The biogeography of giant kelp submarine forests at the sub-Antarctic latitudes of South America

Alejandra Mora-Soto

St. Peter's College



University of Oxford

A thesis presented for the degree of

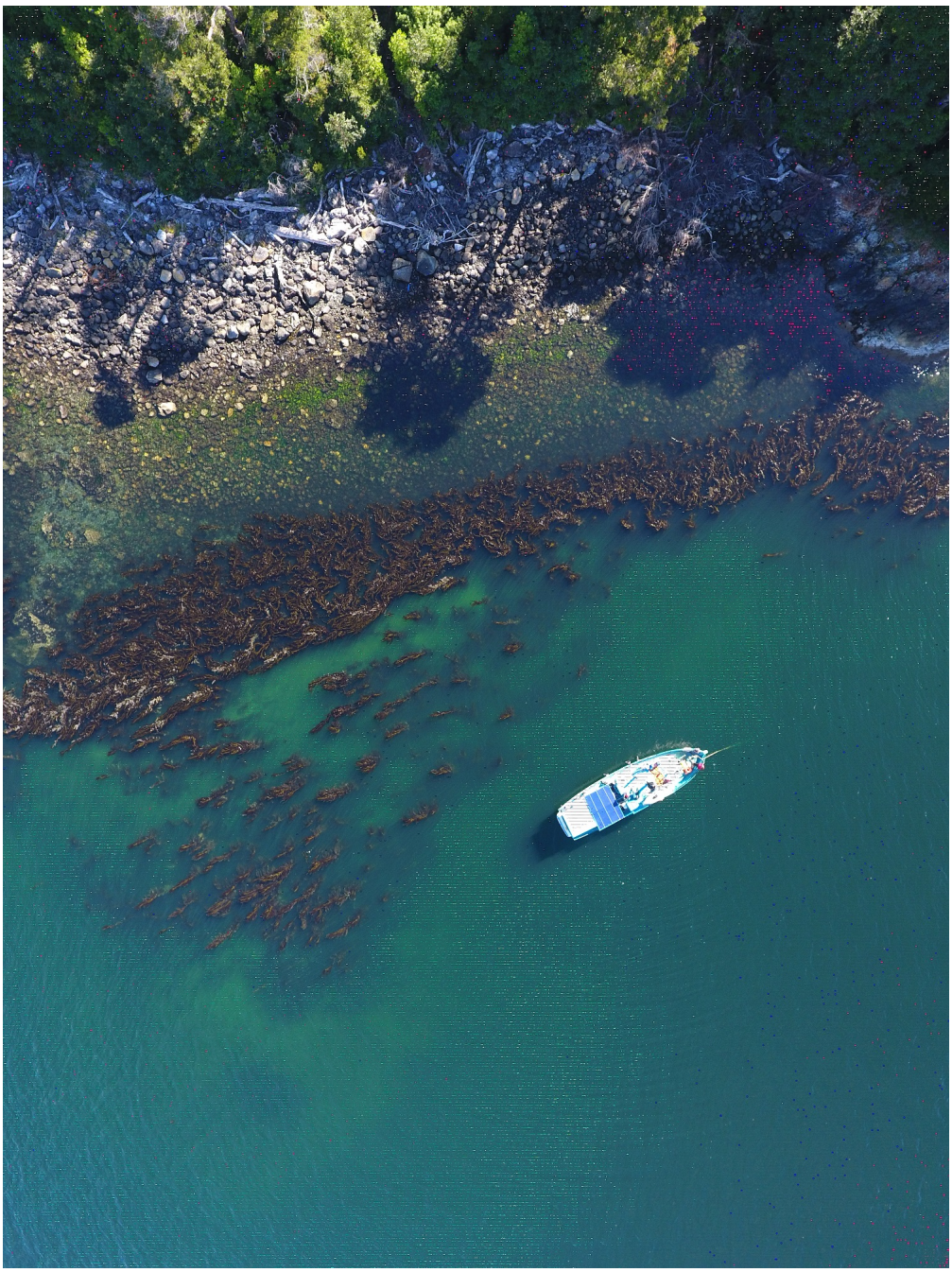
Doctor of Philosophy

Trinity 2021

Dedicated to all the day-dreamers

searching for new worlds

waiting round the corner.



Copyright © 2021 by Alejandra Mora-Soto
All Rights Reserved

Me habéis preguntado qué hila el crustáceo entre sus patas de oro
y os respondo: El mar lo sabe.
Me decís qué espera la ascidia en su campana transparente? Qué espera?
Yo os digo, espera como vosotros el tiempo.
Me preguntáis a quién alcanza el abrazo del alga *Macrocystis*?
Indagadlo, indagadlo a cierta hora, en cierto mar que conozco.

— Pablo Neruda, Los Enigmas

You've asked me what the lobster is weaving there with his golden feet?
I reply, the ocean knows this.
You say, what is the ascidia waiting for in its transparent bell?
What is it waiting for?
I tell you it is waiting for time, like you.
You ask me whom the *Macrocystis* alga hugs in its arms?
Study, study it, at a certain hour, in a certain sea I know.

— Pablo Neruda, Enigmas

There is one marine production, which from its importance is worthy of a particular history. It is the kelp, or *Macrocystis pyrifera* (...) I can only compare these great aquatic forests of the Southern Hemisphere, with the terrestrial ones in the intertropical regions. Yet if in any country a forest was destroyed, I do not believe nearly so many species of animals would perish as would here, from the destruction of the kelp.

— Charles Darwin, The Voyage of the Beagle

Acknowledgements

First and foremost, I am extremely grateful to my supervisor Marc Macias-Fauria for his unwavering support with this research, for giving me the most incredible intellectual freedom at the same time as being so patient and strong-willed in guiding my journey as a researcher, not to mention his endless sense of humour. Many thanks for always having been by my side during this adventure of good old-fashioned science. Additionally, my 'spiritual' gratitude to Charles Darwin for being such an inspiration with his Voyage of the Beagle, which was the awe-inspiring starting point of this research.

I would like to express my sincere gratitude to the colleagues and institutions that advocated this research by facilitating fieldwork resources in Chile and the Falklands. In particular, thanks to Centro IDEAL, represented by José Luis Iriarte, Iván Gómez and Pirjo Huovinen; Centro de Estudios de la Patagonia (CIEP), represented by Giovanni Daneri; South Atlantic Environmental Research Institute (SAERI), represented by Neil Golding; and Shallow Marine Surveys Group, represented by Paul Brewin. This research would never have come so far without your help.

I am deeply grateful to my colleagues that very generously shared with me their knowledge of marine biology and, most importantly, their love for giant kelp. Thanks to Mauricio Palacios (Universidad Austral de Chile), Erasmo Macaya (ALGALAB, Universidad de Concepción), Alejandro Pérez Matus (SUBELAB, Pontificia Universidad Católica de Chile), Américo Montiel (Instituto de la Patagonia), Carolina Oyarzo (Universidad Andrés Bello), Catalina Velasco-Charpentier (Universidad de Magallanes, Fundación Mar y Ciencia), Alan Friedlander and Whitney Goodell (National Geographic, Program Pristine Seas), Paul Dayton

(Scripps Institution of Oceanography, University of California), Mary Young (Deakin University), and Brigitta Van Tussenbroek (Universidad Nacional Autónoma de México).

Many thanks to the colleagues from the areas of zoology (Tom Hart, University of Oxford), oceanography (Catalina Aguirre, Universidad de Valparaíso) and geographical information systems (Austin Capsey, UK Hydrographic Office) for their generous help in providing data and new perspectives for this research.

I would also like to express my gratitude for the great opportunity of being part of the Biogeosciences Group. To my colleagues Maria Dance, Georgia Melodie Hole, Marcus Spiegel, Nicola Kuhn, William Hartz, Andrew Martin and Danielle Sinclair: thank you for sharing your knowledge and thoughts, supporting words and new ideas to improve this research. It has been wonderful to see the evolution of each other's projects and I am very thankful for having been able to stay in contact all this time, despite the COVID-19 pandemic and the physical distance.

Thanks to all my friends from OUEEG for teaching me to dive in the tempestuous Cornwall coastline. A special thanks to my instructors Penny, Kirill, Giles, Tom, Clare, Max and my diving mates Razia, Rona, Jenny, and Mi Jun. Diving in the UK was the best experience and nothing compares in difficulty; I can now dive with confidence thanks to you. *In aqua laetitia!*.

I would like to thank my beloved friends in Oxford: Samuel León, Carlita Pérez Martínez, Paola Castañeda, Tamsin Hong, Meriç Özölçer, Bushra Malik, and all the St. Peter's gang, for the most wonderful and unforgettable times in the city of dreaming spires. Thanks to my adopted family in the UK: Ruby, Paula, Javiera and Chany for their loving support, happiness and, above all, the music.

Dani Manuschevich, thank you for your beautiful and constant mentorship.

A big thanks to my beloved parents, Francisco Mora and Ana Soto, to all my family, and all my friends for always being there; thank you for your love and continuous patience and understanding.

Lastly, my deepest gratitude to Pablo E. Cartes for saving my life with his love and care.

Abstract

This doctoral thesis presents the first work on the extent, spatial dynamics, and long-term trends of the giant kelp (*Macrocystis pyrifera*) ecosystem in southern South America and sub-Antarctic latitudes. This work was based on an interdisciplinary approach of remote sensing using satellite images, unmanned aerial vehicles (UAV), geographical information systems, underwater exploration, and a collection of historical sources and secondary information from international collaborations.

The first research paper of this thesis (Chapter 3) presents a mapping methodology of giant kelp derived from filtering values from the satellite Sentinel-2. This method was validated with secondary sources (previous kelp surveys) and primary sources of data, such as detailed orthomosaics made with UAV. Because of the high overall accuracy of this method, it was possible to map and measure the surface of the complete distribution of the giant kelp ecosystem by ecoregion and province.

The second paper (Chapter 4) is based on the mapping methodology from Chapter 3, developing a spatial analysis of the sub-Antarctic kelp from South America, Falkland Islands (Malvinas) and South Georgia to understand the abiotic patterns that could predict the typical size of a giant kelp forest. Additionally, these patterns were compared in a temporal analysis stretching as far back as the 19th century to assess the persistence of this ecosystem. The results of this paper indicate that sub-Antarctic giant kelp is one of the least modified and most persistent marine ecosystems on Earth.

Chapter 5 analyses the spatial distribution of marine sea surface temperature (SST) heatwaves and marine cold spells in the Channels and Fjords ecoregion in past

decades, with a focus on understanding the climatological trends as they can affect giant kelp ecosystems. This paper established that, in contrast to the main global trend pointing towards SST warming, the frequency of marine cold spells in the nearshore coastlines of southernmost South America has in fact increased in the decade of 2010. We identified two main mechanisms as possible causes for this trend: increased frequency of storms driven by the Antarctic Circumpolar Current and glacier melting in the Patagonian fjords. Cold waters favour the persistence of giant kelp and associated biodiversity, hence the lack of SST warming highlights the region as a potential refugium for the ecosystem. However, more studies are needed to understand these new dynamics, and we conclude the paper with a summary of potential stressors to giant kelp ecosystems in the study area.

Finally, Chapter 6 provides an overview of the main findings of this thesis and recommendations for future research, highlighting the need for further interdisciplinary studies on the Magellanic marine province as a climatic refugium for the giant kelp ecosystem.

Keywords— Giant Kelp, *Macrocystis pyrifera*, Patagonia, South America, sub-Antarctic, marine ecosystems, persistent ecosystems.

Table of Contents

List of Figures xv

List of Tables xxii

1 Introduction 1

1.1 Giant kelp forests: an overview 1

1.2 Sub-Antarctic giant kelp: overview and research gaps 3

1.3 Mapping kelp ecosystems: overview and research gaps 5

1.4 Research aims and thesis structure 7

References 8

2 Research approach 17

2.1 Giant kelp mapping 17

2.2 Giant kelp exploration 19

2.3 Characterization of the abiotic habitat 20

2.4 Historical cartography 21

2.5 Sea surface temperature trends 21

2.6 Remote sensing and GIS tools 23

2.7 A statement for the south 23

References 24

3 Chapter 3: Paper 1 27

3.1 Linking statement 27

3.1.1 Author contribution statement 28

3.2 A high-resolution global map of Giant Kelp (*Macrocystis pyrifera*) forests and intertidal green algae (*Ulvophyceae*) with Sentinel-2 imagery . . . 29
3.2.1 Abstract . . . 30
3.2.2 Keywords . . . 31
3.2.3 Introduction . . . 31
3.2.4 Materials and Methods . . . 37
3.2.4.1 Training data . . . 37
3.2.4.2 Kelp filter algorithm . . . 38
3.2.4.3 Validation at high spatial resolution . . . 41
3.2.4.4 Kelp filter algorithm in Google Earth Engine . . . 42
3.2.4.5 Validation at low spatial resolution . . . 45
3.2.5 Results . . . 45
3.2.5.1 Kelp filter algorithm . . . 45
3.2.5.2 Validation at high resolution . . . 47
3.2.5.3 Validation at low resolution . . . 49
3.2.6 Discussion . . . 49
3.2.6.1 Kelp detection and mapping . . . 49
3.2.6.2 Spatial and biophysical patterns . . . 51
3.2.6.3 False negatives . . . 53
3.2.6.4 False positives . . . 54
3.2.6.5 Notes on UAV surveying . . . 55
3.2.6.6 Additional considerations about the global map 55
3.2.7 Conclusions . . . 56
References . . . 58

4 Chapter 4: Paper 2 71
4.1 Linking statement: Submitted for publication . . . 71

4.1.1 Author Contribution Statement 72
4.2 One of the least disturbed marine coastal ecosystems on Earth: Spatial and temporal persistence of Darwin's sub-Antarctic giant kelp forests 73
4.3 Abstract 75
4.3.1 Aim 75
4.3.2 Location 75
4.3.3 Taxon 75
4.3.4 Methods 75
4.3.5 Results 76
4.3.6 Main conclusions 76
4.3.7 Keywords 76
4.4 Introduction 77
4.4.1 Characterising the abiotic niche 79
4.4.2 Long-term persistence 80
4.5 Methodology 81
4.5.1 Study area 81
4.5.2 The abiotic niche 83
4.5.2.1 Spatial identification of a sample of present kelp forests (2016-2019) 83
4.5.2.2 Statistical analyses 84
4.5.2.3 Decadal trends of Sea Surface Temperature (1981-2020) 86
4.5.3 Long-term persistence 86
4.5.3.1 Long-term kelp canopy extent monitoring . . . 86
4.5.3.2 Second half of 20th century 87
4.6 Results 90

4.6.1 Characterising the abiotic niche 90
4.6.1.1 The landscape/seascape of present kelp forests . 90
4.6.1.2 Multidecadal SST trends 95
4.6.2 Long-term persistence 95
4.7 Discussion 96
4.7.1 Anthropogenic changes and kelp persistence 102
4.8 Acknowledgements 107
References 108

5 Chapter 5: Paper 3 **124**
5.1 Linking Statement: Soon to be submitted for publication. 124
5.1.1 Author Contribution Statement 125
5.2 A song of wind and ice: geographical distribution of marine heatwaves (MHW) and marine cold-spells (MCS) in southwestern Patagonia and their possible effects on giant kelp forests 126
5.3 Abstract 127
5.4 Introduction 128
5.5 Methodology 130
5.5.1 Area of study 130
5.5.2 MHW and MCS definition and characterisation 131
5.6 Results 135
5.6.1 Overview of SST per marine ecoregion 135
5.6.2 Overview of MHW and MCS in Southwestern Patagonia (1981 to 2020) 135
5.6.2.1 Marine Heatwaves (MHW) 135
5.6.2.2 Marine cold spells (MCS) 139
5.6.3 SST, U10 and V10 Anomaly maps for severe and extreme events 140

5.7 Discussion . . . 145
5.7.1 Satellite versus in-situ data . . . 145
5.7.2 Observations on MHW and MCS events . . . 146
5.7.3 MCS and giant kelp forests . . . 148
5.8 Conclusion . . . 151
References . . . 151

6 Chapter 6: Conclusions **162**
6.1 Overall findings . . . 162
6.1.1 Giant kelp forest extent . . . 162
6.1.2 Abiotic factors of giant kelp by ecoregions and landscape units . . . 164
6.1.3 Long-term trends of giant kelp . . . 165
6.1.4 Future trends of sub-Antarctic giant kelp . . . 166
6.2 Future research needs and directions . . . 167
6.3 Concluding remarks . . . 168
References . . . 169

Appendix A Supplementary Materials **173**
A.1 Supplementary Materials Paper 1 . . . 173
A.2 Supplementary Materials Paper 2 . . . 174
A.2.1 Data availability statement . . . 174
A.2.2 Additional tables and figures . . . 175
A.3 Supplementary Materials Paper 3 . . . 177
A.3.1 Satellite versus in-situ SST data . . . 177
A.3.2 SST, U10 and V10 Anomaly maps for severe and extreme events . . . 178

List of Figures

2.1 Giant kelp canopy, as seen from the shore. San Isidro Lighthouse, Strait of Magellan 18

2.2 Sketches of kelp forests from the field campaign 1, in a) the Strait of Magellan and b) the Patagonian fjords. 20

2.3 Comparing historical and present-time giant kelp records. Subsection 1: Kelp canopies were drawn as leaves near the coastline in a chart made in 1834. The following images show averaged kelp area by year using satellite detection. 22

3.1 Mean $\pm$ SD reflectance values for each Region of Interest (ROI) used as training data in this study, computed for all Sentinel-2 bands (central wavelength of each band (in nm) and band number indicated in the x axis). Classes or ROIs: Coast; Foam; GA= Green Algae; Kelp; LV= Land vegetation; Ocean; OW= Organic water; RG: River grass. 39

3.2 Box and whisker plot of B11 reflectance values (90 grid cells per class). All grid cells with B11 $\geq$ 0.028 (indicated with a dashed line) were masked out to separate Coast and Land Vegetation from the other ROIs. Classes or ROIs: Coast; Foam; GA= Green Algae; Kelp; LV= Land vegetation; Ocean; OW= Organic water; RG: River grass. 40

3.3 Map of the surveyed sites for validation at high-resolution of giant kelp forests. Cartographic projection EPSG3857. Maps in this article are South-oriented to highlight the connectivity of kelp forests at Sub-Antarctic latitudes. 44

3.4 Location of the training data (black dots) and the low-resolution validation sites (red dots). Cartographic projection EPSG: 54042. Maps in this article are South-oriented to highlight the connectivity of kelp forests at Sub-Antarctic latitudes. 46

3.5 Ground-truthing process. A: 'True' canopy is delineated as the black line in the UAV orthomosaic. B, C and D: maps obtained through the kelp filter algorithm applied on FAI, KD and NDVI respectively. Higher values show higher concentrations of kelp canopy, although each index shows different levels of sensitivity. Site: San Isidro (Strait of Magellan). Cartographic projection EPSG3857, South-oriented. 67

3.6 A: Buque Quemado intertidal forest (Strait of Magellan), at 10 cm of depth in low tide and 9 m in high tide. B: Measuring the length of the plants of site A. (People in photos A and B are included for scale). C: Permanent subtidal forest (delineated in black) in Puerto Amparo (area= 0.3 ha). D: Underwater canopies of Puerto Amparo (max. depth: 7.9 m). (Photos: Alejandra Mora S.) 69

4.1 A) Ecoregions of Channels and Fjords of Southern Chile, Falkland Islands (Malvinas) and the island of South Georgia in context with the main oceanic currents. The colour palette in the ocean indicates the Eastward mean velocity at the surface in 2019, according to the Hybrid Coordinate Ocean Model (HYCOM; (Chassignet et al.; 2009)); the labels indicate the mean ±2 Standard Deviations (the velocity layer is included for reference only). B, C, D) Overview of the United Kingdom Hydrographical Office (UKHO) historical Nautical Charts, kelp sites and SST sites, and internal currents, for B) Channels and Fjords and Patagonian Shelf; C) Falkland Islands (Malvinas); D) South Georgia. Map projection EPSG:3857. 82

4.2 Kelp canopy cover (ha) by: A) currents, B) slope class, C) geoform, and D) exposure. Boxplots are mean ± standard error of the size of sampled kelp forests per ecoregion, and the red labels indicate number of kelp forests per class. A) Ocean currents: CH = Cape Horn, Channels = Chilean Patagonia Channels, SM = Strait of Magellan, FC = Falkland Current, FS = Falkland Sound, ACC = Antarctic Circumpolar Current. B) Slope Class: Level (flat or gently sloping) = <4°, Sloping = 4-15°, Steep = 15-35°, Very steep = > 35°. C) Geoform, D) Exposure. 91

4.3 Kelp forest size (ha) in relation to coastal orientation: A) Channels and Fjords, B) Falkland Islands (Malvinas), and C) South Georgia. Values are mean ± standard error of the sampled kelp forests per orientation. Refer to Figure 4.1A to compare with the main oceanic currents of each ecoregion. 92

4.4 Conditional inference tree (non-parametric regression tree). Currents: ACC = Antarctic Circumpolar Current. Channels = Channels of Southern Chile. CH = Cape Horn Current. FC = Falkland Current. FS = Falklands Sound. SM = Strait of Magellan. Ecoregions: CFSCh = Channels and Fjords of Southern Chile. Falkland = Falkland Islands (Malvinas). SGeorgia= South Georgia. Exposure: open = Open ocean. Sheltered = Sheltered or protected areas. The threshold of large or small forests is the median area of the total of kelp forests (7 ha). 94

4.5 A general model of the sub-Antarctic kelp forest in relation to coastal geomorphology. The area of a kelp forest depends on the available substrate originated by geological orogeny followed by glacial, marine, alluvial, or organic weathering and/or sedimentation. Topographic slope classes: A) Level to sloping; B) steep; C) vertical and over-hanging walls. Exposure to the ocean has an inverse correlation with the growth rate and positive correlation with the life span of the canopies (Van Tussenbroek, 1989a, 1989c). 99

4.6 1) Royal Bay and Moltke Harbour, South Georgia, as seen from the original georeferenced Imperial German Survey, 1882. The extent of kelp forests is indicated with a red contour. 2) Satellite-detected kelp forests, derived from the KF algorithm. The extent of kelp is indicated with green (2019), red (2018), purple (2017), and yellow (2016) pixels, respectively. The approximate distance between the front line of the Ross Glacier drawn in 1882 and the present time is 6.3 km. (Background image: Earthstar Geographics (TerraColor NextGen) imagery, ESRI). 104

5.1 Figure 1. Map of the marine ecosystems mentioned in this study: 1) Gulf of Penas; 2) Offshore Kaweskar; 3) Inner Channels Kaweskar; 4) Western Strait; 5) Central Strait; 6) Bahia Inutil; 7) Eastern Strait; 8) Offshore Magellan; 9) Nearshore Beagle Ballenero; 10) Nearshore Nassau Hornos. The in-situ sensor is indicated with a red star; the centroids of each satellite-detected kelp forest are indicated with green points. 132

5.2 Map of mean SST per marine ecosystem in the period 1981-2020. Each label in the map indicates the mean temperature per ecosystem. See Figure 1 for marine ecosystem name. Background map: © OpenStreetMap contributors. 136

5.3 Box and whisker plot of daily SST 1981-2020 (in degree Celsius) per marine ecosystem. The vertical line shows temperature mean for the total of the area of study (8.2°C). 137

5.4 Number of events categories II (strong), III (severe) and IV (extreme) for the period 1982-2020 per MHW for the total of ecosystems in the area of study. 139

5.5 Choropleth map labelled with the count of MHW category and ecosystem for the period 1981-2020. MHW, categories II (strong, a), III (severe, b) and IV (extreme, c). Each colour legend and labels in bold indicate the number of events per ecosystem. Background map: © OpenStreetMap contributors. 140

5.6 Number events categories II (strong), III (severe) and IV (extreme) for the period 1982-2020 per A) MHW; B) MCS for the total of ecosystems in the area of study. 143

5.7 Choropleth map labelled with the count of MCS events per category and ecosystem for the period 1981-2020. Categories II (strong, a), III (severe, b) and IV (extreme, c). Each colour legend and labels in bold indicate the number of events per ecosystem. Background map: © OpenStreetMap contributors. 144

6.1 Summary of research aims and paper structure of this thesis. . . . 163

A.1 Time series of NOAA Sea Surface Temperature (°C) from 1981 to 2020 in the SST-representative pixels per ecoregion. 176
A.2 Linear model of SST *in situ* versus SST Statellite. 177
A.3 1) MCS: BH2 1981, MCS E4 1981 179
A.4 2) MCS: CE2 1982a, E4 1982b, C1 1982 180
A.5 3) MCS: CE1 1982a 181
A.6 4) MCS: E1 1982b 182
A.7 5) MCS: E3 1982 183
A.8 6) MCS: E1 1984b 184
A.9 7) MHW: E2 1984b, E3 1984, CE2 1984 185
A.10 8) MCS: CE1 1991 186
A.11 9) MCS: BH2 1995a 187
A.12 10) MHW: CE1 1998b, CE3 1998a, BH2 1998, C1 1998b, E4 1998b, BH1 1998, E2 1998b, E1 1998 188
A.13 11) MCS: E4 2007b 189
A.14 12) MCS: E3 2008 190
A.15 13) MCS: E3 2011 191
A.16 14) MCS: BH2 2014 192
A.17 15) MCS: E4 2015 193
A.18 16) MCS: C1 2015b 194

A.19 17) MCS: BH1 2015 195
A.20 18) MHW: CE2 2016a, CE1 2016a 196
A.21 19) MCS: BH2 2016 197
A.22 20) MHW: CE1 2016d 198
A.23 21) MCS: BH1 2017 199
A.24 22) MCS: C1 2018d 200
A.25 23) MCS: BH2 2019a 201
A.26 24) MCS: BH2 2019b 202
A.27 25) MCS: E2 2019 203
A.28 26) MCS: BH1 2019 204
A.29 27) MHW: BH1 2020b 205

List of Tables

3.1 Sites selected as training data in this study 38

3.2 Masking out threshold by index. 41

3.3 Summary of validation sites, their coordinates, extent of the kelp stand (ha), and climate zone. Climate acronyms Csb, Warm temperate climate with dry and warm summer. Cfb, Warm temperate climate, fully humid and warm summer. Cfc, Warm temperate climate, fully humid and cold summer. ET, Polar tundra (Koweek et al., 2017) 43

3.4 Remaining grid cells out of 90 Giant kelp and 90 Green algae original observations (total = 180) after the application of the kelp filter algorithm to the training data. 47

3.5 Confusion matrix results for maps obtained using the kelp filter algorithm employing FAI, NDVI and KD in forests larger than 1 hectare. PA = Producer's Accuracy (%). UA = User's Accuracy (%). OA = Overall Accuracy (%). Overall Accuracies > 80 and Kappa coefficients > 0.6 are highlighted in bold. 48

3.6 Remaining grid cells out of 90 Giant kelp and 90 Green algae original observations (total = 180) after the application of the kelp filter algorithm to the training data. 49

3.7 Area in km^2 per marine ecoregion and province with detected giant kelp and intertidal green algae, and number of detected grid cells versus total of georeferenced sites per ecoregion in a range of 300 m. 68

3.8 Table 3.7 *(Cont.)* 69

4.1 Attributes of the giant kelp (*Macrocystis pyrifera*) forests used in this study. * Dependent variable; [1]: Independent variable 85
4.2 Descriptive statistics for size (ha) of kelp forests per ecoregion. Qu. = quartile. 92
4.3 Kruskal-Wallis rank sum test of the significant variables associated with size of the kelp canopies. KMO = Kaiser-Meyer-Olkin (KMO) Measure of Sampling Adequacy. KMO values >0.5 and significant Bartlett's Test indicate that the variables are adequate for factor analysis. 93
4.4 Summary of the total of kelp forests drawn on the UKHO nautical charts and satellite-detected kelp. 97
4.5 List of sites with kelp forests from their first records on nautical charts, and anthropogenic and environmental changes occurred in the last two centuries. 103

5.1 MHW events, categories III and IV per ecosystem in the period 1982-2020. Start, peak, end date= days of the event (peak day in bold); i_max = maximum intensity [°C]; var = Standard deviation; duration= total days of the event (note that there could be gap days in the duration of the event). More details of each event are disaggregated in Supplementary Material A.3.2. 138
5.2 MCS events, categories III and IV per ecosystem in the period 1982-2020. Start, peak, end date= days of the event (peak day in bold); i_max = maximum intensity [°C]; var = Standard deviation; duration= total days of the event (note that there could be gap days in the duration of the event). More details of each event are disaggregated in Supplementary Material A.3.2. 141
5.3 Table 5.2 (cont.) 142

5.4 Summary of possible effects on giant kelp forests by marine ecosystem, according to geographical characteristics and warm and cold events observed in this study. Giant kelp area was calculated using the map of Mora-Soto et al. (2020). 150

A.1 Table S1 Descriptive statistics of SST (°C) for the representative NOAA-SST sites by ecoregion. 175

List of Abbreviations

ACC . . . . . Antarctic Circumpolar Current

CART . . . . . Classification and Regression Trees

FAI . . . . . Floating Algae Index

GEE . . . . . Google Earth Engine

KD . . . . . Kelp Difference

KF . . . . . Kelp Filter algorithm

MCS . . . . . Marine cold spells

MESMA . . . . . Multiple Endmember Spectral Mixture Analysis

MHW . . . . . Marine heatwaves

MSS . . . . . Multispectral Scanner (*Landsat sensor*)

NDVI . . . . . Normalised Difference Vegetation Index

NIR . . . . . Near Infrared band

OLI . . . . . Operational Land Imager (*Landsat sensor*)

PCA . . . . . Principal Component Analysis

RGB . . . . . Band composite Red Green Blue; Visible Light

ROI . . . . . Regions of Interest

SMA . . . . . Spectral Mixture Analysis

SPOT . . . . . Satellite Pour l'Observation de la Terre

SST . . . . . Sea Surface Temperature

TM . . . . . Thematic Mapper (*Landsat sensor*)

UAV . . . . . Unmanned aerial vehicle; also known as *drone*





1 | Introduction

1.1 Giant kelp forests: an overview

The giant kelp, *Macrocystis pyrifera*, is one of the longest biogenic structures and one of the most conspicuous and extensively distributed species on the planet (Graham et al.; 2007). This algae can be found on the temperate coastlines of South America, Africa, Australia, New Zealand and Subantarctic Islands, as well as the north Pacific coast of North America from Baja California to Alaska, showing a remarkable capacity to adapt its physiology to different environmental conditions (Macaya and Zuccarello; 2010).

Giant kelp is considered a foundation species and an ecosystem engineer, as its presence creates ideal nursery grounds and protection for a high diversity of organisms that settle and move around the algae's holdfasts to its blades, and also for the physical role that forms against the effect of waves and currents, sedimentation, and incoming light into the water column (Miller et al.; 2018; Steneck et al.; 2002; Teagle et al.; 2017).

Generally speaking, the main abiotic factors for giant kelp are: hard substratum, cold temperatures, light intensities equivalent to 1% or greater than the incoming light on the surface, nitrate concentrations above 1 μmol L^{-1}, and protection from extreme water motion (Schiel and Foster; 2015). On the other hand, where there is a lack of light and a rocky substratum, as well as sea urchin grazing, giant kelp distribution is stunted (Graham et al.; 2007). These broad factors plus their biotic requirements interplay in complex ways, enhancing or constraining their success as individual organisms and as ecosystems (Graham et al.; 2007; Schiel and Foster; 2015).

There is an age-old bond between giant kelp and humans. Some scholars consider that the early human settlement in the American continent, from the Bering Strait to Patagonia, could be explained by migration routes following the kelp-bordered coasts (the Kelp Highway hypothesis; (Erlandson et al.; 2007)). This hypothesis is supported by the discovery of remains of *Macrocystis pyrifera* and other seaweed at the earliest archaeological site of South America, Monte Verde (14,000 years BP; (Dillehay et al.; 2008)) among other archaeological sites (Steneck et al.; 2002). Nowadays, there is an overall agreement that giant kelp is a provider of several ecosystem services, in direct ways, like seaweed production (Buschmann et al.; 2014), and in indirect ways, because of their related biodiversity and cultural heritage, their coastal protection capabilities and carbon sequestration potential (Duarte et al.; 2005; Filbee-Dexter and Wernberg; 2018; Vásquez et al.; 2014).

Despite their significance, giant kelp as well as the overall kelp biome has been reduced by multiple stressors at different regions of the world's ocean. Ocean warming, increased storms, overharvesting, and pollution (with or without eutrophication) are some of their most relevant threats (Wernberg et al.; 2019). A global analysis on the status and trends of kelp forests detected that 38% of forests are declining, 27% are increasing and 35% have no detectable changes, in the 34 ecoregions with long-term databases out of the 99 ecoregions where kelp exists (Krumhansl et al.; 2016). One of the extensive and important marine ecoregions where no data were available was the Channels and Fjords of Southern Chile ecoregion in the Magellanic province (Spalding et al.; 2007), located in sub-Antarctic South America. The main goal of this thesis is to fill this gap.

1.2 Sub-Antarctic giant kelp: overview and research gaps

The sub-Antarctic marine ecoregions of South America (42°-55°S) are some of the least studied in the world (Escribano et al.; 2003). The marine environment is influenced by the West Wind Drift, which carries sub-Antarctic water from the Pacific Ocean flowing poleward in the Cape Horn Current; nearshore, this water encounters with estuarine waters from rivers, glaciers, and fjords (Camus; 2001), forming a sharp vertical gradient of low salinity and low density waters in the top layer over a denser, high-salinity bottom layer (Dávila et al.; 2002). The land is dominated by the Andes mountain range, which is a great orographic barrier: at latitude 53°S the windward side receives between 6000 and 7000 mm of annual precipitation at sea level, whereas the leeward side, the city of Punta Arenas in the Strait of Magellan, receives only 430 mm (Schneider et al.; 2003). The coastal landscape is a very complex network of channels between islands and archipelagos resulting from the combined effect of tectonics and glaciation (Camus; 2001). The extreme south also represents the southernmost biogeographical distribution for numerous taxa (Rozzi et al.; 2007), including giant kelp.

One of the first mentions of the kelp habitat was made by Charles Darwin during the Beagle expedition, a hydrographic survey organised by the British Admiralty, with the aim of making precise nautical charts of southern South America (King et al.; 1836). On his accounts of the voyage, Darwin mentions how prevalent giant kelp was on the coastline of Tierra del Fuego and Patagonia and the diversity of species that depended on the kelp ("I can only compare these great aquatic forests of the southern hemisphere, with the terrestrial ones in the intertropical regions" (Darwin; 1845)). Despite this interesting observation made almost two centuries

ago, the first studies that explicitly focused on kelp ecosystems and kelp physiology in the extreme south only started in the decades of 1970 and 1980 (Barrales and Lobban; 1975; Castilla and Moreno; 1982; Dayton; 1985a,9; Moreno and Jara; 1984; Ojeda and Santelices; 1984; Santelices and Ojeda; 1984; Van Tussenbroek; 1989a,9,9,9,9); these works opened a new focus on the ecology and environment of giant kelp at these latitudes (Graham et al.; 2007; Steneck et al.; 2002; Wernberg et al.; 2019).

In recent years, there has been an increasing awareness of the associated biodiversity and conservation challenges of *Macrocystis pyrifera* forests, through integrated ecological assessments developed in the Cape Horn archipelago, Diego Ramírez Islands and Francisco Coloane National Park (Friedlander et al.; 2018); Tierra del Fuego and Isla de los Estados (Friedlander et al.; 2020), and Kaweskar National Park (Friedlander et al.; 2021). These studies agree that the giant kelp at the end of the continent is one of the last remaining intact marine ecosystems on Earth. However, the first — and so far, the only — marine protected area that has included giant kelp as an object of conservation is Seno Almirantazgo, in Tierra del Fuego (Vila et al.; 2010). External anthropogenic pressures, such as the negative environmental effects of salmon farming (for example, increased nutrient discharge in fjords or salmon as an invasive species), constitute current threats to the biodiversity of the region (Friedlander et al.; 2021). An open question was to confirm whether these and/or other pressures have reduced the former levels of distribution of kelp.

1.3 Mapping kelp ecosystems: overview and research gaps

Treating kelp forests as 'forests' is an effective communication tool: it is easily understandable by the wider public, as this concept highlights its functionality as an essential foundation ecosystem (Wernberg and Filbee-Dexter; 2019). In the same way, including kelp forests in a map of national ecosystems emphasizes their presence and therefore their conservation status would become priority.

When I began this research (2017), there were already important developments on kelp mapping. The most significant innovation was the use of satellite imagery from the SPOT and LANDSAT sensors to map giant kelp canopies (Bell et al.; 2018,0; Cavanaugh et al.; 2010,0; Jensen et al.; 1980); but the extent of such mapping exercises was landscape to regional, and they had been only applied to the regions where ground-truthing data was available. This largely restricted the geographical scope of the thesis, since a full set of ground truthing data is incredibly hard to obtain *a priori* in a very long and complex coastline such as western Patagonia. For my investigation, I had to create a methodology with enough predictive power to locate kelp forests and to validate them with a dataset of known sites, even if they were outside my area of study. This was the first and most important challenge of this thesis. The general methodological approach to create this map is explained in Chapter 2, section 2.1, and in more detail in Chapter 3.

Having a basemap with the location of sub-Antarctic kelp forests introduces new possibilities of understanding their drivers and dynamics. In other latitudes such as the north Atlantic and the north Pacific, environmental factors such as depth, slope, wave exposure, wave disturbance, and nitrate availability, among others,

play a role in defining the distribution of kelp (Bekkby et al.; 2009,0; Bell et al.; 2015). However, the distribution of kelp species is site-specific at small scales and there is a need for expanding the knowledge of their behaviour to other marine ecoregions and provinces (Teagle et al.; 2017). To understand the abiotic factors of kelp habitats at sub-Antarctic latitudes, I compared the main geographical characteristics of 309 kelp forests from Channels and Fjords of Southern Chile, Falkland Islands and South Georgia, to create a predictive model of kelp forest size. The general methodological approach to create this model is explained in Chapter 2, sections 2.2 & 2.3, and in more detail in Chapter 4.

A distribution map enables studies regarding past and future trends of this marine ecosystem. Previous examples of historical assessments examining changes were developed at coral reefs (Hamylton and East; 2012), and during the course of this research, two papers were published about long-term trends of kelp forests in the northeast Pacific (Costa et al.; 2020; Pfister et al.; 2018), employing both long-term satellite data and field-based kelp presence maps which date back to nautical charts from the first half of the 19th century. My research expanded on this analysis, investigating the historical changes in the south using as reference the predictive model mentioned above. A typical expected forest size was a parameter to analyse if the current forests, compared with historical data, were persistent at the same places. The general methodological approach to create this historical comparison is explained in Chapter 2, section 2.4 , and in more detail in Chapter 4.

Finally, a novel research corpus has arisen in the last years, studying the extent, duration and intensity of marine heatwaves and marine cold spells in the world ocean (Holbrook et al.; 2020). Most of the research has been focused on the trends of the warming ocean, including their origins and effects (Marin et al.; 2021; Oliver et al.; 2018), while less attention has been given to the cooling trend, which

has been observed to occur in the Western Australia and South African coastlines (Feng et al.; 2021; Schlegel et al.; 2017). To date, there are no reported analyses on long-term trends of temperature anomalies in the sea near South America and their possible effects on kelp forests (Smale; 2019), which is another open question that this thesis aims to develop. The general methodological approach to analyse the sea surface temperature trends and their effects on kelp forests is explained in Chapter 2, section 2.5, and in more detail in Chapter 5.

1.4 Research aims and thesis structure

My DPhil explores the geography and the temporal trends of the giant kelp ecosystem in southern South America and the sub-Antarctic latitudes, with special focus on the Magellanic province and particularly the Channels and Fjords of Southern Chile ecoregion, deriving from the classification of marine ecosystems from (Spalding et al.; 2007). Consequently, this research was structured with the following aims:

1. To detect the extension of the giant kelp forest in the Magellanic province, from Chiloé Island to Cape Horn;
2. To create a model to understand the abiotic factors that explain the observed distribution of giant kelp forests;
3. To explore the differences between giant kelp forests in varying ecoregions and landscape units;
4. To explore the long-term trends of giant kelp;
5. To explore the future trends of sub-Antarctic kelp forests.

This thesis was written as a series of scientific papers that addresses the given

aims: aim 1 was covered by the first paper (**Chapter 3**) which explores a mapping methodology for the Magellanic province and the complete distribution of the giant kelp ecosystem; the second paper (**Chapter 4**) is based on the map obtained in Chapter 3 and covers aims 2, 3 and 4, specifically looking at a spatial analysis of the sub-Antarctic kelp from South America to South Georgia and at a temporal analysis that stretches as far back as to the 19th century; the third paper (**Chapter 5**) covers aims 3, 4 and 5 of this thesis, analysing the spatial distribution of marine heatwaves and marine cold spells in the Channels and Fjords ecoregion in past decades, and outlines future trends for giant kelp. Finally, **Chapter 6** provides an overview of the main findings of this thesis and recommendations for future research.

References

Barrales, H. L. and Lobban, C. S. (1975). The comparative ecology of Macrocystis pyrifera, with emphasis on the forests of Chubut, Argentina, *The Journal of Ecology* pp. 657–677.

Bekkby, T., Rinde, E., Erikstad, L. and Bakkestuen, V. (2009). Spatial predictive distribution modelling of the kelp species Laminaria hyperborea, *ICES Journal of Marine Science* **66**(10): 2106–2115.

Bekkby, T., Rinde, E., Gundersen, H., Norderhaug, K. M., Gitmark, J. K. and Christie, H. (2014). Length, strength and water flow: relative importance of wave and current exposure on morphology in kelp Laminaria hyperborea, *Marine Ecology Progress Series* **506**: 61–70.

Bell, T. W., Allen, J. G., Cavanaugh, K. C. and Siegel, D. (2018). Three decades of

variability in California's Giant Kelp forests from the Landsat satellites, *Rem. Sens. of Env.* p. 110811.

Bell, T. W., Cavanaugh, K. C., Reed, D. C. and Siegel, D. A. (2015). Geographical variability in the controls of Giant Kelp biomass dynamics, *J. of Biogeography* **42**(10): 2010–2021.

Buschmann, A. H., Prescott, S., Potin, P., Faugeron, S., Vásquez, J. A., Camus, C., Infante, J., Hernández-González, M. C., Gutiérrez, A. and Varela, D. A. (2014). *Chapter Six - The Status of Kelp Exploitation and Marine Agronomy, with Emphasis on Macrocystis pyrifera, in Chile*, Vol. 71, Academic Press, pp. 161–188.
URL: *https://www.sciencedirect.com/science/article/pii/B9780124080621000068*

Camus, P. A. (2001). Biogeografía marina de Chile continental, *Revista Chilena de Historia Natural* **74**(3): 587–617.

Castilla, J. and Moreno, C. (1982). Sea urchins and *Macrocystis pyrifera*: experimental test of their ecological relations in Southern Chile, *Proceedings of the International Echinoderm Conference, Tampa Bay, Florida, USA, ed. JM Lawrence*, pp. 257–263.

Cavanaugh, K. C., Siegel, D. A., Kinlan, B. P. and Reed, D. C. (2010). Scaling Giant Kelp field measurements to regional scales using satellite observations, *Mar. Ecology Progress Series* **403**: 13–27.

Cavanaugh, K. C., Siegel, D. A., Reed, D. C. and Dennison, P. (2011). Environmental controls of giant-kelp biomass in the Santa Barbara Channel, California, *Mar. Ecology Progress Series* **429**: 1–17.

Costa, M., Le Baron, N., Tenhunen, K., Nephin, J., Willis, P., Mortimor, J. P.,

Dudas, S. and Rubidge, E. (2020). Historical distribution of kelp forests on the coast of British Columbia: 1858-1956, *Applied Geography* **120**: 102230.

Darwin, C. (1845). *The Voyage of the Beagle: Journal of Researches into the Natural History and Geology of the Countries Visited During the Voyage of HMS Beagle Round the World: Under the Command of Capt. Fitz Roy, R.N.*, GB.

Dávila, P. M., Figueroa, D. and Müller, E. (2002). Freshwater input into the coastal Ocean and its relation with the salinity distribution off austral Chile (35-55°s), *Continental Shelf Research* **22**(3): 521–534.
URL: *https://www.sciencedirect.com/science/article/pii/S0278434301000723*

Dayton, P. K. (1985a). Ecology of kelp communities, *Annu. Rev. Ecol. Syst.* **16**(1): 215–245.

Dayton, P. K. (1985b). The structure and regulation of some South American kelp communities, *Ecological monographs* **55**(4): 447–468.

Dillehay, T. D., Ramírez, C., Pino, M., Collins, M. B., Rossen, J. and Pino-Navarro, J. (2008). Monte Verde: seaweed, food, medicine, and the peopling of South America, *science* **320**(5877): 784–786.

Duarte, C. M., Middelburg, J. J. and Caraco, N. (2005). Major role of marine vegetation on the Oceanic carbon cycle, *Biogeosciences* **2**(1): 1–8.

Erlandson, J. M., Graham, M. H., Bourque, B. J., Corbett, D., Estes, J. A. and Steneck, R. S. (2007). The kelp highway hypothesis: marine ecology, the coastal migration theory, and the peopling of the Americas, *The Journal of Island and Coastal Archaeology* **2**(2): 161–174.

Escribano, R., Fernández, M. and Aranís, A. (2003). Physical-chemical processes

and patterns of diversity of the Chilean eastern boundary pelagic and benthic marine ecosystems: an overview, *Gayana* **67**(2): 190–205.

Feng, M., Caputi, N., Chandrapavan, A., Chen, M., Hart, A. and Kangas, M. (2021). Multi-year marine cold-spells off the west coast of Australia and effects on fisheries, *Journal of Marine Systems* **214**: 103473.
URL: *https://www.sciencedirect.com/science/article/pii/S0924796320301688*

Filbee-Dexter, K. and Wernberg, T. (2018). Rise of turfs: a new battlefront for globally declining kelp forests, *Bioscience* **68**(2): 64–76.

Friedlander, A. M., Ballesteros, E., Bell, T. W., Caselle, J. E., Campagna, C., Goodell, W., Hüne, M., Muñoz, A., Salinas-de León, P. and Sala, E. (2020). Kelp forests at the end of the earth: 45 years later, *Plos one* **15**(3): e0229259.

Friedlander, A. M., Ballesteros, E., Bell, T. W., Giddens, J., Henning, B., Hüne, M., Muñoz, A., Salinas-de León, P. and Sala, E. (2018). Marine biodiversity at the end of the World: Cape Horn and Diego Ramírez Islands, *PloS one* **13**(1): e0189930.

Friedlander, A. M., Ballesteros, E., Goodell, W., Hüne, M., Muñoz, A., Salinas-de León, P., Velasco-Charpentier, C. and Sala, E. (2021). Marine communities of the newly created Kawésqar National Reserve, Chile: From glaciers to the Pacific Ocean, *PLOS ONE* **16**(4): e0249413.
URL: *https://doi.org/10.1371/journal.pone.0249413*

Graham, M. H., Vasquez, J. A. and Buschmann, A. H. (2007). Global ecology of the Giant Kelp Macrocystis: from ecotypes to ecosystems, *Oceanography and Marine Biology* **45**: 39.

Hamylton, S. and East, H. (2012). A geospatial appraisal of ecological and geo-

morphic change on Diego Garcia Atoll, Chagos Islands (british indian Ocean-territory), *Remote Sensing* **4**(11): 3444–3461.

Holbrook, N. J., Sen Gupta, A., Oliver, E. C. J., Hobday, A. J., Benthuysen, J. A., Scannell, H. A., Smale, D. A. and Wernberg, T. (2020). Keeping pace with marine heatwaves, *Nature Reviews Earth & Environment* **1**(9): 482–493. **URL:** *https://doi.org/10.1038/s43017-020-0068-4*

Jensen, J. R., Estes, J. and Tinney, L. (1980). Remote sensing techniques for kelp surveys, *Photogrammetric Eng. and Rem. Sen.* **46**(6): 743–755.

King, P. P., Stokes, P. and Fitz-Roy, R. (1836). Sketch of the surveying voyages of His Majesty's ships Adventure and Beagle, 1825-1836, *The Journal of the Royal Geographical Society of London* **6**: 311–343.

Krumhansl, K. A., Okamoto, D. K., Rassweiler, A., Novak, M., Bolton, J. J., Cavanaugh, K. C., Connell, S. D., Johnson, C. R., Konar, B., Ling, S. D., Micheli, F., Norderhaug, K. M., Pérez-Matus, A., Sousa-Pinto, I., Reed, D. C., Salomon, A. K., Shears, N. T., Wernberg, T., Anderson, R. J., Barrett, N. S., Buschmann, A. H., Carr, M. H., Caselle, J. E., Derrien-Courtel, S., Edgar, G. J., Edwards, M., Estes, J. A., Goodwin, C., Kenner, M. C., Kushner, D. J., Moy, F. E., Nunn, J., Steneck, R. S., Vásquez, J., Watson, J., Witman, J. D. and Byrnes, J. E. K. (2016). Global patterns of kelp forest change over the past half-century, *PNAS* **113**(48): 13785.

Macaya, E. C. and Zuccarello, G. C. (2010). DNA barcoding and genetic divergence in the Giant Kelp Macrocystis (Laminariales) 1, *J. of Phycology* **46**(4): 736–742.

Marin, M., Feng, M., Phillips, H. E. and Bindoff, N. L. (2021). A global, multiproduct analysis of coastal marine heatwaves: Distribution, charac-

teristics, and long-term trends, *Journal of Geophysical Research: Oceans* **126**(2): e2020JC016708.
URL: *https://agupubs.onlinelibrary.wiley.com/doi/abs/10.1029/2020JC016708*

Miller, R. J., Lafferty, K. D., Lamy, T., Kui, L., Rassweiler, A. and Reed, D. C. (2018). Giant Kelp increases faunal diversity through physical engineering, *P. Biol. sciences* **285**(1874).

Moreno, C. A. and Jara, F. (1984). Ecological studies on fish fauna associated with Macrocystis pyrifera belts in the South of fueguian Islands, Chile, *Marine ecology progress series. Oldendorf* **15**(1): 99–107.

Ojeda, F. and Santelices, B. (1984). Invertebrate communities in holdfasts of the kelp Macrocystis pyrifera from Southern Chile, *Marine ecology progress series. Oldendorf* **16**(1): 65–73.

Oliver, E. C., Donat, M. G., Burrows, M. T., Moore, P. J., Smale, D. A., Alexander, L. V., Benthuysen, J. A., Feng, M., Gupta, A. S. and Hobday, A. J. (2018). Longer and more frequent marine heatwaves over the past century, *Nature communications* **9**(1): 1–12.

Pfister, C. A., Berry, H. D. and Mumford, T. (2018). The dynamics of kelp forests in the Northeast Pacific Ocean and the relationship with environmental drivers, *J. of Ecology* **106**(4): 1520–1533.

Rozzi, R., Massardo, F., Mansilla, A., Anderson, C. B., Berghofer, A., Mansilla, M., Gallardo, M. R., Plana, J., Berghofer, U. and Arango, X. (2007). La reserva de biosfera cabo de hornos: un desafío para la conservación de la biodiversidad e implementación del desarrollo sustentable en el extremo austral de América, *Anales Del Instituto De La Patagonia* **35**(1): 55 – 70.

Santelices, B. and Ojeda, F. (1984). Population dynamics of coastal forests *Macro-*

cystis pyrifera in Puerto Toro, Isla Navarino, Southern Chile, *Marine ecology progress series. Oldendorf* **14**(2): 175–183.

Schiel, D. R. and Foster, M. S. (2015). *The biology and ecology of Giant Kelp forests*, Ebook central, University of California Press, Oakland, California.

Schlegel, R. W., Oliver, E. C., Wernberg, T. and Smit, A. J. (2017). Nearshore and offshore co-occurrence of marine heatwaves and cold-spells, *Progress in Oceanography* **151**: 189–205.

Schneider, C., Glaser, M., Kilian, R., Santana, A., Butorovic, N. and Casassa, G. (2003). Weather observations across the Southern Andes at 53°s, *Physical Geography* **24**(2): 97–119.
URL: *https://doi.org/10.2747/0272-3646.24.2.97*

Smale, D. A. (2019). Impacts of Ocean warming on kelp forest ecosystems, *New Phytologist* .

Spalding, M. D., Fox, H. E., Allen, G. R., Davidson, N., Ferdaña, Z. A., Finlayson, M., Halpern, B. S., Jorge, M. A., Lombana, A. and Lourie, S. A. (2007). Marine ecoregions of the World: a bioregionalization of coastal and shelf areas, *BioScience* **57**(7): 573–583.

Steneck, R. S., Graham, M. H., Bourque, B. J., Corbett, D., Erlandson, J. M., Estes, J. A. and Tegner, M. J. (2002). Kelp forest ecosystems: biodiversity, stability, resilience and future, *Environmental conservation* pp. 436–459.

Teagle, H., Hawkins, S. J., Moore, P. J. and Smale, D. A. (2017). The role of kelp species as biogenic habitat formers in coastal marine ecosystems, *J. of Exp. Marine Biology and Ecology* **492**(C): 81–98.

Van Tussenbroek, B. (1989a). The life-span and survival of fronds of Macrocystis

pyrifera (Laminariales, phaeophyta) in the Falkland Islands, *British Phycological Journal* **24**(2): 137–141.

Van Tussenbroek, B. (1989b). Morphological variations of Macrocystis pyrifera in the Falkland Islands in relation to environment and season, *Marine Biology* **102**(4): 545–556.

Van Tussenbroek, B. (1989c). Observations on branched Macrocystis pyrifera (l.) c. agardh (Laminariales, phaeophyta) in the Falkland Islands, *Phycologia* **28**(2): 169–180.

Van Tussenbroek, B. (1989d). Seasonal growth and composition of fronds of Macrocystis pyrifera in the Falkland Islands, *Marine Biology* **100**(3): 419–430.

Van Tussenbroek, B. (1993). Plant and frond dynamics of the Giant Kelp, Macrocystis pyrifera, forming a fringing zone in the Falkland Islands, *European Journal of Phycology* **28**(3): 161–165.

Vásquez, J. A., Zuñiga, S., Tala, F., Piaget, N., Rodríguez, D. C. and Vega, J. A. (2014). Economic valuation of kelp forests in Northern Chile: values of goods and services of the ecosystem, *Journal of Applied Phycology* **26**(2): 1081–1088.

Vila, A., Falabella, V., Gálvez, M., Farías, A., Droguett, D. and Saavedra, B. (2010). Identificación de áreas marinas y costeras de alto valor de conservación en la ecorregión de canales y fiordos australes, *Punta Arenas, Chile. WCS y WWF* **110**.

Wernberg, T. and Filbee-Dexter, K. (2019). Missing the marine forest for the trees, *Marine Ecology Progress Series* **612**: 209–215.
URL: *https://www.int-res.com/abstracts/meps/v612/p209-215/*

Wernberg, T., Krumhansl, K., Filbee-Dexter, K. and Pedersen, M. F. (2019). *Status and trends for the World's kelp forests*, Elsevier, pp. 57–78.



2 | Research approach

In this section I will introduce the rationale behind the research for the three papers of my thesis. The methodologies will be explained in detail in each paper.

2.1 Giant kelp mapping

As a canopy-forming species, giant kelp is easily detected from a vessel, and several nautical charts and maps have included some indications of their presence since at least the 19th century (Costa et al.; 2020; Pfister et al.; 2018). However, it is not an easy task to map their area and perimeter with accuracy, because of the inherent optical dynamics of the surface and water column of the ocean, and the very narrow range where kelp forests grow along the coastline (Figure 2.1).

A satellite that was not yet fully used for kelp mapping was Sentinel-2, from the European Space Agency (ESA; 2015). This sensor has some advantages over other multispectral satellites, namely its increased spatial resolution, with 10 m for RGB and NIR bands, and increased spectral resolution, with three additional bands of 20 m in the red edge area of the electromagnetic spectrum (ESA; 2015). My research was able to determine that the red edge bands are more sensitive at detecting giant kelp canopy than the NIR, which is the standard for remote sensing of land vegetation. To isolate giant kelp reflectance, I created a formula with two threshold filters, condensed into a mapping algorithm. An advantage of using reflectance indices derived from multispectral bands to detect algae is that they don't depend on other variables, allowing to determine the characteristics of the habitat independently.

To validate this method, I had two possible sources of information: 1) collecting references of giant kelp sites, and 2) mapping giant kelp myself:



Figure 2.1: Giant kelp canopy, as seen from the shore. San Isidro Lighthouse, Strait of Magellan

1. For the former, I had the great opportunity of being in contact with marine biologists from Chile, the Falkland Islands (Malvinas) and Australia. They shared their field knowledge with me, which constitutes the basis for a dataset of known sites. They also collaborated as co-authors in the first paper.

2. For mapping kelp, I was able to develop a data collection of georeferenced RGB orthomosaics using drones (DJI Phantom 4 UAV). The first field campaign was carried out in the summer of 2019 (January- March) in Southern Chile, from the Strait of Magellan (53°S, 70°W), to the Patagonian fjords of the Aysén Region (44°S, 72°W) and then up to the town of Maitencillo in Central Chile (32.6°S, 71.4°W). The second campaign was carried out in

the winter of 2019 (July- August) in the Falkland Islands (51°S, 57°W) and the Yendegaia Fjord at the south of Tierra del Fuego (54.8°S, 68.7°W). To my knowledge, this is so far the largest collection of kelp orthomosaics of South America, and they could be relied on in future research.

To determine the accuracy of this method, I applied a confusion matrix to the ground-truth orthomosaics to compare the performance of the filtered algorithm with other known vegetation indices, such as Normalised Difference Vegetation Index or NDVI (Ashley and Rea; 1975) and Floating Algae Index or FAI (Hu; 2009), using similar filtering parameters. Although the computed accuracy of my filter algorithm — KD, or Kelp Difference — was slightly higher, an advantage of NDVI and FAI is that they can be used with other multispectral sensors of larger temporal coverage, such as Landsat or SPOT.

2.2 Giant kelp exploration

Along with drone mapping, I explored giant kelp forests with the aid of SCUBA diving and an underwater drone (Chasing Gladius Mini). This part of my research did not form part of a sampling plan by itself, but it was nevertheless fundamental for understanding the environmental characteristics of the forests from an internal perspective, and the role that coastal geomorphology and ocean exposure play in defining kelp extent. The notes I was able to take were key for the development of the discussion on the abiotic factors for kelp growth in the second paper (Figure 2.2). These notes and observations were critically reviewed by kelp experts who have undertaken research of their own on sub-Antarctic kelp forests in the past; their ecological and biological knowledge helped to complement the scope of my second paper.

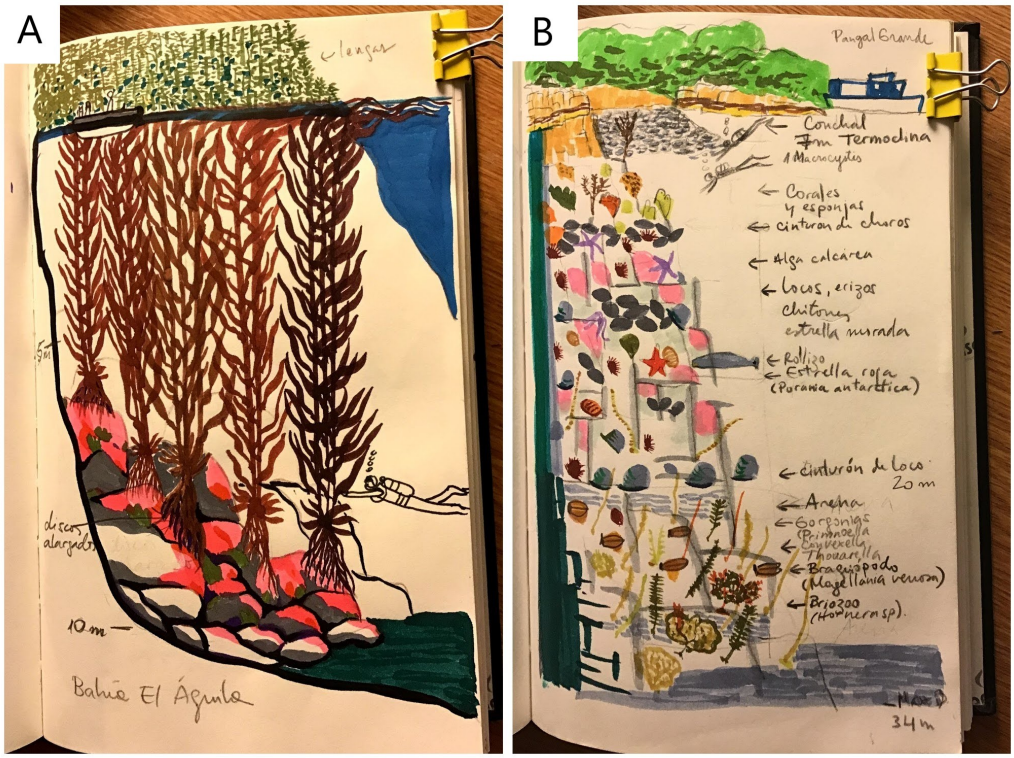


Figure 2.2: Sketches of kelp forests from the field campaign 1, in a) the Strait of Magellan and b) the Patagonian fjords.

2.3 Characterization of the abiotic habitat

For the second paper, in order to understand how the abiotic factors shape the typical size of a giant kelp forest, I selected a random sample of $\sim$ 100 kelp forests from each of the ecoregions of Channels and Fjords of Southern Chile, Falkland Islands and South Georgia. I calculated the size of each forest in hectares, and characterised them according to their ocean current, orientation, level of exposure, geoform (a visual assessment of the geomorphological setting of the coastline), latitude, longitude, and slope, to determine the role of each factor to predict forest size. I used the statistically significant variables in a conditional inference tree (Hothorn et al.; 2006), taking as a parameter the median of the size of the total

sample.

2.4 Historical cartography

I developed a work on long-term historical changes of kelp forests, which involved archival research, followed by scanning and georeferencing the multiple charts, maps, and aerial imagery collected from the archives of the United Kingdom Hydrographic Office (Beagle Kelp charts); in the nautical charts, areas with kelp were drawn as leaves on the surface. I applied the same protocol as (Costa et al.; 2020) of delineating the perimeter of the mapped kelp forests only. Satellite-detected canopy areas could change with tidal height, and therefore if a year had a limited number of images, and they were taken during high tide, kelp canopies could only be partially seen. For this reason, my criteria to assess the persistence of kelp forests was the analysis of the drawn shape of the kelp forests on the historical records versus the current satellite detection using the Kelp Difference algorithm. If the forests were similar in shape between both layers, I could determine whether kelp was persistent at the same locations (Figure 2.3).

2.5 Sea surface temperature trends

During the time of this thesis, several advancements were made in the field of measuring and understanding marine heatwaves (MHW) and marine cold spells (MCS) (Hobday et al.; 2018,0; Schlegel et al.; 2017). For the third paper, I made the most of the newly available research methods and drew on their methodologies to test their use when applying them to different marine ecosystems of the Channels and Fjords ecoregion, an area that had been identified as an area with no clear warming trends but which had not been assessed in detail. In that sense, the

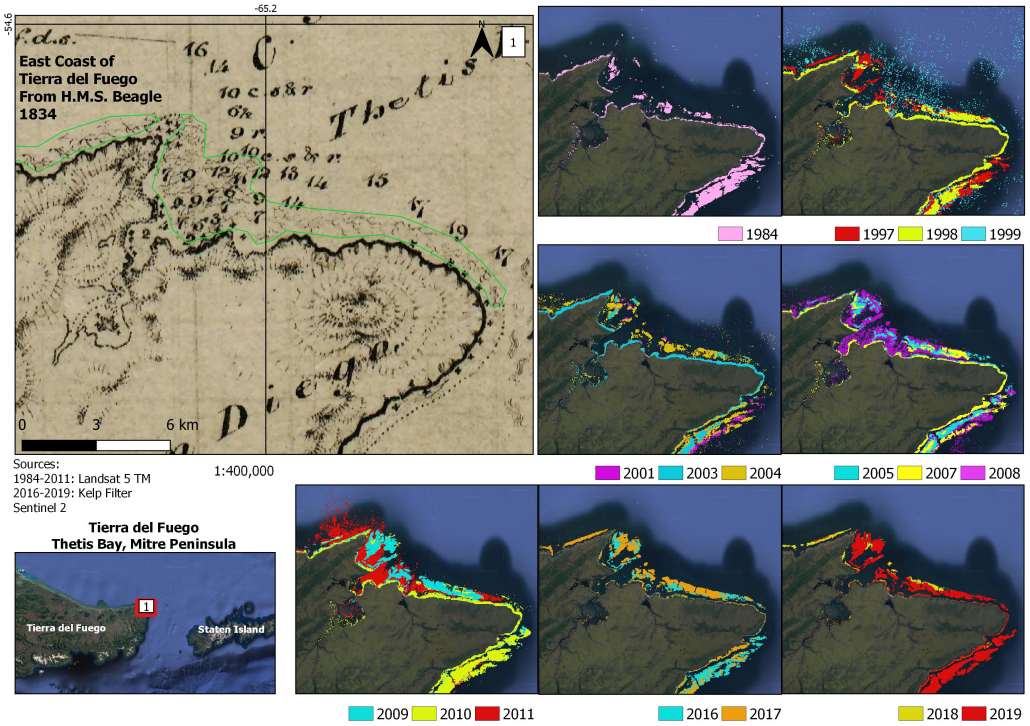


Figure 2.3: Comparing historical and present-time giant kelp records. Subsection 1: Kelp canopies were drawn as leaves near the coastline in a chart made in 1834. The following images show averaged kelp area by year using satellite detection.

third paper has a management approach, as it divides the ecoregion in landscape units called marine ecosystems *sensu* (Rovira and Herreros; 2016) and observes the number and intensity of warm and cold events over the last decades since 1981. I computed the daily mean temperature per ecosystem using as source the NOAA 1/4° daily Optimum Interpolation Sea Surface Temperature (or daily OISST) (Banzon et al.; 2014), and then calculated the levels of intensity of the MHW or MCS (moderate, strong, severe, and extreme) using the difference between the SST temperature computed over a period of at least 5 day versus the climatological mean of the time of the year (Hobday et al.; 2016,0). The number of events, classified in categories of intensity, were analysed in terms of their temporal duration, and choropleth maps helped to analyse the distribution of those

events. Additionally, warm and cold events were compared with wind anomalies for the equivalent period using the northward (V10) and eastward (U10) components of wind from the ERA5 reanalysis dataset (Hersbach et al.; 2020), to determine possible causal mechanisms. This analysis allowed the comparison of the drivers and distribution of warm and cold events, as well as their possible effects on kelp forests.

2.6 Remote sensing and GIS tools

Google Earth Engine (GEE) is an application that allows petabytes of satellite imagery collections to be processed using JavaScript programming language (Gorelick et al.; 2017). In my personal opinion, the scope and global scale of this research could not have been possible without this tool, considering the previous software technology only allowed such images to be processed one by one. An additional outcome of this research was the unprecedented possibility of presenting the results as online maps for the wider public. Nonetheless, it must be noted that the aforementioned previous software technology plus QGIS and R, were open-source tools that were pivotal for analysing and generating results on cartography and statistics. The resultant global map of kelp forests is at this map, and the repository for the additional material created for this DPhil is at this repository.

2.7 A statement for the south

The first paper of this thesis is one of the first scientific papers in history — if not the first — that presents maps orientated towards the south. This is a cultural proposal: through this map, I present the southern hemisphere as *oceanic* in itself, where the space we map and work with is easily seen as smaller land masses sur-

rounded by water. On this oceanic planet, our human presence is still limited, and the coastline offers us interesting new perspectives from which we can renew our understanding of natural history within the current context of the climate crisis.

References

Ashley, M. D. and Rea, J. (1975). Seasonal vegetation differences from ERTS imagery, *Am. Soc. of Photogrammetry* **41**(6).

Banzon, V. F., Reynolds, R. W., Stokes, D. and Xue, Y. (2014). A 1/4°-spatial-resolution daily sea surface temperature climatology based on a blended satellite and in situ analysis, *Journal of Climate* **27**(21): 8221 – 8228.

Costa, M., Le Baron, N., Tenhunen, K., Nephin, J., Willis, P., Mortimor, J. P., Dudas, S. and Rubidge, E. (2020). Historical distribution of kelp forests on the coast of British Columbia: 1858-1956, *Applied Geography* **120**: 102230.

ESA, E. S. A. (2015). Sentinel-2 user handbook, *Report*, European Space Agency, European Union.

Gorelick, N., Hancher, M., Dixon, M., Ilyushchenko, S., Thau, D. and Moore, R. (2017). Google Earth Engine: Planetary-scale geospatial analysis for everyone, *Rem. Sens. of Env.* **202**: 18–27.

Hersbach, H., Bell, B., Berrisford, P., Hirahara, S., Horányi, A., Muñoz-Sabater, J., Nicolas, J., Peubey, C., Radu, R., Schepers, D. et al. (2020). The era5 global reanalysis, *Quarterly Journal of the Royal Meteorological Society* **146**(730): 1999–2049.

Hobday, A. J., Alexander, L. V., Perkins, S. E., Smale, D. A., Straub, S. C., Oliver, E. C., Benthuysen, J. A., Burrows, M. T., Donat, M. G. and Feng, M. (2016). A

hierarchical approach to defining marine heatwaves, *Progress in Oceanography* **141**: 227–238.

Hobday, A. J., Oliver, E. C., Gupta, A. S., Benthuysen, J. A., Burrows, M. T., Donat, M. G., Holbrook, N. J., Moore, P. J., Thomsen, M. S. and Wernberg, T. (2018). Categorizing and naming marine heatwaves, *Oceanography* **31**(2): 162–173.

Hothorn, T., Hornik, K. and Zeileis, A. (2006). Unbiased recursive partitioning: A conditional inference framework, *Journal of Computational and Graphical statistics* **15**(3): 651–674.

Hu, C. (2009). A novel Ocean color index to detect floating algae in the global Oceans, *Rem. Sens. of Env.* **113**(10): 2118–2129.

Pfister, C. A., Berry, H. D. and Mumford, T. (2018). The dynamics of kelp forests in the Northeast Pacific Ocean and the relationship with environmental drivers, *J. of Ecology* **106**(4): 1520–1533.

Rovira, J. and Herreros, J. (2016). Clasificación de ecosistemas marinos Chilenos de la zona económica exclusiva, *Departamento de Planificación y Políticas en Biodiversidad. División de Recursos Naturales y Biodiversidad. Ministerio del Medio Ambiente* .

Schlegel, R. W., Oliver, E. C., Wernberg, T. and Smit, A. J. (2017). Nearshore and offshore co-occurrence of marine heatwaves and cold-spells, *Progress in Oceanography* **151**: 189–205.



3 | Chapter 3: Paper 1

3.1 Linking statement

Remote Sensing 2020, 12(4), 694; https://doi.org/10.3390/rs12040694

This paper addresses the first aim of my thesis: **"To detect the extension of the giant kelp forest in the Magellanic province, from Chiloé Island to Cape Horn."** In this paper we produced a high-resolution global map of giant kelp forests derived from Sentinel-2 satellite imagery. To develop this map, I classified the spectral signature of giant kelp and other coastal classes to identify their typical signatures. Then, analysing the values of reflectance per band, I isolated giant kelp from other classes, except for green algae (*Ulvophyceae*), which had a very similar signature, but is usually located in intertidal areas, whereas giant kelp is found in intertidal to subtidal areas. To validate this filter algorithm, I mapped giant kelp forests from central to southern Chile and Falkland Islands (Malvinas) with a UAV (drone) and compared the performance of this filter algorithm with Normalised Difference Vegetation Index (NDVI) and Floating Algae Index (FAI). I obtained an Overall Accuracy > 0.88 for the three indices with canopies greater than 1 hectare. Additionally, I produced a dataset of georeferenced sites with giant kelp from previous surveys, and 66% of them were in the vicinity of satellite-detected kelp in a range of 300 m. As the results were so promising, I expanded this algorithm to the global distribution of this ecosystem, computing the coverage of giant kelp and intertidal green algae per ecoregion. This work was also presented as an interactive online map, which can be seen and explored at this link.

3.1.1 Author contribution statement

A. M.-S. and M. M.-F. conceptualised the research and methodology. The collection of data, formal analysis, the administration of the project, the creation of the remote sensing code and the original draft preparation were developed by A.M.-S. The validation of kelp forests on the field was contributed by M.P., A.M.-S., E.C.M., A.P.-M., N.G., M. Young, P.H. and I.G.; M.P., P.H., I.G., N.G. and A. M-S. provided funding and resources for fieldwork; M.T. helped with data curation of the first version of the global kelp map; the draft was reviewed and edited by A.M.-S., M.P., E.C.M., A.P.-M., N.G., M.Y., M. Yaqub, P.H., I.G. and M.M.-F. ; the online map was edited by A.M.-S. and M. Yaqub. This project was supervised by M.M.-F.

This chapter was submitted for publication on the 6th December 2019, accepted on the 18th February 2020 and published in Remote Sensing on the 20th February 2020.

3.2 A high-resolution global map of Giant Kelp (*Macrocystis pyrifera*) forests and intertidal green algae (*Ulvophyceae*) with Sentinel-2 imagery

Alejandra Mora-Soto [1*], Mauricio Palacios [2, 3, 4, 5], Erasmo C. Macaya [3, 5, 7], Iván Gómez [2, 5], Pirjo Huovinen [2, 5], Alejandro Pérez-Matus [8], Mary Young [9], Neil Golding [10], Martin Toro [11], Mohammad Yaqub [12] and Marc Macias-Fauria [1]

[1] Biogeosciences Group, School of Geography and the Environment, University of Oxford, Oxford OX1 3QY, U.K.

[2] Instituto de Ciencias Marinas y Limnológicas, Facultad de Ciencias, Universidad Austral de Chile, Valdivia, Chile.

[3] Facultad de Ciencias, Universidad de Magallanes, Punta Arenas, Chile.

[4] Programa de Doctorado en Biología Marina, Universidad Austral de Chile, Valdivia, Chile.

[5] Centro FONDAP de Investigación en Dinámica de Ecosistemas Marinos de Altas Latitudes (IDEAL), Valdivia, Chile.

[6] Laboratorio de Estudios Algales (ALGALAB), Departamento de Oceanografía, Universidad de Concepción, Casilla 160-C, Concepción, Chile.

[7] Millenium Nucleus Ecology and Sustainable Management of Oceanic Islands (ESMOI), Coquimbo, Chile.

[8] Subtidal Ecology Laboratory, Departamento de Ecología, Estación Costera de Investigaciones Marinas, Pontificia Universidad Católica de Chile, Casilla 114-D, Santiago, Chile.

[9] Centre for Integrative Ecology, Life and Environmental Sciences, Deakin University, Princes Hwy, Warrnambool, 3280, Australia.

[10] South Atlantic Environmental Research Institute (SAERI), Stanley, Falkland Islands.

[11] Instituto de Geografía, Pontificia Universidad Católica de Chile. Macul, Santiago.

[12] IT Services, University of Oxford, Oxford OX2 6NN, U.K.

* Correspondence: alejandra.morasoto@ouce.ox.ac.uk.

Received: 6 December 2019 / Revised: 13 February 2020 / Accepted: 18 February 2020 / Published: 20 February 2020

3.2.1 Abstract

Giant kelp (*Macrocystis pyrifera*) is the most widely distributed kelp species on the planet, but detailed information of its distribution is entirely missing in some marine ecoregions, especially in the high latitudes of the Southern Hemisphere. Here we present an algorithm based on a series of filter thresholds to detect giant kelp and intertidal green algae (*Ulvophyceae*) employing Sentinel-2 imagery. The kelp filter algorithm was applied separately to vegetation indices FAI, NDVI, and a novel formula (Kelp Difference, KD). Training data from previously surveyed kelp forests and other coastal and ocean features were used to identify reflectance threshold values. This procedure was validated with independent field data collected with UAV imagery at high spatial resolution and point-georeferenced sites at low spatial resolution. At comparing UAV with Sentinel data (high-resolution validation), an average overall accuracy ≥ 0.88 and Cohen's kappa ≥ 0.64 coefficients were found in all three indices for canopies reaching the surface with

extensions greater than 1 hectare, with KD showing the highest average kappa score (0.66). Measurements between previously surveyed georeferenced points and remotely-sensed kelp grid cells (low-resolution validation) showed that 66% of georeferenced points had grid cells indicating kelp presence within a linear distance of 300 m. We employed KD in our kelp filter algorithm to estimate the global extent of giant kelp and intertidal green algae per marine ecoregion and province, producing in a high-resolution global map of giant kelp and intertidal green algae, powered by Google Earth Engine.

3.2.2 Keywords

Giant kelp, *Macrocystis pyrifera*, Google Earth Engine, UAV, Sentinel-2, *Ulvophyceae*.

3.2.3 Introduction

Kelp forests provide a variety of ecosystem services: they protect and modify the substrate and surrounding water column and act as habitat for several species, increasing the complexity of coastal trophic networks (Miller et al.; 2018; Teagle et al.; 2017). Although the term 'kelp'is used to refer to all large brown algae (Fraser; 2012), the focus of this study is the commonly called giant kelp *Macrocystis pyrifera* (Laminariales, Phaeophyceae), Earth's most widespread kelp species, which forms one of the most productive and diverse ecosystems on the planet (Mann; 1973; Reed et al.; 2008; Smale; 2019). *M. pyrifera* forests (giant kelp hereafter) can be found in the temperate and subpolar coastlines of South America, Western North America, South Africa, Australia, New Zealand, as well as the South Atlantic and the majority of the sub-Antarctic islands (Dayton; 1985; Graham; 2004; Graham et al.; 2007). Despite the importance of kelp forests as a global biome, kelp monitoring has mostly been implemented locally and gener-

ally without temporal replication, which obscures the dynamics in many marine regions (Krumhansl et al.; 2016). Mapping kelp's global distribution and biomass dynamics is thus a necessary first step to understand its contemporary distribution and identify possible threats in a context of global change (Schiel and Foster; 2015). This information can contribute to the sustainable development agenda of the UN by 2030, specifically goal 14: "Conserve and sustainably use the oceans, seas and marine resources for sustainable development" (Division for Sustainable Development Goals; 2016).

Canopies (fronds) of giant kelp reach the surface of the ocean and can be easily seen from aerial platforms at low latitudes (Cavanaugh et al.; 2010). However, observation using satellite imagery makes it difficult to establish a clear distinction between kelp canopies and open ocean water, because of elements like sun glint, breaking waves, sediments, dissolved organic matter or phytoplankton blooms that also contribute to water reflectance (Cavanaugh et al.; 2011). Sensors used for kelp mapping have included aerial photogrammetry (Pfister et al.; 2018; Schiel and Foster; 2015), Landsat Multispectral Scanner System (MSS) (Jensen et al.; 1980), Landsat Thematic Mapper (TM) (Cavanaugh et al.; 2010,0), Landsat Operational Land Imager (OLI) (Nijland et al.; 2019), Sentinel-2 (Huovinen et al.; 2019), Satellite Pour l'Observation de la Terre (SPOT) (Augenstein et al.; 1991; Deysher; 1993) and aircraft multispectral sensors with spatial resolutions $\sim 2m$ (Nijland et al.; 2019). Methodologies employed to detect kelp canopies using such imagery have been varied: from using brightness values ratios per band to indices like Normalized Difference Vegetation Index (NDVI; (Ashley and Rea; 1975)) to methods like unsupervised classification (Augenstein et al.; 1991; Deysher; 1993), supervised maximum likelihood classification (Jensen et al.; 1980; Nijland et al.; 2019; Stekoll et al.; 2006), Principal Component Analysis (PCA; (Cavanaugh et al.; 2010)), Spectral Mixture Analysis (SMA; (Adams et al.; 1986)), (Huovi-

nen et al.; 2019), and particularly Multiple Endmember Spectral Mixture Analysis (MESMA; (Roberts et al.; 1998)), (Cavanaugh et al.; 2011) which has been effective in studying different characteristics of kelp ecology, such as genetic differentiation within geographic clusters (Johansson et al.; 2015), long-term biomass trends (Bell et al.; 2018), fish, invertebrate and algae assemblages in kelp communities (Lamy et al.; 2018), biogeochemical (Koweek et al.; 2017) and physical (Cavanaugh et al.; 2011) dynamics.

The above - mentioned methods have been applied at local to regional scales, e.g. in the Santa Barbara Channel (Southern California) or the Francisco Coloane Marine Park, Cape Horn archipelago and Diego Ramirez islands in southern Chile (Friedlander et al.; 2018). These studies were not scaled up to the global distribution for the operative costs of human hours required for pre-processing and classifying images, as well as providing pure endmember data, especially along extensive coastlines (but see (Rosenthal et al.; 2018)). Previous research using citizen science data found that at least 4 different people were required to identify and classify the same grid cell as kelp in order to make an optimal supervised classification (Rosenthal et al.; 2018). In a similar way, Machine Learning methods such as Random Forest or Classification and Regression Trees (CART) (Breiman; 2001) require categorical variables to split grid cell values in a series of thresholds in a tree-like structure, predicting a categorical label for each cell (Mishra and Datta-Gupta; 2017). In these classification algorithms, data classes define the size of the tree. That is, with limited training data, kelp fraction cover (ground-truthing) is logistically challenging to obtain in remote locations or in the absence of high-resolution imagery, many classes might result in the model underestimating the predicted error. On the contrary, a small tree might not be able to classify new values (Borsuk; 2008). Classification algorithms have thus proven effective but, due to their statistical data-adaptive nature, they are more reliable

in local areas and less scalable to broader spatial scales, unless a large, spatially comprehensive (global) collection of training data (Traganos, Aggarwal, Poursanidis, Topouzelis, Chrysoulakis and Reinartz; 2018) – not currently existing for this ecosystem – is available. For these reasons, there are still large areas where giant kelp forests remain undetected, and the lack of a baseline distribution map hampers the detection of their temporal trends. In the last global assessment of kelp forest change, only 34 of the 99 marine ecoregions with kelp were surveyed, and of these, only nine had giant kelp data records longer than 5 years; none of them were from Sub-Antarctic ecoregions (Krumhansl et al.; 2016).

Key recent developments show the potential to revolutionise the remote detection of the global distribution of giant kelp. These are:

a) New sensors onboard the recently launched European Space Agency's (ESA) Sentinel satellites offer an alternative to Landsat in the remote detection of giant kelp forests. Although individual kelp blades can show different photo-acclimation responses to variable conditions of light, the concentration of pigments chlorophylls a and c and fucoxanthin (Fuc) give the plants a conspicuous brownish colour, with a higher concentration with increasing depth (Colombo Pallotta et al.; n.d.). These characteristics result in the highest spectral reflectance of kelp canopies being in the Near-Infrared (780 - 890 nm) (Augenstein et al.; 1991), the lowest being in the blue (400 - 500 nm) and red (675 nm) areas (Colombo Pallotta et al.; n.d.), with reflectance increasing strongly in the red-edge area (Jensen et al.; 1980). The sensors onboard Sentinel-2, with three additional red-edge bands of 20 m of spatial resolution, can strongly contribute to highlight this spectral area with a level of detail that other multispectral sensors – such those in Landsat of 30 m of spatial resolution – do not possess.

b) Cloud-based platforms such as Google Earth Engine (GEE, (Gorelick et al.;

2017)) enable access to petabytes of open-access satellite imagery paired with an interactive development environment. Previous research in GEE in similar environments includes the analysis of the capabilities of Landsat imagery to detect kelp forests in British Columbia (Nijland et al.; 2019) and the use of Sentinel-2 imagery to estimate satellite-derived bathymetry (Traganos, Poursanidis, Aggarwal, Chrysoulakis and Reinartz; 2018) and to map seagrass (Traganos, Aggarwal, Poursanidis, Topouzelis, Chrysoulakis and Reinartz; 2018). Using GEE helps in processing large amounts of data to detect spatially persistent areas of giant kelp forests, taking into consideration that persistent kelp areas tend to occur at the centres of the forests, whereas borders are more variable (Young et al.; 2016). This persistence has been associated with abiotic factors like water depth, presence of a rocky substrate, substrate topology, and connectivity between the forests (Young et al.; 2016). In contrast, variability is associated with ocean dynamics like wave height and sea-surface temperature (Cavanaugh et al.; 2011), more than seasonality), tidal ranges or zenith angles (Huovinen et al.; 2019). Therefore, the central areas of forests should provide optimal material to build a global map of giant kelp.

c) The use of Unmanned Aerial Vehicles (UAV) for coastal habitat mapping is a simple, cost-effective and reliable technology (Turner et al.; 2016) that has been successfully used to map and validate intertidal biogenic reefs (Collin et al.; 2019), saltmarsh biomass (Doughty and Cavanaugh; 2019) and algal blooms (Kislik et al.; 2018). Recent surveys to detect macroalgae in temperate coastlines have shown that RGB and multispectral cameras mounted on UAVs produce accurate imagery able to detect water turbidity and a range of taxonomical groups of algae in surface or shallow water, with the exception of spectrally similar species (Huovinen et al.; 2019; Tait et al.; 2019). To our knowledge, there are yet no standardized protocols for marine or coastal mapping with UAVs (Kislik et al.;

2018).

The present study capitalises on these advances to produce an algorithm based on a series of filters to detect giant kelp forests at different latitudes and coastal contexts, to generate a global map of their distribution. We analysed the multi-band reflectance values of a set of classes or Regions of Interest (ROI) and defined a threshold-based approach that sequentially refined the kelp reflectance signal. This filtering algorithm was tested with three different spectral indices: the widely used Normalised Difference Vegetation Index (NDVI (Ashley and Rea; 1975), an index used in remote sensing to detect vegetation based on the differential reflectance of vegetation between wavelengths within the photosynthetically active radiation and the near infrared); the Floating Algae Index (FAI (Hu; 2009), an index specifically designed to detect floating algae) and the Kelp Difference (KD) we introduce in this paper. Spectral signatures were extracted from Sentinel 2 L1C imagery; masking thresholds were globally applied in Google Earth Engine employing an average image composition from 2015 to 2019. Forests detected with this algorithm were validated at high-resolution with UAV-obtained orthomosaics. Our methodology successfully isolates giant kelp from the surrounding ocean and land except for green algae (*Ulvophyceae*). *Ulvophyceae* is a conspicuous class of algae found in intertidal environments such as estuaries or rocky areas (Baweja and Sahoo; 2015) that has a similar spectral reflectance to giant kelp (Tait et al.; 2019) and can share the same habitat only when giant kelp forests occur on shallow rocky intertidal areas (Huovinen et al.; 2019). Hence, in those geographical contexts, our map cannot distinguish between giant kelp and *Ulvophyceae*. As a result, a global map of kelp forests and intertidal algae is presented. The code is available in GEE, and the resulting map can be accessed online.

3.2.4 Materials and Methods

3.2.4.1 Training data

We used Sentinel-2 Level 1C (Copernicus Service information) imagery provided by Google Earth Engine (GEE). Sentinel-2 L1C consists of ortho and radiometrically corrected images showing Top of Atmosphere (TOA) reflectance originally scaled by 10000 (Sentinel, 2013) and rescaled by 10^{-4} for this study. Training areas consisted of previously studied kelp forest regions located at different latitudes and oceans, identified with their respective coordinates. An average 0.01°x 0.01°image was produced for each selected area employing the tool developed by (Simonetti et al.; 2015) to remove areas affected by cloud cover. This involved scanning the complete Sentinel-2 L1C dataset (23rd June 2015 to 31st July 2018) with cloud cover < 90%. The number of images processed thus varied for each site (Table 1). The final composite image represents 3 years of cloud - free grid cells. It emphasizes the temporal continuity of grid cell reflectance and includes all the possible zenith angles in this lapse of time. For each image, the following ROIs or classes were selected based on the literature and field experience: *Giant Kelp*, defined as giant kelp canopy; *Coast*, defined as grid cells laying between 0 and 1 m of elevation – such as rocks, beaches, human artefacts (e.g. docks, vessels) and any other elements close to the coastline and not permanently covered by water; *Ocean*, defined as areas of open ocean surface; *Foam*, defined as grid cells in an extensive (10 km) surf zone; *Organic water*, defined as highly productive waters; *River grass* in an estuarial area; *Green algae*, i.e. intertidal green algae (*Ulvophyceae*); and *Land vegetation* that can be found between 0 and 1 m above sea level and could be misinterpreted as kelp grid cells. We sampled 90 points per ROI, totalling a training data set of 720 observations (Table 3.1).

For each ROI, the multispectral reflectance of their respective grid cells was ex-

Table 3.1: Sites selected as training data in this study

Class (ROI)	Site	Long, Lat	Images processed	Reference
Kelp, Coast, Ocean	S. Australia – Warrnambool	142.46, -38.4	163	(Macaya and Zuccarello; 2010)
	S. Africa – Oudekraal	18.35, -33.98	310	(Macaya and Zuccarello; 2010)
	UK - Falkland Islands (Malvinas)	-57.75, -51.61	73	(Macaya and Zuccarello; 2010)
	W. Canada – Nuchatlitz Islands	-126.53, 49.6	258	(Macaya and Zuccarello; 2010)
	USA – Carmel Bay	-121.93, 36.55	76	(Macaya and Zuccarello; 2010)
	C. Chile – Punta Parra	-72.97, -36.66	171	(Macaya; 2018)
	S. Chile – Grevy Island (Cape Horn)	-67.61, -55.52	93	(Friedlander et al.; 2018)
	France – Kerguelen Islands	69.68, -49.20	98	(Belsher and Mouchot; 1992)
	UK – South Georgia	-36.71, -54.11	129	(Wells et al.; 2011)
Foam	S. Chile – Queule	-73.21, -39.35	77	This study
River Grass	S. Chile – Queule	-73.21, -39.35	77	This study
Land vegetation	S. Chile – Queule	-73.21, -39.35	77	This study
Green algae (Ulvophyceae)	S. Chile – Puyuhuapi Channel	-72.76, -44.71	78	This study
	S. Argentina - Puerto Deseado	-65.86, -47.85	147	
Organic water	USA – Santa Barbara Channel	-119.95, 34.03	282	This study
	S. Chile – Puyuhuapi Channel	-72.71, -44.73	78	
	New Zealand – Kaimaumau	173.31, -34.96	136	

tracted from the averaged image using R (packages: raster, rgeos, sp, maptools, dplyr), and mean and standard deviation were calculated per class for all Sentinel-2 Bands (Figure 3.1).

3.2.4.2 Kelp filter algorithm

A 3-step process was followed to optimise giant kelp identification from the multispectral reflectance values of the ROIs:

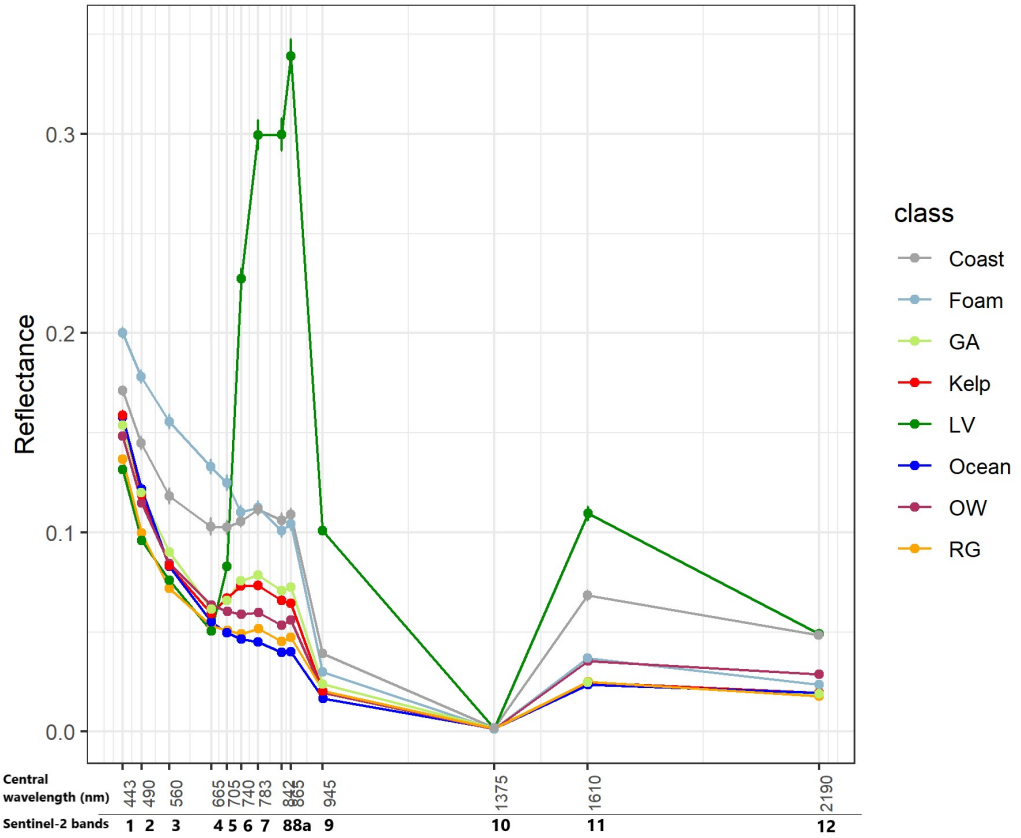


Figure 3.1: Mean ± SD reflectance values for each Region of Interest (ROI) used as training data in this study, computed for all Sentinel-2 bands (central wavelength of each band (in nm) and band number indicated in the x axis). Classes or ROIs: Coast; Foam; GA= Green Algae; Kelp; LV= Land vegetation; Ocean; OW= Organic water; RG: River grass.

- **Band-based threshold**. The multispectral profiles of Land Vegetation, Coast, and Foam are clearly distinctive (Figure 3.1). One hundred percent of all Coast and Land Vegetation observations in the training data were larger or equal than B11 = 0.0286, which corresponds to the minimum value of Coast ROI at B11 (1610 nm at central wavelength, Figure 3.2). Consequently, all observations with value B11 > 0.028 were masked out, which resulted in 305 training data grid cells remaining. This eliminated 21 observations in the upper quartile of the original kelp sample (Figure 3.2). This was done

to avoid misclassification with coastal features at the expense of identifying some kelp-occupied grid cells with higher-than average reflectance values in band B11. These were found to be marginal portions of the identified kelp forest ROIs – i.e. grid cells occupying the periphery of kelp stands.

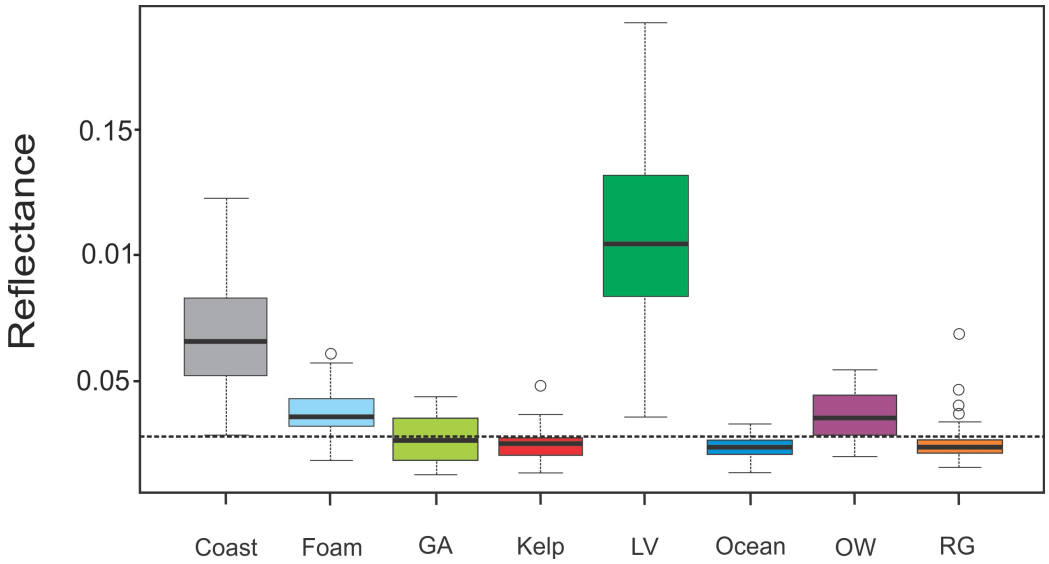


Figure 3.2: Box and whisker plot of B11 reflectance values (90 grid cells per class). All grid cells with B11 $\geq$ 0.028 (indicated with a dashed line) were masked out to separate Coast and Land Vegetation from the other ROIs. Classes or ROIs: Coast; Foam; GA= Green Algae; Kelp; LV= Land vegetation; Ocean; OW= Organic water; RG: River grass.

- **Kelp Difference (KD)**. Giant kelp grid cells exhibited a conspicuous large difference in reflectance between bands in the red edge area of the spectrum (Bands 5, 6 and 7) and the red band (B4). Selecting B6 (central wavelength = 740 nm) as the band with the largest difference with B4 (Figure 1), we defined a Kelp Difference (KD) as the difference between both band values. Step 2 was applied after the band-based masking (Step 1), although the order of these two steps would not alter the result:

$$KD = R_{B6} - R_{B4}$$

- **KD-based threshold**. A second masking threshold was applied to the KD-converted training dataset. This enabled 100% of the grid cells not belonging to Giant Kelp or Green Algae to be removed (Table 3.2 and Supplementary Material). The reflectance values for Giant Kelp and Green Algae were found too similar to be efficiently discriminated. In order to compare the performance of the KD in relation to other indices used to remotely detect algae in the past, we separately implemented this step employing NDVI and FAI. This resulted in the production of three different kelp maps.

Table 3.2: Masking out threshold by index.

Index	Masking threshold	Defined by
NDVI	>-0.003411	*River grass* max value
FAI	>0.005352	*Organic water* max value
KD	>0.003216	*River grass* max value

3.2.4.3 Validation at high spatial resolution

Independent data of giant kelp forests were collected along the Chilean coastline and the Falkland Islands (Malvinas) covering a latitudinal distance of 2,470 km. This distance accounts for the wide range of environments where giant kelp occurs in different climates – from warm temperate (Csb, Cfb and Cfc) to tundra (ET) according to the Köppen-Geiger climate classification (Kottek et al.; 2006) – and from the Pacific to the Atlantic oceans (Table 3.3, Figure 3.3). The ground-truthing process was conducted during the austral summer and winter of 2019, between 24th January and 18th February in the Strait of Magellan, 21st February to 9th March in the Patagonian Channels and Fjords, 15th March in Niebla, 24th March in Maitencillo, 11th July in the Tussac Islands, and 21st July in Yendegaia. For each site, a mapping mission flew a DJI-Phantom 4 unmanned aerial vehicle (UAV) with an RGB camera mounted on it (FOV 84°8.8 mm/24 mm (35 mm format equivalent) f/2.8-f/11 auto focus at 1 m-∞). The overlap of the im-

ages was 80%, and the height was between 70 to 100 m depending on coastal topography. The time of the day for the flights was between 10 am - 4 pm. The aerial images were processed using either the application DroneDeploy or Agisoft Metashape (in the case of the Falkland Islands). Because of bad weather conditions during the fieldwork campaign in the Strait of Magellan, the kelp forests of Buque Quemado, San Gregorio and Chabunco were only partially mapped. In each ground-truth orthomosaic (10 cm spatial resolution), kelp forests – defined as the presence of clearly visible canopies in the RGB high-resolution image – were visually identified and delineated in the form of polygon shapefiles. They were then converted into a binary raster format: kelp and no-kelp, at 10 m of spatial resolution. Ground-truthed layers were compared with the filtered kelp grid cells calculated separately for NDVI, FAI and KD over the same extents at 10 m of spatial resolution, averaged over the 3 months prior to the survey and converted to binary values of kelp and no-kelp using the values in Table 2 as thresholds.

Ground-truth images were compared with filtered NDVI, FAI and KD with Confusion Matrix in ENVI 4.7 to obtain their Producer's, User's and Overall Accuracy plus the Cohen's kappa (Cohen; 1960) statistics.

3.2.4.4 Kelp filter algorithm in Google Earth Engine

The kelp detection product with the best overall accuracy and kappa coefficient was applied over the temperate coastlines of the planet using GEE through the following steps:

- **a)** cloud-free tool of (Simonetti et al., 2015) over Sentinel-2 grid cells scaled at 10-4 from 26th June 2015 to 23rd June 2019;
- **b)** kelp filter threshold;
- **c)** masking of all grid cells with elevation above sea level > 0 m using two

Table 3.3: Summary of validation sites, their coordinates, extent of the kelp stand (ha), and climate zone. Climate acronyms Csb, Warm temperate climate with dry and warm summer. Cfb, Warm temperate climate, fully humid and warm summer. Cfc, Warm temperate climate, fully humid and cold summer. ET, Polar tundra (Koweek et al., 2017)

Main area	**Site**	**Long, Lat**	**Area (ha)**	**Köppen-Geiger climate classification**
C. Chile	Maitencillo	-71.44199, -32.64762	0.5	Csb
S. C. Chile	Niebla	-73.40054, -39.87498	2.1	Cfb
Channels and Fjords	Lobera María Isabel	-73.42381, -44.90923	0.3	Cfb
Channels and Fjords	San Andrés 1 and 2	-73.32865, -44.9348	0.3 1	Cfb
Channels and Fjords	Puerto Amparo	-73.28257, -44.89874	0.3	Cfb
Strait of Magellan	San Isidro	-70.97483, -53.78515	5.0	Cfc
Strait of Magellan	Santa Ana Sur	-70.92467, -53.63006	0.4	Cfc
Strait of Magellan	Santa Ana Norte	-70.91918, -53.62731	1.1	Cfc
Strait of Magellan	Punta Carrera	-70.93902, -53.55859	5.2	Cfc
Strait of Magellan	Chabunco	-70.81101, -52.98648	1.4	Cfc
Strait of Magellan	San Gregorio	-70.07255, -52.57044	0.8	Cfc
Strait of Magellan	Buque Quemado	-69.47702, -52.33489	1.2	Cfc
Beagle Channel	Yendegaia	-68.70262, -54.9045	1.5	ET
Falkland Islands (Malvinas)	Tussac Islands: Kelly Rocks, Bottom, Top	-57.74472, -51.67233	11.5 16.3 11.8	ET

digital elevation models: Advanced Land Observing Satellite (ALOS) and Shuttle Radar Topography Mission (SRTM), both at 30 m of spatial resolution. This last procedure was done to avoid any misclassification of elements on land with similar reflectance to giant kelp that were not included

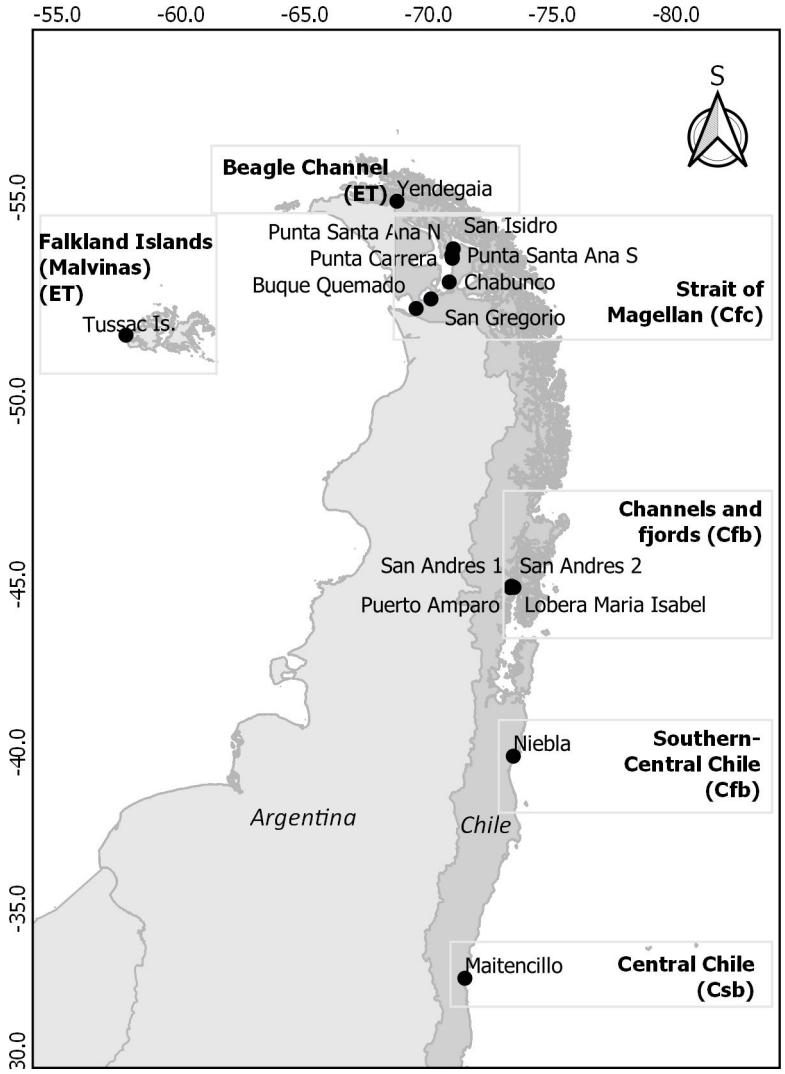


Figure 3.3: Map of the surveyed sites for validation at high-resolution of giant kelp forests. Cartographic projection EPSG3857. Maps in this article are South-oriented to highlight the connectivity of kelp forests at Sub-Antarctic latitudes.

in our ROI training data set. To improve the readability of the index, digital numbers were rescaled to values from 0 to 255 in the maps.

The ALOS digital elevation model fills the void grid cells of other digital elevation models and thus has higher accuracy than SRTM (more information in (Tadono et al.; 2016)). ALOS in GEE does not cover the following archipelagos:

Chatham, Prince Edward, Tristan da Cunha, Gough Island and the extreme NW of South Georgia. In these cases, SRTM was used. No digital elevation models were available for the Diego Ramirez archipelago. In this case, a polygon shapefile of the coastline was used as a mask. As Sentinel-2 imagery does not cover some of the Southern Ocean islands (Amsterdam and Saint-Paul, Bouvet, Antipodes and Bounty Islands), those areas had to be excluded from the map. The code for the GEE algorithm in JavaScript is available in Supplementary Material.

3.2.4.5 Validation at low spatial resolution

To validate the global map, we measured the linear distance between kelp grid cells and previously surveyed or observed giant kelp forests. To this end, we employed a dataset of 157 locations in South and North America, New Zealand, Southern Australia and Tasmania, South Georgia and Sub-Antarctic islands, recorded in a multipoint layer in Google Earth (Figure 3.4 and Supplementary Material). As these stands were identified at different times and degrees of accuracy, the linear distance in breaks of 50, 100, 200 and 300 m was measured from each point to the closest mapped kelp grid cell. A workflow of this methodology is shown in Supplementary Material. The detected grid cells were summarized by marine ecoregion and province following the classification of Spalding et al. (2007).

3.2.5 Results

3.2.5.1 Kelp filter algorithm

Using the original training data of 90 grid cells per ROI (720 grid cells in total), the applied protocol preserved a fraction of Giant kelp grid cells, which were concentrated at the centre of the observed kelp canopies – and thus represented the purest grid cells or at least the grid cells most dominated by kelp canopy, and



Figure 3.4: Location of the training data (black dots) and the low-resolution validation sites (red dots). Cartographic projection EPSG: 54042. Maps in this article are South-oriented to highlight the connectivity of kelp forests at Sub-Antarctic latitudes.

Green algae grid cells on rocky intertidal areas (Table 3.4). Excluded Giant kelp grid cells were located at the peripheries of identified Giant kelp stands, where they were more likely to display mixed reflectances with Ocean, Foam, Organic water, or River grass in some areas. Zero grid cells belonging to any of the other ROIs remained after the application of the kelp filter algorithm. The use of the KD in the algorithm preserved the highest quantity of Giant kelp grid cells in the training area, followed by FAI and NDVI. As our algorithm cannot distinguish between Giant kelp (*M. pyrifera*) and Green algae (*Ulvophyceae*), our resulting map shows M. pyrifera and rocky intertidal Ulvophyceae cover.

Table 3.4: Remaining grid cells out of 90 Giant kelp and 90 Green algae original observations (total = 180) after the application of the kelp filter algorithm to the training data.

Index	**No. of observations Total**	**No. of observations kelp**	**No. of observations Green Algae**
NDVI	102	50	52
FAI	103	50	53
KD	114	61	53

3.2.5.2 Validation at high resolution

The ground-truthing process is illustrated in Figure 3.5, where filtered grid cells are overlain on an UAV orthomosaic that is used as ground-truthed imagery (see Supplementary Material for the complete collection of UAV imagery). Maps obtained employing KD, FAI and NDVI show higher values at the centre of the giant kelp canopy, with decreasing values towards their periphery. Levels of sensitivity are different with each index, with NDVI showing more saturation and homogeneous values over the canopy.

Confusion matrix results (Table 3.5) show similar levels of accuracy for all forests > 1 ha, with an overall accuracy (OA) $\geq$ 78% and a kappa coefficient $\geq$ 0.52 for the three indices, and with a slightly better overall kappa coefficient for maps obtained using KD (mean = 0.66) over FAI and NDVI (means of 0.65 and 0.64 respectively). Smaller kelp forests (Maitencillo, Lobera María Isabel, San Andrés 1 and 2, Santa Ana Sur) showed only sparse grid cells over the ground-truthed areas, and their levels of accuracy were much lower. The forest of Puerto Amparo, which is composed of mostly underwater canopy, was only detected as sparse grid cells over the area. Finally, the forests of San Gregorio and Buque Quemado, located in areas of high tidal range (9 m) were undetected in the averaged image.

Regarding Producer's and User's accuracy metrics, the three maps show percent-

ages of accuracy > 51% for all the sites > 1 ha, with averages $\geq$ 64% for PA and $\geq$ 81% for UA (Table 3.5). In agreement with the conservative approach used in our kelp filter algorithm (i.e. our algorithm aimed at minimising false detections), Producer's accuracy (an indicator of omission error or underestimation of the canopy extent) is slightly lower than User's accuracy (that indicates commission errors or the overestimation of the canopy on the water surface). The map with the least underestimation was obtained using KD (73.1% Producer's Accuracy) and the map with the least overestimation was obtained using FAI (82.8% User's Accuracy). KD showed the highest average and the most balanced (lowest standard deviation) combination of accuracy metrics.

Table 3.5: Confusion matrix results for maps obtained using the kelp filter algorithm employing FAI, NDVI and KD in forests larger than 1 hectare. PA = Producer's Accuracy (%). UA = User's Accuracy (%). OA = Overall Accuracy (%). Overall Accuracies > 80 and Kappa coefficients > 0.6 are highlighted in bold.

	FAI				**NDVI**				**KD**			
	PA	**UA**	**OA**	**Kappa**	**PA**	**UA**	**OA**	**Kappa**	**PA**	**UA**	**OA**	**Kappa**
Punta Santa Ana Norte	59.3	84.3	92.3	0.65	61.2	80	91.9	0.65	62.5	75	91.3	0.63
San Isidro	69.2	76.7	92.9	0.69	71	74.4	92.7	0.68	75.1	67.4	91.6	0.66
Chabunco	69.2	76.8	92.7	0.69	72	73.9	92.5	0.69	82.7	64.5	91.2	0.67
Punta Carrera	76	94.6	91.9	0.79	78.7	93.7	92.4	0.8	84.2	92.9	93.7	0.84
Niebla	62.6	79.7	80.9	0.56	66.5	77	80.9	0.57	67.9	69.8	78	0.52
Tussac Kelly	66.2	89.5	86.2	0.67	61	90.9	85	0.63	72.8	87.4	87.5	0.71
Tussac Bottom	60.8	88.4	89.4	0.66	57.6	88.4	88.8	0.63	71.4	85.5	90.8	0.72
Tussac Top	69.1	74.6	80.8	0.57	60.8	76.4	79.6	0.53	77.6	73.6	82.3	0.62
Yendegaia	56.1	80.8	89.3	0.6	51.2	82.1	88.8	0.57	63.2	71.2	88.4	0.6
Total average	65.4	82.8	88.5	0.65	64.4	81.9	88.1	0.64	73.1	76.4	88.3	0.66

3.2.5.3 Validation at low resolution

We computed the global map employing the KD, since it produced the best validation statistics. For a total of 157 georeferenced sites, 59 (37.6 %) were found to be within a range of 100 m, 103 (65.6 %) within a range of 300 m, and 54 sites (34.4 %) more than 300 m away of a reported kelp stand (Table 3.6). The ecoregions with the lowest detection ($\leq$ 50 %) were Humboldtian, Western Bassian, Bounty-Antipodes and Central New Zealand, whereas all other ecoregions had $\geq$ 66 % of detection. Considering that this is a global map at a grid cell resolution of 10 m, our results indicate a moderate to strong ability of this filtering algorithm to detect areas with kelp within a range of 300 m, with more success at higher latitudes and larger kelp forest areas. Tables 3.7 and 3.8 provide a summary of the detected area of giant kelp and intertidal green algae per marine ecoregion and province.

Table 3.6: Remaining grid cells out of 90 Giant kelp and 90 Green algae original observations (total = 180) after the application of the kelp filter algorithm to the training data.

Range (m)	**N**	**%**	**cumulative %**
50	42	26.8	26.8
100	17	10.8	37.6
200	27	17.2	54.8
300	17	10.8	65.6
>300, undetected	54	34.4	100
Total	157	100	

3.2.6 Discussion

3.2.6.1 Kelp detection and mapping

Our methodology simplifies the giant kelp detection process by refining the parameters to detect canopies. Although it is recommendable to use KD, this method

can be done using well-known and widely used indices such as NDVI and FAI, which can be applied to databases with longer records than Sentinel-2, such as Landsat, in averaged or non-averaged imagery. However, this algorithm has limitations: 7 out of 17 high-resolution and 54 out of 157 low-resolution validation sites used in this research were not detected. At high-resolution, the best results occurred when detecting kelp forests $\geq$ 1 hectare with Sentinel-2 imagery at 10 m spatial resolution. This represents a large improvement in relation to the Landsat 30 m resolution: in the Santa Barbara Channel where (Cavanaugh et al.; 2014) found a mean patch size of 0.28 km^2 (28 ha), a much larger value than the largest observed forest in the Falklands training data in this study (Bottom Island, 16.3 ha). A similar minimal mapping unit of 1 hectare was recommended for the Global Mangrove Watch initiative, made with a fusion of multispectral (Landsat) and ALOS imagery classified with the Extremely Randomized Trees algorithm. In this case, more than 50,000 training points were used (Bunting et al.; 2018; Gandhi and Jones; 2019). As would be expected due to limited training data, applying our training data to classification algorithms like CART or Random Forests yielded poor results and hence were not included in the main results of this study, although they can be examined in the supplementary material). The sources of River grass, Green algae and Organic water observations in our training dataset were limited to specific areas because of our local knowledge and sources of secondary data. The training dataset volume used in this study is in line with previous remote sensing studies that have been carried with similar training numbers, e.g. 17 sampling sites (Chen et al.; 2005) and five sampling classes (Karnieli; 1997), both with high levels of accuracy when tested with independent field data. Like ours, these studies avoided the use of machine-learning algorithms, since they work well with large amounts of training data but show lower performance otherwise, and proposed instead working with combinations of reflectance bands as

an optimal way to detect targeted ROIs. Further research is required to establish which method is best as ground data availability increases, as well as to detect other coastal and marine ecosystems (e.g. subtidal kelp forests).

The low-resolution validation represents a very demanding test for the kelp filter algorithm, and its results need to be placed in perspective. First of all, the spatial precision of the validation data points is variable, and hence observed accuracies between the mapped distribution and the published kelp canopies of < 300 m are notable. Second, the array of low-resolution stands includes observations made over a period of 15 years, with the oldest ones dating from 2004, and 75% made before the start of the satellite observation period used in the current study. Third, the metadata in the low-resolution calibration test does not contain information on the size of the reported kelp stands, which can be smaller than 1 ha and thus not detectable with this method. Lastly, our 4-yr averaged map does not detect seasonality in the canopy extent and shows only permanent grid cells over the same area. Highly variable canopies may thus be undetected. The finding that 65.6% of the reported low-resolution sites fall within 300 m of KD-detected stands – which are based on spatial resolutions of 20 m (B6) and 10 m (B4) – needs to be interpreted under this light.

3.2.6.2 Spatial and biophysical patterns

Maps produced with the kelp filter algorithm show larger values in the centre of the forests and lower values at their peripheries in the validation sites, as reported for the kelp forests characterized by Young et al. (2016) and Cavanaugh et al. (2010). This may indicate mixed spectral signatures on the edges of the kelp stands due to lower frond density, as it was observed in fieldwork and with our high-resolution UAV images. Edge effects in kelp forests have an important impact on ecological processes (e.g., herbivory) as well as on mechanical action

effects (e.g., turbulence) outside and inside the forest (Dayton; 1985).

Previous research has identified low average NDVI values in kelp canopy forests (< 0.30, Cavanaugh et al. (2010)) and Nijland et al. (2019) used a threshold of NDVI > 0.05 in two or more scenes to detect kelp. Both results agree with the values found in our study sites. Considering the similarities of the maps created using FAI, KD and NDVI, it can be hypothesized that KD and FAI are related to biomass in a similar way than NDVI, although more data are needed to test if the use of this algorithm would help to detect this biophysical variable. Previous research completed in the Santa Barbara Channel found correlations between giant kelp estimates of canopy biomass computed using Landsat imagery and adult plant density (R^2 = 0.85, P < 0.001; (Cavanaugh et al.; 2013)) and total forest biomass (R^2= 0.73, P < 0.001; (Cavanaugh et al.; 2010)), and between kelp fraction index and canopy biomass (R^2= 0.64, P < 0.001; (Cavanaugh et al.; 2011)), with total biomass values that ranged from 4.14 x 106 to 4.74 x 108 kg in 25 years (mostly affected by large winter storms) for a study area c. 1500 km in length (Bell, Cavanaugh, Reed and Siegel; 2015). The positive results obtained with Landsat hold promise for the use of Sentinel-2 imagery in a similar fashion in the near future.

On the other hand, the phenotypic plasticity of giant kelp implies that it can adopt different shapes and sizes in the ecomorphs 'pyrifera', 'integrifolia', 'angustifolia', and 'laevis', named after their differences in holdfasts and blade texture (Graham et al.; 2007; Macaya and Zuccarello; 2010; Schiel and Foster; 2015). Although our global map seems to detect canopies in their complete distribution, the low number of detected sites in the Humboldtian ecoregion where the ecomorph 'integrifolia' occurs (Graham et al.; 2007) requires more sampling sites to test our detection thresholds.

3.2.6.3 False negatives

An important characteristic of giant kelp plants is that they form canopies on the surface, but this is not a mandatory rule. In fact, the plants of Buque Quemado in the Atlantic side of the Strait of Magellan are subjected to tidal ranges > 9 m, and at high water tend not to be visible in Sentinel-2 imagery, while at low tide the plants are completely exposed (Figures 3.6 A, B). In British Columbia, a 2 m increase in tide decreased the detected kelp extent by 40% (Nijland et al.; 2019), an effect that may also be reflected in our results (e.g., the intertidal forest of Niebla). However, tidal ranges < 4 m have shown not to affect or to produce large biases in the estimates of kelp forest extent, as observed by Cavanaugh et al. (2010,0) in the Santa Barbara Channel forests. Coastlines with tidal ranges > 9 m where giant kelp might be present are restricted to the south-eastern coast of South America and western North America (British Columbia and Alaska) (Masselink and Hughes; 2014), and hence those areas could be underestimated in our global kelp map.

Forests with few plants reaching the surface were not successfully detected, as was the case with Puerto Amparo in the Channels and Fjords area. In our in-situ observation, the plants looked stressed and not reproductive under the water (Figures 3.6 C, D). There are other areas in the world where the canopy never reaches the surface, such as around the Channel Islands in Southern California (Edwards; 2004). A similar case was found in our study site of Maitencillo in central Chile, which could be explained by summer temperatures reaching sub-lethal levels with monthly SST between 17°- 18°C (OBPG, NASA) before our survey. According to Buschmann et al. (2014), mortality of macroscopic sporophytes of giant kelp increases with temperatures > 15-17°C, following previously observed patterns of seasonality (Graham et al.; 2007). The low number of detected sites in the

Humboldtian and Western Bassian ecoregion may be explained by kelp harvesting (Vásquez; 2008) or climate-driven shifts (Wernberg et al.; 2016). Finally, San Andrés 1 and Lobera María Isabel were small patches almost completely undetected by the spatial resolution of the Sentinel sensor.

3.2.6.4 False positives

The presence of kelp canopies > 25 m^2 can be detected in a grid cell with 20 m spatial resolution (Augenstein et al.; 1991), but the elements that fall into that instantaneous field of vision may cause commission errors. In this research, reflectance thresholds, combination of values of key reflectance bands, and topography filters were used to isolate giant kelp grid cells, and our training data were focused on the presence of giant kelp, which is the only canopy-forming kelp species in South America, and *Ulvophyceae*, which is a conspicuous class of algae in rocky intertidal areas. This procedure did not mask out intertidal areas because giant kelp can also grow in these environments (Graham et al.; 2007), therefore *Ulvophyceae* can be considered as part of the positive error of this research, but restricted to rocky intertidal areas only. Due to lack of georeferenced data to generate ROIs for our calibration dataset, we did not include the intertidal-subtidal *Durvillaea antarctica*, a southern member of order Fucales that can sometimes reach the surface, or *Nereocystis luetkeana* of North America, which also forms canopies (Pfister et al.; 2018). The same applied to the presence of floating (detached) specimens of *D. antarctica* and giant kelp. Floating kelp can reach > 1000 kg km^2 in the Patagonian Fjords (Hinojosa et al.; 2011); these kelp rafts are not uniform, and temporal variation occurs (Hinojosa et al.; 2010). Hence it was assumed that their ephemeral occurrence was not detected in our 4-year composite images. The use of other sensors (most notably hyperspectral (Bell, Cavanaugh and Siegel; 2015)) may help to separate actual giant kelp from reflectances of other algae, or alterna-

tively more ROIs in Sentinel-2 can help to confirm the capacity of this method to effectively detect intertidal algae.

3.2.6.5 Notes on UAV surveying

Our high-resolution validation confirmed that RGB cameras mounted on UAVs can be successfully used for giant kelp (Huovinen et al.; 2019). The length of canopy blades floating on water (min length of an individual blade= 13.85 cm, M. Palacios personal communication) makes fronds and canopies easily detectable with spatial resolutions of 10 cm. Integrating UAV orthomosaics and GEE-processed images in either a GEE or a GIS environment is a smooth process that can be easily used for ground-truthing satellite imagery of land or coastal classes. Some technical challenges observed in the field were that RGB cameras can be easily blinded by solar reflection on water. The use of a polarizing filter on the camera lens to cut solar flaring could be explored to avoid this problem. We also advise to include a fraction of land on the surveyed area to facilitate the ground-control of the orthomosaic.

3.2.6.6 Additional considerations about the global map

The global KD map was created using satellite imagery composited over four years. This represents the first complete high-resolution map of giant kelp, the distribution of which is particularly unknown in many areas of the Southern Hemisphere. Our method offers the opportunity to implement a dynamic monitoring system using validated areas as reference and can be used to detect other intertidal kelp areas in other marine ecoregions. The global map was developed using a Sentinel-2 dataset and does not consider differences in tidal heights. It may have errors caused by the elevation mask, since ALOS DSM and SRTM are not accurate at very fine scales (< 30 m of spatial resolution) between land and sea.

Further analyses will be done with a land mask of finer resolution when this becomes available. The tool created by Simonetti et al. (2015) to clean up the effect of clouds was found to be a good option for making an averaged map of permanent cloud-free grid cells. However, permanent clouds could have covered some kelp forests for the whole period in some extreme environments.

3.2.7 Conclusions

The results of this research show that the use of the kelp filter algorithm presented here provides a simple, reliable and inexpensive way of detecting and monitoring giant kelp forests covering areas larger than one hectare and in regions with tidal fluctuations < 4 m at different temporal and spatial scales. The method can be applied to indices NDVI and FAI, but it works best when applied to the KD. This system does not discriminate between giant kelp and green intertidal algae, but it discriminates between those signatures and other land and water grid ROIs. The filter algorithm was successfully validated with UAV imagery. Additionally, the platform provided by GEE provides pre-processed images and constantly updated datasets, and the code is open for application by any user. This methodology provides a repeatable and robust process to assess the distribution and abundance of giant kelp forests, allowing this tool to contribute to wider temporal monitoring of giant kelp communities. This dynamic approach would have the potential to address questions linked to their connectivity in their widespread extension in the world's ocean (Dayton; 1985) and to kelp's global changes in distribution and abundance.

- *Funding:* The fieldwork of this research was funded by CONICYT (scholarship 296776-21171029 awarded to M. Palacios), Centro de Investigación de Ecosistemas Marinos de Altas Latitudes (FONDAP – IDEAL grant 15150003 from CONICYT), Centro de Investigación de Ecosistemas de la Patago-

nia (CIEP), South Atlantic Environmental Research Institute (SAERI), the School of Geography and the Environment - University of Oxford, St Peter's College (Graduate Awards) and Santander Academic Travel Awards. This research is part of A.M-S's PhD funded by CONICYT- Becas Chile. Drone imagery collection from the Falklands Islands was undertaken by Neil Golding at SAERI, as part of the Darwin DPLUS065 Coastal Habitat Mapping project, grant aided by the Darwin Initiative through UK Government funding.

- *Acknowledgments:* We gratefully acknowledge the contribution to this publication made by the Falkland Islands IMS-GIS data centre. Thanks to Giovanni Daneri and Madeleine Hamamé (CIEP), Federico Betti (U. Genoa), Mathias Hüne and Fernando Luchsinger (Fundación Ictiológica), Pamela Fernández (i-Mar), Austin Capsey (UKHO) and Tom Hart (U. Oxford) for providing kelp data and commenting on the results. Thanks to IDEAL, CIEP, Américo Montiel (UMAG), Celestino Ancamil (Puerto Cisnes), Miguel Herrera (Maitencillo), SAERI and Shallow Marine Surveys Group (Falkland Is.) for their logistic help. The constructive suggestions from three anonymous reviewers and the editors helped to improve the final manuscript. We are grateful to the colleagues that commented on the manuscript on earlier versions: Daniela Manuschevich (UAHC) and José Luis Iriarte (UACh). Finally, thanks to Noel Gorelick, Nicholas Clinton and David Carmichael of GEE for their classes and assistance.

- *Conflicts of Interest:* The authors declare no conflict of interest. The funders had no role in the design of the study; in the collection, analysis, or interpretation of data; in the writing of the manuscript, or in the decision to publish the results.

References

Adams, J. B., Smith, M. O. and Johnson, P. E. (1986). Spectral mixture modeling: A new analysis of rock and soil types at the Viking Lander 1 site, *Journal of Geophysical Research: Solid Earth* **91**(B8): 8098–8112.

Ashley, M. D. and Rea, J. (1975). Seasonal vegetation differences from ERTS imagery, *Am. Soc. of Photogrammetry* **41**(6).

Augenstein, E. W., Stow, D. and Hope, A. (1991). Evaluation of SPOT HRV-XS data for kelp resource inventories, *Photogrammetric Eng. and Rem. Sen.* .

Baweja, P. and Sahoo, D. (2015). *Classification of Algae*, Springer, pp. 31–55.

Bell, T. W., Allen, J. G., Cavanaugh, K. C. and Siegel, D. (2018). Three decades of variability in California's Giant Kelp forests from the Landsat satellites, *Rem. Sens. of Env.* p. 110811.

Bell, T. W., Cavanaugh, K. C., Reed, D. C. and Siegel, D. A. (2015). Geographical variability in the controls of Giant Kelp biomass dynamics, *J. of Biogeography* **42**(10): 2010–2021.

Bell, T. W., Cavanaugh, K. C. and Siegel, D. (2015). Remote monitoring of Giant Kelp biomass and physiological condition: An evaluation of the potential for the hyperspectral infrared imager (HyspIRI) mission, *Rem. Sens. of Env.* **167**: 218–228.

Belsher, T. and Mouchot, M.-C. (1992). Evaluation, par télédétection satellitaire, des stocks de Macrocystis pyrifera dans le golfe du Morbihan (archipel de Kerguelen), *Oceanologica acta* **15**(3): 297–307.

Borsuk, M. (2008). *Statistical Prediction*, pp. 3362–3373.

Breiman, L. (2001). Random forests, *Machine learning* **45**(1): 5–32.

Bunting, P., Rosenqvist, A., Lucas, R., Rebelo, L.-M., Hilarides, L., Thomas, N., Hardy, A., Itoh, T., Shimada, M. and Finlayson, C. (2018). The global mangrove watch: a new 2010 global baseline of mangrove extent, *Remote Sensing* **10**(10): 1669.

Buschmann, A. H., Pereda, S. V., Varela, D. A., Rodríguez-Maulén, J., López, A., González-Carvajal, L., Schilling, M., Henríquez-Tejo, E. A. and Hernández-González, M. C. (2014). Ecophysiological plasticity of annual populations of Giant Kelp (Macrocystis pyrifera) in a seasonally variable coastal environment in the Northern Patagonian Inner Seas of Southern Chile, *J. of Applied Phycology* **26**(2): 837–847.

Cavanaugh, K. C., Kendall, B. E., Siegel, D. A., Reed, D. C., Alberto, F. and Assis, J. (2013). Synchrony in dynamics of Giant Kelp forests is driven by both local recruitment and regional environmental controls, *Ecology* **94**(2): 499–509.

Cavanaugh, K. C., Siegel, D. A., Kinlan, B. P. and Reed, D. C. (2010). Scaling Giant Kelp field measurements to regional scales using satellite observations, *Mar. Ecology Progress Series* **403**: 13–27.

Cavanaugh, K. C., Siegel, D. A., Raimondi, P. T. and Alberto, F. (2014). Patch definition in metapopulation analysis: a graph theory approach to solve the mega-patch problem, *Ecology* **95**(2): 316–328.

Cavanaugh, K. C., Siegel, D. A., Reed, D. C. and Dennison, P. (2011). Environmental controls of giant-kelp biomass in the Santa Barbara Channel, California, *Mar. Ecology Progress Series* **429**: 1–17.

Chen, J., Zhang, M. Y., Wang, L., Shimazaki, H. and Tamura, M. (2005). A new

index for mapping lichen-dominated biological soil crusts in desert areas, *Rem. Sens. of Env.* **96**(2): 165–175.

Cohen, J. (1960). A coefficient of agreement for nominal scales, *Educ. Psych. Measurement* **20**(1): 37–46.

Collin, A., Dubois, S., James, D. and Houet, T. (2019). Improving intertidal reef mapping using UAV surface, Red Edge, and Near-Infrared data, *Drones* **3**(3): 67.

Colombo Pallotta, M. F., García Mendoza, E. and Ladah, L. B. (n.d.). Photosynthetic performance, light absorption, and pigment composition of Macrocystis pyrifera (l.

Dayton, P. K. (1985). Ecology of kelp communities, *Annu. Rev. Ecol. Syst.* **16**(1): 215–245.

Deysher, L. (1993). Evaluation of remote sensing techniques for monitoring Giant Kelp populations., *Hydrobiologia* **261**: 307–312.

Division for Sustainable Development Goals, U. N. (2016). Transforming our World: The 2030 agenda for sustainable development.
URL: *https://sustainabledevelopment.un.org/post2015/transformingourWorld*

Doughty, C. L. and Cavanaugh, K. C. (2019). Mapping coastal wetland biomass from high resolution unmanned aerial vehicle (UAV) imagery, *Remote Sensing* **11**(5): 540.

Edwards, M. S. (2004). Estimating scale-dependency in disturbance impacts: El niños and Giant Kelp forests in the Northeast Pacific, *Oecologia* **138**(3): 436–447.

Fraser, C. (2012). Is bull-kelp kelp? The role of common names in science, *New Zealand Journal of Marine Freshwater Research* **46**(2): 279–284.

Friedlander, A. M., Ballesteros, E., Bell, T. W., Giddens, J., Henning, B., Hüne, M., Muñoz, A., Salinas-de León, P. and Sala, E. (2018). Marine biodiversity at the end of the World: Cape Horn and Diego Ramírez Islands, *PloS one* **13**(1): e0189930.

Gandhi, S. and Jones, T. G. (2019). Identifying mangrove deforestation hotspots in South Asia, Southeast Asia and Asia-Pacific, *Remote Sensing* **11**(6): 728.

Gorelick, N., Hancher, M., Dixon, M., Ilyushchenko, S., Thau, D. and Moore, R. (2017). Google Earth Engine: Planetary-scale geospatial analysis for everyone, *Rem. Sens. of Env.* **202**: 18–27.

Graham, M. H. (2004). Effects of local deforestation on the diversity and structure of Southern California Giant Kelp forest food webs, *Ecosystems* **7**(4): 341–357.

Graham, M. H., Vasquez, J. A. and Buschmann, A. H. (2007). Global ecology of the Giant Kelp Macrocystis: from ecotypes to ecosystems, *Oceanography and Marine Biology* **45**: 39.

Hinojosa, I. A., Pizarro, M., Ramos, M. and Thiel, M. (2010). Spatial and temporal distribution of floating kelp in the channels and fjords of Southern Chile, *Estuarine, Coastal and Shelf Science* **87**(3): 367–377.

Hinojosa, I. A., Rivadeneira, M. M. and Thiel, M. (2011). Temporal and spatial distribution of floating objects in coastal waters of central–Southern Chile and Patagonian fjords, *Cont. Shelf Research* **31**(3-4): 172–186.

Hu, C. (2009). A novel Ocean color index to detect floating algae in the global Oceans, *Rem. Sens. of Env.* **113**(10): 2118–2129.

Huovinen, P., Ramírez, J., Palacios, M. and Gómez, I. (2019). Satellite-derived mapping of kelp distribution and water optics in the glacier impacted Yendegaia fjord (Beagle channel, Southern Chilean Patagonia), *Science of The Total Environment* p. 135531.

Jensen, J. R., Estes, J. and Tinney, L. (1980). Remote sensing techniques for kelp surveys, *Photogrammetric Eng. and Rem. Sen.* **46**(6): 743–755.

Johansson, M. L., Alberto, F., Reed, D. C., Raimondi, P. T., Coelho, N. C., Young, M. A., Drake, P. T., Edwards, C. A., Cavanaugh, K. and Assis, J. (2015). Seascape drivers of Macrocystis pyrifera population genetic structure in the Northeast Pacific, *Molecular ecology* **24**(19): 4866–4885.

Karnieli, A. (1997). Development and implementation of spectral crust index over dune sands, *Int. J. of Rem. Sen.* **18**(6): 1207–1220.

Kislik, C., Dronova, I. and Kelly, M. (2018). Uavs in support of algal bloom research: a review of current applications and future opportunities, *Drones* **2**(4): 35.

Kottek, M., Grieser, J., Beck, C., Rudolf, B. and Rubel, F. (2006). World map of the köppen-geiger climate classification updated, *Meteorologische Zeitschrift* **15**(3): 259–263.

Koweek, D. A., Nickols, K. J., Leary, P. R., Litvin, S. Y., Bell, T. W., Luthin, T., Lummis, S., Mucciarone, D. A. and Dunbar, R. B. (2017). A year in the life of a central California kelp forest: physical and biological insights into biogeochemical variability, *Biogeosciences* **14**(1): 31–44.

Krumhansl, K. A., Okamoto, D. K., Rassweiler, A., Novak, M., Bolton, J. J., Cavanaugh, K. C., Connell, S. D., Johnson, C. R., Konar, B., Ling, S. D., Micheli, F., Norderhaug, K. M., Pérez-Matus, A., Sousa-Pinto, I., Reed, D. C., Salomon,

A. K., Shears, N. T., Wernberg, T., Anderson, R. J., Barrett, N. S., Buschmann, A. H., Carr, M. H., Caselle, J. E., Derrien-Courtel, S., Edgar, G. J., Edwards, M., Estes, J. A., Goodwin, C., Kenner, M. C., Kushner, D. J., Moy, F. E., Nunn, J., Steneck, R. S., Vásquez, J., Watson, J., Witman, J. D. and Byrnes, J. E. K. (2016). Global patterns of kelp forest change over the past half-century, *PNAS* **113**(48): 13785.

Lamy, T., Reed, D. C., Rassweiler, A., Siegel, D. A., Kui, L., Bell, T. W., Simons, R. D. and Miller, R. (2018). Scale-specific drivers of kelp forest communities, *Oecologia* **186**(1): 217–233.

Macaya, E. (2018). Personal communication.

Macaya, E. C. and Zuccarello, G. C. (2010). DNA barcoding and genetic divergence in the Giant Kelp Macrocystis (Laminariales) 1, *J. of Phycology* **46**(4): 736–742.

Mann, K. H. (1973). Seaweeds: Their productivity and strategy for growth: The role of large marine algae in coastal productivity is far more important than has been suspected, *Science* **182**(4116): 975.

Masselink, G. and Hughes, M. G. (2014). *An introduction to coastal processes and geomorphology*, Routledge.

Miller, R. J., Lafferty, K. D., Lamy, T., Kui, L., Rassweiler, A. and Reed, D. C. (2018). Giant Kelp increases faunal diversity through physical engineering, *P. Biol. sciences* **285**(1874).

Mishra, S. and Datta-Gupta, A. (2017). *Applied Statistical Modeling and Data Analytics: A Practical Guide for the Petroleum Geosciences*, Elsevier.

Nijland, W., Reshitnyk, L. and Rubidge, E. (2019). Satellite remote sensing of

canopy-forming kelp on a complex coastline: A novel procedure using the Landsat image archive, *Rem. Sens. of Env.* **220**: 41–50.

Pfister, C. A., Berry, H. D. and Mumford, T. (2018). The dynamics of kelp forests in the Northeast Pacific Ocean and the relationship with environmental drivers, *J. of Ecology* **106**(4): 1520–1533.

Reed, D. C., Rassweiler, A. and Arkema, K. K. (2008). Biomass rather than growth rate determines variation in net primary production by Giant Kelp., *Ecology* **89**(9): 2493–2505.

Roberts, D. A., Gardner, M., Church, R., Ustin, S., Scheer, G. and Green, R. O. (1998). Mapping chaparral in the Santa Monica Mountains using multiple endmember spectral mixture models, *Rem. Sens. of Env.* **65**(3): 267–279.

Rosenthal, I. S., Byrnes, J. E., Cavanaugh, K. C., Bell, T. W., Harder, B., Haupt, A. J., Rassweiler, A. T., Pérez-Matus, A., Assis, J. and Swanson, A. (2018). Floating Forests: Quantitative validation of citizen science data generated from consensus classifications, *arXiv* .

Schiel, D. R. and Foster, M. S. (2015). *The biology and ecology of Giant Kelp forests*, Ebook central, University of California Press, Oakland, California.

Simonetti, D., Simonetti, E., Szantoi, Z., Lupi, A. and Eva, H. (2015). First results from the phenology-based synthesis classifier using Landsat 8 imagery, *IEEE Geosc. Rem. Sens. letters* **12**(7): 1496–1500.

Smale, D. A. (2019). Impacts of Ocean warming on kelp forest ecosystems, *New Phytologist* .

Spalding, M. D., Fox, H. E., Allen, G. R., Davidson, N., Ferdaña, Z. A., Finlayson, M., Halpern, B. S., Jorge, M. A., Lombana, A. and Lourie, S. A. (2007). Ma-

rine ecoregions of the World: a bioregionalization of coastal and shelf areas, *BioScience* **57**(7): 573–583.

Stekoll, M., Deysher, L. and Hess, M. (2006). A remote sensing approach to estimating harvestable kelp biomass, *Eighteenth International Seaweed Symposium*, Springer, pp. 97–108.

Tadono, T., Nagai, H., Ishida, H., Oda, F., Naito, S., Minakawa, K. and Iwamoto, H. (2016). Generation of the 30 m-mesh global digital surface model by ALOS prism, *Int. Archives of the Photogrammetry, Rem. Sens. and Spatial Inf. Sciences* **41**.

Tait, L., Bind, J., Charan-Dixon, H., Hawes, I., Pirker, J. and Schiel, D. (2019). Unmanned aerial vehicles (uavs) for monitoring macroalgal biodiversity: Comparison of rgb and multispectral imaging sensors for biodiversity assessments, *Remote Sensing* **11**(19): 2332.

Teagle, H., Hawkins, S. J., Moore, P. J. and Smale, D. A. (2017). The role of kelp species as biogenic habitat formers in coastal marine ecosystems, *J. of Exp. Marine Biology and Ecology* **492**(C): 81–98.

Traganos, D., Aggarwal, B., Poursanidis, D., Topouzelis, K., Chrysoulakis, N. and Reinartz, P. (2018). Towards global-scale seagrass mapping and monitoring using Sentinel-2 on google earth engine: The case study of the aegean and ionian seas, *Remote Sensing* **10**(8): 1227.

Traganos, D., Poursanidis, D., Aggarwal, B., Chrysoulakis, N. and Reinartz, P. (2018). Estimating satellite-derived bathymetry (sdb) with the google earth engine and Sentinel-2, *Remote Sensing* **10**(6): 859.

Turner, I. L., Harley, M. D. and Drummond, C. D. (2016). Uavs for coastal surveying, *Coastal Engineering* **114**: 19–24.

Vásquez, J. A. (2008). Production, use and fate of Chilean brown seaweeds: resources for a sustainable fishery, *Nineteenth Int. Seaweed Symposium*, Springer, pp. 7–17.

Wells, E., Brewin, P. and Brickle, P. (2011). Intertidal and subtidal benthic seaweed diversity of South Georgia, *Report*, South Georgia Heritage Trust, Joint Nature Conservation Committee Survey, Scotland.

Wernberg, T., Bennett, S., Babcock, R. C., De Bettignies, T., Cure, K., Depczynski, M., Dufois, F., Fromont, J., Fulton, C. J. and Hovey, R. K. (2016). Climate-driven regime shift of a temperate marine ecosystem, *Science* **353**(6295): 169–172.

Young, M., Cavanaugh, K., Bell, T., Raimondi, P., Edwards, C. A., Drake, P. T., Erikson, L. and Storlazzi, C. (2016). Environmental controls on spatial patterns in the long - term persistence of Giant Kelp in central California, *Ecological Monographs* **86**(1): 45–60.

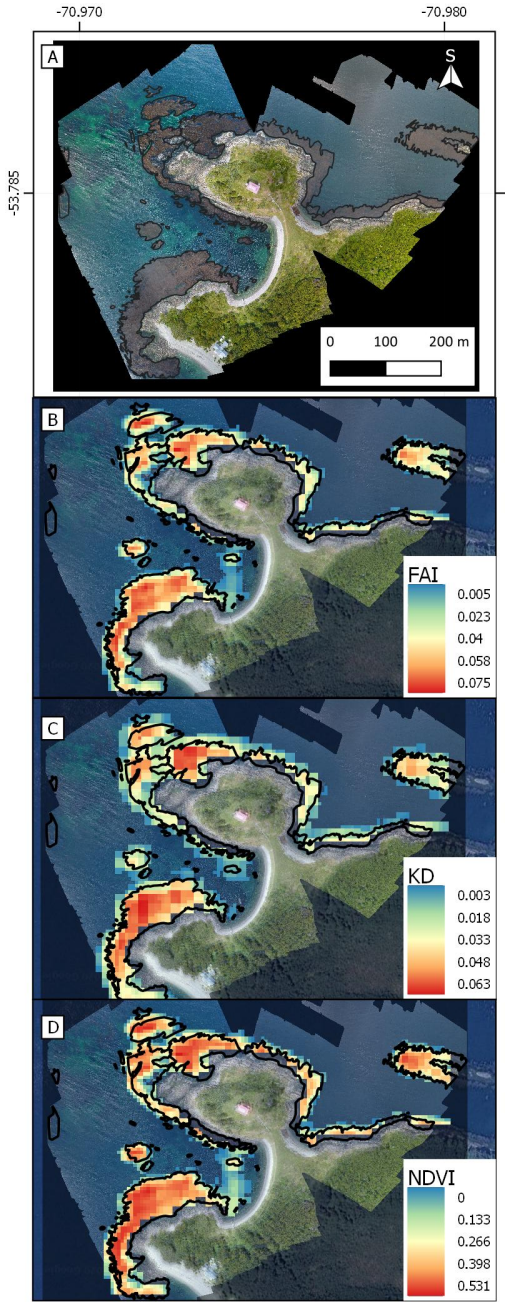


Figure 3.5: Ground-truthing process. A: 'True' canopy is delineated as the black line in the UAV orthomosaic. B, C and D: maps obtained through the kelp filter algorithm applied on FAI, KD and NDVI respectively. Higher values show higher concentrations of kelp canopy, although each index shows different levels of sensitivity. Site: San Isidro (Strait of Magellan). Cartographic projection EPSG3857, South-oriented.

Table 3.7: Area in km^2 per marine ecoregion and province with detected giant kelp and intertidal green algae, and number of detected grid cells versus total of georeferenced sites per ecoregion in a range of 300 m.

Province	**Ecoregion**	**km2**	**Detected/ georeferenced**
Agulhas	Agulhas Bank	136.2	
	Natal	1.7	
Benguela	Namaqua	96.5	1/1
Cold Temperate Northeast Pacific	Gulf of Alaska	483.9	
	North American Pacific Fjordland	2074.2	
	Northern California	193.7	1/1
	Oregon, Washington, Vancouver Coast and Shelf	333.6	
	Puget Trough/ Georgia Basin	118.2	
Magellanic	Channels and Fjords of Southern Chile	4840.7	23/32
	Chiloense	687.0	17/22
	Falkland Islands (Malvinas)	3081.1	1/1
	Patagonian Shelf	144.5	
Northern New Zealand	Northeastern New Zealand	76.6	
	Three Kings–North Cape	0.6	
Scotia Sea	South Georgia	145.9	2/2
Southeast Australian Shelf	Bassian	389.3	10/13
	Cape Howe	128.4	
	Western Bassian	42.4	1/3
Southern New Zealand	Central New Zealand	75.7	5/11
	Chatham Island	23.3	1/1
	Snares Island	ND	
	South New Zealand	148.8	7/8
Subantarctic Islands	Crozet Islands	73.6	
	Heard and McDonald Islands	0.5	
	Kerguelen Islands	3397.6	
	Macquarie Island	17.2	
	Prince Edward Islands	46.4	1/1

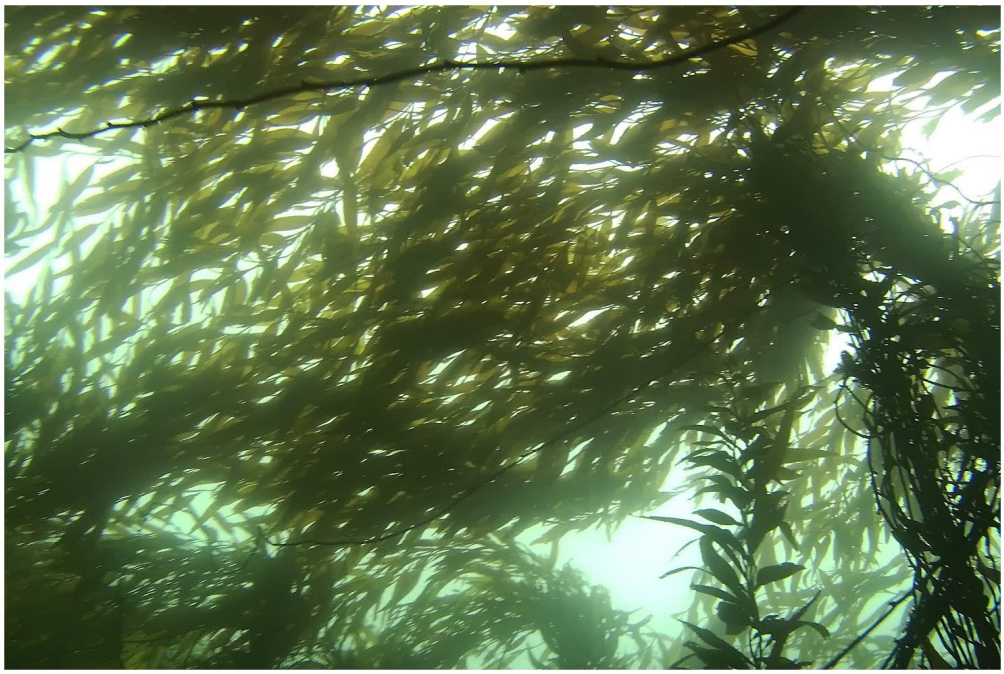
Table 3.8: Table 3.7 *(*Cont.)

Province	**Ecoregion**	**km2**	**Detected/ georeferenced**
Subantarctic New Zealand	Auckland Island	29.1	1/1
	Bounty and Antipodes Islands	0.6	1/2
	Campbell Island	1.5	1/1
Tristan Gough	Tristan Gough	6.0	
Warm Temperate Northeastern Pacific	Southern California Bight	222.1	
Warm Temperate Southeastern Pacific	Araucanian	54.9	12/18
	Central Chile	11.7	9/10
	Humboldtian	4.7	9/29



Figure 3.6: A: Buque Quemado intertidal forest (Strait of Magellan), at 10 cm of depth in low tide and 9 m in high tide. B: Measuring the length of the plants of site A. (People in photos A and B are included for scale). C: Permanent subtidal forest (delineated in black) in Puerto Amparo (area= 0.3 ha). D: Underwater canopies of Puerto Amparo (max. depth: 7.9 m). (Photos: Alejandra Mora S.)





4 | Chapter 4: Paper 2

4.1 Linking statement: Submitted for publication

The second paper of this thesis is based on the results of the global map introduced in Chapter 2. As that map revealed the location of giant kelp along different coastlines around the world, it created a new opportunity to explore the main geographical and historical characteristics of giant kelp beyond South America to the sub-Antarctic ecoregions of Falkland Islands (Malvinas) and South Georgia. Consequently, this paper addresses the second, third and fourth aims of this thesis: **"to create a model to understand the abiotic factors that explain the observed distribution of giant kelp forests"; "to explore the differences of giant kelp forests between ecoregions and landscape units"**; and **"to explore the long-term trends of giant kelp"** in a holistic approach.

The proposal of the paper is that kelp forests occupy different landscape units according to the geomorphology of the coastline and the level of exposure to the open ocean. These characteristics, without direct human intervention but stable temperatures, should be enough to maintain the giant kelp's locations in the long term. To prove these points, I classified kelp forests by their abiotic characteristics (ecoregion, slope, latitude, longitude, current, exposition, orientation, geoform); analysed a long-term record of sea surface temperatures at the three ecoregions; and compared multi-temporal records of giant kelp, including the nautical charts made during the Beagle Expedition (King et al.; 1836) as well as the first systematic surveys of giant kelp made during the 1970s and 1980s, up to the present. This approach allows us to say that sub-Antarctic kelp could be one of the last undisturbed marine ecosystems on the planet. The results of the long-term persistence of giant kelp forests can be explored at this online map.

4.1.1 Author Contribution Statement

A.M.-S. and M. M.-F. Conceived the ideas and conceptualised the research and methodology. A.M-S, M.P., N.G. and T.H. conducted the fieldwork, A.M-S collected and analysed the data, and led the writing; A.C., A.M.F., M.P., P.B., N.G., P.D., B.V.T., A.M., W.G., C.V-C., T.H., E.C.M, A.P-M. and M.M-F. critically reviewed and edited the manuscript.

It is important to mention that all of my collaborators have developed surveys directly or indirectly focused on giant kelp in those latitudes, including some of the first scientific publications on giant kelp performed in Patagonia, Tierra del Fuego and the Falkland Islands; their field knowledge was important to clarify and validate the points that I presented in this manuscript. This paper was submitted for publication on the 12th of January 2021 to the *Journal of Biogeography*; it is currently under second revision.

4.2 One of the least disturbed marine coastal ecosystems on Earth: Spatial and temporal persistence of Darwin's sub-Antarctic giant kelp forests

Short title: Persistence of sub-Antarctic kelp forests

Alejandra Mora-Soto[*1], Austin Capsey[2], Alan M. Friedlander[3,4], Mauricio Palacios[5, 6, 7, 8], Paul E. Brewin[9 10], Neil Golding[9], Paul Dayton[11], Brigitta Van Tussenbroek[12], Américo Montiel[13], Whitney Goodell[3 14], Catalina Velasco-Charpentier[15 16], Tom Hart[17], Erasmo C. Macaya[7 18], Alejandro Pérez-Matus[19], Marc Macias-Fauria[1]

[1] Biogeosciences Group, School of Geography and the Environment, University of Oxford, Oxford OX1 3QY, United Kingdom.

[2] UK Hydrographic Office, Admiralty Way, Taunton, Somerset TA1 2DN, United Kingdom.

[3] Pristine Seas, National Geographic Society, Washington DC.

[4] Hawaii Institute of Marine Biology, University of Hawaii, Kaneohe, Hawaii.

[5] Programa de Doctorado en Biología Marina, Universidad Austral de Chile, Valdivia, Chile.

[6] Facultad de Ciencias, Universidad de Magallanes, Punta Arenas, Chile.

[7] Centro FONDAP de Investigación en Dinámica de Ecosistemas Marinos de Altas Latitudes (IDEAL), Valdivia, Chile.

[8] Wildlife Conservation Society Marine Program- Chile.

[9] South Atlantic Environmental Research Institute (SAERI), Stanley FIQQ 1ZZ, Falkland Islands.

[10] Shallow Marine Surveys Group (SMSG), Stanley, FIQQ 1ZZ, Falkland Islands.

[11] Scripps Institution of Oceanography, University of California, San Diego, La Jolla, California 92.093.

[12] Unidad Académica Sistemas Arrecifales-Puerto Morelos, Instituto de Ciencias del Mar y Limnología, Universidad Nacional Autónoma de México, México.

[13] Laboratorio de Ecología Funcional, Instituto de la Patagonia, Universidad de Magallanes, Punta Arenas, Chile.

[14] Exploration Technology Lab, National Geographic Society, Washington DC.

[15] Centro de investigación Gaia Antartica, University of Magallanes, Av. Bulnes 01855, Punta Arenas, Chile.

[16] Fundación Mar y Ciencia, Chile.

[17] Penguin Watch, Department of Zoology, University of Oxford. Oxford OX1 3SZ, United Kingdom.

[18] Laboratorio de Estudios Algales (ALGALAB), Departamento de Oceanografía, Universidad de Concepción, Casilla 160-C, Concepción, Chile.

[19] Subtidal Ecology Laboratory, Estación Costera de Investigaciones Marinas, Departamento de Ecología, Facultad de Ciencias Biológicas, Pontificia Universidad Católica de Chile, Casilla 114: D, Santiago, Chile.

* Corresponding author. Email: alejandra.morasoto@ouce.ox.ac.uk

4.3 Abstract

4.3.1 Aim

Marine habitats and their dynamics are difficult to systematically monitor, particularly those in remote locations. This is the case with the sub-Antarctic ecosystem of the giant kelp *Macrocystis pyrifera*, which was already noted by Charles Darwin in his accounts on the Voyage of the Beagle and recorded on the nautical charts made during that expedition. We combined these and other nautical charts from the 19th and early 20th centuries with surveys conducted in the 1970s and 1980s and satellite detection algorithms from 1984 to 2019, to analyse kelp distribution through time and the factors that correlate with it.

4.3.2 Location

Marine ecoregions of Channels and Fjords of Southern Chile, Falkland Islands (Malvinas), and the island of South Georgia.

4.3.3 Taxon

Macrocystis pyrifera

4.3.4 Methods

We characterised 309 giant kelp forests by their coastal geospatial attributes. Statistically significant variables were included in a conditional inference tree to predict kelp forest size. Sea surface temperature (SST) records were analysed to confirm temperature ranges over the last four decades. Nautical charts, historical surveys, aerial photogrammetry, unmanned aerial vehicle (UAV) surveys,

and satellite imagery were overlaid to assess spatial distribution of kelp forest canopies, spanning the period 1829-2020.

4.3.5 Results

Considering the extensive natural and human caused changes over the last two centuries, this diverse kelp ecosystem is remarkably persistent. We found that the ocean currents and wave exposure, combined with the geomorphological settings of the coastline are the most critical factors predicting the extent of the kelp forests.

4.3.6 Main conclusions

We have described the long-term ecological persistence of the kelp forests in this vastly under-studied region that offers a conceptual biogeographical model supporting the global importance proposed by Charles Darwin 200 years ago (Darwin; 1845). In the current context of global change, the need for conservation of this persistent and well-preserved marine ecosystem has never been more important.

4.3.7 Keywords

Coastal biogeography, historical cartography, kelp forests, *Macrocystis pyrifera*, nautical charts, persistent ecosystems, remote sensing, sub-Antarctic marine ecosystems, *the Voyage of the Beagle*.

4.4 Introduction

There is an increasing awareness of the need to protect the last remaining terrestrial forest ecosystems with limited anthropogenic impact (Watson et al.; 2018). Intact forests on continents are periodically monitored by remote sensing systems to better understand changes in the quantity and quality of these ecosystems (Hansen et al.; 2013; Potapov et al.; 2017,0). In contrast, there has been less attention to the status of intact or pristine underwater ecosystems, particularly kelp forests. Kelps are considered "foundation" species, as their presence increases the number and diversity of species by the control of the physical environment in the water column, also known as physical engineering (Lamy et al.; 2020; Miller et al.; 2018). In many regions of the planet, kelp forests are degrading under multiple stressors such as ocean warming, pollution, or over-harvesting (Krumhansl et al.; 2016; Wernberg et al.; 2019).

A missing area in the recent account of the global trends of kelp forests is the sub-Antarctic region (Krumhansl et al.; 2016), which paradoxically was one of the first kelp ecosystems mentioned in natural history studies. In the *Voyage of the Beagle*, Charles Darwin commented on the conspicuous forests of the giant kelp (*Macrocystis pyrifera*) surrounding Tierra del Fuego, saying "I can only compare these great aquatic forests of the southern hemisphere, with the terrestrial ones in the intertropical regions. Yet if in any country a forest was destroyed, I do not believe nearly so many species of animals would perish as would here, from the destruction of the kelp" (Darwin; 1845). These tenets forged the pillars of kelp ecology (Miller et al.; 2018). Darwin was not the first to record the giant kelp: the first written description of *M. pyrifera* was made by Juan Ladrilleros during his expedition through the Strait of Magellan in 1557-58, which illustrates how prevalent this alga was in the region (Martinic Beros; 1982).

The combined extent of the giant kelp canopies of *M. pyrifera* on the sea surface (kelp forests hereafter) detected with satellite imagery of the Chilean Fjords, Falkland Islands (Malvinas), and the island of South Georgia is 8067.7 km^2, which accounts for more than 47% of its known distribution (Mora-Soto et al.; 2020). Recent evidence suggests that this ecosystem is adapting to environmental change (Palacios et al.; 2021). A previous study reported that the abundances and composition of the kelp forests at Isla de los Estados (Argentina, 54°47'S 64°15'W) experienced little changes over the last four decades (Friedlander et al.; 2020). Furthermore, kelp forests in a nearby fjord (Yendegaia, Beagle Channel, Chile, 54°52'S 68°44'W) showed physiological tolerance to the indirect effects of glacier melting such as reduced light availability and increased turbidity (Huovinen et al.; 2019; Palacios et al.; 2021). Contrary to other kelp regions suffering thermal stress, the sub-Antarctic currents at present, do not show signs of tropicalization (Vergés et al.; 2014).

The sub-Antarctic kelp forests in this region are found along a high gradient of geographic coastal diversity, from the fjordlands of Southern Chile, to the extensive coastal shelf of the Falkland Islands and the rugged and heavily glaciated landscapes of South Georgia. These coastlines have been subject to direct and indirect influences of humans for thousands of years. Indigenous peoples in the Chilean Fjordland region have utilized *M. pyrifera* and other local seaweed species for food and medicine over at least 14,000 years BP (Dillehay et al.; 2008). The Falkland Islands and South Georgia, without human occupation before European arrival, have seen successive waves of economic activity since the mid-18th century, such as livestock grazing and seal and whale hunting (Alonso Marchante; 2014; Bridges; 1987; Palomares and Pauly; 2015), but the impact of these activities on kelp forests is unknown. At present, the spread of the salmon farming industry in Chile has had a devastating impact in the northern Patagonia coastal region, and

is now threatening the coastal and fjord ecosystems in the southernmost regions of the country (Friedlander et al.; 2018; Quiñones et al.; 2019). Still, the nature and extent of the impacts of this activity on kelp forests are poorly understood.

In the present study, we aim to characterise key aspects of the biophysical characteristics of sub-Antarctic giant kelp forests, and to observe the long-term patterns in their distribution as inferred from observational records. By addressing these questions, we aim to develop a broad biogeographical conceptual model of the environmental adaptations and long-term trends in these unique ecosystems.

4.4.1 Characterising the abiotic niche

Abiotic variables such as depth, complexity of the rocky substrate, and wave stress are essential in determining kelp presence and persistence (Young et al.; 2016). However, detailed bathymetric data of the sub-Antarctic is sparse, which precludes a comprehensive overview of the ecosystem. For this reason, this paper will analyse the abiotic niche of kelp forests based on the geomorphology of the coastline, exposure to the ocean, and sea surface temperatures.

Geomorphology informs on the general patterns of rocky nearshore ecosystems. In glacial and paraglacial regions with parallel glacial history such as in the Chilean Fjordland and South Georgia (Hodgson et al.; 2014), coastal and submarine geoforms like lateral or terminal moraines, erratic rocks and sills, may provide available rocky substrates at the borders of trough valleys or U-shaped fjords. In contrast, the Falkland Islands experienced limited glacial presence (Clapperton; 1990) with a large shelf, which provided an ecological refugium during the Pleistocene for some marine species (González-Wevar et al.; 2012; Leese et al.; 2008). Following this premise, similar geomorphological processes may be linked to similar coastal configurations and spatial patterns of kelp forests. Consequently, if the ge-

omorphological origin of a rocky substrate has been under a slow geological pace of marine sedimentation, the substratum for kelp forests should remain persistent within modern records, unless direct disturbance led to local extinctions.

Oceanographic variables like exposure to currents can also support habitat persistence or shifts. Kelp generally grows best under high hydrodynamic regimes due to the increased flow of nutrients and inorganic carbon (Parnell et al.; 2010; Wernberg et al.; 2019). On exposed coastlines, kelp attains higher biomass and growth rates in open waters with more water movement, as observed by (Van Tussenbroek; 1989b) in the Falkland Islands and by (Dayton; 1985b) at Isla de Los Estados and southern Tierra del Fuego. However, we have limited evidence of kelp forest sizes in exposed or sheltered areas in sub-Antarctic kelp ecoregions, or whether strong storms are able to remove kelp forests in the most exposed areas.

In addition, Sea Surface Temperature (SST) records can help to confirm temperature ranges for kelp persistence. At latitude 42°S, north of the Chilean Fjordland, SST > 15-17°C were observed to increase the mortality of annual populations of kelp sporophytes (Buschmann et al.; 2014). It is not yet clear whether sub-Antarctic SST records for the last decades are fully within the optimal thermal tolerance of kelp.

4.4.2 Long-term persistence

Estimating long-time resilience of kelp forest ecosystems in these three different ecoregions is challenging, considering the limited temporal range of ecological studies in this region (Barnes et al.; 2006; Castilla and Moreno; 1982; Dayton; 1985b; Van Tussenbroek; 1989c). Instead, the concept of persistence (sensu (Connell and Sousa; 1983)) refers to a population that did not go extinct, or if it did go extinct locally or regionally, it recolonized during a given period of time in a

given area.

To gain perspective on the long-term persistence of sub-Antarctic kelp forests, we compared the first detailed cartographical records made during the voyages of the HMS Beagle and Adventure in 1826-36 (King et al.; 1836) and similar early charts from South Georgia made in 1882-1931 with surveys and remote sensing imagery from the second half of the 20th century up to the present.

4.5 Methodology

4.5.1 Study area

Our area of study encompasses the western side of South America from Peninsula Tres Montes at latitude 47°S to Cape Horn at latitude 56°S; and from longitudes 35°W to 76°W along the Chilean coastline to South Georgia (Figure 4.1A). This area includes the marine ecoregions of Channels and Fjords of Southern Chile, the Falkland Islands (Malvinas), and the island of South Georgia (excluding the South Sandwich Islands) (Spalding et al.; 2007), and is oceanographically connected with the Pacific and the Atlantic oceans by the Cape Horn Current, the Falkland Current, and the Circumpolar Antarctic Current around the South Georgia Shelf (Brandon; 2000). The Channels and Fjords ecoregion is connected by a network of channels (called Channels hereafter, described in González et al. (2013)) and the Strait of Magellan that separates the South American continent from Tierra del Fuego. The Falkland Islands ecoregion is bisected by Falkland Sound, which separates the West and East Falkland Islands. In this study, we consider the Patagonian Shelf ecoregion that includes Puerto Deseado (Argentina) and the Chiloense ecoregion (Chile, latitude 41-46°S) for historical analysis only, because the kelp forests in the former occur within a region of large tidal ranges, which may render

them invisible to satellite sensors (Mora-Soto et al.; 2020), while in the latter kelp forests are less stable, with weaker attachments to the substrate (Darwin; 1845; Dayton; 1985b).

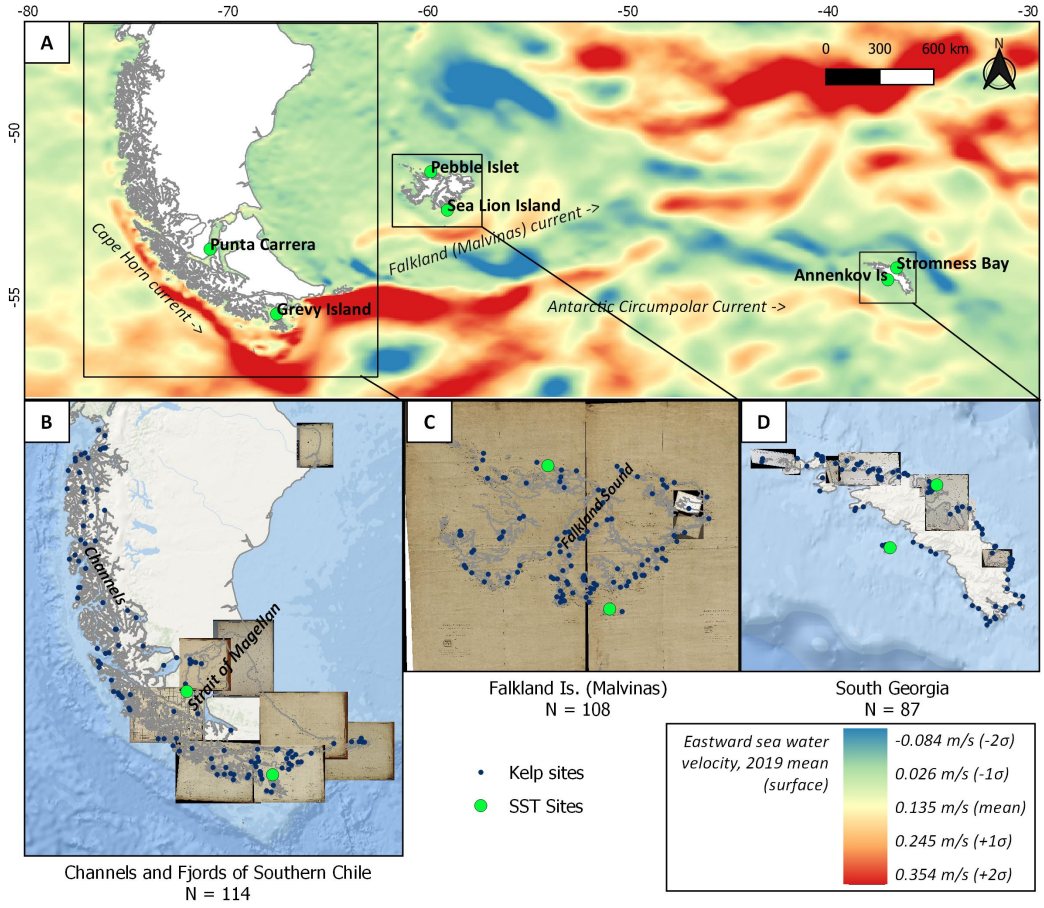


Figure 4.1: A) Ecoregions of Channels and Fjords of Southern Chile, Falkland Islands (Malvinas) and the island of South Georgia in context with the main oceanic currents. The colour palette in the ocean indicates the Eastward mean velocity at the surface in 2019, according to the Hybrid Coordinate Ocean Model (HYCOM; (Chassignet et al.; 2009)); the labels indicate the mean ±2 Standard Deviations (the velocity layer is included for reference only). B, C, D) Overview of the United Kingdom Hydrographical Office (UKHO) historical Nautical Charts, kelp sites and SST sites, and internal currents, for B) Channels and Fjords and Patagonian Shelf; C) Falkland Islands (Malvinas); D) South Georgia. Map projection EPSG:3857.

4.5.2 The abiotic niche

4.5.2.1 Spatial identification of a sample of present kelp forests (2016-2019)

We extracted present giant kelp canopy extents using remote sensing imagery. The extent of each canopy on the sea surface was detected with the Kelp Filter (KF) algorithm developed by Mora-Soto et al. (2020) and applied to Sentinel-2 Level-1C (Copernicus Service) satellite imagery from the Austral Spring 2015, starting on 21st September through to Austral Summer 2020, ending on 21st March. KF highlights the presence of kelp canopies through the difference of the red-edge (Band 6, 740 nm) and red reflectance (Band 4, 665 nm) of the Sentinel-2 spectral bands at 20 m resolution. The algorithm further masks values to discard other land or ocean elements, except for *Ulvophyceae* (a class of green algae) in intertidal areas, due to their similar reflectance. We applied this algorithm in seasonally-averaged images to increase the detection of kelp forests, as they often otherwise remain invisible due to heavy cloud cover, potentially persistent swell, or very small canopies over the study area. Subsequently, all seasons were averaged to calculate a representative extent of kelp canopy for the total range of time.

We aimed to obtain a representative sample of kelp forests per ecoregion. In QGIS (version 3.14.15), a random multipoint layer was created within the limits of each ecoregion. If any of those random points were in a range of 500 m near a kelp forest as identified by the KF algorithm, the forest was selected as a sample, and the process was repeated until the number of samples was close to 100 per ecoregion. The final number of sites were 108, 114, and 87 for Falkland Islands, Channels, and South Georgia, respectively. For each of these kelp forests, a polygon was delineated covering the maximum extent of the observed canopy, including an inland range of 500 m if the forest was next to a coastline. Sites were double-checked with visible canopies on very high resolution Google Earth

true colour images to avoid false positives (Mora-Soto et al.; 2020). If the Google Earth image had low resolution, or was obstructed by cloud cover, we used KF pixels that showed a permanent overlay of pixels identified as kelp in concentrated areas, avoiding estuarine or beach areas. The polygon drawing scale ranged from 1:5,000 to 1:20,000.

4.5.2.2 Statistical analyses

Kelp forests were characterized by their coastal geospatial attributes (Table 4.1). Orientation, level of exposure to the open ocean, and the coastal setting of the surrounding land (geoform) were manually classified using Sentinel-2 and a topographic layer (Advanced Land Observing Satellite Global Digital Surface Model – ALOS AW3D30, (Tadono et al.; 2016)) for context. For kelp forests next to land, the maximum slope in a range of 500 m was calculated with ALOS and the Zonal Statistics tool in QGIS version 3.14. Kelp forest size was classified according to the median size of the complete number of samples (6.6 ha, rounded to 7 ha), in two classes: "small" (< 7 ha) and "large" (>7 ha).

A Kruskal–Wallis (1952) rank sum test was applied to determine whether kelp forest size was significantly different along the categorical variables exposure to the ocean, geoform, ocean current, and aspect per each ecoregion. Significant p-values were adjusted and compared with the Benjamini and Hochberg (1995) method. Additionally, Kaiser-Meyer-Olkin (KMO) and Bartlett's Tests (R version 4.0.2, package: psych, (Revelle and Revelle; 2015)) were used to assess the adequacy of each factor. Spearman's rank-order correlation (Spearman; 1987) was used to identify whether kelp forest size was correlated with the continuous variables of adjacent land slope, longitude, and latitude. Statistically significant categorical variables were included in a conditional inference tree (Hothorn et al.; 2006) (R package: partykit, (Hothorn and Zeileis; 2015)) to investigate the asso-

Table 4.1: Attributes of the giant kelp (*Macrocystis pyrifera*) forests used in this study. * Dependent variable; [1]: Independent variable

Name	Definition and levels	Type of variable and test
Size*	Total area covered by canopy, in hectares.	Continuous, Spearman rank-order correlation
Slope [1]	Maximum topographic slope in degrees (source: ALOS AW3D30) of the surrounding land in a range of 500 m.	
Latitude, Longitude [1]	Coordinates in decimal degrees (WGS 84).	
Size class*	Small (< 7 ha) or Large (> 7 ha).	Categorical, Kruskal–Wallis rank-sum test (compared with Size in hectares and Size class).
Slope class [1]	Classification of topographic slope ranges: < 4° = level, 4-15° = sloping, 15-35° = steep, > 35° = Very steep.	
Exposure [1]	Exposition to the open sea: wave exposed or sheltered.	
Geoform [1]	Visual assessment of the geomorphological setting of the forest site: concave (bay), convex coastline, straight coastline, small island, intertidal rock (islet).	
Orientation [1]	Visual assessment of the orientation or aspect of the kelp forest next to a coastline (flat or circular is omitted): North, North East, East, South East, South, South West, West, North West.	
Current [1]	Oceanic currents: Antarctic Circumpolar, Cape Horn, Falkland Islands. Straits and sounds: Channels (in the Chilean Fjordland), Falkland Sound, Strait of Magellan.	
Ecoregion [1]	Channels and Fjords of Southern Chile, Falkland Islands, South Georgia.	

ciation between forest size and geospatial variables, using 80% of all forests of the three bioregions combined (N = 254) for calibration and the remaining 20% (N= 55) as an evaluation dataset.

4.5.2.3 Decadal trends of Sea Surface Temperature (1981-2020)

We obtained long-term daily SST records surrounding sub-Antarctic kelp forests. SST trends were analysed using the NOAA CDR OISST: Optimum Interpolation Sea Surface Temperature product (Banzon et al.; 2014) employing the Google Earth Engine API. As this imagery dataset has a coarser scale (0.25 arc degrees) than the one used for delimitating kelp forests, we selected two representative points for each ecoregion between the kelp forests and the open ocean (Figure 4.1A). Daily records from 01 September 1981 to 30 March 2020 were tested for stationarity using the Augmented Dickey-Fuller Test (R package: adf.test (Fuller; 2009)). The selected sites were as follows: 1) Channels and Fjords ecoregion: Punta Carrera, in the Strait of Magellan; Grevy Island in the Cape Horn Archipelago; 2) Falkland Islands ecoregion: Sea Lion Island, at the South of East Falkland; Pebble Islet, at the North of West Falkland; 3) South Georgia ecoregion: Annenkov Island at the western side of the island; Stromness Bay at its eastern side.

4.5.3 Long-term persistence

4.5.3.1 Long-term kelp canopy extent monitoring

To examine the variability of kelp forest extent over the longest observational time frame possible, we made use of historical nautical charts, airborne (from aircraft and unmanned aerial vehicles [UAVs]), and satellite imagery, spanning the period 1829-2020.

- 1829- 2019. Nautical charts and visual assessments of kelp forests

  The original HMS “Beagle” Nautical Charts of the Strait of Magellan, Tierra del Fuego, and Falkland Islands (1829-1834) (King et al.; 1836), along with

the HMS "Sappho" (1905), HMS "Dartmouth" (1920), RRS "Discovery" (1925-1930), and German International Polar Year Expedition (1882-1914) Nautical Charts of South Georgia were manually scanned at the archives of the United Kingdom Hydrographic Office (UKHO) using a hand-held scanner. The images were georeferenced in QGIS using a first-order polynomial transformation and ground control points using distinctive coastal features, choosing the georeference with the minimum root mean square (RMS) error (Figure 4.1B-D). With this transformation, we opted to maintain the main coordinates of the historical chart rather than stretching the chart to fit the actual coastline, in consideration of the cartographic technology at the time. The observed kelp forest areas, depicted with symbols of stipes and blades, were delineated as polygon shapefiles along a wide perimeter around the fronds, following the protocol of Costa et al. (2020). The range of the drawing scale was 1:5,000 to 1:10,000.

4.5.3.2 Second half of 20th century

- Airborne imagery

  Aerial photographic archives containing kelp forests from Port Stanley and surrounding area (Falkland Islands) were scanned and georeferenced along with the nautical charts. The date of the aerial survey was 14-22 March 1976 (Sortie number: 1186). The flight was conducted at $\sim$ 1,800 m with a camera of focal length of 152:46 mm at a scale of 1:12,000. The boundaries of the kelp canopies were manually drawn in shape polygons following the contour of the fronds in the photographs.

  Contemporary kelp forests were recorded from UAV mapping missions during 2019 and 2020 in the Falkland Islands (Golding et al.; 2019) and South

Georgia, using a DJI Phantom 4 and DJI Mavic Pro 2 Pro equipped with an RGB camera. Along track and across track overlap of images was 80%, with flying altitude ranging from 70 to 100 m above ground level (AGL); time of flights was between 10 a.m. and 4 p.m. Orthomosaics were created from processing the still images in Agisoft Metashape Professional (Version 1.6.4) with a spatial resolution of 10 cm. Observed canopies were manually drawn as shapefile polygons following the same protocol as with the aerial photography.

Sketches and observations from geolocated diving surveys and footage records using a Chasing Gladius Mini underwater drone were included in this analysis in addition to the visual assessment of kelp canopies. Surveys were conducted in the Strait of Magellan, Yendegaia Fjord (Beagle Channel), the Magdalena Channel (Aysén Region, Chilean Patagonia) and Tussac Islands (Falkland Islands) from January to July 2019.

- Historical kelp surveys (1972-1987)

  The first ecological and ecophysiological studies on sub-Antarctic kelp were conducted in the 1970s and 1980s (Dayton; 1985b; Moreno and Jara; 1984; Ojeda and Santelices; 1984; Santelices and Ojeda; 1984; Van Tussenbroek; 1989a,9,9,9,9). We located the surveys on the map and verified if satellite-detected kelp forests exist in the vicinities of the locations indicated in these studies (either in maps or registered coordinates), using the same layered procedure as mentioned above. Finally, we compared the charts with data on human impact using geographical records of historical and current land use from Geographical Information Systems of the local governments and institutions (Chile: Región de Magallanes (Magallanes; 2020); UK Overseas Territories (BAS; 2020; SAERI; 2020) as main sources.

- Multidecadal assessments of kelp forests with satellite imagery (1984-2019)

  Charted kelp forests drawn on the UKHO historical nautical charts were compared with the extent of kelp forests from the satellite imagery provided by Google Earth Engine (Gorelick et al.; 2017). The detection algorithms were: Normalised Difference Vegetation Index (NDVI; (Tucker; 1979)) derived from the Landsat 5 TM Tier 1 calibrated top-of-atmosphere (TOA) reflectance of 30 m resolution (Nijland et al.; 2019); and the KF derived from Sentinel-2 (note that KF cannot be computed from Landsat due to lack of adequate reflectance bands). As the available Landsat 5 TM images from 1984 to 2011 were few in comparison to Sentinel-2 images from 2016 to 2019, all images were averaged annually. Only Sentinel-2 images were available for South Georgia.

  The following protocol was applied to the annually-averaged Landsat 5 TM: cloud masking with the aid of the Quality Assessment band (USGS); land masking of elevation values > 0 m using the Advanced Land Observing Satellite Global Digital Surface Model (ALOS AW3D30, (Tadono et al.; 2016)); NDVI calculation and filtering of values ≥ 0.01; selection of annual images with filtered NDVI pixels over the targeted kelp forests. In the case of Sentinel-2, we followed the KF protocol mentioned above.

  Kelp canopies can be covered by persistent clouds resulting in underestimation of their total extent, and kelp areas in the historical nautical charts were not outlined precisely and are thus prone to not insignificant margins of error. Therefore, the polygons corresponding to each canopy drawn on the UKHO charts were overlaid with the satellite-detected kelp areas to analyse spatial concordance, and we classified this visual assessment in four categories:

1. The satellite-detected kelp areas covered the charted kelp in similar form and extent.
2. The satellite-detected kelp areas had spare pixels over the target kelp canopy: this may mean that the forest is small or with sparse fronds, largely undetected by the satellite sensor.
3. The satellite-detected kelp areas showed patterns not associated with kelp forests.
4. No satellite-detected kelp pixels over the targeted kelp.

4.6 Results

4.6.1 Characterising the abiotic niche

4.6.1.1 The landscape/seascape of present kelp forests

The landscape and seascape characteristics allowed the identification of key characteristics defining the kelp forests in the three studied ecoregions: e.g., the mean size of individual kelp forests in the Falkland Islands ecoregion is three times larger than that of the forests in the Channels and Fjords ecoregion, and twenty times larger than the forests in the South Georgia Ecoregion (Table 4.2). The largest forests are associated with the Falklands Current, Falklands Sound, and the Cape Horn Current, whereas smaller forests are found in areas that are influenced by the less powerful currents of the Channels, Strait of Magellan, and the Antarctic Circumpolar Current near South Georgia (Figure 4.2A). Post-hoc pairwise comparison indicates that forest size is not significantly different between Falklands Current and Falklands Sound, and between Strait of Magellan and Cape Horn and Channels. However, forest canopies are larger when their surrounding

coastline is oriented towards the dominant oceanic currents. This corresponds with directions from southwest to east in Channels, and from south to northeast at both the Falkland Islands and South Georgia (Figures 4.1A and 4.3).

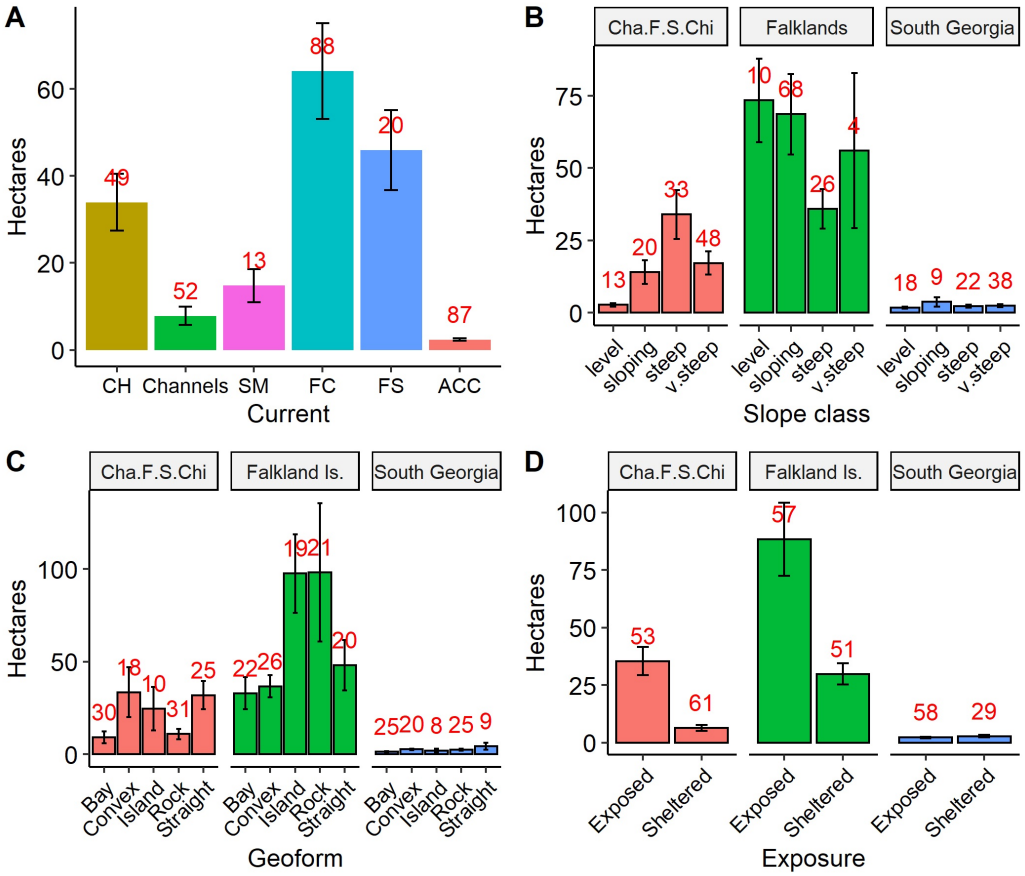


Figure 4.2: Kelp canopy cover (ha) by: A) currents, B) slope class, C) geoform, and D) exposure. Boxplots are mean ± standard error of the size of sampled kelp forests per ecoregion, and the red labels indicate number of kelp forests per class. A) Ocean currents: CH = Cape Horn, Channels = Chilean Patagonia Channels, SM = Strait of Magellan, FC = Falkland Current, FS = Falkland Sound, ACC = Antarctic Circumpolar Current. B) Slope Class: Level (flat or gently sloping) = <4°, Sloping = 4-15°, Steep = 15-35°, Very steep = > 35°. C) Geoform, D) Exposure.

Kelp forests differ in size and number according to the slope class of the nearby land, but follow different patterns in each ecoregion (Figure 4.2B and Table 4.3).

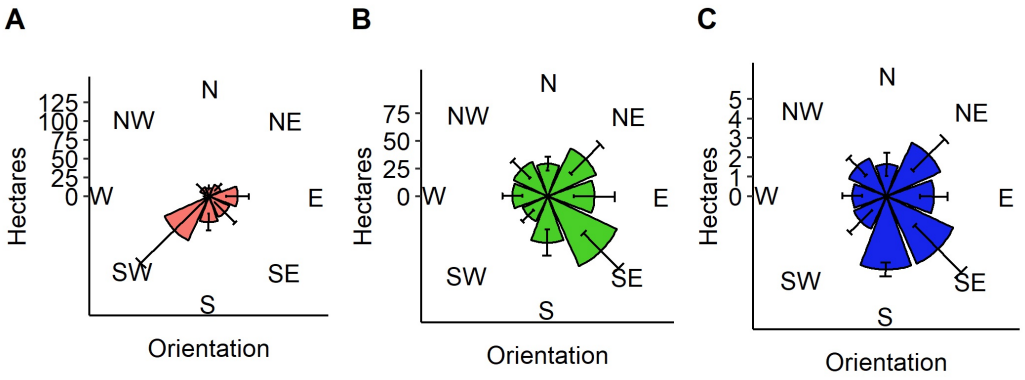


Figure 4.3: Kelp forest size (ha) in relation to coastal orientation: A) Channels and Fjords, B) Falkland Islands (Malvinas), and C) South Georgia. Values are mean ± standard error of the sampled kelp forests per orientation. Refer to Figure 4.1A to compare with the main oceanic currents of each ecoregion.

Table 4.2: Descriptive statistics for size (ha) of kelp forests per ecoregion. Qu. = quartile.

	N forests	Mean	St.Dev	Median	1st Q	3rd Q	Min	Max
Falklands	108	60.72	94.6	35.73	14.70	77.79	0.28	820.53
Channels	114	19.84	34.1	6.03	2.11	21.24	0.08	220.51
South Georgia	87	2.38	2.9	1.54	0.49	2.97	0.07	18.69

The majority and the larger kelp forests are adjacent to steep (15-35°) to very steep (>35°) terrain in the Channels and Fjords; in South Georgia, slightly larger kelp forests are associated with sloping lands (4-15°) (Figure 4.2B). In the Falkland Islands, most of the kelp forests are located around flat to gently sloping gradients. Regarding geoforms, in the Channels and Fjords ecoregion and in South Georgia, larger kelp forests are associated with convex headlands and straight coastlines, and dominate in number in bays and around intertidal rocky islets. In the Falkland Islands ecoregion, larger forests are found around islands or intertidal rocky islets (Figure 4.2C). Finally, a significant difference is observed among forests in sheltered versus exposed areas facing the main ocean currents in both Channels and Fjords and the Falkland Islands (Figure 4.2D).

Table 4.3: Kruskal-Wallis rank sum test of the significant variables associated with size of the kelp canopies. KMO = Kaiser-Meyer-Olkin (KMO) Measure of Sampling Adequacy. KMO values >0.5 and significant Bartlett's Test indicate that the variables are adequate for factor analysis.

	x^2	df	p-value	KMO
Ecoregion	119.65	2	< 0.001	0.54
Slope class	44.525	3	< 0.001	0.53
Current	143.63	5	< 0.001	0.53
Exposure	16.199	1	< 0.001	0.51
Geoform	18.059	4	0.001	0.53
Overall KMO				0.54
Bartlett's Test of Sphericity				
Approx. Chi-Square				207.2
df				15
p-value				< 0.001

The continuous variables of longitude, latitude, and slope display significant correlations with the size of the kelp forests. These are overall weak and tend to confirm the patterns displayed by categorical variables. Kelp forest size is negatively correlated with longitude ($\rho = -0.19$; p-value < 0.001; i.e., in a hump-shaped relationship from the continent to the very large forests of the Falkland Islands and becoming smaller towards South Georgia in the east). Similarly, kelp forest size decreases with increasing latitude ($\rho = 0.26$; < 0.001). Kelp forest size is negatively correlated with land slope, although this relationship is not as strong as with latitude or longitude ($\rho = -0.14$; p-value = 0.015).

The significant variables are used in a conditional inference tree to predict the size of the kelp forests (Figure 4.4). Small forests are linked to the Antarctic Circumpolar Current on the South Georgia Shelf (94.6%) and the Channels of Southern Chile (76.6%). Larger forests are related to the main oceanic currents (Cape Horn, Falkland Current, Falkland Sound, and Strait of Magellan, p < 0.001), but they vary in relation to how exposed they are to the open ocean. In sheltered

areas, including the Strait of Magellan and Falkland Sound, small forests make up 40% of the total, whereas larger forests dominate in the open oceanic areas facing the Cape Horn and Falkland currents, accounting for 77% and 100% of the kelp forests, respectively. The prediction level of the conditional inference tree is 81% (p-value =0.001).

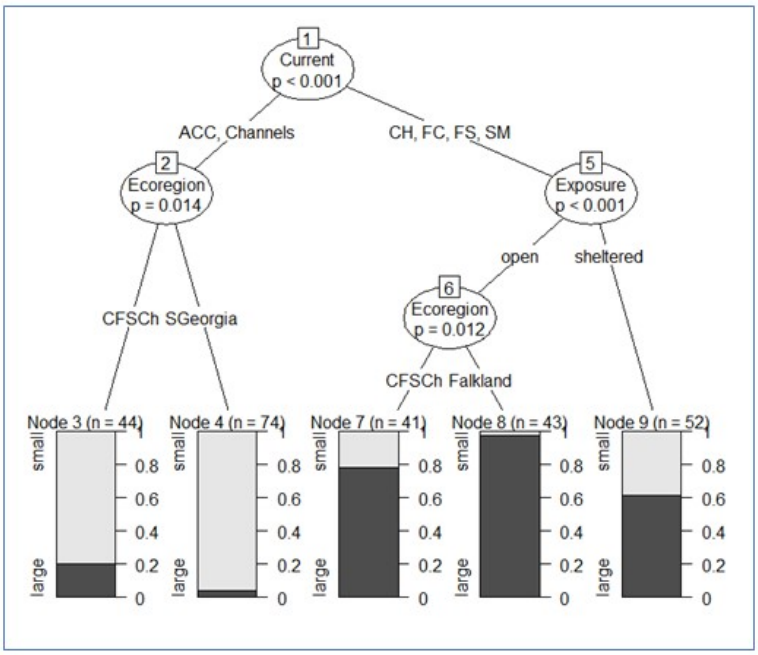


Figure 4.4: Conditional inference tree (non-parametric regression tree). Currents: ACC = Antarctic Circumpolar Current. Channels = Channels of Southern Chile. CH = Cape Horn Current. FC = Falkland Current. FS = Falklands Sound. SM = Strait of Magellan. Ecoregions: CFSCh = Channels and Fjords of Southern Chile. Falkland = Falkland Islands (Malvinas). SGeorgia= South Georgia. Exposure: open = Open ocean. Sheltered = Sheltered or protected areas. The threshold of large or small forests is the median area of the total of kelp forests (7 ha).

4.6.1.2 Multidecadal SST trends

The long daily record (1981-2020) of NOAA SST data shows stationary trends for all the representative pixels (Dickey-Fuller test= stationary; p-value = 0.01 for all the sites; Supplementary Figure A.1). Minimum SST record is -1.74°C at Stromness, South Georgia, while the maximum recorded temperature is 12.77°C at Pebble Island in the Falkland Islands (Supplementary Table A.1). No temperatures above the thermal range of kelp survival are recorded between 1981 and 2020. This record demonstrates that SSTs have been stable during the last three decades in the study area.

4.6.2 Long-term persistence

The complete coverage of UKHO Nautical Charts and satellite-detected kelp forests can be found in the following online resource. Multi-annual kelp time-series, detected with KF from Sentinel-2 and NDVI derived from Landsat 5 TM, show spatial coincidence with contemporary kelp forests, with differences mostly attributable to cloud cover in the averaged satellite images. A multi-decadal assessment of kelp forest area was not possible due to lack of continuous cloudless data, but the overlay of annual detected kelp forest shows patterns of spatial coincidence, indicating a persistence of kelp forests from 1984 to 2019. All of the surveys made in the 1970s and 1980s are in the vicinity of the recent satellite-detected kelp areas.

Contemporary kelp forests also displayed a general spatial coincidence with kelp canopies drawn on the historical UKHO survey charts (Table 4.4). The cartographic details of the UKHO charts vary greatly in their accuracy; consequently, some sheltered coastlines have generally more details, sugesting more elaboration time, usually including kelp canopies as a warning for navigation. The best equiv-

alence between past and present inferred kelp forests is in the Falkland Islands charts, with 200 out of 223 kelp forests along the complete coastline, and only 4 non-detected forests in exposed areas of Choiseul Sound, Eagle Passage, Falkland Sound, and Berkeley Sound. South Georgia has 231 out of 304 satellite-detected kelp forests with similar presence and shape of charted kelp forests in the areas of Larsen Harbour, Royal Bay, Cumberland Bay, Stromness Bay, Fortuna Bay, Posession Bay, Bay of Isles, Prince Olaf Harbour, Right Whale Bay, Elsehul, Undine Harbour, and Bird Islands, with few confirmed kelp forest removals in the exposed areas of Barff Point, Elsehul, and Prince Olaf Harbour. The Channels and Fjords of the Southern Chile ecoregion has less coincidence of kelp forests (21 out of 38) along the Strait of Magellan, Navarino and Wollaston Island, Hardy Peninsula, and south of Tierra del Fuego, with 11 areas of sparse pixels and 6 noisy areas in the middle of the first and second narrows of the Strait of Magellan. The Patagonian Shelf ecoregion has 4 out of 8 areas with similar presence and shape near Puerto Deseado, Cape Virgins, and southeast coast of Tierra del Fuego, one missing area from Cape Espiritu Santo to Peninsula El Paramo, and two missing kelp forests in the exposed area of Puerto Deseado.

4.7 Discussion

In this study, we demonstrate that in addition to bathymetry used in other studies to locate potential sites of kelp forests (Costa et al.; 2020), currents, coastal geomorphology, and exposure can help to successfully predict broad spatial kelp patterns, in line with studies on sub-Antarctic benthic fauna (Barnes et al.; 2006). In the words of Dayton et al. (1994), p. 90), "geological history and oceanographic processes are the warp and woof of the biological understanding of any marine habitat". Although the predictive value of each explanatory variable was

Table 4.4: Summary of the total of kelp forests drawn on the UKHO nautical charts and satellite-detected kelp.

		Marine ecoregion			
		Channels and Fjords of Southern Chile	Falkland Islands (Islas Malvinas)	South Georgia	Patagonian Shelf
Historical nautical charts	Number of charts	11	4	24	4
	Year of elaboration	1834	1834-35	1882-1931	1929-1834
	Number of charted kelp forests	38	223	304	8
Kelp forests on nautical charts versus contemporary detections	Similar shape	21 55.3%	200 89.7%	231 76%	4 50%
	Spare pixels	11 29%	19 8.5%	48 15.8%	1 12.5%
	Noise	6 16%	0	0	0
	Empty	0	4 1.8%	25 8.2%	3 37.5%

low (KMO > 0.5), their combination generated a robust model that successfully predicted expected kelp forest sizes in the region.

Relatively small patches of kelp are abundant in bays and rocky islets in South Georgia, in contrast to the large extent of kelp forests in the Falkland Islands. This may reflect paraglacial patterns (Hodgson et al.; 2014) of fjords and moraines and restricted glacial history and extensive shallow shelf (Clapperton; 1990) respectively. This pattern is also supported by the surrounding land slope and anecdotal observations in the field. The spatial extent of sub-Antarctic kelp forests along coastlines is broader on flat to inclined slopes and narrower along vertical slopes. Level to sloping lands dominate at the Falkland Islands, steep to vertical lands dominate in South Georgia and Chilean Fjords. Vertical and over-hanging walls are a niche for animal forests like bivalves, polychaetes, and soft-corals, which can coexist with macroalgae (Cárdenas and Montiel; 2017). Regarding the exter-

nal boundary for *M. pyrifera* forests, previous surveys in the Channels and Fjords and Falkland Islands have reported that some forests are bordered by a narrow band of *Lessonia flavicans*, small boulders, and sand, although *L. flavicans* can grow intermixed with *M. pyrifera* (Beaton et al.; 2020; Dayton; 1985b; Santelices and Ojeda; 1984; Van Tussenbroek; 1989d). We illustrate this general conceptual model of kelp forest habitats in Figure 4.5. The patchy response of *M. pyrifera* to a variety of abiotic (geomorphology, SST) and biotic (competitive interactions) between species of kelps presents analytical challenges; understanding their differentiation / integration in response to contemporary environmental pressures would benefit modelling and monitoring of kelp forests in all regions.

In the ecoregions of Channels and Fjords and Falkland Islands, the dominant orientation of larger kelp forests towards the oceanic currents corroborates previous findings (Dayton; 1985b; Van Tussenbroek; 1989b,9), supporting the concept that water motion and turbulence play a primary role on nutrient assimilation for kelp (Dayton; 1985a). This prevalent quality ends when maximum wave energy limits kelp canopy, resulting in a hump-shaped relationship between kelp forest size and wave energy (Young et al.; 2016). On the other hand, in areas of very low energy, i.e., the fjords of South Georgia and the internal Channels of Southern Chile, kelp forests are strongly influenced by freshwater coming from glaciers and snow fields and rainfall. Previous work in the Beagle Channel has shown that *M. pyrifera* has adapted their photosynthetic activity to this paraglacial environment, including overshadowing due to high turbidity (Palacios et al.; 2021) or adopting a loose-lying form on the bottom and small pneumatocysts, undetectable from the surface (Gerard and Kirkman; 1984; Van Tussenbroek; 1989c). Therefore, kelp forests in fjords can persist despite being considered stressed (Dayton; 1985b; Mora-Soto et al.; 2020), even with the increased glacial melting rates of the last three decades (Meier et al.; 2018).

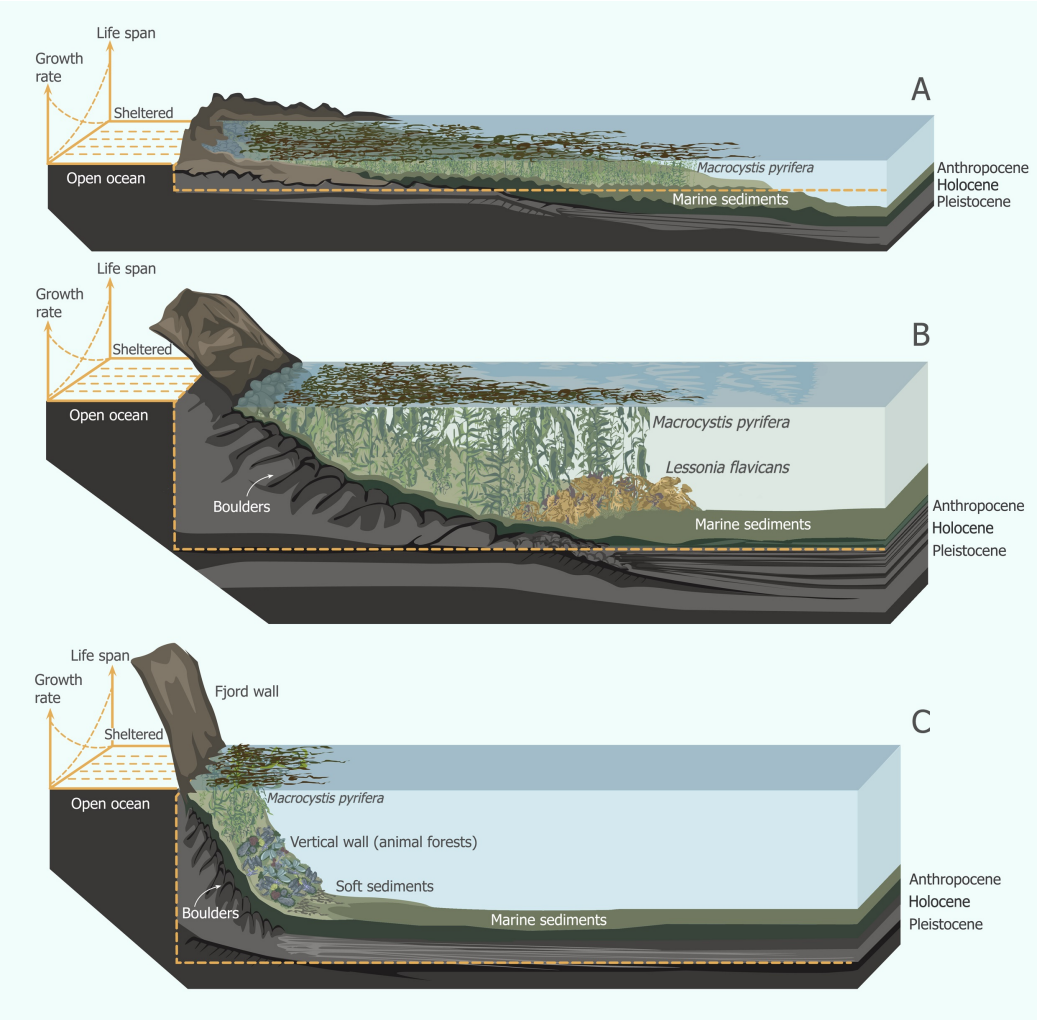


Figure 4.5: A general model of the sub-Antarctic kelp forest in relation to coastal geomorphology. The area of a kelp forest depends on the available substrate originated by geological orogeny followed by glacial, marine, alluvial, or organic weathering and/or sedimentation. Topographic slope classes: A) Level to sloping; B) steep; C) vertical and over-hanging walls. Exposure to the ocean has an inverse correlation with the growth rate and positive correlation with the life span of the canopies (Van Tussenbroek, 1989a, 1989c).

In the current global context, kelp forests are severely affected by marine heatwaves, ocean acidification, increased frequency of storms, and over-harvesting (Krumhansl et al.; 2016; Wernberg et al.; 2019). However, kelp persistence seems

to follow a neutral relationship with SST at higher latitudes, i.e., bull kelp *Nereocystis luetkeana* in Oregon (Hamilton et al.; n.d.). Furthermore, our SST analysis confirms that the currents near our study areas show no trends of tropicalization, a major cause of thermal stress and shifts on kelp distributions in other regions, i.e. Western Australia (Wernberg et al.; 2013), or Tasmania, with a sharp decline of kelp canopies since the year 2000 (Butler et al.; 2020). The low SST ranges in South Georgia, located south of the Antarctic Polar Front (Moore et al.; 1999), could mean that this ecosystem may cope well with polar temperatures, which might be a signal for potential colonisation of the Antarctic, but the small sizes of their canopies might also mean they are close to their lower temperature limit. On the other hand, acidification could have a negative impact on the development of calcareous organisms that feed on kelp, but not the kelp itself (Brown et al.; 2014). An increased frequency of subpolar westerly winds and strong storms is affecting the distribution of some species like the bull kelp *Durvillaea antarctica* (Fraser et al.; 2018). Although SSTs have remained stable and the present study supports the long-term stability observed in this marine ecosystem (Friedlander et al.; 2020,0), more local long-term studies on persistence after storms are needed to confirm this region as a climatic refugium for kelp.

Our work compared present-time with late-modern period records. The large number of kelp forests drawn in the nautical charts is explained by the words of Captain FitzRoy of the HMS Beagle: "there is no danger in any of the Falkland harbours that is not distinctly buoyed by kelp."((FitzRoy; 1839), p. 265). The process of georeferencing the charts with modern techniques confirmed the remarkable accuracy of the coordinates calculated in the Beagle charts, which meant a significant improvement from the previous cartography made in the times of the Spanish Empire (King et al.; 1836). South Georgia charts have more errors, but they improved in accuracy in successive editions from 1882 to 1931, refin-

ing the outline of the coastlines and charted kelp area. However, the location of very exposed kelp forests may be less accurate than kelp forests close to land. Similar sources of data to estimate kelp persistence were also used with success by (Costa et al.; 2020) in British Columbia, and (Pfister et al.; 2018) in the state of Washington. This research confirms their convenience for integrated historical studies.

The results of the temporal comparison showed 0%, 1.8%, 8.2% and 37.5% of empty kelp areas in Channels and Fjords of Southern Chile, Falkland Islands, South Georgia, and Patagonian Shelf, respectively. For present-time records, our kelp-detecting method with satellite imagery might have generated false negatives (empty cells) in narrow kelp canopy fringes or in canopies of low density, as the resolution of the satellites (30 m for Landsat TM and 20 m for Sentinel-2) might be too coarse to detect them, and in the eastern side of Tierra del Fuego and the Patagonian Shelf, kelp forests can be hidden under high tides (Mora-Soto et al.; 2020). In South Georgia, empty areas could be explained by the marginal distribution of the species, a high dynamism of the coastline due to glacial activity, or direct anthropogenic intervention. Some Landsat-5 TM images can also show some noisy stripes at the border of the original images. In the middle of the Strait of Magellan (Paso Ancho), a higher number of false positives (16%) was detected than elsewhere. A possible cause for this could be due to local areas of higher photosynthetic activity associated with phytoplankton (Saggiomo et al.; 2011) or to floating kelp (Wichmann et al.; 2012).

The remote sensing approach used in this study was based on previous studies that used KF (Mora-Soto et al.; 2020) and NDVI (Nijland et al.; 2019), with high levels of overall accuracy at detecting kelp canopy extent in remote locations. This study, however, does not include ground-truthed estimations of kelp canopy biomass, frond density, and kelp density linked with satellite imagery. Those

variables could help to explain the environmental dynamics of the forests further, but would need a significant long term sampling effort through SCUBA diving, as done in previous works developed in the Southern California coastline (Bell et al.; 2018; Cavanaugh et al.; 2013,0). The baseline presented in this study could be expanded to a similar kind of environmental research in the future.

4.7.1 Anthropogenic changes and kelp persistence

A number of places in our area of study have experienced important landscape changes in the last two centuries caused by direct or indirect human interventions in the environment. Nevertheless, kelp forests have generally persisted in the same areas (Table 4.5). The main landscape alterations are the following:

- *Glacier retreat*: The German International Polar Year Expedition stayed at Royal Bay (South Georgia) between 1882 and 1883, where they mapped the bay including Molkte Harbour and Ross Glacier, a tidewater glacier. Although the map had some errors, the trends of this glacier show a slight advancement until 1965 (Hayward; 1983) followed by a high rate of retreat since the 1990s (Cook et al.; 2010) with an area loss of 0.88 $\pm$ 0.04 km^2 yr^{-1} between 2003 and 2016 (Farías-Barahona et al., 2020). The kelp forests of Molkte Harbour are still in the same location despite the distance to the ice front (currently < 10 km) (Figure 4.6). Other retreating glaciers with persistent kelp forests are Turnback and Purvis glaciers, among others.

- *Indigenous (Yaghan) people*: Yaghan people, local canoe sailors, lived traditionally in the intertidal environment of the Beagle Channel and the Cape Horn Archipelago (south of Tierra del Fuego). Kelp forests were an essential source of food and meant a central part of their worldview (Ojeda et al.; 2018). The most detailed charts of these coastlines were made on Goree

Table 4.5: List of sites with kelp forests from their first records on nautical charts, and anthropogenic and environmental changes occurred in the last two centuries.

Description	Site	Longitude	Latitude	Ecoregion
Glacier retreat	Moltke Harbour (Ross Glacier)	-36.0729	-54.5238	South Georgia
Glacier retreat	Fortuna Bay (Turnback Glacier)	-36.8292	-54.1286	South Georgia
Glacier retreat	Possession Bay (Purvis Glacier)	-37.1624	-54.0925	South Georgia
Glacier retreat	Beckmann Fjord	-37.1993	-54.0588	South Georgia
Glacier retreat	Sea Leopard Fjord	-37.2418	-54.0798	South Georgia
Sealing site	Larsen Harbour	-36.0114	-54.8399	South Georgia
Sealing site	Darthmouth Point	-36.4451	-54.3147	South Georgia
Sealing site	Discovery Point	-36.4848	-54.3042	South Georgia
Sealing site	Maiviken	-36.5147	-54.2464	South Georgia
Sealing site	Alert Cove	-36.6957	-54.1868	South Georgia
Sealing site	Tonsberg Point	-36.6540	-54.1681	South Georgia
Sealing site	Prion Island	-37.2622	-54.0312	South Georgia
Sealing site	Rosita Harbour	-37.4586	-54.0156	South Georgia
Sealing site	Right Whale Bay	-37.6876	-54.0044	South Georgia
Sealing site	Elsehul	-37.9664	-54.0264	South Georgia
Sealing site	Undine Harbour	-37.9687	-54.0343	South Georgia
Sealing site	Thetis Bay, Mitre Peninsula	-65.2159	-54.6374	Cha.F.S.Chi
Sealing site	Jason Harbour	-36.5835	-54.1940	South Georgia
Urban development	Stanley	-57.8651	-51.6928	Falkland Is. (Malvinas)
Urban development	Puerto Deseado (Port Desire)	-65.8703	-47.7608	Patagonian Shelf
Urban development	Agua Fresca (Freshwater Bay)	-70.9558	-53.3719	Cha.F.S.Chi
Urban development	Laredo Peninsula (Punta Arenas)	-70.6988	-52.8980	Cha.F.S.Chi
Whaling station	Godthul	-36.0729	-54.5238	South Georgia
Whaling station	Grytviken	-36.5017	-54.2814	South Georgia
Whaling station	Husvik	-36.7104	-54.1796	South Georgia
Whaling station	Stromness	-36.7126	-54.1596	South Georgia
Whaling station	Leith Harbour	-36.6865	-54.1413	South Georgia
Whaling station	Prince Olaf Harbour	-37.1570	-54.0606	South Georgia
Yaghan people	Goeree Roads, Navarino and Lennox Islands	-67.1075	-55.2707	Cha.F.S.Chi
Yaghan people	Wollaston Island	-67.2889	-55.7345	Cha.F.S.Chi
Yaghan people	Packsaddle Bay	-68.0974	-55.4489	Cha.F.S.Chi

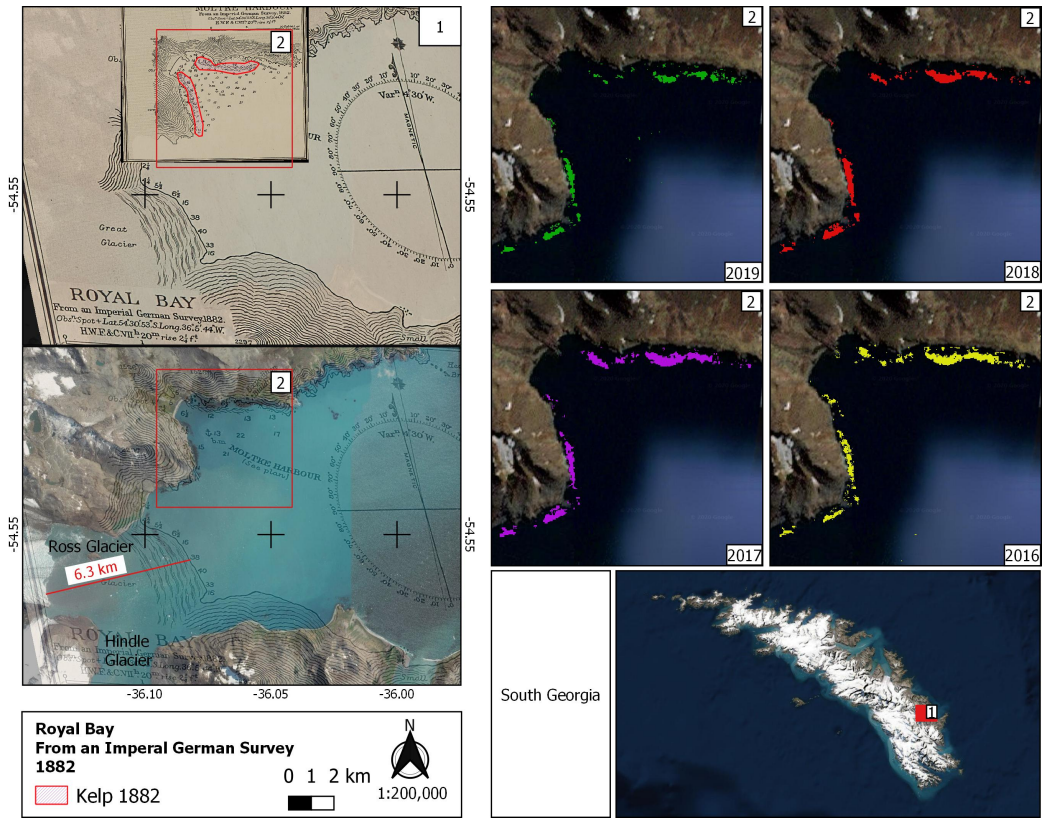


Figure 4.6: 1) Royal Bay and Moltke Harbour, South Georgia, as seen from the original georeferenced Imperial German Survey, 1882. The extent of kelp forests is indicated with a red contour. 2) Satellite-detected kelp forests, derived from the KF algorithm. The extent of kelp is indicated with green (2019), red (2018), purple (2017), and yellow (2016) pixels, respectively. The approximate distance between the front line of the Ross Glacier drawn in 1882 and the present time is 6.3 km. (Background image: Earthstar Geographics (TerraColor NextGen) imagery, ESRI).

Roads on the 7th, Packsaddle Bay on the 18th, and Middle Cove (Wollaston Island) on the 19th of February 1833, where Yaghans were in close contact with the HMS Beagle crew (FitzRoy; 1839). The number of Yaghan people declined dramatically after the first contacts with Europeans, Chileans, and Argentinians during the 19th and 20th centuries, and Yaghan descendants now live in Ushuaia (Argentina) and Puerto Williams and Puerto Natales

(Chile). Although we don't know if the Yaghan had a positive or negative impact on kelp forests, our results indicate that kelp forests have persisted in historical Yaghan areas.

- *Urban development*: The Beagle Expedition finished their surveys of South America and the Falkland Islands in 1834. Some years later, in 1843, the city of Port Stanley (Falkland Islands) was founded in Port William (Royle; 1985), and in 1848 the city of Punta Arenas (Chile) was founded in the Strait of Magellan (Martinic Beros; 2002). Both cities have seen population and infrastructure growth since their founding, but kelp forests persist around both settlements, as does the kelp forest near the city of Puerto Deseado (Argentina).

- *Whaling/sealing areas*: The Beagle anchored in Thetis Bay, between St. Vincent and St. Diego capes on 21st February 1834 (Keynes; 2001). Between 1940 and 1948, a pinniped slaughterhouse operated in the bay, where 200 people worked; more than 30,000 sea lions were killed until the installation was closed and abandoned (Vázquez and Santiago; 2014). The southern elephant seals (*Mirounga leonina*) and whales that were processed in South Georgia from the mid-nineteen to mid-twentieth centuries (Palomares and Pauly; 2015) in the factories of Leith, Grytviken, Husvik, Prince Olaf, and Stromness Harbours, among others, suffered a similar fate, all of which had detailed charts indicating kelp forests that are still present today.

Estimations of past distributions of sub-Antarctic kelp forests remain as open questions. Terrestrial references indicate that the maximum extent of the Patagonian Icefields occurred around 14,600 years BP and was followed by a relatively gradual warming (Glasser et al.; 2004) that opened coastal spaces for conifers and moorlands (Villagran; 2001), whereas closed-canopy Nothofagus forests in

Patagonia have been in place since ∼10,000 cal yr BP (Moreno et al.; 2019). Shell middens along the Beagle Channel indicate human occupation of the coastline during at least the last 6,500 years, with a stable marine biota (Estévez et al.; 2001). A 14,000 yr multiproxy record of seabird guano and tussac grass (*Poa flabellata*) in the Falkland Islands showed an abrupt establishment of *P. flabellata* and seabird colonies ∼5,000 yr BP (Groff et al.; 2020), which in turn could have meant massive nutrient inputs for kelp growth. In turn, seabirds like the kelp gull *Larus dominicanus* can forage on bivalves growing on kelp blades like *Gaimardia trapesina* (Friedlander et al.; 2020; Hockey; 1988). Molecular studies have suggested a northern hemisphere origin of giant kelp, with a later dispersal to the southern hemisphere (Astorga et al.; 2012; Coyer et al.; 2001; Macaya and Zuccarello; 2010). Specifically, (Coyer et al.; 2001) indicate that multiple inter-hemisphere crossings occurred between 3.1 Mya and as recent 0.01 Mya. More specific research is needed to complement these convergent lines to estimate an age of sub-Antarctic kelp forests.

The observed persistence does not necessarily imply that sub-Antarctic kelp forests are not threatened by local anthropogenic factors. To the north of our study area, kelp forests are harvested with different levels of protection in central and northern Chile. This has a strong overall influence over kelp forest morphology and biomass (Gouraguine et al.; 2021; Krumhansl et al.; 2016; Vásquez; 2008). The effect of marine traffic on kelp canopies in the region, particularly near the Strait of Magellan and the Cape Horn is a question that requires future research. The major impending threat to the region is probably the rapid expansion of salmon farming; however, overexploitation of fisheries stocks, destructive fishing practices, and threats associated with climate change will all require proactive management actions to mitigate potential negative impacts (Friedlander et al.; 2021). To sustain this ecosystem in the long term, it is imperative to develop specific

plans for conservation, like the creation of marine protected areas (Friedlander et al.; 2020,0; Rozzi et al.; 2007), regulation of kelp harvesting, intensive salmon farming, destructive fishing practices, and pollution (Hinojosa et al.; 2010; Iriarte et al.; 2010), evaluation of carbon sequestration and ecosystem services (Bayley et al.; 2021) as well as encouraging indigenous rights for the protection of the maritorio (seascape) in Patagonia.

4.8 Acknowledgements

We thank Nacho Juárez and Walter Huaraca (U. of Oxford), Giles Richardson (MAST), Rachel Keay, Ray Paice and the Archives and Research Department of UKHO; Alex Muñoz (National Geographic Pristine Seas), and Daphne Damm for their help at different stages of this project. We are very grateful for the careful, constructive anonymous reviews of the manuscript. This research is part of A.M-S's PhD funded by ANID-Becas Chile. Drone imagery collection from the Falklands Islands was undertaken by Neil Golding at SAERI, as part of the Darwin DPLUS065 Coastal Habitat Mapping project, grant aided by the Darwin Initiative through UK Government funding. Drone imagery collection from South Georgia was undertaken by Tom Hart (Penguin Watch). Thanks to volunteers of the Shallow Marine Surveys Group for assistance during collection of underwater ROV surveys in the Falkland Islands. The historic nautical charts, hydrographic surveys and aerial survey photography referred to can be accessed in the UK Hydrographic Office (UKHO) Archive.

References

Alonso Marchante, J. (2014). *Menéndez, rey de la Patagonia*, Catalonia, Santiago de Chile.

Astorga, M., Hernández, C. E., Valenzuela, C., Llautureo, J. A. and Westermeier, R. (2012). Origin, diversification, and historical biogeography of the Giant Kelps genus Macrocystis: Evidences from bayesian phylogenetic analysis, *Revista de biología marina y Oceanografía* **47**(3): 573–579.

Banzon, V. F., Reynolds, R. W., Stokes, D. and Xue, Y. (2014). A 1/4°-spatial-resolution daily sea surface temperature climatology based on a blended satellite and in situ analysis, *Journal of Climate* **27**(21): 8221 – 8228.

Barnes, D. K., Linse, K., Waller, C., Morely, S., Enderlein, P., Fraser, K. P. and Brown, M. (2006). Shallow benthic fauna communities of South Georgia Island, *Polar Biology* **29**(3): 223–228.

BAS (2020). South Georgia GIS.
URL: *https://www.sggis.gov.gs/*

Bayley, D., Brickle, P., Brewin, P., Golding, N. and Pelembe, T. (2021). Valuation of kelp forest ecosystem services in the falkland islands: A case study integrating blue carbon sequestration potential, *One Ecosystem* **6**: e62811.

Beaton, E. C., Kupper, F. C., van West, P., Brewin, P. E. and Brickle, P. (2020). The influence of depth and season on the benthic communities of a Macrocystis pyrifera forest in the Falkland Islands, *POLAR BIOLOGY* **43**(5): 573–586.

Bell, T. W., Allen, J. G., Cavanaugh, K. C. and Siegel, D. (2018). Three decades of variability in California's Giant Kelp forests from the Landsat satellites, *Rem. Sens. of Env.* p. 110811.

Benjamini, Y. and Hochberg, Y. (1995). Controlling the false discovery rate: a practical and powerful approach to multiple testing, *Journal of the Royal statistical society: series B (Methodological)* **57**(1): 289–300.

Brandon, M. A., M. E. J. T. P. N. . B. D. G. (2000). Physical Oceanographic conditions to the Northwest of the sub-Antarctic Island of South Georgia., *Journal of Geophysical Research: Oceans* **105**: 23983–23996.

Bridges, E. L. (1987). *The uttermost part of the earth*, Random House (UK).

Brown, M. B., Edwards, M. S. and Kim, K. Y. (2014). Effects of climate change on the physiology of Giant Kelp, Macrocystis pyrifera, and grazing by purple urchin, Strongylocentrotus purpuratus, *Algae* **29**(3): 203–215.

Buschmann, A. H., Pereda, S. V., Varela, D. A., Rodríguez-Maulén, J., López, A., González-Carvajal, L., Schilling, M., Henríquez-Tejo, E. A. and Hernández-González, M. C. (2014). Ecophysiological plasticity of annual populations of Giant Kelp (Macrocystis pyrifera) in a seasonally variable coastal environment in the Northern Patagonian Inner Seas of Southern Chile, *J. of Applied Phycology* **26**(2): 837–847.

Butler, C. L., Lucieer, V. L., Wotherspoon, S. J. and Johnson, C. R. (2020). Multi-decadal decline in cover of giant kelp macrocystis pyrifera at the southern limit of its australian range, *Marine Ecology Progress Series* **653**: 1–18.

Cárdenas, C. A. and Montiel, A. (2017). Coexistence in cold waters: animal forests in seaweed-dominated habitats in Southern high latitudes, *Marine Animal Forests: The Ecology of Benthic Biodiversity Hotspots* pp. 257–276.

Castilla, J. and Moreno, C. (1982). Sea urchins and *Macrocystis pyrifera*: experimental test of their ecological relations in Southern Chile, *Proceedings of*

the International Echinoderm Conference, Tampa Bay, Florida, USA, ed. JM Lawrence, pp. 257–263.

Cavanaugh, K. C., Kendall, B. E., Siegel, D. A., Reed, D. C., Alberto, F. and Assis, J. (2013). Synchrony in dynamics of Giant Kelp forests is driven by both local recruitment and regional environmental controls, *Ecology* **94**(2): 499–509.

Cavanaugh, K. C., Siegel, D. A., Reed, D. C. and Dennison, P. (2011). Environmental controls of giant-kelp biomass in the Santa Barbara Channel, California, *Mar. Ecology Progress Series* **429**: 1–17.

Chassignet, E. P., Hurlburt, H. E., Metzger, E. J., Smedstad, O. M., Cummings, J. A., Halliwell, G. R., Bleck, R., Baraille, R., Wallcraft, A. J., Lozano, C., Tolman, H. L., Srinivasan, A., Hankin, S., Cornillon, P., Weisberg, R., Barth, A., He, R., Werner, F. and Wilkin, J. (2009). US GODAE: Global Ocean Prediction with the HYbrid Coordinate Ocean Model (HYCOM), *Oceanography* **22**(2): 64–75.

Clapperton, C. M. (1990). Quaternary glaciations in the Southern Ocean and Antarctic Peninsula area, *Quaternary Science Reviews* **9**(2-3): 229–252.

Connell, J. H. and Sousa, W. P. (1983). On the evidence needed to judge ecological stability or persistence, *The American Naturalist* **121**(6): 789–824.

Cook, A. J., Poncet, S., Cooper, A. P. R., Herbert, D. and Christie, D. (2010). Glacier retreat on South Georgia and implications for the spread of rats, *Antarctic Science* **22**(3): 255–263.

Costa, M., Le Baron, N., Tenhunen, K., Nephin, J., Willis, P., Mortimor, J. P., Dudas, S. and Rubidge, E. (2020). Historical distribution of kelp forests on the coast of British Columbia: 1858-1956, *Applied Geography* **120**: 102230.

Coyer, J. A., Smith, G. J. and Andersen, R. A. (2001). Evolution of Macrocys-

tis spp.(phaeophyceae) as determined by its1 and its2 sequences1, *Journal of Phycology* **37**(4): 574–585.

Darwin, C. (1845). *The Voyage of the Beagle: Journal of Researches into the Natural History and Geology of the Countries Visited During the Voyage of HMS Beagle Round the World: Under the Command of Capt. Fitz Roy, R.N.*, GB.

Dayton, P. K. (1985a). Ecology of kelp communities, *Annu. Rev. Ecol. Syst.* **16**(1): 215–245.

Dayton, P. K. (1985b). The structure and regulation of some South American kelp communities, *Ecological monographs* **55**(4): 447–468.

Dayton, P. K., Mordida, B. and Bacon, F. (1994). Polar marine communities, *American Zoologist* **34**(1): 90–99.

Dillehay, T. D., Ramírez, C., Pino, M., Collins, M. B., Rossen, J. and Pino-Navarro, J. (2008). Monte Verde: seaweed, food, medicine, and the peopling of South America, *science* **320**(5877): 784–786.

Estévez, J., Piana, E., Schiavini, A. and Juan-Muns, N. (2001). Archaeological analysis of shell middens in the Beagle Channel, Tierra del Fuego Island, *International Journal of Osteoarchaeology* **11**(1-2): 24–33.

FitzRoy, R. (1839). *Narrative of the Surveying Voyages of His Majesty's Ships Adventure and Beagle Between the Years 1826 and 1836: Describing Their Examination of the Southern Shores of South America, and the Beagle's Circumnavigation of the Globe*, Vol. 2, H. Colburn.

Fraser, C. I., Morrison, A. K., Hogg, A. M., Macaya, E. C., van Sebille, E., Ryan, P. G., Padovan, A., Jack, C., Valdivia, N. and Waters, J. M. (2018). Antarctica's

ecological isolation will be broken by storm-driven dispersal and warming, *Nature climate change* **8**(8): 704–708.

Friedlander, A. M., Ballesteros, E., Bell, T. W., Caselle, J. E., Campagna, C., Goodell, W., Hüne, M., Muñoz, A., Salinas-de León, P. and Sala, E. (2020). Kelp forests at the end of the earth: 45 years later, *Plos one* **15**(3): e0229259.

Friedlander, A. M., Ballesteros, E., Bell, T. W., Giddens, J., Henning, B., Hüne, M., Muñoz, A., Salinas-de León, P. and Sala, E. (2018). Marine biodiversity at the end of the World: Cape Horn and Diego Ramírez Islands, *PloS one* **13**(1): e0189930.

Friedlander, A. M., Ballesteros, E., Goodell, W., Hüne, M., Muñoz, A., Salinas-de León, P., Velasco-Charpentier, C. and Sala, E. (2021). Marine communities of the newly created Kawésqar National Reserve, Chile: From glaciers to the Pacific Ocean, *PLOS ONE* **16**(4): e0249413.
URL: *https://doi.org/10.1371/journal.pone.0249413*

Fuller, W. A. (2009). *Introduction to statistical time series*, Vol. 428, John Wiley & Sons.

Gerard, V. and Kirkman, H. (1984). Ecological observations on a branched, loose-lying form of Macrocystis pyrifera (l.) c. agardh in New Zealand, *Botanica marina* **27**(3): 105–110.

Glasser, N. F., Harrison, S., Winchester, V. and Aniya, M. (2004). Late pleistocene and holocene palaeoclimate and glacier fluctuations in Patagonia, *Global and planetary change* **43**(1-2): 79–101.

Golding, N., Black, B., Blake, D., Brewin, P., Harte, M., Havercroft, H., James, R. and Jones, G. (2019). Long-term coastal habitat mapping and monitoring handbook. examples based on work undertaken in the Falkland Islands and South

Georgia. dplus065 coastal habitat mapping project, *Report*.
URL: *shorturl.at/wESW3*

González, H., Castro, L., Daneri, G., Iriarte, J., Silva, N., Tapia, F., Teca, E. and Vargas, C. (2013). Land–Ocean gradient in haline stratification and its effects on plankton dynamics and trophic carbon fluxes in Chilean Patagonian fjords (47–50 s), *Progress in Oceanography* **119**: 32–47.

González-Wevar, C. A., Hüne, M., Cañete, J. I., Mansilla, A., Nakano, T. and Poulin, E. (2012). Towards a model of postglacial biogeography in shallow marine species along the Patagonian province: lessons from the limpet Nacella Magellanica (Gmelin, 1791), *BMC Evolutionary Biology* **12**(1): 139.

Gorelick, N., Hancher, M., Dixon, M., Ilyushchenko, S., Thau, D. and Moore, R. (2017). Google Earth Engine: Planetary-scale geospatial analysis for everyone, *Rem. Sens. of Env.* **202**: 18–27.

Gouraguine, A., Moore, P., Burrows, M. T., Velasco, E., Ariz, L., Figueroa-Fábrega, L., Muñoz-Cordovez, R., Fernandez-Cisternas, I., Smale, D. and Pérez-Matus, A. (2021). The intensity of kelp harvesting shapes the population structure of the foundation species Lessonia trabeculata along the Chilean coastline, *Marine Biology* **168**(5): 66.
URL: *https://doi.org/10.1007/s00227-021-03870-7*

Groff, D. V., Hamley, K. M., Lessard, T. J. R., Greenawalt, K. E., Yasuhara, M., Brickle, P. and Gill, J. L. (2020). Seabird establishment during regional cooling drove a terrestrial ecosystem shift 5000 years ago, *Science Advances* **6**(43): eabb2788.
URL: *https://advances.sciencemag.org/content/advances/6/43/eabb2788.full.pdf*

Hamilton, S. L., Bell, T. W., Watson, J. R., Grorud-Colvert, K. A. and Menge,

B. A. (n.d.). Remote sensing: generation of long-term kelp bed data sets for evaluation of impacts of climatic variation, *Ecology* **101**(7): e03031.
URL: *https://esajournals.onlinelibrary.wiley.com/doi/abs/10.1002/ecy.3031*

Hansen, M. C., Potapov, P. V., Moore, R., Hancher, M., Turubanova, S. A., Tyukavina, A., Thau, D., Stehman, S., Goetz, S. J. and Loveland, T. R. (2013). High-resolution global maps of 21st-century forest cover change, *science* **342**(6160): 850–853.

Hayward, R. (1983). Glacier fluctuations in South Georgia, 1883–1974, *British Antarctic Survey Bulletin* **52**: 47–61.

Hinojosa, I. A., Pizarro, M., Ramos, M. and Thiel, M. (2010). Spatial and temporal distribution of floating kelp in the channels and fjords of Southern Chile, *Estuarine, Coastal and Shelf Science* **87**(3): 367–377.

Hockey, P. A. R. (1988). Kelp gulls Larus dominicanus as predators in kelp Macrocystis pyrifera beds, *Oecologia* **76**(1): 155–157.

Hodgson, D. A., Graham, A. G., Griffiths, H. J., Roberts, S. J., Cofaigh, C. Ó., Bentley, M. J. and Evans, D. J. (2014). Glacial history of sub-Antarctic South Georgia based on the submarine geomorphology of its fjords, *Quaternary Science Reviews* **89**: 129–147.

Hothorn, T., Hornik, K. and Zeileis, A. (2006). Unbiased recursive partitioning: A conditional inference framework, *Journal of Computational and Graphical statistics* **15**(3): 651–674.

Hothorn, T. and Zeileis, A. (2015). partykit: A modular toolkit for recursive partytioning in r, *The Journal of Machine Learning Research* **16**(1): 3905–3909.

Huovinen, P., Ramírez, J., Palacios, M. and Gómez, I. (2019). Satellite-derived mapping of kelp distribution and water optics in the glacier impacted Yende-

gaia fjord (Beagle channel, Southern Chilean Patagonia), *Science of The Total Environment* p. 135531.

Iriarte, J. L., González, H. E. and Nahuelhual, L. (2010). Patagonian fjord ecosystems in Southern Chile as a highly vulnerable region: Problems and needs, *AMBIO* **39**(7): 463–466.
URL: *https://doi.org/10.1007/s13280-010-0049-9*

Keynes, R. D. (2001). *Charles Darwin's Beagle Diary*, Cambridge University Press.

King, P. P., Stokes, P. and Fitz-Roy, R. (1836). Sketch of the surveying voyages of His Majesty's ships Adventure and Beagle, 1825-1836, *The Journal of the Royal Geographical Society of London* **6**: 311–343.

Krumhansl, K. A., Okamoto, D. K., Rassweiler, A., Novak, M., Bolton, J. J., Cavanaugh, K. C., Connell, S. D., Johnson, C. R., Konar, B., Ling, S. D., Micheli, F., Norderhaug, K. M., Pérez-Matus, A., Sousa-Pinto, I., Reed, D. C., Salomon, A. K., Shears, N. T., Wernberg, T., Anderson, R. J., Barrett, N. S., Buschmann, A. H., Carr, M. H., Caselle, J. E., Derrien-Courtel, S., Edgar, G. J., Edwards, M., Estes, J. A., Goodwin, C., Kenner, M. C., Kushner, D. J., Moy, F. E., Nunn, J., Steneck, R. S., Vásquez, J., Watson, J., Witman, J. D. and Byrnes, J. E. K. (2016). Global patterns of kelp forest change over the past half-century, *PNAS* **113**(48): 13785.

Lamy, T., Koenigs, C., Holbrook, S. J., Miller, R. J., Stier, A. C. and Reed, D. C. (2020). Foundation species promote community stability by increasing diversity in a Giant Kelp forest, *Ecology* **101**(5): e02987.

Leese, F., Kop, A., Wägele, J.-W. and Held, C. (2008). Cryptic speciation in a

benthic isopod from Patagonian and Falkland Island waters and the impact of glaciations on its population structure, *Frontiers in zoology* **5**(1): 19.

Macaya, E. C. and Zuccarello, G. C. (2010). DNA barcoding and genetic divergence in the Giant Kelp Macrocystis (Laminariales) 1, *J. of Phycology* **46**(4): 736–742.

Magallanes, G. R. (2020). SIG Magallanes.
URL: *http://www.sigmagallanes.cl/*

Martinic Beros, M. (1982). Antecedentes para la historia del conocimiento botánico y zoológico de la región del estrecho de Magallanes, *Anales del Instituto de la Patagonia*.

Martinic Beros, M. (2002). Breve historia de Magallanes.

Meier, W. J.-H., Grießinger, J., Hochreuther, P. and Braun, M. H. (2018). An updated multi-temporal glacier inventory for the Patagonian Andes with changes between the little ice age and 2016, *Frontiers in Earth Science* **6**: 62.

Miller, R. J., Lafferty, K. D., Lamy, T., Kui, L., Rassweiler, A. and Reed, D. C. (2018). Giant Kelp increases faunal diversity through physical engineering, *P. Biol. sciences* **285**(1874).

Moore, J. K., Abbott, M. R. and Richman, J. G. (1999). Location and dynamics of the Antarctic polar front from satellite sea surface temperature data, *Journal of Geophysical Research: Oceans* **104**(C2): 3059–3073.
URL: *https://agupubs.onlinelibrary.wiley.com/doi/abs/10.1029/1998JC900032*

Mora-Soto, A., Palacios, M., Macaya, E. C., Gómez, I., Huovinen, P., Pérez-Matus, A., Young, M., Golding, N., Toro, M. and Yaqub, M. (2020). A high-resolution global map of Giant Kelp (Macrocystis pyrifera) forests and

intertidal green algae (Ulvophyceae) with Sentinel-2 imagery, *Remote Sensing* **12**(4): 694.

Moreno, C. A. and Jara, F. (1984). Ecological studies on fish fauna associated with Macrocystis pyrifera belts in the South of fueguian Islands, Chile, *Marine ecology progress series. Oldendorf* **15**(1): 99–107.

Moreno, P., Simi, E., Villa-Martínez, R. P. and Vilanova, I. (2019). Early arboreal colonization, postglacial resilience of deciduous nothofagus forests, and the Southern westerly wind influence in central-east andean Patagonia, *Quaternary Science Reviews* **218**: 61–74.
URL: *http://www.sciencedirect.com/science/article/pii/S0277379119301222*

Nijland, W., Reshitnyk, L. and Rubidge, E. (2019). Satellite remote sensing of canopy-forming kelp on a complex coastline: A novel procedure using the Landsat image archive, *Rem. Sens. of Env.* **220**: 41–50.

Ojeda, F. and Santelices, B. (1984). Invertebrate communities in holdfasts of the kelp Macrocystis pyrifera from Southern Chile, *Marine ecology progress series. Oldendorf* **16**(1): 65–73.

Ojeda, J., Rozzi, R., Rosenfeld, S., Contadora, T., Massardo, F., Malebrán, J., González-Calderón, J. and Mansilla, A. (2018). Interacciones bioculturales del pueblo yagán con las macroalgas y moluscos: una aproximación desde la filosofía ambiental de campo, *Magallania (Punta Arenas)* **46**(1): 155–181.

Palacios, M., Osman, D., Ramírez, J., Huovinen, P. and Gómez, I. (2021). Photobiology of the Giant Kelp Macrocystis pyrifera in the land-terminating glacier fjord Yendegaia (Tierra del Fuego): A look into the future?, *Science of The Total Environment* **751**: 141810.

Palomares, M. L. D. and Pauly, D. (2015). Fisheries of the Falkland Islands and the South Georgia, South sandwich and South orkney Islands., *Report*.

Parnell, P. E., Miller, E. F., Cody, C. E. L., Dayton, P. K., Carter, M. L. and Stebbinsd, T. D. (2010). The response of giant kelp (macrocystis pyrifera) in southern california to low-frequency climate forcing, *Limnology and Oceanography* **55**(6): 2686–2702.

Pfister, C. A., Berry, H. D. and Mumford, T. (2018). The dynamics of kelp forests in the Northeast Pacific Ocean and the relationship with environmental drivers, *J. of Ecology* **106**(4): 1520–1533.

Potapov, P., Hansen, M. C., Laestadius, L., Turubanova, S., Yaroshenko, A., Thies, C., Smith, W., Zhuravleva, I., Komarova, A. and Minnemeyer, S. (2017). The last frontiers of wilderness: Tracking loss of intact forest landscapes from 2000 to 2013, *Science advances* **3**(1): e1600821.

Potapov, P., Yaroshenko, A., Turubanova, S., Dubinin, M., Laestadius, L., Thies, C., Aksenov, D., Egorov, A., Yesipova, Y., Glushkov, I., Karpachevskiy, M., Kostikova, A., Manisha, A., Tsybikova, E. and Zhuravleva, I. (2008). Mapping the World's intact forest landscapes by remote sensing, *Ecology and Society* **13**(2).
URL: *http://www.jstor.org/stable/26267984*

Quiñones, R. A., Fuentes, M., Montes, R. M., Soto, D. and León-Muñoz, J. (2019). Environmental issues in Chilean salmon farming: a review, *Reviews in Aquaculture* **11**(2): 375–402.
URL: *https://onlinelibrary.wiley.com/doi/abs/10.1111/raq.12337*

Revelle, W. and Revelle, M. W. (2015). Package 'psych', *The comprehensive R archive network* .

Royle, S. A. (1985). The Falkland Islands, 1833-1876: the establishment of a colony, *Geographical Journal* pp. 204–214.

Rozzi, R., Massardo, F., Mansilla, A., Anderson, C. B., Berghofer, A., Mansilla, M., Gallardo, M. R., Plana, J., Berghofer, U. and Arango, X. (2007). La reserva de biosfera cabo de hornos: un desafío para la conservación de la biodiversidad e implementación del desarrollo sustentable en el extremo austral de América, *Anales Del Instituto De La Patagonia* **35**(1): 55 – 70.

SAERI (2020). Coastal habitat mapping of the Falkland Islands.
URL: *shorturl.at/mnxM5*

Saggiomo, V., Santarpia, I., Saggiomo, M., Margiotta, F. and Mangoni, O. (2011). Primary production processes and photosynthetic performance of a unique periAntarctic ecosystem: the Strait of Magellan, *Polar Biology* **34**(9): 1255–1267.

Santelices, B. and Ojeda, F. (1984). Population dynamics of coastal forests *Macrocystis pyrifera* in Puerto Toro, Isla Navarino, Southern Chile, *Marine ecology progress series. Oldendorf* **14**(2): 175–183.

Spalding, M. D., Fox, H. E., Allen, G. R., Davidson, N., Ferdaña, Z. A., Finlayson, M., Halpern, B. S., Jorge, M. A., Lombana, A. and Lourie, S. A. (2007). Marine ecoregions of the World: a bioregionalization of coastal and shelf areas, *BioScience* **57**(7): 573–583.

Spearman, C. (1987). The proof and measurement of association between two things, *The American Journal of Psychology* **100**(3/4): 441–471.
URL: *http://www.jstor.org/stable/1422689*

Tadono, T., Nagai, H., Ishida, H., Oda, F., Naito, S., Minakawa, K. and Iwamoto, H. (2016). Generation of the 30 m-mesh global digital surface model by ALOS

prism, *Int. Archives of the Photogrammetry, Rem. Sens. and Spatial Inf. Sciences* **41**.

Tucker, C. J. (1979). Red and photographic infrared linear combinations for monitoring vegetation, *Remote Sensing of Environment* **8**(2): 127–150.
URL: *https://doi.org/10.1016/0034-4257(79)90013-0*

Van Tussenbroek, B. (1989a). The life-span and survival of fronds of Macrocystis pyrifera (Laminariales, phaeophyta) in the Falkland Islands, *British Phycological Journal* **24**(2): 137–141.

Van Tussenbroek, B. (1989b). Morphological variations of Macrocystis pyrifera in the Falkland Islands in relation to environment and season, *Marine Biology* **102**(4): 545–556.

Van Tussenbroek, B. (1989c). Observations on branched Macrocystis pyrifera (l.) c. agardh (Laminariales, phaeophyta) in the Falkland Islands, *Phycologia* **28**(2): 169–180.

Van Tussenbroek, B. (1989d). Seasonal growth and composition of fronds of Macrocystis pyrifera in the Falkland Islands, *Marine Biology* **100**(3): 419–430.

Van Tussenbroek, B. (1993). Plant and frond dynamics of the Giant Kelp, Macrocystis pyrifera, forming a fringing zone in the Falkland Islands, *European Journal of Phycology* **28**(3): 161–165.

Vásquez, J. A. (2008). Production, use and fate of Chilean brown seaweeds: resources for a sustainable fishery, *Nineteenth Int. Seaweed Symposium*, Springer, pp. 7–17.

Vázquez, M. and Santiago, F. (2014). Explotación industrial de pinnípedos en la factoría de bahía tethis (Tierra del Fuego, argentina): Una aproximación zooarqueológica, *Revista Chilena de Antropología* (29).

Vergés, A., Steinberg, P. D., Hay, M. E., Poore, A. G., Campbell, A. H., Ballesteros, E., Heck Jr, K. L., Booth, D. J., Coleman, M. A. and Feary, D. A. (2014). The tropicalization of temperate marine ecosystems: climate-mediated changes in herbivory and community phase shifts, *Proceedings of the Royal Society B: Biological Sciences* **281**(1789).

Villagran, C. (2001). Un modelo de la historia de la vegetación de la cordillera de la costa de Chile central-sur: la hipótesis glacial de darwin, *Revista Chilena de historia natural* **74**(4): 793–803.

Watson, J. E. M., Evans, T., Venter, O., Williams, B., Tulloch, A., Stewart, C., Thompson, I., Ray, J. C., Murray, K., Salazar, A., McAlpine, C., Potapov, P., Walston, J., Robinson, J. G., Painter, M., Wilkie, D., Filardi, C., Laurance, W. F., Houghton, R. A., Maxwell, S., Grantham, H., Samper, C., Wang, S., Laestadius, L., Runting, R. K., Silva-Chávez, G. A., Ervin, J. and Lindenmayer, D. (2018). The exceptional value of intact forest ecosystems, *Nature Ecology & Evolution* **2**(4): 599–610.
URL: *https://doi.org/10.1038/s41559-018-0490-x*

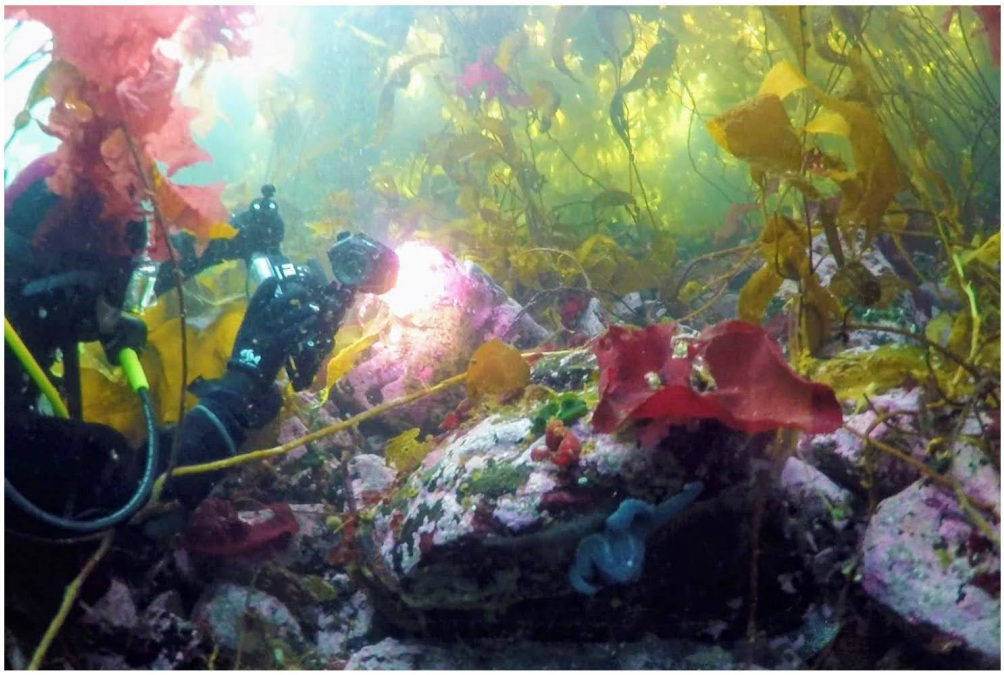
Wernberg, T., Krumhansl, K., Filbee-Dexter, K. and Pedersen, M. F. (2019). *Status and trends for the World's kelp forests*, Elsevier, pp. 57–78.

Wernberg, T., Smale, D. A., Tuya, F., Thomsen, M. S., Langlois, T. J., de Bettignies, T., Bennett, S. and Rousseaux, C. S. (2013). An extreme climatic event alters marine ecosystem structure in a global biodiversity hotspot, *Nature Climate Change* **3**(1): 78–82.
URL: *https://doi.org/10.1038/nclimate1627*

Wichmann, C.-S., Hinojosa, I. A. and Thiel, M. (2012). Floating kelps in Patagonian fjords: an important vehicle for rafting invertebrates and its relevance for

biogeography, *Marine Biology* **159**(9): 2035–2049.
URL: *https://doi.org/10.1007/s00227-012-1990-x*

Young, M., Cavanaugh, K., Bell, T., Raimondi, P., Edwards, C. A., Drake, P. T., Erikson, L. and Storlazzi, C. (2016). Environmental controls on spatial patterns in the long - term persistence of Giant Kelp in central California, *Ecological Monographs* **86**(1): 45–60.





5 | Chapter 5: Paper 3

5.1 Linking Statement: Soon to be submitted for publication.

In the previous chapter, I presented the case of the long-term stability of giant kelp in sub-Antarctic latitudes. In this chapter, I dive deeper into the main driver of environmental stress for giant kelp: sea surface temperature. This variable was analysed to address the third, fourth, and fifth aims of the thesis: **"To explore the differences of giant kelp forests between ecoregions and landscape units"; "to explore the long-term trends of giant kelp"; "To explore the future trends of sub-Antarctic kelp forests"**.

In this paper, I explored the main distribution and times of extreme warm and cold marine events in the last four decades (1981-2020) in the Channels and Fjords ecoregion. The ecoregion was divided in landscape units called *marine ecosystems*, following the previous classification made by Rovira and Herreros (2016) which considers the links among land, benthos, and ocean. Partitioning the space in this way allowed us to overview the past trends and to discuss the possible trends for kelp in the future.

This research allowed to detect an increment of extreme cold events in the past decade, in stark contrast with other marine ecoregions of the world ocean. Those events were likely driven by two indirect drivers of climate change: wind anomalies linked to increased westerlies and changes in the Polar Front, and glacier melting in the inner fjords and channels. Both drivers, along with global oceanic oscillations (e.g., El Niño - Southern Oscillation, ENSO), together with potentially new stressing factors for kelp ecosystems, open new areas for kelp research

in Patagonia.

This paper is advanced draft form and will soon be submitted to the *Journal of Geophysical Research: Oceans*.

5.1.1 Author Contribution Statement

A.M.-S. and M. M.-F. Conceived the ideas and conceptualised the research and methodology. A.M-S led the writing, collected and analysed the data, except for the wind variable which was contributed by C.A.; M.M-F. critically reviewed and edited the manuscript.

5.2 A song of wind and ice: geographical distribution of marine heatwaves (MHW) and marine cold-spells (MCS) in southwestern Patagonia and their possible effects on giant kelp forests

Alejandra Mora-Soto[*1], Catalina Aguirre [2, 3], José Luis Iriarte [4,5,6], Mauricio Palacios[4, 7, 8, 9], Marc Macias-Fauria[1]

[1] Biogeosciences Group, School of Geography and the Environment, University of Oxford, Oxford OX1 3QY, United Kingdom

[2] School of Ocean Engineering, Faculty of Engineering, Universidad de Valparaíso, Valparaíso, Chile

[3] Center for Climate and Resilience Research, Universidad de Chile, Santiago, Chile

[4] Centro FONDAP de Investigación en Dinámica de Ecosistemas Marinos de Altas Latitudes (IDEAL), Valdivia, Chile

[5] Centro COPAS-Sur Austral, Universidad de Concepción, Concepción, Chile

[6] Centro de Investigación en Ecosistemas de la Patagonia (CIEP), Francisco Bilbao 449, Coyhaique, Chile

[7] Programa de Doctorado en Biología Marina, Universidad Austral de Chile, Valdivia, Chile

[8] Facultad de Ciencias, Universidad de Magallanes, Punta Arenas, Chile

[9] Wildlife Conservation Society Marine Program- Chile.

* Corresponding author. Email: alejandra.morasoto@ouce.ox.ac.uk

5.3 Abstract

In contrast to other coastal regions of the world, convergent evidence from the southeast Pacific region (southwestern Patagonia) indicates that the giant kelp (*Macrocystis pyrifera*) ecosystem, a foundation species that predominates in the coastal border of its islands, channels, and fjords, has been persistent in area and associated biodiversity in the last decades. In this ecoregion, Sea Surface Temperature (SST) records have consistently remained below the upper thermal threshold for kelp survival; however, no studies have analysed the spatiotemporal variability of SST and their anomalies across the geographical diversity of the southwestern Patagonian coastline. In this study, we explored the geographical distribution of extreme warm and cold events in this region from latitudes 47° to 56° S in a range of 1,000 km. Specifically, we identified the dates and spatial distribution of Marine Heatwaves (MHW) and Marine Cold-Spells (MCS) from 1981 to 2020. Results show that extreme MHW events have been non-existent since the great El Niño year of 1998. Additionally, the 2014-2019 period has had more severe and extreme MCS events. These dynamics could partly explain the long-term persistence of this ecosystem. We discuss the origin of these events with a focus on three main processes: geographically constrained cold events caused by glacier melting, regional cold events caused by extreme winds linked to the position of the polar front, and extensive SST anomalies linked to planetary-scale events such as El Niño and La Niña. Overall, those processes were conducive to counteract global warming trends locally or regionally, and may result in southwestern Patagonia being a climatic refugium for the giant kelp ecosystem. We conclude by identifying new research challenges stemming from our findings.

5.4 Introduction

Increased evidence in the last decade has shown that the world ocean has been warming with more frequent and intense Marine Heatwaves (MHW). These events, sensu Hobday et al. (2016), are defined as discrete prolonged anomalously warm water events that occur in a particular location. A flourishing corpus of methodologies and analyses has arisen in the last years to explain their causes, signalling blocking high-pressure systems, oceanic oscillations such as El Niño, and shifts in winds and currents, as well as their disturbance effects on foundation species such as corals, seagrasses and kelp (Holbrook et al.; 2020). Much uncertainty remains about Marine Cold-Spells (MCS), which appear to co-occur in nearshore waters caused by coastal upwelling, and which have been associated with enhanced primary production, as observed in the coastlines of South Africa and Western Australia (Feng et al.; 2021; Schlegel et al.; 2017).

Even less is known about the southeast Pacific region in southwestern Patagonia, which was less affected by MHW in the period 1982-2016 than most regions in the world ocean (Oliver et al.; 2018), with less frequency and duration (Marin et al.; 2021) and less thermal displacement (Jacox et al.; 2020). Additionally, climate models show that this region will experience less heat intensity than other areas of the ocean in the next century (Oliver et al.; 2019). Forced upwelling and northwards cold water advection by the Antarctic Circumpolar Current (ACC) have been proposed as causing such lack of warming trends (Armour et al.; 2016; Oliver et al.; 2019); alternatively, internal ocean variability may be linked to a temporal hiatus over a general warming pattern (Marin et al.; 2021). However, no previous study has investigated the location and intensity of MHW and MCS with a focus on the long and complex coastline of islands, channels, and fjords of Patagonia, which constitutes one of the least studied marine ecoregions in the

world (Escribano et al.; 2003; Iriarte et al.; 2014).

The coastline of this marine ecoregion, also known as Channels and Fjords of Southern Chile (Spalding et al.; 2007), is conspicuously bordered by the least disturbed giant kelp (*Macrocystis pyrifera*) forests on the planet (Dayton; 1985; Mora-Soto et al.; 2020). A study carried out on giant kelp in the southernmost coast of Tierra del Fuego and Isla de Los Estados in 2018 compared densities and holdfast diameter of giant kelp with previous surveys performed in 1973; there were no significant differences between these two surveys conducted 45 years apart (Friedlander et al.; 2020). Moreover, a comparison between present-day giant kelp forests and giant kelp forests drawn in 19th century nautical charts in the Strait of Magellan and Cape Horn archipelago determined that at least 84% of the kelp forests showed spatial overlap (Mora-Soto et al., *Chapter 4*). The observed marine biodiversity of these forests gives support to consider that these are one of the last intact ecosystems on Earth (Friedlander et al.; 2018,0).

In contrast, at other latitudes kelp forests are experiencing the direct and indirect effects of ocean warming, such as decreased abundances, contraction of the historical range of distribution (Wernberg et al.; 2013), increased grazing from herbivorous fish and sea urchins (Rogers-Bennett and Catton; 2019; Vergés et al.; 2014), and/or competition with invasive species, such as turf-forming algae (Filbee-Dexter and Wernberg; 2018). So far, however, there are no reports of climate-driven changes in the kelp forests of the southwestern coastline of South America (see a review in Smale (2019)), although some populations in central and northern Chile are under direct pressures of anthropogenic origin (Pérez-Matus et al.; 2017; Vásquez; 2008; Vásquez et al.; 2012). For this reason, it is important *i)* to determine the spatiotemporal variability of sea surface temperatures in the south of the continent, as it can directly and/or indirectly affect giant kelp, and *ii)* to identify the drivers of those anomalies.

The present study provides a geographical overview of warm and cold extreme events in southwestern Patagonia during the last four decades. Specifically, our aim is to outline the spatial patterns and trends of these anomalies, in order to discuss their possible causes and the impacts on the giant kelp forests of this ecoregion.

5.5 Methodology

5.5.1 Area of study

The area of study spans the marine ecoregion of Channels and Fjords of Southern Chile (Spalding et al.; 2007), from the Gulf of Penas to the Cape Horn archipelago (47°to 56°S; $\sim$ 1,000 km in straight line) and a longitudinal range from the Pacific Ocean (75°W) to the eastern entrance of the Strait of Magellan (68°W). This region is dominated by the Andes mountain range, which acts as a strong orographic barrier for the ACC and the dominant eastward atmospheric circulation. As a consequence, the western side of the Andes receives permanent strong westerly winds and annual rainfall accumulations that range from 6,000 to 7,000 mm at sea level, while the eastern side is under a rain shadow effect (Schneider et al.; 2003). The mountain range comprises the Northern and Southern Patagonian Icefields and numerous glaciers, as well as Cordillera Darwin in Tierra del Fuego. Glaciers in the region show different rates of retreat, and even some advances (Bown et al.; 2014; Sakakibara and Sugiyama; 2014). The coastal geomorphology is characterized by the presence of fjords, channels, straits and embayments; beyond the presence of giant kelp forests along the coastal border, the almost vertical deep underwater walls of the fjords are habitat for a high marine biodiversity including cold-water hydrocorals (Häussermann and Försterra; 2007).

Rovira and Herreros (2016), integrating previous studies and expert knowledge, subdivided this ecoregion in marine ecosystems, defined as spatial units encompassing similar areas of benthic depth, type of substrate, main geoforms, sea-coast interface, and ecological processes (figure 5.1). From north to south, these are: Gulf of Penas, an exposed and turbulent area open to the Pacific Ocean; Offshore and Inner coast Kaweskar, in the archipelagos and fjords near the Southern Patagonian Ice Field; the Western, Central, Eastern, and Bahía Inutil sections of the Strait of Magellan; and the Magellanic areas, subdivided among Offshore Magellan, the Beagle Channels and Canal Ballenero, and the areas surrounding the Cape Horn at the end of the continent (Nassau Hornos). Hence, we consider ten main marine ecosystems covering 73% of the total Channels and Fjords ecoregion; we excluded smaller areas like inner fjords and sounds due to the lack of satellite-detected SST data (see below), as well as the Atlantic side of this ecoregion (eastern Tierra del Fuego and Isla de Los Estados). We further limited our study area to a bathymetric range down to 200m depth, since we focus on giant kelp habitat.

5.5.2 MHW and MCS definition and characterisation

In this study, we used the classification of MHW defined as "a prolonged discrete anomalously warm water event that can be described by its duration, intensity, rate of evolution and spatial extent" by Hobday et al. (2016). MCS follow the same definition, except for being "anomalously cold water events" (Schlegel et al.; 2017). They are identified when a daily climatological time series exceeds a threshold of the 90th (MHW), or fall below the 10th percentile (MCS), for more than 5 days. This is calculated in a climatological-centred window of 11 days where the mean and the threshold are calculated in a satellite-derived SST series for at least 30 years. In this study, we used the complete time series from 1

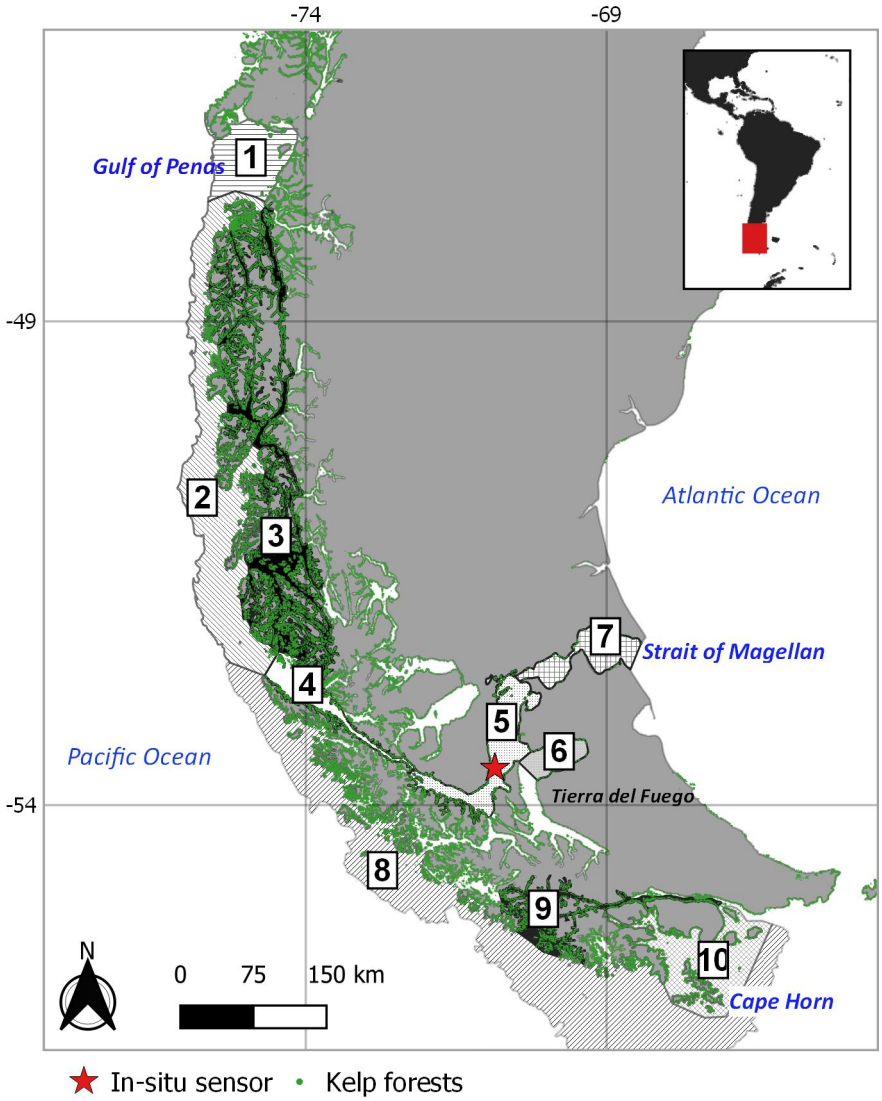


Figure 5.1: Figure 1. Map of the marine ecosystems mentioned in this study: 1) Gulf of Penas; 2) Offshore Kaweskar; 3) Inner Channels Kaweskar; 4) Western Strait; 5) Central Strait; 6) Bahia Inutil; 7) Eastern Strait; 8) Offshore Magellan; 9) Nearshore Beagle Ballenero; 10) Nearshore Nassau Hornos. The in-situ sensor is indicated with a red star; the centroids of each satellite-detected kelp forest are indicated with green points.

September 1981 to 30 December 2020. Further, MHW (MCS) are categorized as Category I, II, III and IV when the local difference between the intensity of the MHW (MCS) and the climatological mean is one, two, three or four times or more

than the climatological 90th (10th) percentile, respectively, using as reference the maximum intensity (*I max*), which is specific to the location and time of the year where/when is calculated. A detailed explanation on this method and classification is given by Hobday et al. (2016,0). We obtained SST measurements from the NOAA CDR OISST v02r01: Optimum Interpolation Sea Surface Temperature (Banzon et al.; 2014). This dataset was elaborated with observations from ships and buoys, and satellite observations, and corrected with an optimum interpolation analysis to deal with irregularly spaced data. We extracted daily mean SST per marine ecosystem through zonal statistics, with a spatial resolution of 0.25 arc degrees, using a Google Earth Engine script (Gorelick et al.; 2017). Despite the vast temporal coverage, we found a gap of data between 31-Dec-1984 to 01-Sep-1985, not included in the analysis.

To explore the accuracy of satellite-detected SST data in the inner waters of Patagonia, which could be potentially less well remotely sensed than the open seas of the Southern Hemisphere (Banzon et al.; 2014), we compared in-situ data from a conductivity, temperature, and depth (CTD) SeaBird sensor (SeaBird SBE model 19) at the surface (50 cm), located at the central part of the Strait of Magellan with an SST satellite pixel at the same location (53°38' 16"S, 70°51' 29.9"W; Figure 5.1). To our knowledge, this is the only permanent CTD sensor with a temporal range of more than a year in our area of study. The *in-situ* series was elaborated with monthly SST measurements starting in January 2018 to January 2020. A Pearson's correlation and a linear model were applied comparing daily in-situ/satellite records.

Computations of MHW and MCS, as well as their categories of intensity according to Hobday et al. (2018), were calculated using the heatwaveR package in R (Schlegel and Smit; 2018). Descriptive statistics and simple linear regressions were used to explore general trends of MHW and MCS per year, selecting cate-

gories II (strong), III (severe), and IV (extreme) for our analysis (Hobday et al.; 2018; Schlegel et al.; 2017). Choropleth maps per marine ecosystem were created to identify the spatial patterns of these events in QGIS version 3.14.15. Additionally, category III and IV events were examined using NOAA OISST anomaly maps at 0.25 arc degrees, calculating the per-pixel difference between the start and end dates of the event and the same averaged SST days during the period 1981-2020. Data were downloaded and processed in R using the package rgee (Aybar et al.; 2020).

Finally, we compared MHW and MCS categories III and IV with the regional surface wind conditions to determine if those events could be explained by wind anomalies. We employed the variables of northward (V10) and eastward (U10) winds 10 m above the surface, computed each 6 hours, from the ERA5 reanalysis for the period 1981–2020, and obtained anomalies by subtracting the averaged values for the days of the event from start to end minus the same time range averaged for the complete period. The ERA5 reanalysis is generated by the European Centre for Medium-Range Weather Forecast (ECMWF) and consists of a global-scale regular grid of 0.25° spatial resolution (Hersbach et al.; 2020). Data were also downloaded and processed in R:rgee. The extent of the giant kelp forest coverage (Figure 5.1) per ecosystem was computed from a kelp layer derived from Sentinel-2 imagery spanning the period 2015-2019 (Mora-Soto et al.; 2020). This layer was clipped per marine ecosystem to obtain an estimate of the total area employing an ellipsoidal WGS-84 datum. We analysed the main geographical and oceanographic characteristics of each ecosystem to discuss the observed MHW and MCS trends, and possible effects on giant kelp forests.

5.6 Results

5.6.1 Overview of SST per marine ecoregion

Satellite and in-situ SST measurements in the Strait of Magellan were highly correlated (Pearson's r = 0.93, p-value < 0.005, N= 22). This relationship can be expressed as a linear model (SST in situ = 1.386 + 0.837*SST Satellite). That is, while in situ SST variability was very well captured by satellite data, observed temperatures were slightly overestimated by satellite data when they were $\sim <$ 8ºC and slightly underestimated when they were $\sim >$8ºC (Supplementary Material A.3.1). Total mean temperature of the complete area of study was 8.2°C, with maximum mean temperature in Gulf of Penas (10.8°C) and minimum mean in Eastern Strait of Magellan (7.25°C), in a descending pattern from north to south and west to east. Daily maximum temperature was 16.7°C in Gulf of Penas (22-Jan-2016) and minimum temperature was 0.72°C in Western Strait of Magellan (07-Jul-2015) throughout the entire period of study (Figures 5.2 and 5.3).

5.6.2 Overview of MHW and MCS in Southwestern Patagonia (1981 to 2020)

5.6.2.1 Marine Heatwaves (MHW)

A total of 150 MHW events were detected in the area of study. Among them, 135 were category II (strong), 13 category III (severe) and 2 category IV (extreme). The years with the highest frequency of MHW were 1998 (20), 2020 (15), 2006 (14) and 2016 (13), whereas the years with severe events were 1984 (2), 1998 (7), 2016 (3), and 2020 (1) (Figure 5.4 and Table 5.1). The two recorded extreme MHW events occurred in 1984 and in 1998.

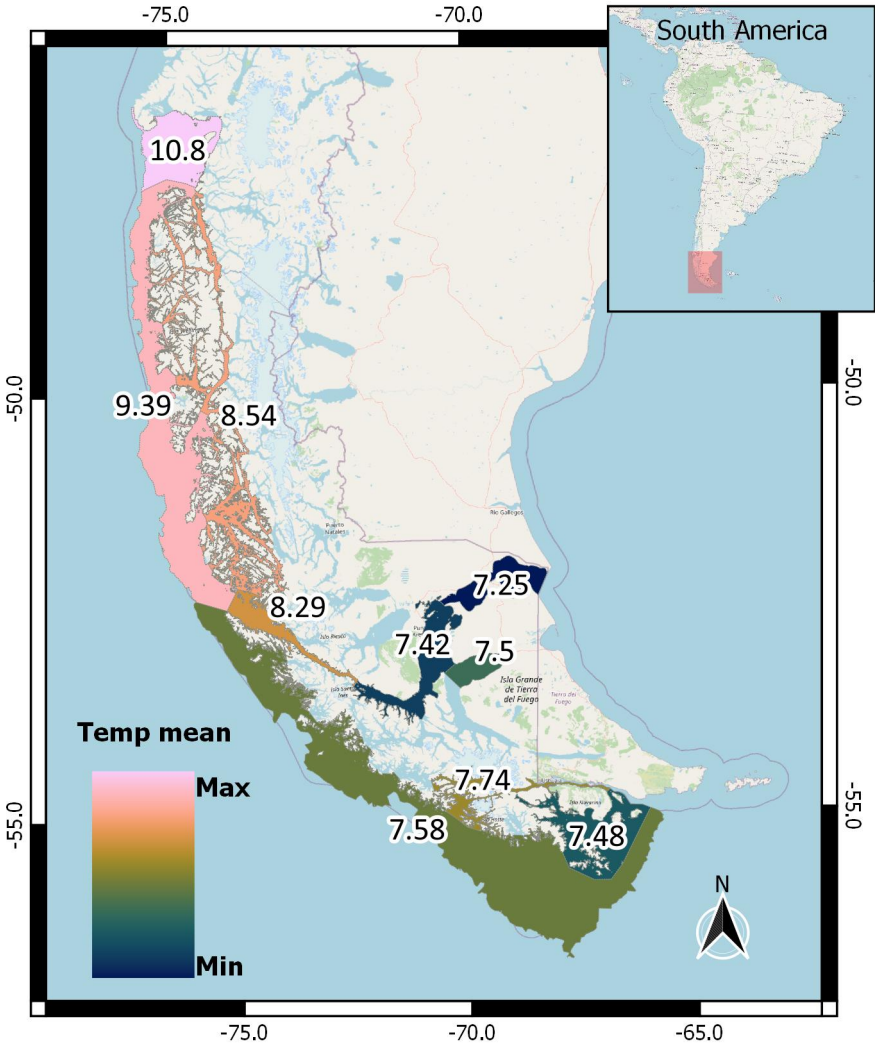


Figure 5.2: Map of mean SST per marine ecosystem in the period 1981-2020. Each label in the map indicates the mean temperature per ecosystem. See Figure 1 for marine ecosystem name. Background map: © OpenStreetMap contributors.

The period with the most severe and extreme events occurred in July-September 1998 (winter on a strong El Niño year) and extended over almost all the marine ecosystems of our area of study, from Gulf of Penas to Nearshore Nassau-Hornos, with a maximum intensity of 2.42°C above the climatological mean (Nearshore Nassau-Hornos), and a maximum period of 181 days (Eastern Strait of Magellan). December 1984 (spring/summer) was also highly anomalous, with an event that

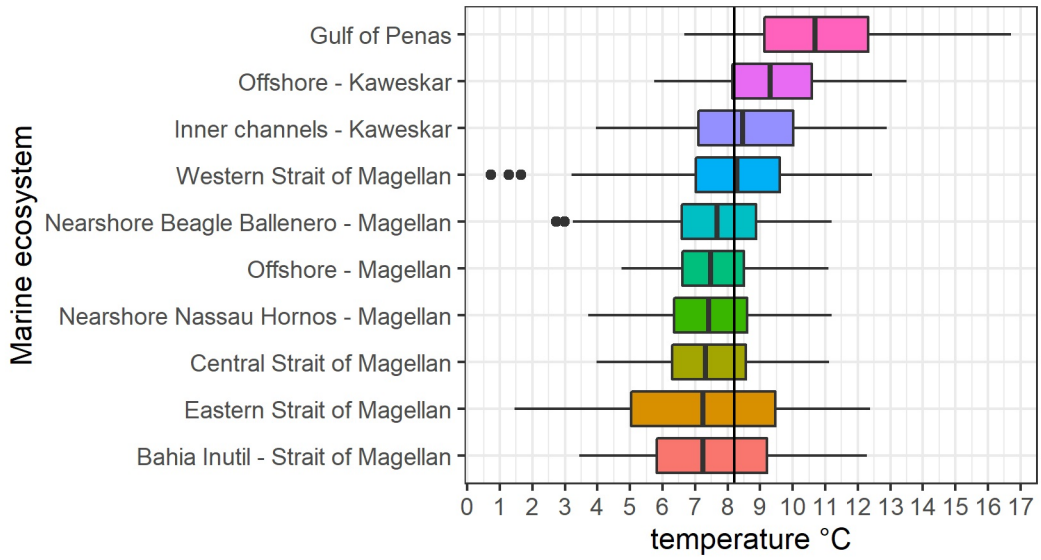


Figure 5.3: Box and whisker plot of daily SST 1981-2020 (in degree Celsius) per marine ecosystem. The vertical line shows temperature mean for the total of the area of study (8.2°C).

achieved a maximum intensity (SST anomaly) of 2.6°C and lasted for 16 days (Central Strait of Magellan).

There were no extreme events recorded in the period 1999 to 2020, but severe events were recorded in January 2016 (Offshore Kaweskar and Gulf of Penas) during summer on a strong El Niño year, November 2016 (Gulf of Penas), and June 2020 (Nearshore Beagle Ballenero). These events lasted for a maximum of 35 days. Choropleth maps (Figure 5.5) show that most of the MHW category II events occurred near the Gulf of Penas in the northern part of our area of study (Figure 5.5a), whereas the severe and extreme events were in the Central Strait of Magellan and Nassau Hornos (Figures 5.5b, 5.5c).

Table 5.1: MHW events, categories III and IV per ecosystem in the period 1982-2020. Start, peak, end date= days of the event (peak day in bold); i_max = maximum intensity [°C]; var = Standard deviation; duration= total days of the event (note that there could be gap days in the duration of the event). More details of each event are disaggregated in Supplementary Material A.3.2.

event name	**start date**	**peak date**	**end date**	**category**	**i_max**	**var (sd)**	**duration**	**season**	**ecosystem**
E2 1984b	15-12-1984	26-12-1984	30-12-1984	IV Extreme	2.62	0.53	16	Spring	Central Strait
E3 1984	18-12-1984	26-12-1984	30-12-1984	III Severe	2.64	0.44	13	Spring	Bahia Inutil - Strait
CE2 1984	15-12-1984	27-12-1984	30-12-1984	III Severe	2.53	0.52	16	Spring	Offshore Kaweskar
CE1 1998b	24-05-1998	05-07-1998	12-09-1998	III Severe	2.19	0.4	112	Fall/ Winter	Gulf of Penas
CE3 1998a	10-04-1998	05-07-1998	11-08-1998	III Severe	2.32	0.38	124	Fall/ Winter	Offshore Magallanes
BH2 1998	14-04-1998	13-07-1998	06-09-1998	IV Extreme	2.42	0.4	146	Fall/ Winter	Nearshore Nassau Hornos
C1 1998b	10-06-1998	14-07-1998	13-09-1998	III Severe	3.01	0.57	96	Fall/ Winter	Inner Channels Kaweskar
E4 1998b	17-06-1998	14-07-1998	05-08-1998	III Severe	3.84	0.72	50	Fall/ Winter	Western Strait
BH1 1998	02-06-1998	24-07-1998	03-08-1998	III Severe	2.93	0.62	63	Fall/ Winter	Nearshore Beagle Ballenero
E2 1998b	12-04-1998	31-07-1998	14-09-1998	III Severe	1.58	0.22	156	Fall/ Winter	Central Strait
E1 1998	19-03-1998	05-09-1998	15-09-1998	III Severe	2.35	0.3	181	Winter	Eastern Strait
CE2 2016a	14-01-2016	21-01-2016	08-02-2016	III Severe	2.5	0.45	26	Summer	Offshore Kaweskar
CE1 2016a	12-01-2016	22-01-2016	15-02-2016	III Severe	3.62	0.63	35	Summer	Gulf of Penas
CE1 2016d	20-11-2016	27-11-2016	11-12-2016	III Severe	2.92	0.59	22	Spring	Gulf of Penas
BH1 2020b	23-05-2020	11-06-2020	13-06-2020	III Severe	3.68	0.85	22	Fall	Nearshore Beagle Ballenero

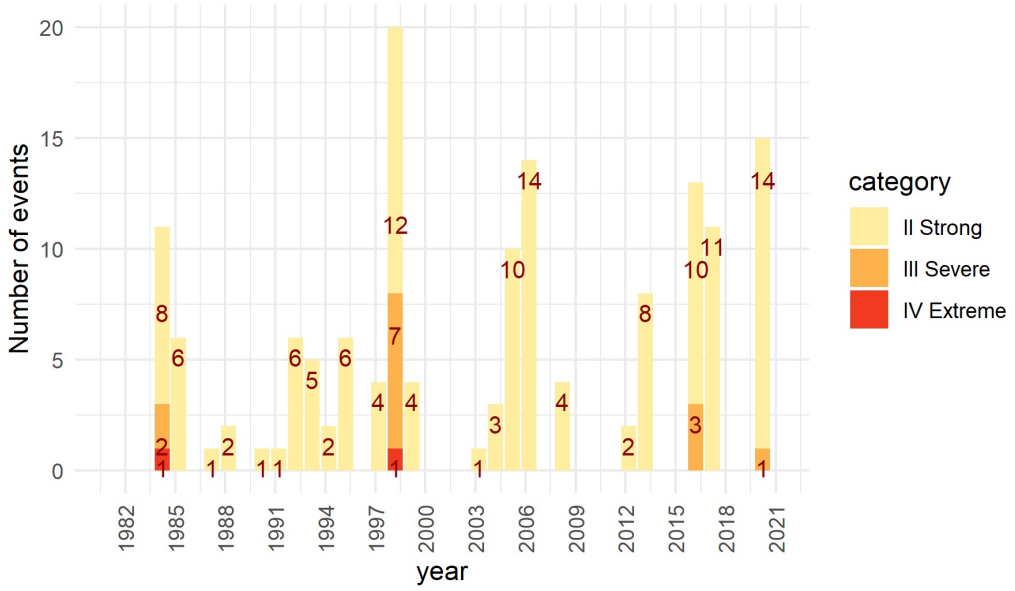


Figure 5.4: Number of events categories II (strong), III (severe) and IV (extreme) for the period 1982-2020 per MHW for the total of ecosystems in the area of study.

5.6.2.2 Marine cold spells (MCS)

There were 163 MCS events during the period 1981-2020 in the area of study; 138 category II (strong), 17 category III (severe) and 8 category IV (extreme) events. The year with the highest frequency of MCS was 1984 (18), followed by 1982 (15), 2009 (10), 2011 (10) and 2014 (10). The years with the most severe events were 1982 (4) and 2019 (3). The years 1982, 2014, 2015, 2016, 2017, 2018 and 2019 recorded extreme events. The frequency of these events in the last decade is remarkable in an overall warming planet. Among them, the two events of 1982 occurred in the Inner Channels Kaweskar and Bahia Inutil, and the events from 2014 to 2019 were in Nassau-Hornos (3) and one each in Inner channels-Kaweskar, Beagle Ballenero, and Western Strait of Magellan, the latter of which with the event with maximum intensity (-5.93°C) in a relatively short period (16 days). All of these events occurred in the fall to winter midseason (Tables 5.2 and

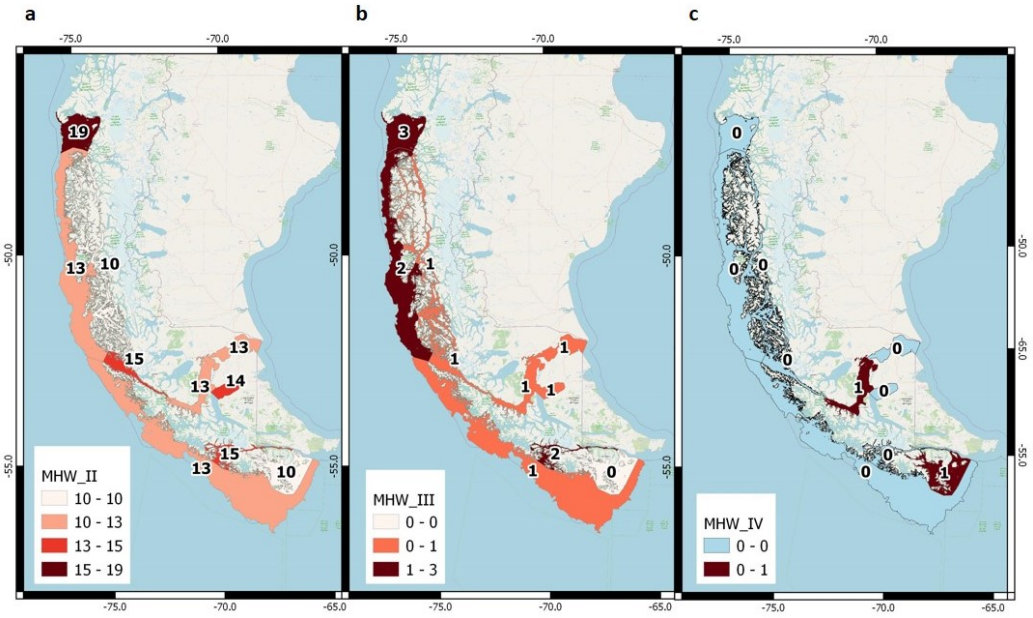


Figure 5.5: Choropleth map labelled with the count of MHW category and ecosystem for the period 1981-2020. MHW, categories II (strong, a), III (severe, b) and IV (extreme, c). Each colour legend and labels in bold indicate the number of events per ecosystem. Background map: © OpenStreetMap contributors.

5.3; Figure 5.6; supplementary material).

Choropleth maps show that category II events are concentrated in the Inner Channels Kaweskar (Figure 5.7a), and categories III and IV have more presence in the Inner Channels Kaweskar, Beagle Ballenero, Western Strait of Magellan and Nassau Hornos (Figures 5.7b and 5.7c).

5.6.3 SST, U10 and V10 Anomaly maps for severe and extreme events

We found four main wind-SST patterns associated with warm and cold events. These are displayed in more detail in Supplementary Material (A.3.2).

- *Cold events with strong winds:* We found a predominance of zonal winds

Table 5.2: MCS events, categories III and IV per ecosystem in the period 1982-2020. Start, peak, end date= days of the event (peak day in bold); i_max = maximum intensity [°C]; var = Standard deviation; duration= total days of the event (note that there could be gap days in the duration of the event). More details of each event are disaggregated in Supplementary Material A.3.2.

event name	start date	peak date	end date	category	i_max	var (sd)	duration	season	name
BH2 1981	08-10-1981	10-10-1981	19-10-1981	III Severe	-1.79	0.27	12	Spring	Nassau Hornos
E4 1981	08-10-1981	10-10-1981	13-10-1981	III Severe	-2.75	0.64	6	Spring	Western Strait
CE2 1982a	01-04-1982	02-04-1982	06-04-1982	III Severe	-2.43	0.75	6	Fall	Offshore Kaweskar
E4 1982b	01-04-1982	02-04-1982	13-04-1982	III Severe	-3.51	0.98	13	Fall	Western Strait
C1 1982	01-04-1982	03-04-1982	07-04-1982	IV Extreme	-3.34	0.62	7	Fall	Inner Channels Kaweskar
CE1 1982a	19-04-1982	20-04-1982	23-04-1982	III Severe	-2.83	0.33	5	Fall	Gulf of Penas
E1 1982b	05-07-1982	26-07-1982	19-10-1982	III Severe	-2.36	0.41	107	Winter/ Spring	Eastern Strait
E3 1982	20-09-1982	21-09-1982	25-09-1982	IV Extreme	-1.84	0.26	6	Winter	Bahia Inutil Strait
E1 1984b	04-05-1984	17-08-1984	02-11-1984	III Severe	-2.56	0.44	183	Fall/ Spring	Eastern Strait
CE1 1991	29-05-1991	31-05-1991	16-06-1991	III Severe	-2.47	0.62	19	Fall	Gulf of Penas
BH2 1995a	18-04-1995	22-04-1995	26-04-1995	III Severe	-1.94	0.57	9	Fall	Nassau Hornos
E4 2007b	13-12-2007	17-12-2007	23-12-2007	III Severe	-2.83	0.62	11	Spring	Western Strait
E3 2008	18-08-2008	29-08-2008	05-09-2008	III Severe	-1.85	0.39	19	Winter	Bahia Inutil Strait
E3 2011	03-05-2011	09-05-2011	11-05-2011	III Severe	-1.84	0.45	9	Fall	Bahia Inutil Strait
BH2 2014	09-02-2014	26-03-2014	21-04-2014	IV Extreme	-2.47	0.27	72	Summer/ Fall	Nassau Hornos
E4 2015	04-07-2015	07-07-2015	19-07-2015	IV Extreme	-5.93	1.4	16	Winter	Western Strait
C1 2015b	12-08-2015	23-08-2015	06-09-2015	III Severe	-2.58	0.41	26	Winter	Inner Channels Kaweskar

Table 5.3: Table 5.2 (cont.)

event name	start date	peak date	end date	category	i_max	var (sd)	duration	season	name
BH1 2015	23-08-2015	27-08-2015	28-08-2015	III Severe	-2.53	0.62	6	Winter	Nearshore Beagle Ballenero
BH2 2016	14-04-2016	18-04-2016	09-05-2016	IV Extreme	-4.65	1.26	26	Fall	Nassau Hornos
BH1 2017	05-08-2017	07-08-2017	18-08-2017	IV Extreme	-3.43	0.86	14	Winter	Nearshore Beagle Ballenero
C1 2018d	08-03-2018	06-04-2018	19-05-2018	IV Extreme	-4.04	0.99	73	Summer/ Fall	Inner Channels Kaweskar
BH2 2019a	20-02-2019	24-02-2019	28-02-2019	III Severe	-2.12	0.61	9	Summer	Nassau Hornos
BH2 2019b	13-04-2019	19-04-2019	21-04-2019	IV Extreme	-2.4	0.6	9	Fall	Nassau Hornos
E2 2019	02-06-2019	05-06-2019	07-06-2019	III Severe	-2.09	0.51	6	Fall	Central Strait
BH1 2019	15-08-2019	18-08-2019	21-08-2019	III Severe	-2.89	0.75	7	Winter	Nearshore Beagle Ballenero

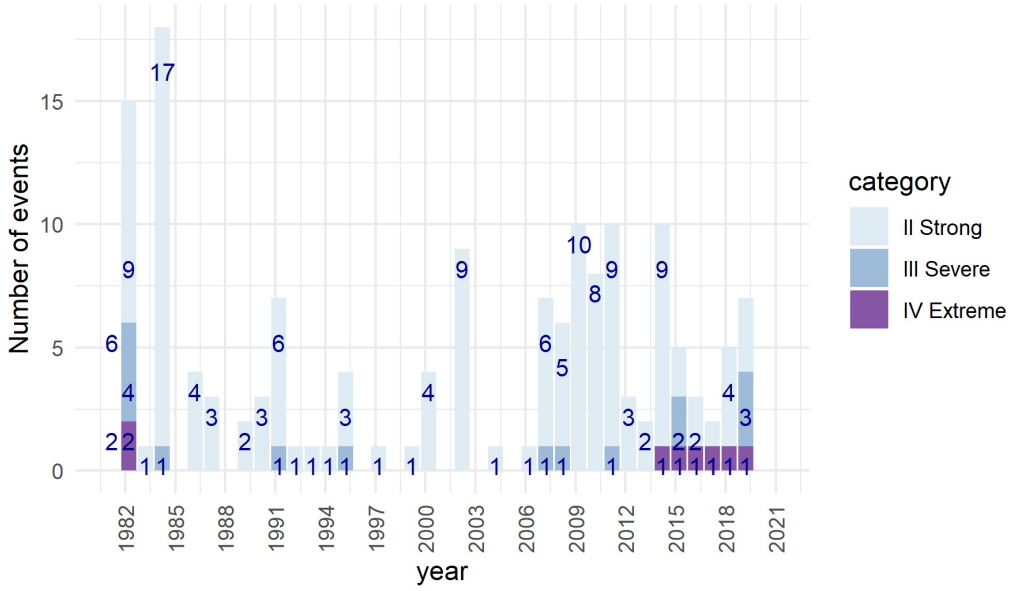


Figure 5.6: Number events categories II (strong), III (severe) and IV (extreme) for the period 1982-2020 per A) MHW; B) MCS for the total of ecosystems in the area of study.

(U10) either in their positive (west to east) to negative (east to west) flows, and positive northward winds (V10), in the southernmost ecosystems of Nearshore Nassau-Hornos, Beagle Ballenero, Bahía Inútil and Western Strait. Among them, the most extreme winds occurred in 2015 (A.19), 2016 (A.21), and 2019 (A.25, A.26, A.27, A.28), and moderate winds associated with positive zonal (U10) flows around the Western Strait (A.3 and A.4). North of our area of study, one event of Gulf of Penas in 1991 (A.10) seems to be associated to upwelling events due to the presence of southerly winds alongshore (Ekman transport) and surface wind divergence (Ekman Pumping).

- *Cold events without strong winds:* These events have a very localized presence in the interior of the fjords, with extreme spikes in temperature with a short duration. Cold anomalies lasting for two to three months in the east-

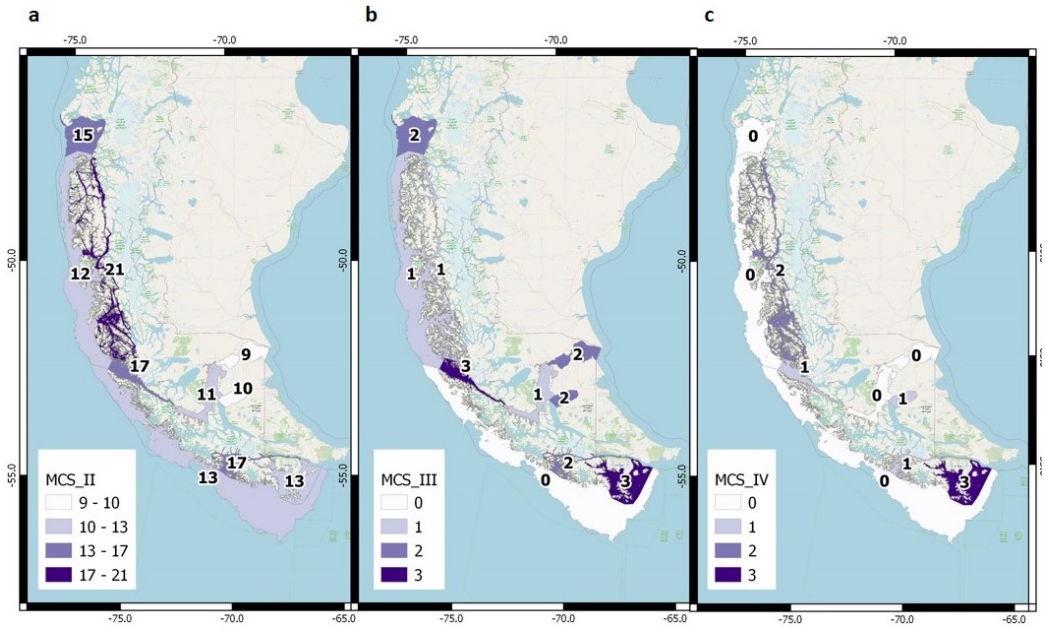


Figure 5.7: Choropleth map labelled with the count of MCS events per category and ecosystem for the period 1981-2020. Categories II (strong, a), III (severe, b) and IV (extreme, c). Each colour legend and labels in bold indicate the number of events per ecosystem. Background map: © OpenStreetMap contributors.

ern side of the continent also occurred unrelated to strong winds. In the first case, the most relevant events occurred in Gulf of Penas (A.5), Western Strait (A.13, Nassau Hornos (A.11, A.16), and Inner Channels Kaweskar (A.18); the latter case occurred in Eastern Strait in 1982 (A.6) and 1984 (A.8).

- *Warm events with strong winds:* Observed in the warm event of 1984 (A.9), with strong northward and westward winds (from the continent to the Pacific Ocean). This event was not entirely recorded due to a data gap after the 30th Dec 1984.

- *Warm events without strong winds:* Observed in the massive event of 1998 (A.12), two events in in Gulf of Penas and Offshore Kaweskar in 2016 (A.20, A.22), and one event in Nearshore Beagle Ballenero in 2020 (A.29).

On the duration of the warm and cold events, the median and mean duration for severe and extreme MCS were 11 and 27 days, respectively. Severe and extreme MHW lasted a median of 50 and 72 days on average. Durations were statistically different (Wilcoxon rank sum test, p-value > 0.01). The longer duration of warm events means that over the study period, severe and extreme warm SST anomalies occurred for a total of 1,078 days, vs. 676 for severe and extreme cold SST anomalies. However, this trend is reversed in the last decade starting in 2011, with a total of 273 days under severe and extreme cold SST anomalies vs. 105 days under warm severe and extreme SST anomalies, despite the longer average and median durations of MHWs.

5.7 Discussion

5.7.1 Satellite versus in-situ data

In the complete area of study, we only have one validation site located in the Strait of Magellan. From the observed relationship, we identify a risk to overestimate very cold temperatures and underestimate very high temperatures in the sheltered waters of the channels and fjords (i.e., temperatures identified via satellite are likely to be slightly buffered if compared with those in situ). However, given that *i)* the mean is around the range of least disagreement (see SM A.3.1), deviations are very likely <1C; and *ii)* the correlation shows that the variance is very well captured by satellites, the estimates of variability and extreme events are likely to be quite accurate.

5.7.2 Observations on MHW and MCS events

The observed distribution of MCS in the decade of 2010-2020 in western Patagonia shows patterns of spatially- constrained nearshore distributions, in line with previous research from South Africa and western Australia (Feng et al.; 2021; Schlegel et al.; 2017). However, the South African and western Australian studies indicate temporal short-term sequences of cold and warm events, whereas in Patagonia this pendular oscillation was only observed in 1982-84, with a series of cold events in 1982 followed by a series of warm events in 1984. In the decade of 2010s, there was a series of three warm severe events in 2016 in the northern and exposed part of the study area (Gulf of Penas and Offshore Kaweskar; A.20 and A.22), but the extreme cold event occurred in the southernmost marine ecosystem (A.21). The lack of extreme warm events in the last two decades confirms the main trends observed for this region (Marin et al.; 2021; Oliver et al.; 2018). Moreover, Gulf of Penas is the marine ecoregion with the largest quantity of warm events in the study region: 19 category II and 3 category III MHW in four decades, which is in itself a much lower frequency of MHWs than many other regions across the planet (Marin et al.; 2021).

According to Garreaud et al. (2013), one of the main climate drivers of Patagonia are the westerlies centred around 50°S: when these are weaker than average, winters are colder and summers are warmer. Contemporary trends show that there has been a reduction of westerlies north of 50°S, whereas there is an increment of westerlies – and precipitation – near the 55°S in the extreme south of the continent, which may increase upwelling and colder SSTs as consequence (Winckler et al.; 2020). This trend has been observed, together with a negative trend on atmospheric sea level pressure, which itself has been linked to a positive trend in the Southern Annular Mode (SAM) and, in a minor way, to the Pacific Decadal Oscil-

lation (PDO) (Winckler et al.; 2020). The increase in zonal and meridional winds – causing possible upwelling events or else advecting cold surface waters from higher latitudes – could be a possible cause of severe cold events in the southernmost marine ecoregions facing the south of the Pacific Ocean, whereas SST on the eastern side of the Strait seemed to be less affected by wind.

In the nearshore area of the fjords, sea surface temperature is generally colder than deep water. This is caused by low salinity, nitrate-poor cold continental freshwater (Modified Subantarctic Water) entering the fjords and channels and forming vertical stratification (halocline and pycnocline) over denser, warmer, and nutrient-rich oceanic waters (Subantarctic Surface Water- SAAW) (Iriarte; 2018; Valdenegro and Silva; 2003). Vertical mixing occurs in winter-spring, when decreased fluxes of freshwater discharge from the main rivers increase light penetration in the water column, increasing net primary production, as well as CO2 capture in the fjords (González et al.; 2013; Iriarte et al.; 2014). Hence in these regions wind-related cold events might be related to cold surface water advection. The presence of very cold waters in fall and winter causing extreme MCS events in the nearshore areas and not associated to wind anomalies could be explained by increased atmospheric anomalies causing glacier melting and associated freshening (Iriarte; 2018), as it seems to be indicated by the generalised retreat of the glaciers in the ecoregion (Meier et al.; 2018). We infer that this may be the reason behind the relatively short span of the extreme cold events in the fjords area, in contrast with the longer duration of the warm events which seem to be related with offshore oceanographic oscillations, such as El Niño in 1998 and 2016 and La Niña in 2020. The warm event of 1984, associated with strong winds, occurred during a La Niña year.

Regarding the method used to detect and classify MHW and MCS (Hobday et al.; 2016,0), a minimization of the threshold period to detect severe and extreme MCS

using less than 5 days could help to identify pulses of cold freshwater entering the fjord system with more precision.

In contrast with nearshore cold events, the observed offshore upwelling in the Gulf of Penas in 1982 has not been documented prior to this study; the southernmost upwelling pattern to date was observed in the Chiloense ecoregion in summer months (42-44°S; (Saldías et al.; 2021)), which has a slightly different oceanographic system with the presence of large rivers adding high volumes of cold freshwater, which generates permanent surface stratification over sub-Antarctic oceanic waters (Iriarte; 2018). Reduced freshwater input in summer could play a role in increased mixing in the upper layer in the northern section of Patagonia.

5.7.3 MCS and giant kelp forests

In the study region and during the whole study period, maximum temperatures – even with MHW – stayed below 15-17°C, the temperature threshold above which giant kelp shows a decline germination and growth (Buschmann et al.; 2014,0; Fernández et al.; 2021). Given the observed trends, it is difficult to foresee any clear positive trends on SST in the near future, which agrees with the observed persistence of this important marine ecosystem for Patagonia and the world ocean (Mora-Soto, *Chapter 4*). The interplay between dynamic forcing (be it wind-caused upwelling or cold-water advection) and freshwater outputs seems to be very efficient in keeping SST trends in check in most of the study region; however, warm events driven by ENSO tend to be long-lasting (more than one month) in the area, causing possible thermic stress in these ecosystems.

Sediment from melting glaciers can increase water turbidity and block light, hence becoming a possible stressing factor for the photosynthetic performance of giant kelp. However, a recent study conducted in a fjord with marked glacier retreat in

southern Tierra del Fuego with elevated seasonal turbidity (Huovinen et al.; 2019) showed that giant kelp has a strong adaptability in their photobiological traits to this environmental change (Palacios et al.; 2021).

Previous studies have been carried on the effects of MHW in communities, distribution, and resilience of giant kelp forests at the temperate coastlines of the Pacific Ocean (Arafeh-Dalmau et al.; 2019; Beas-Luna and Ladah; 2014; Cavanaugh et al.; 2019; Smale; 2019; Wernberg et al.; 2016,0); nevertheless, the lack of research on cold events opens a new frontier in kelp studies. As water temperature is the most important driver of giant kelp performance (Fernández et al.; 2021), current trends in the study region could mean favourable conditions for giant kelp as foundation species for a multitude of organisms (Friedlander et al.; 2020,0,0; Ríos and Mutschke; 2009). However, there are additional stressing factors on giant kelp: increased UV radiation, reduced salinity and ice cover, increased runoff and turbidity (Filbee-Dexter et al.; 2019; Huovinen et al.; 2019), or extreme turbulence in exposed offshore causing high canopy removal (Van Tussenbroek; 1989) and increasing the competition for light for subtidal algae (Bartsch et al.; 2016) or colonization of new spaces (Bolton et al.; 2012; Krumhansl et al.; 2016; Palacios et al.; 2021).

We outline possible effects of these events on giant kelp by ecosystem in Table 5.4, all of them are yet unanswered research questions that require further development. Overall, we foresee those nearshore areas closer to the fjords will be more affected by freshening due to glacier melting; exposed areas will be more affected by a higher frequency of strong winds and storms, and areas facing the polar front could be favoured by the presence of cold and nutrient-rich waters.

Table 5.4: Summary of possible effects on giant kelp forests by marine ecosystem, according to geographical characteristics and warm and cold events observed in this study. Giant kelp area was calculated using the map of Mora-Soto et al. (2020).

Nearshore/ offshore	**Marine ecosystem**	**Giant kelp area (ha)**	**Main geographical and oceanographical features**	**Main research gaps on giant kelp forests (open research questions)**
Nearshore	Inner Channels - Kaweskar	67,874	Southern Patagonia Icefield; glacio-nival freshwater input (Meier et al., 2018)	Expansion to new deglaciated areas (Filbee-Dexter et al., 2019); Increased glacial turbidity; Increased photobiotic stress (Palacios et al., 2021); severe and extreme storms carrying cold, nutrient-rich water favourable for giant kelp.
Nearshore	Beagle Ballenero - Magellan	27,528	Cordillera Darwin Icefield; glacio-nival freshwater input (Bown et al., 2014)	
Offshore	Gulf of Penas	3,109	Northern Patagonia Icefield; glacio-nival freshwater input (Meier et al., 2018); Observed upwelling (event in 1982).	
Offshore	Exposed coast - Kaweskar	62,438	Windward side of the continent (Kaweskar); extreme rainfall (Schneider et al., 2003)	Increased turbulence; nutrient mixing, shorter lifespan of the canopies due to more frequency of storms (Van Tussenbroek,1989a, 1989b)
Offshore	Exposed coast - Magellan	77,103	Windard side of the continent (Magellan); extreme rainfall (Schneider et al., 2003)	
Nearshore	Central Strait of Magellan	11,621	Orographic threshold from the windward (Pacific) to the leeward sides of Patagonia.	Increment of the frequency of strong winds
Nearshore	Bahía Inutil Strait of Magellan	1,376	Shallow waters; rain shadow (Schneider et al., 2003)	
Nearshore	Eastern Strait of Magellan	409	First Narrow to the Atlantic Ocean; high tidal amplitude.	Not observed
Nearshore	Nassau Hornos Magellan	72,214	Cape Horn Archipelago and Hardy Peninsula	Severe and extreme storms (Winckler et al., 2020) carrying cold, nutrient-rich water favourable for giant kelp.
Nearshore	Western Strait of Magellan	29,741	Windward side of the continent; extreme rainfall (Schneider et al., 2003); entrance of the Pacific towards the Atlantic Ocean.	

5.8 Conclusion

Western Patagonia has experienced a high frequency of extreme cold events in the decade of 2010-2020 that could be explained by freshening events nearshore by the fjords area, as well as strong wind anomalies delivering cold water from the higher latitudes or facilitating upwellings, from the western entrance of the Strait of Magellan to the Cape Horn Archipelago. We also identified warm events that could be explained by the wider-range oscillations of El Niño and La Niña, but were not as short and extreme as the cold events. As cold-water temperature is a positive factor for giant kelp, this trend gives support to previous observations of persistence of this ecosystem in this ecoregion. We identify research lines to address the wider range of possible stressors that the giant kelp ecosystem may face, such as freshening and increased storms and turbulence.

References

Arafeh-Dalmau, N., Montaño-Moctezuma, G., Martínez, J. A., Beas-Luna, R., Schoeman, D. S. and Torres-Moye, G. (2019). Extreme marine heatwaves alter kelp forest community near its equatorward distribution limit, *Frontiers in Marine Science* **6**: 499.

Armour, K. C., Marshall, J., Scott, J. R., Donohoe, A. and Newsom, E. R. (2016). Southern Ocean warming delayed by circumpolar upwelling and equatorward transport, *Nature Geoscience* **9**(7): 549–554.

Aybar, C., Wu, Q., Bautista, L., Yali, R. and Barja, A. (2020). rgee: An r package for interacting with google earth engine, *Journal of Open Source Software* **5**(51): 2272.

Banzon, V. F., Reynolds, R. W., Stokes, D. and Xue, Y. (2014). A 1/4°-spatial-resolution daily sea surface temperature climatology based on a blended satellite and in situ analysis, *Journal of Climate* **27**(21): 8221 – 8228.

Bartsch, I., Paar, M., Fredriksen, S., Schwanitz, M., Daniel, C., Hop, H. and Wiencke, C. (2016). Changes in kelp forest biomass and depth distribution in Kongsfjorden, Svalbard, between 1996–1998 and 2012–2014 reflect Arctic warming, *Polar Biology* **39**(11): 2021–2036.

Beas-Luna, R. and Ladah, L. B. (2014). Latitudinal, seasonal, and small-scale spatial differences of the Giant Kelp, Macrocystis pyrifera, and an herbivore at their Southern range limit in the Northern hemisphere, *Botanica Marina* **57**(2): 73–83.

Bolton, J., Anderson, R., Smit, A. and Rothman, M. (2012). South African kelp moving eastwards: the discovery of Ecklonia maxima (osbeck) Papenfuss at De Hoop Nature Reserve on the South coast of South Africa, *African Journal of Marine Science* **34**(1): 147–151.

Bown, F., Rivera, A., Zenteno, P., Bravo, C. and Cawkwell, F. (2014). *First Glacier Inventory and Recent Glacier Variation on Isla Grande de Tierra Del Fuego and Adjacent Islands in Southern Chile*, Springer Berlin Heidelberg, Berlin, Heidelberg, pp. 661–674.

Buschmann, A. H., Pereda, S. V., Varela, D. A., Rodríguez-Maulén, J., López, A., González-Carvajal, L., Schilling, M., Henríquez-Tejo, E. A. and Hernández-González, M. C. (2014). Ecophysiological plasticity of annual populations of Giant Kelp (Macrocystis pyrifera) in a seasonally variable coastal environment in the Northern Patagonian Inner Seas of Southern Chile, *J. of Applied Phycology* **26**(2): 837–847.

Buschmann, A. H., Vásquez, J., Osorio, P., Reyes, E., Filún, L., Hernández-González, M. and Vega, A. (2004). The effect of water movement, temperature and salinity on abundance and reproductive patterns of Macrocystis spp.(phaeophyta) at different latitudes in Chile, *Marine Biology* **145**(5): 849–862.

Cavanaugh, K. C., Reed, D. C., Bell, T. W., Castorani, M. C. N. and Beas-Luna, R. (2019). Spatial variability in the resistance and resilience of Giant Kelp in Southern and Baja California to a multiyear heatwave, *Frontiers in Marine Science* **6**(413).
URL: *https://www.frontiersin.org/article/10.3389/fmars.2019.00413*

Dayton, P. K. (1985). The structure and regulation of some South American kelp communities, *Ecological monographs* **55**(4): 447–468.

Escribano, R., Fernández, M. and Aranís, A. (2003). Physical-chemical processes and patterns of diversity of the Chilean eastern boundary pelagic and benthic marine ecosystems: an overview, *Gayana* **67**(2): 190–205.

Feng, M., Caputi, N., Chandrapavan, A., Chen, M., Hart, A. and Kangas, M. (2021). Multi-year marine cold-spells off the west coast of Australia and effects on fisheries, *Journal of Marine Systems* **214**: 103473.
URL: *https://www.sciencedirect.com/science/article/pii/S0924796320301688*

Fernández, P. A., Navarro, J. M., Camus, C., Torres, R. and Buschmann, A. H. (2021). Effect of environmental history on the habitat-forming kelp Macrocystis pyrifera responses to Ocean acidification and warming: a physiological and molecular approach, *Scientific reports* **11**(1): 1–15.

Filbee-Dexter, K. and Wernberg, T. (2018). Rise of turfs: a new battlefront for globally declining kelp forests, *Bioscience* **68**(2): 64–76.

Filbee-Dexter, K., Wernberg, T., Fredriksen, S., Norderhaug, K. M. and Pedersen, M. F. (2019). Arctic kelp forests: Diversity, resilience and future, *Global and Planetary Change* **172**: 1–14.
URL: *https://www.sciencedirect.com/science/article/pii/S0921818118301826*

Friedlander, A. M., Ballesteros, E., Bell, T. W., Caselle, J. E., Campagna, C., Goodell, W., Hüne, M., Muñoz, A., Salinas-de León, P. and Sala, E. (2020). Kelp forests at the end of the earth: 45 years later, *Plos one* **15**(3): e0229259.

Friedlander, A. M., Ballesteros, E., Bell, T. W., Giddens, J., Henning, B., Hüne, M., Muñoz, A., Salinas-de León, P. and Sala, E. (2018). Marine biodiversity at the end of the World: Cape Horn and Diego Ramírez Islands, *PloS one* **13**(1): e0189930.

Friedlander, A. M., Ballesteros, E., Goodell, W., Hüne, M., Muñoz, A., Salinas-de León, P., Velasco-Charpentier, C. and Sala, E. (2021). Marine communities of the newly created Kawésqar National Reserve, Chile: From glaciers to the Pacific Ocean, *PLOS ONE* **16**(4): e0249413.
URL: *https://doi.org/10.1371/journal.pone.0249413*

Garreaud, R., Lopez, P., Minvielle, M. and Rojas, M. (2013). Large-scale control on the Patagonian climate, *Journal of Climate* **26**(1): 215–230.

González, H., Castro, L., Daneri, G., Iriarte, J., Silva, N., Tapia, F., Teca, E. and Vargas, C. (2013). Land–Ocean gradient in haline stratification and its effects on plankton dynamics and trophic carbon fluxes in Chilean Patagonian fjords (47–50 s), *Progress in Oceanography* **119**: 32–47.

Gorelick, N., Hancher, M., Dixon, M., Ilyushchenko, S., Thau, D. and Moore, R. (2017). Google Earth Engine: Planetary-scale geospatial analysis for everyone, *Rem. Sens. of Env.* **202**: 18–27.

Häussermann, V. and Försterra, G. (2007). Extraordinary abundance of hydrocorals (Cnidaria, Hydrozoa, Stylasteridae) in shallow water of the Patagonian fjord region, *Polar Biology* **30**(4): 487–492.

Hersbach, H., Bell, B., Berrisford, P., Hirahara, S., Horányi, A., Muñoz-Sabater, J., Nicolas, J., Peubey, C., Radu, R., Schepers, D. et al. (2020). The era5 global reanalysis, *Quarterly Journal of the Royal Meteorological Society* **146**(730): 1999–2049.

Hobday, A. J., Alexander, L. V., Perkins, S. E., Smale, D. A., Straub, S. C., Oliver, E. C., Benthuysen, J. A., Burrows, M. T., Donat, M. G. and Feng, M. (2016). A hierarchical approach to defining marine heatwaves, *Progress in Oceanography* **141**: 227–238.

Hobday, A. J., Oliver, E. C., Gupta, A. S., Benthuysen, J. A., Burrows, M. T., Donat, M. G., Holbrook, N. J., Moore, P. J., Thomsen, M. S. and Wernberg, T. (2018). Categorizing and naming marine heatwaves, *Oceanography* **31**(2): 162–173.

Holbrook, N. J., Sen Gupta, A., Oliver, E. C. J., Hobday, A. J., Benthuysen, J. A., Scannell, H. A., Smale, D. A. and Wernberg, T. (2020). Keeping pace with marine heatwaves, *Nature Reviews Earth & Environment* **1**(9): 482–493.
URL: *https://doi.org/10.1038/s43017-020-0068-4*

Huovinen, P., Ramírez, J., Palacios, M. and Gómez, I. (2019). Satellite-derived mapping of kelp distribution and water optics in the glacier impacted Yendegaia fjord (Beagle channel, Southern Chilean Patagonia), *Science of The Total Environment* p. 135531.

Iriarte, J. L. (2018). Natural and human influences on marine processes in Patagonian subAntarctic coastal waters, *Frontiers in Marine Science* **5**: 360.

Iriarte, J. L., Pantoja, S. and Daneri, G. (2014). Oceanographic processes in Chilean fjords of Patagonia: from small to large-scale studies, *Progress in Oceanography* **129**: 1–7.

Jacox, M. G., Alexander, M. A., Bograd, S. J. and Scott, J. D. (2020). Thermal displacement by marine heatwaves, *Nature* **584**(7819): 82–86.

Krumhansl, K. A., Okamoto, D. K., Rassweiler, A., Novak, M., Bolton, J. J., Cavanaugh, K. C., Connell, S. D., Johnson, C. R., Konar, B., Ling, S. D., Micheli, F., Norderhaug, K. M., Pérez-Matus, A., Sousa-Pinto, I., Reed, D. C., Salomon, A. K., Shears, N. T., Wernberg, T., Anderson, R. J., Barrett, N. S., Buschmann, A. H., Carr, M. H., Caselle, J. E., Derrien-Courtel, S., Edgar, G. J., Edwards, M., Estes, J. A., Goodwin, C., Kenner, M. C., Kushner, D. J., Moy, F. E., Nunn, J., Steneck, R. S., Vásquez, J., Watson, J., Witman, J. D. and Byrnes, J. E. K. (2016). Global patterns of kelp forest change over the past half-century, *PNAS* **113**(48): 13785.

Marin, M., Feng, M., Phillips, H. E. and Bindoff, N. L. (2021). A global, multiproduct analysis of coastal marine heatwaves: Distribution, characteristics, and long-term trends, *Journal of Geophysical Research: Oceans* **126**(2): e2020JC016708.
URL: *https://agupubs.onlinelibrary.wiley.com/doi/abs/10.1029/2020JC016708*

Meier, W. J.-H., Grießinger, J., Hochreuther, P. and Braun, M. H. (2018). An updated multi-temporal glacier inventory for the Patagonian Andes with changes between the little ice age and 2016, *Frontiers in Earth Science* **6**: 62.

Mora-Soto, A., Palacios, M., Macaya, E. C., Gómez, I., Huovinen, P., Pérez-Matus, A., Young, M., Golding, N., Toro, M. and Yaqub, M. (2020). A high-resolution global map of Giant Kelp (Macrocystis pyrifera) forests and

intertidal green algae (Ulvophyceae) with Sentinel-2 imagery, *Remote Sensing* **12**(4): 694.

Oliver, E. C., Burrows, M. T., Donat, M. G., Sen Gupta, A., Alexander, L. V., Perkins-Kirkpatrick, S. E., Benthuysen, J. A., Hobday, A. J., Holbrook, N. J. and Moore, P. J. (2019). Projected marine heatwaves in the 21st century and the potential for ecological impact, *Frontiers in Marine Science* **6**: 734.

Oliver, E. C., Donat, M. G., Burrows, M. T., Moore, P. J., Smale, D. A., Alexander, L. V., Benthuysen, J. A., Feng, M., Gupta, A. S. and Hobday, A. J. (2018). Longer and more frequent marine heatwaves over the past century, *Nature communications* **9**(1): 1–12.

Palacios, M., Osman, D., Ramírez, J., Huovinen, P. and Gómez, I. (2021). Photobiology of the Giant Kelp Macrocystis pyrifera in the land-terminating glacier fjord Yendegaia (Tierra del Fuego): A look into the future?, *Science of The Total Environment* **751**: 141810.

Pérez-Matus, A., Carrasco, S. A., Gelcich, S., Fernandez, M. and Wieters, E. A. (2017). Exploring the effects of fishing pressure and upwelling intensity over subtidal kelp forest communities in central Chile, *Ecosphere* **8**(5): e01808.
URL: *https://esajournals.onlinelibrary.wiley.com/doi/abs/10.1002/ecs2.1808*

Ríos, C. and Mutschke, E. (2009). Aporte al conocimiento de Macrocystis pyrifera: revisión bibliográfica sobre los "huirales" distribuidos en la Región de Magallanes, *Anales del Instituto de la Patagonia*, Vol. 37, Universidad de Magallanes, pp. 97–102.

Rogers-Bennett, L. and Catton, C. (2019). Marine heat wave and multiple stressors tip bull kelp forest to sea urchin barrens, *Scientific reports* **9**(1): 1–9.

Rovira, J. and Herreros, J. (2016). Clasificación de ecosistemas marinos Chilenos

de la zona económica exclusiva, *Departamento de Planificación y Políticas en Biodiversidad. División de Recursos Naturales y Biodiversidad. Ministerio del Medio Ambiente* .

Sakakibara, D. and Sugiyama, S. (2014). Ice-front variations and speed changes of calving glaciers in the Southern Patagonia Icefield from 1984 to 2011, *Journal of Geophysical Research: Earth Surface* **119**(11): 2541–2554.
URL: *https://agupubs.onlinelibrary.wiley.com/doi/abs/10.1002/2014JF003148*

Saldías, G. S., Hernández, W., Lara, C., Muñoz, R., Rojas, C., Vásquez, S., Pérez-Santos, I. and Soto-Mardones, L. (2021). Seasonal variability of sst fronts in the inner sea of chiloé and its adjacent coastal Ocean, Northern Patagonia, *Remote Sensing* **13**(2): 181.

Schlegel, R. W., Oliver, E. C., Wernberg, T. and Smit, A. J. (2017). Nearshore and offshore co-occurrence of marine heatwaves and cold-spells, *Progress in Oceanography* **151**: 189–205.

Schlegel, R. W. and Smit, A. J. (2018). heatwaver: A central algorithm for the detection of heatwaves and cold-spells, .*Journal of Open Source Software* **3**(821).

Schneider, C., Glaser, M., Kilian, R., Santana, A., Butorovic, N. and Casassa, G. (2003). Weather observations across the Southern Andes at 53°s, *Physical Geography* **24**(2): 97–119.
URL: *https://doi.org/10.2747/0272-3646.24.2.97*

Smale, D. A. (2019). Impacts of Ocean warming on kelp forest ecosystems, *New Phytologist* .

Spalding, M. D., Fox, H. E., Allen, G. R., Davidson, N., Ferdaña, Z. A., Finlayson, M., Halpern, B. S., Jorge, M. A., Lombana, A. and Lourie, S. A. (2007). Ma-

rine ecoregions of the World: a bioregionalization of coastal and shelf areas, *BioScience* **57**(7): 573–583.

Valdenegro, A. and Silva, N. (2003). Caracterización Oceanográfica física y química de la zona de canales y fiordos australes de Chile entre el estrecho de magallanes y cabo de hornos (cimar 3 fiordos), *Cienc. Tecnol. Mar* **26**: 19–60.

Van Tussenbroek, B. (1989). The life-span and survival of fronds of Macrocystis pyrifera (Laminariales, phaeophyta) in the Falkland Islands, *British Phycological Journal* **24**(2): 137–141.

Vásquez, J. A. (2008). Production, use and fate of Chilean brown seaweeds: resources for a sustainable fishery, *Nineteenth Int. Seaweed Symposium*, Springer, pp. 7–17.

Vásquez, J. A., Piaget, N. and Vega, J. M. A. (2012). The *Lessonia nigrescens* fishery in Northern Chile: "how you harvest is more important than how much you harvest", *Journal of Applied Phycology* **24**(3): 417–426.

Vergés, A., Steinberg, P. D., Hay, M. E., Poore, A. G., Campbell, A. H., Ballesteros, E., Heck Jr, K. L., Booth, D. J., Coleman, M. A. and Feary, D. A. (2014). The tropicalization of temperate marine ecosystems: climate-mediated changes in herbivory and community phase shifts, *Proceedings of the Royal Society B: Biological Sciences* **281**(1789).

Wernberg, T., Bennett, S., Babcock, R. C., De Bettignies, T., Cure, K., Depczynski, M., Dufois, F., Fromont, J., Fulton, C. J. and Hovey, R. K. (2016). Climate-driven regime shift of a temperate marine ecosystem, *Science* **353**(6295): 169–172.

Wernberg, T., Smale, D. A., Tuya, F., Thomsen, M. S., Langlois, T. J., de Bettignies, T., Bennett, S. and Rousseaux, C. S. (2013). An extreme climatic event

alters marine ecosystem structure in a global biodiversity hotspot, *Nature Climate Change* **3**(1): 78–82.
URL: *https://doi.org/10.1038/nclimate1627*

Winckler, P., Aguirre, C., Farías, L., Contreras-López, M. and Masotti, Í. (2020). Evidence of climate-driven changes on atmospheric, hydrological, and Oceanographic variables along the Chilean coastal zone, *Climatic Change* **163**(2): 633–652.





6 | Chapter 6: Conclusions

> *"... there are several other sources of enjoyment in a long voyage, which are of a more reasonable nature. The map of the world ceases to be a blank; it becomes a picture full of the most varied and animated figures. Each part assumes its proper dimensions (...) it is not until having sailed for weeks along small portions of their shores, that one is thoroughly convinced what vast spaces on our immense world these names imply."*
>
> — Charles Darwin, The Voyage of the Beagle

The planet is not fully explored yet and there are still blank spaces on its maps. This research started with the overall aim of determining where the giant kelp forests in southern Patagonia were, and assessing their changes over the last century, on which there were vast gaps of knowledge that were essential for understanding the kelp biome in a global context (Krumhansl et al.; 2016). This chapter highlights the key findings of chapters 3, 4 and 5 and how they achieve the aims presented in the Introduction (figure 6.1).

6.1 Overall findings

6.1.1 Giant kelp forest extent

In the first research chapter of my thesis (Chapter 3), I developed a novel formula (Kelp Difference, or KD) and a filter algorithm to detect giant kelp canopy. I also compared KD with other widely used vegetation indices such as Floating Algae Index, or FAI (Hu; 2009) and Normalised Difference Vegetation Index,

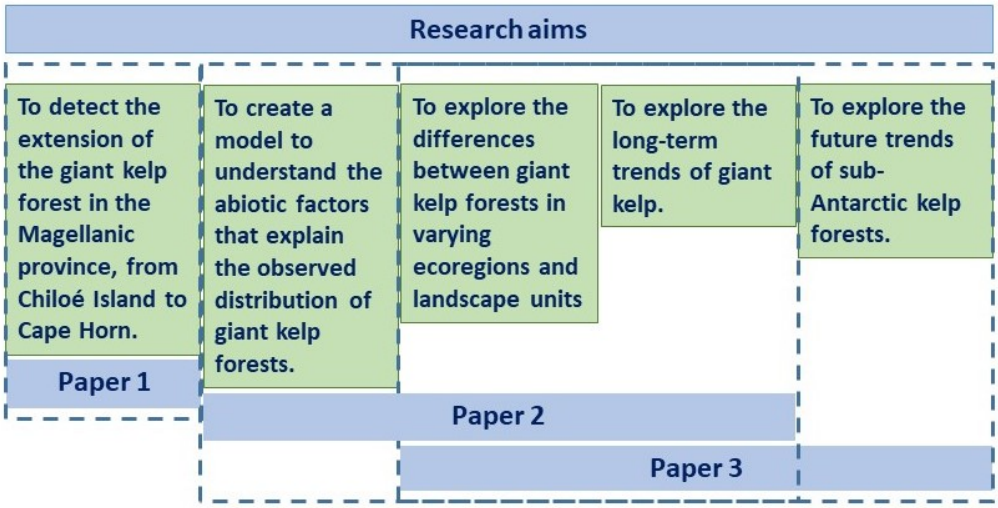


Figure 6.1: Summary of research aims and paper structure of this thesis.

or NDVI (Ashley and Rea; 1975). This method showed a high overall accuracy in average for canopies larger than 1 hectare. These results confirm that using filtering thresholds is a useful tool for detecting kelp forests on the sea surface in a reliable way, and their values could be adjustable if ever they were to be used for other kelp or coastal species. However, this method has some caveats: forests under high tidal ranges, small forests, permanently submerged forests, and highly variable forests are prone to go undetected, while green algae (*Ulvophyceae*) and similar brown algae could also be detected with this method. All these sources of error justify more focused research. The imminent advent of hyperspectral satellite imagery (Bell et al.; 2015) will go at great lengths to solve some of the current limitations, although this alone won't solve the need for monitoring past giant kelp dynamics.

As a result, , and following this method, we estimated the giant kelp extent of the Magellanic province as: Channels and Fjords ecoregion = 4840.7 km^2; Chiloense ecoregion = 687 km^2; Falkland Island (Malvinas) ecoregion = 3081.1 km^2; Patag-

onian Shelf ecoregion = 144.5 km^2; North Patagonian Gulfs ecoregion = undetected. This totals 8753.3 km^2 for the entire province, and 5527.7 km^2 between Chiloense and the Channels and Fjords ecoregions. The Magellanic province accounts for the 51% of the entire global extent detected in this research (17088.3 km^2).

6.1.2 Abiotic factors of giant kelp by ecoregions and landscape units

During the course of this thesis, I found that combinations of abiotic factors are distinguishable by ecoregions and landscape units, and they play different roles in shaping the size and dynamics of giant kelp. For this reason, aims 2 and 3 are completely interlinked.

In the second paper (Chapter 4), I conducted a biogeographical study of the Channels and Fjords, Falkland Islands (Malvinas) and South Georgia ecoregions. I classified the forests according to their size and the main characteristics of the coastline. The mean size of an individual forest in the Falklands is 60.72 ha, 19.84 ha in Channels and Fjords, and 2.38 ha in South Georgia. Kelp forest sizes and numbers differ according to the environment; for instance, size is larger towards exposed areas in Channels and Fjords and Falkland Islands; but kelp forests dominate in number in steep to very steep slopes (> 15°), as well as in bays and intertidal rocks in Channels and Fjords and South Georgia. On the contrary, in the Falkland Islands they dominate in number in gently sloping lands and in size in convex coastlines. These findings reflect how coastal geomorphology gives shape to kelp establishment.

A conditional inference tree was used to predict kelp forest size, finding that the

current and exposition to the open ocean explained in 81% of cases the presence of large or small forests. In sheltered areas of less powerful currents such as the inner Channels and the Antarctic Circumpolar Current around South Georgia, small forests dominated over 80% of the total, whereas in exposed areas towards the Cape Horn and the Falkland (Malvinas) current, large forests dominated more than 70% of the total of forests. The independence of kelp detection indices based on surface reflectance values allowed the direct characterisation of the kelp physical habitats without circularities.

In the third paper (Chapter 5), I subdivided the Channels and Fjords ecoregion by *marine ecoregions* (Rovira and Herreros; 2016), which I consider to be the landscape units of this research, to analyse Sea Surface Temperature (SST) trends during the 39 year period 1981-2020. The main result, in terms of spatial units, is that the nearshore ecosystems in the extreme south of the ecoregion, — namely the Western Strait of Magellan, Inner Channels Kaweskar, Nearshore Beagle Ballenero and Nearshore Nassau Hornos — have experienced an increase in the number of extreme cold events in the last decade. This result, together with the absence of extreme heatwaves, suggests that the fjord ecosystems, with dominance of small forests along the fjord walls, have been protected from ocean warming. The offshore ecoregions, with larger and more exposed forests towards the Cape Horn current, have not experienced any extreme warm or cold events.

6.1.3 Long-term trends of giant kelp

In the second paper (Chapter 4), I explored the long-term trends of giant kelp in the Channels and Fjords, Falkland Island (Malvinas) and South Georgia ecoregions using historical cartography (nautical charts), aerial photogrammetry and historical kelp surveys, along with satellite-detected kelp forests from 1984 to

2019. They showed a remarkable coincidence of similar shapes of kelp forests at the same places where they were first recorded, despite several environmental changes occurring in the last two centuries, including glacier retreat and changes in land/seascape use and occupation. The ecoregion with the best coincidence of records, indicating more persistence, was Falkland Islands (Malvinas) with 89.7% of present-time forests with a similar shape to the first record made in 1834 (200 out of 223 charted kelp forests). This high success might also be linked to the larger average size of kelp forests in this archipelago, and hence a higher detection rate.

On the other hand, seasonal fluctuation assessments of kelp were not possible with the available data. Multispectral satellite imagery in the study region is usually covered, at least partially, by clouds. At sub-Antarctic regions, cloud cover could dominate all year round and seasonal changes were thus undetectable.

With regards to thermal trends, SST have been stable in the sub-Antarctic latitudes with no temperatures above the thermal tolerance of kelp sporophytes in the last four decades (Chapter 4; supplementary material). The results of extreme warm and cold events in the Channels and Fjords ecoregion by month and season made it possible to conclude that the extreme warm events in 1998 and 1984 occurred in winter and spring, whereas extreme cold events (1982, 2014 to 2019) occurred in fall and winter (Chapter 5), driven by increased winds in the extreme south of the region, and possibly by glacier melting in the inner fjordland.

6.1.4 Future trends of sub-Antarctic giant kelp

As an overall result of the SST trends of the last four decades (Chapter 5), the Channels and Fjords ecoregion could be considered a climatic refugia for giant kelp forests and their associated biodiversity. This affirmation is supported by the

thermal stability — and even cooling — marine trend, as well as for the long-term persistence of the sub-Antarctic kelp forests presented in Chapter 4. In Chapter 5, this stability is discussed in depth. The spatial and thermal persistence of giant kelp is good news for this ecosystem, but the future could see other possible outcomes, such as increased frequency of storms coming from the west wind drift, increasing coastal turbulence and kelp canopy removal. Global warming also could lead to the colonisation of new areas freshly exposed by glacier retreat; all these effects are open to future research (see Table 5.4 in Chapter 5).

6.2 Future research needs and directions

The assessment of the extent and persistence of giant kelp is a first step towards a myriad of research avenues on this ecosystem. Among all the possibilities, in my opinion the first and most immediate goal would be detecting biomass fluctuations by season and year, in the same way as it is done in other ecoregions (Bell et al.; 2018; Cavanaugh et al.; 2011). The use of UAV technology is increasingly complementing precise studies on kelp canopy removal and renewal, as well as the effect of tidal fluctuations on canopy optics (Cavanaugh et al.; 2021; Doughty and Cavanaugh; 2019).

The role of giant kelp in the carbon cycle is still an area of scientific research under development (Duarte et al.; 2005), and this gap is even more relevant at high latitudes (Filbee-Dexter et al.; 2019). A recent paper assessed carbon sequestration of kelp detritus of *Laminaria hyperborea* in the Norwegian Fjords (Pedersen et al.; 2021); the Patagonian fjords offers an interesting counterpoint to their findings.

Another research gap is the development of new remote sensing techniques for mapping underwater algae and benthic complexity (Kutser et al.; 2020). This

could include active sensors such as Sentinel-1 combined with expert field knowledge (Hu et al.; 2021). In Chapter 3 the kelp filter algorithm could not differentiate giant kelp from green algae; these and other kelp species with similar reflectance require a convergence of novel methods and technology (e.g., hyperspectral imagery) to get an accurate distinction (Karki et al.; 2021).

A global model between kelp fluctuations and climate could also help to detect strategic areas for kelp conservation and reforestation. Working with climate experts would help to develop a new understanding of kelp fluctuations along with coastal dynamics, towards an effective protection of this ecosystem in the world. The study of the identified non-climate kelp threats (e.g., pollution, overharvesting, biotic interactions) and of their potential synergies with a changing climate is also an important research avenue.

Finally, it has been an enormous surprise and pleasure to see the wider outcomes of this research. After the publication of the first paper, many people have started to mention that Chile has one third of the global distribution of giant kelp forests, and the urgent need for their protection. This has been outlined as part of the roadmap towards blue carbon development in the country (Rehbein Lucero et al.; 2020), and it is currently under conversations to include kelp forests as a NDC for the upcoming UFCCC COP 26 in Glasgow. National media has also covered this message, and new documentaries (*Blue forest*; 2021) are expanding kelp forest awareness to the public.

6.3 Concluding remarks

The contribution of this thesis is the discovery of the extent and singularity of the giant kelp ecosystem at the high latitudes of South America, a step towards com-

pleting the global map of marine biogeography. This research was done through a novel formula developed in the field of remote sensing, but made and improved thanks to interdisciplinary collaboration from the fields of marine biology, geography, cartography, and oceanography. This work helped to unveil sub-Antarctic kelp as one of the least intervened, most intact, and most persistent ecosystems on Earth.

References

Ashley, M. D. and Rea, J. (1975). Seasonal vegetation differences from ERTS imagery, *Am. Soc. of Photogrammetry* **41**(6).

Bell, T. W., Allen, J. G., Cavanaugh, K. C. and Siegel, D. (2018). Three decades of variability in California's Giant Kelp forests from the Landsat satellites, *Rem. Sens. of Env.* p. 110811.

Bell, T. W., Cavanaugh, K. C. and Siegel, D. (2015). Remote monitoring of Giant Kelp biomass and physiological condition: An evaluation of the potential for the hyperspectral infrared imager (HyspIRI) mission, *Rem. Sens. of Env.* **167**: 218–228.

Blue forest (2021).
URL: *https://www.oceansoulsfilms.com/blue-forest*

Cavanaugh, K. C., Siegel, D. A., Reed, D. C. and Dennison, P. (2011). Environmental controls of giant-kelp biomass in the Santa Barbara Channel, California, *Mar. Ecology Progress Series* **429**: 1–17.

Cavanaugh, K., Cavanaugh, K., Bell, T. and Hockridge, E. (2021). An automated method for mapping Giant Kelp canopy dynamics from UAV. front, *Environ. Sci* **8**: 587354.

Doughty, C. L. and Cavanaugh, K. C. (2019). Mapping coastal wetland biomass from high resolution unmanned aerial vehicle (UAV) imagery, *Remote Sensing* **11**(5): 540.

Duarte, C. M., Middelburg, J. J. and Caraco, N. (2005). Major role of marine vegetation on the Oceanic carbon cycle, *Biogeosciences* **2**(1): 1–8.

Filbee-Dexter, K., Wernberg, T., Fredriksen, S., Norderhaug, K. M. and Pedersen, M. F. (2019). Arctic kelp forests: Diversity, resilience and future, *Global and Planetary Change* **172**: 1–14.
URL: *https://www.sciencedirect.com/science/article/pii/S0921818118301826*

Hu, C. (2009). A novel Ocean color index to detect floating algae in the global Oceans, *Rem. Sens. of Env.* **113**(10): 2118–2129.

Hu, Y., Tian, B., Yuan, L., Li, X., Huang, Y., Shi, R., Jiang, X., Wang, l. and Sun, C. (2021). Mapping coastal salt marshes in China using time series of Sentinel-1 sar, *ISPRS Journal of Photogrammetry and Remote Sensing* **173**: 122–134.
URL: *https://www.sciencedirect.com/science/article/pii/S0924271621000034*

Karki, S., Bermejo, R., Wilkes, R., Monagail, M. M., Daly, E., Healy, M., Hanafin, J., McKinstry, A., Mellander, P.-E. and Fenton, O. (2021). Mapping spatial distribution and biomass of intertidal Ulva blooms using machine learning and earth observation, *Frontiers in Marine Science* **8**: 380.

Krumhansl, K. A., Okamoto, D. K., Rassweiler, A., Novak, M., Bolton, J. J., Cavanaugh, K. C., Connell, S. D., Johnson, C. R., Konar, B., Ling, S. D., Micheli, F., Norderhaug, K. M., Pérez-Matus, A., Sousa-Pinto, I., Reed, D. C., Salomon, A. K., Shears, N. T., Wernberg, T., Anderson, R. J., Barrett, N. S., Buschmann, A. H., Carr, M. H., Caselle, J. E., Derrien-Courtel, S., Edgar, G. J., Edwards, M., Estes, J. A., Goodwin, C., Kenner, M. C., Kushner, D. J., Moy, F. E., Nunn,

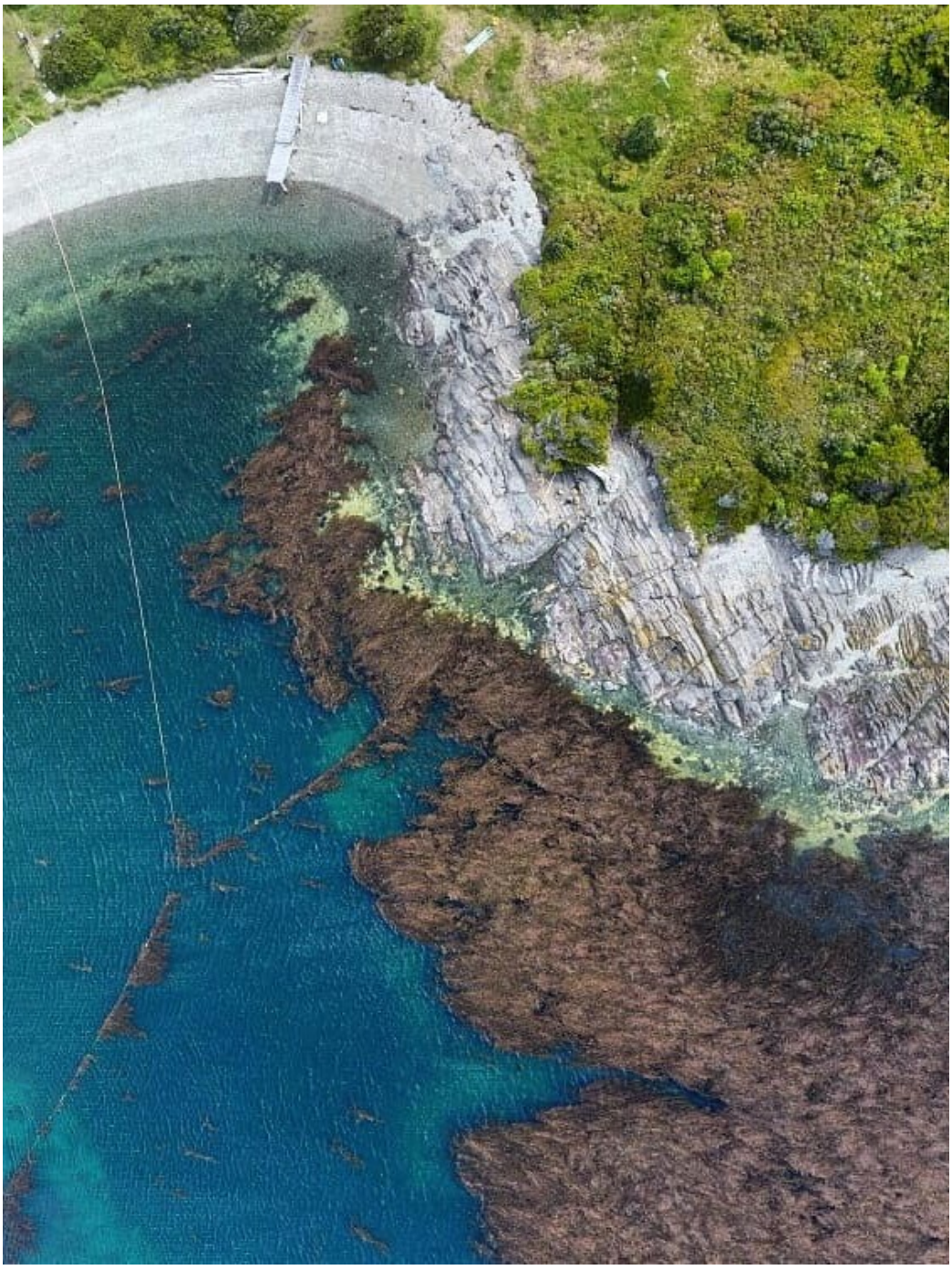
J., Steneck, R. S., Vásquez, J., Watson, J., Witman, J. D. and Byrnes, J. E. K. (2016). Global patterns of kelp forest change over the past half-century, *PNAS* **113**(48): 13785.

Kutser, T., Hedley, J., Giardino, C., Roelfsema, C. and Brando, V. E. (2020). Remote sensing of shallow waters–a 50 year retrospective and future directions, *Remote Sensing of Environment* **240**: 111619.

Pedersen, M. F., Filbee-Dexter, K., Frisk, N. L., Sárossy, Z. and Wernberg, T. (2021). Carbon sequestration potential increased by incomplete anaerobic decomposition of kelp detritus, *Marine Ecology Progress Series* **660**: 53–67.

Rehbein Lucero, J., Encalada, G. and Barbosa, J. (2020). *Propuesta de Hoja de Ruta para el Carbono Azul en Chile. Banco Mundial*.

Rovira, J. and Herreros, J. (2016). Clasificación de ecosistemas marinos Chilenos de la zona económica exclusiva, *Departamento de Planificación y Políticas en Biodiversidad. División de Recursos Naturales y Biodiversidad. Ministerio del Medio Ambiente* .



A | Supplementary Materials

A.1 Supplementary Materials Paper 1

The following are available online at this link

- Kelp filter algorithm (JS code)
- Box and whisker plot of NDVI, FAI and KD and their thresholds
- Methodology workflow
- High-resolution validation (GEE interface)
- Drone-KD-CART and RF comparison
- Low resolution kelp observations (table).

A.2 Supplementary Materials Paper 2

A.2.1 Data availability statement

All the historical nautical charts, previous surveys, and the current kelp distribution layers were uploaded to an online open visualization viewer:

https://biogeoscienceslaboxford.users.earthengine.app/view/beaglekelpcharts with the aim of encouraging scientists and the public to explore the layers interactively.

The datasets generated during the current study are available in the Beagle Kelp charts repository: https://github.com/BiogeosciencesLabOxford/BeagleKelp

A.2.2 Additional tables and figures

- Table A.1: Table S1 Descriptive statistics of SST (°C) for the representative NOAA-SST sites by ecoregion.

- Figure A.1: Time series of NOAA Sea Surface Temperature (°C) from 1981 to 2020 in the SST-representative pixels per ecoregion.

Table A.1: Table S1 Descriptive statistics of SST (°C) for the representative NOAA-SST sites by ecoregion.

Ecoregion	Location	Mean	(+/- sd)	Median	1st Q	3rd Q	Min	Max
Channels	Punta Carrera	7.45	1.28	7.3	6.35	8.56	3.99	11.22
	Isla Grevy	7.45	1.41	7.4	6.23	8.68	3.63	10.79
Falklands	Sea Lion	7.26	1.80	7.09	5.64	8.82	3.03	12.24
	Pebble	7.71	1.99	7.56	5.94	9.48	2.99	12.77
South Georgia	Annenkov	1.88	1.41	1.76	0.69	3.04	-1.76	5.97
	Stromness	1.91	1.35	1.8	0.73	3.04	-1.74	6.06

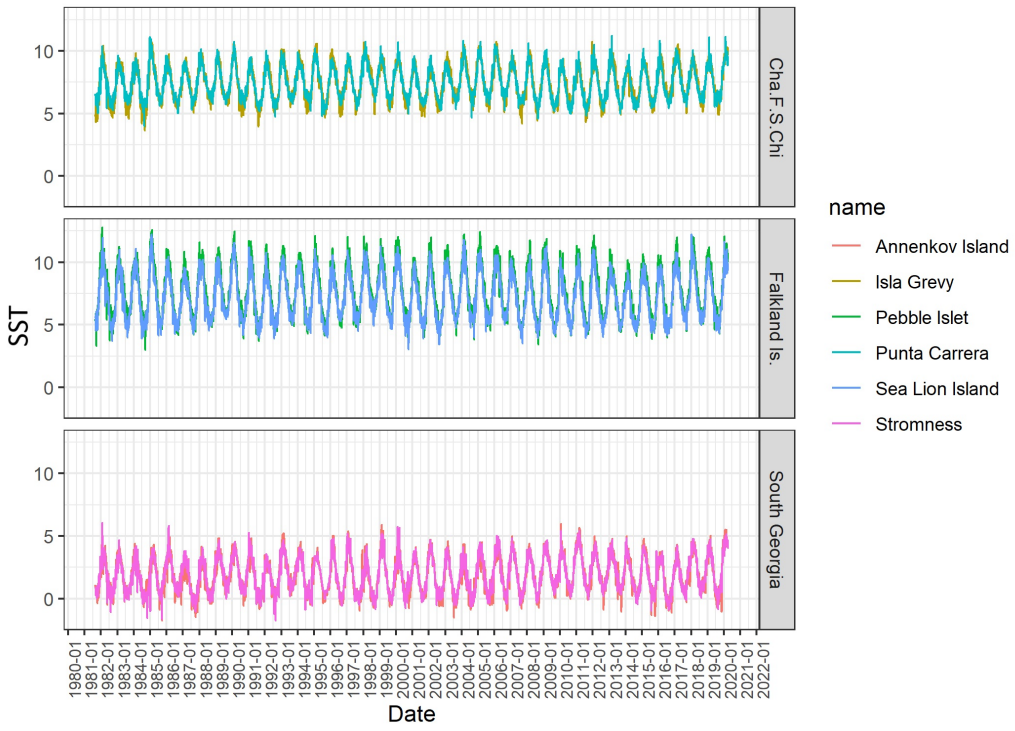


Figure A.1: Time series of NOAA Sea Surface Temperature (°C) from 1981 to 2020 in the SST-representative pixels per ecoregion.

A.3 Supplementary Materials Paper 3

A.3.1 Satellite versus in-situ SST data

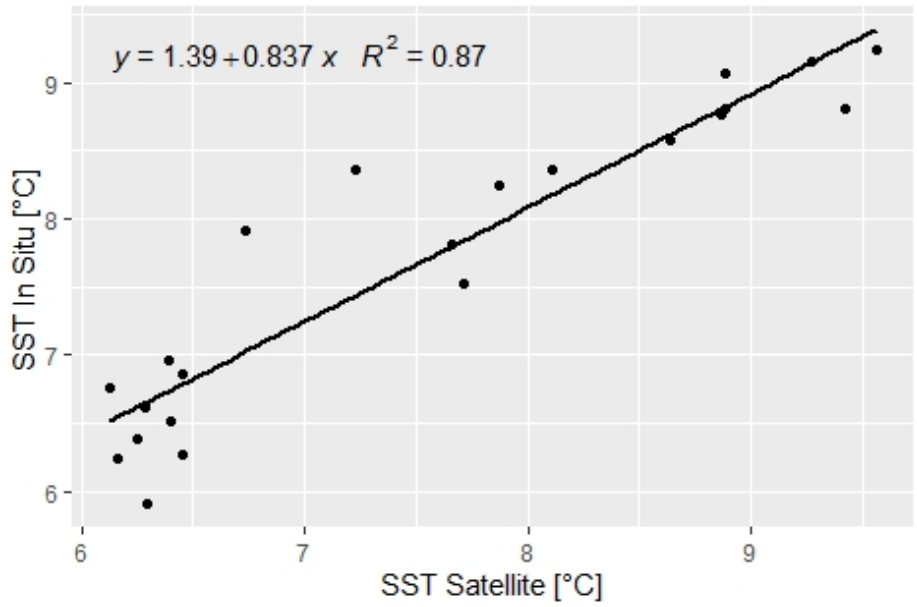


Figure A.2: Linear model of SST *in situ* versus SST Statellite.

A.3.2 SST, U10 and V10 Anomaly maps for severe and extreme events

MHW and MCS events categories III and IV occurred in the area of study, ordered chronologically.

Each image contains

- a table indicating the name of the event, start, peak and end dates, category, maximum intensity (°C), total duration of days, days under the categories moderate (I), strong (II), severe (III) and extreme (IV), season, and name of the ecosystem.
- Anomaly maps of the eastward (U10) and northward (V10) winds 10 m above the surface, computed each 6 hours, from the ERA5 reanalysis, and sea surface temperatures computed from the OISST model. Each anomaly map is a mean from the start to the end dates covering from 1981 to 2020. Ecosystems in focus are indicated with black arrows.
- Plots the largest intensity in the series, considering the start, peak, and end dates of each event.

1) MCS, BH2 1981, MCS E4 1981

even	event_nan	start_date	peak_date	end_date	category	i_max	var (sd)	duration	days_mod	days_sto	days_severe	days_extreme	season	name
2	BH2 1981	08-10-1981	**10-10-1981**	19-10-1981	III Severe	-1.79	0.27	12	2	5	5	0	Spring	Nassau Hornos
1	E4 1981	08-10-1981	**10-10-1981**	13-10-1981	III Severe	-2.75	0.64	6	1	3	2	0	Spring	Western Strait

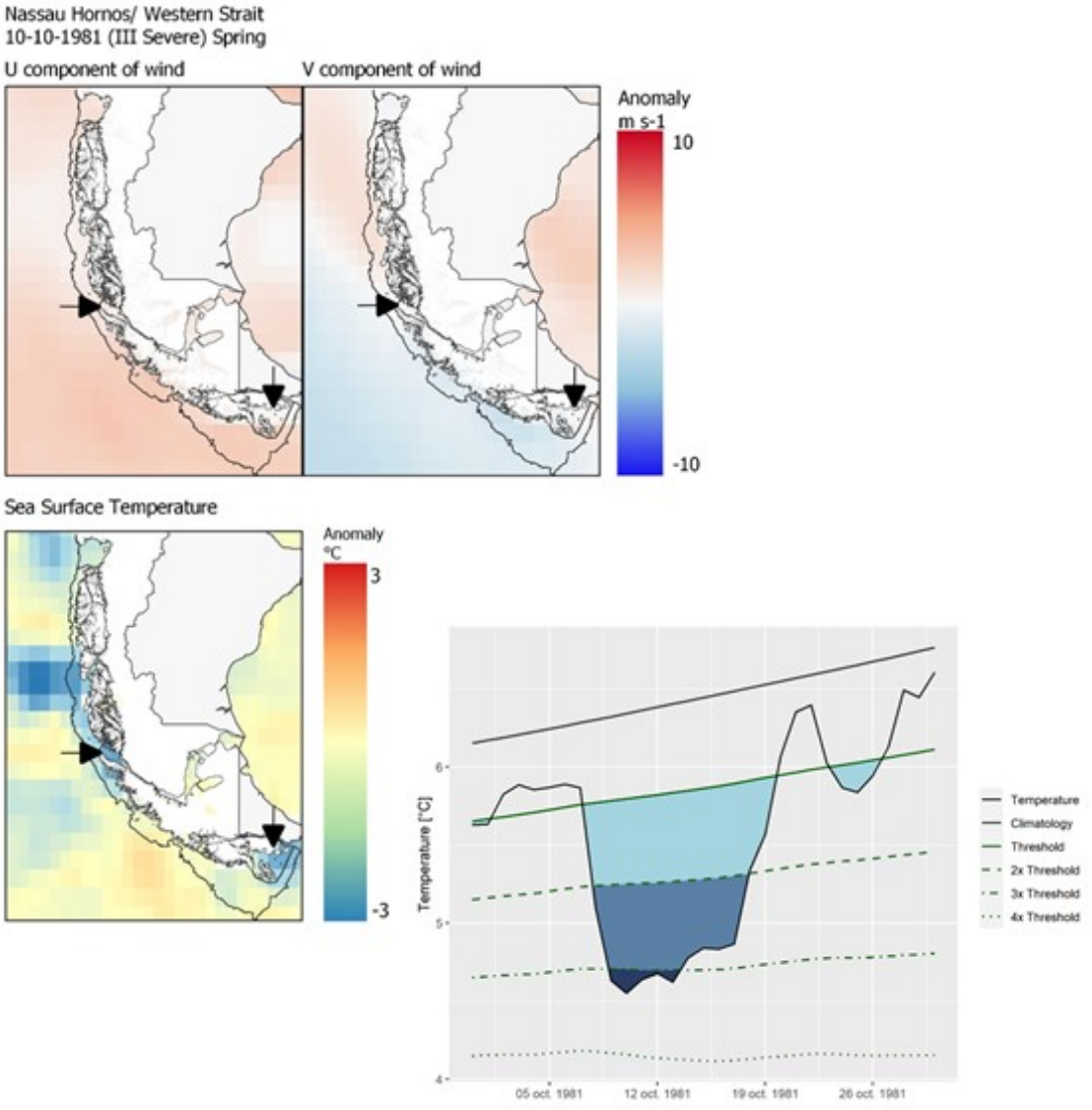


Figure A.3: 1) MCS: BH2 1981, MCS E4 1981

2) MCS, CE2 1982a, E4 1982b, C1 1982

even	event_nan	start_date	peak_date	end_date	category	i_max	var (sd)	duration	days_mod	days_sto	days_severe	days_extreme	season	name
4	CE2 1982a	01-04-1982	**02-04-1982**	06-04-1982	III Severe	-2.43	0.75	6	3	0	3	0	Fall	Offshore Kaweskar
3	E4 1982b	01-04-1982	**02-04-1982**	13-04-1982	III Severe	-3.51	0.98	13	6	1	6	0	Fall	Western Strait
2	C1 1982	01-04-1982	**03-04-1982**	07-04-1982	IV Extreme	-3.34	0.62	7	1	0	4	2	Fall	Inner Channels Kaweskar

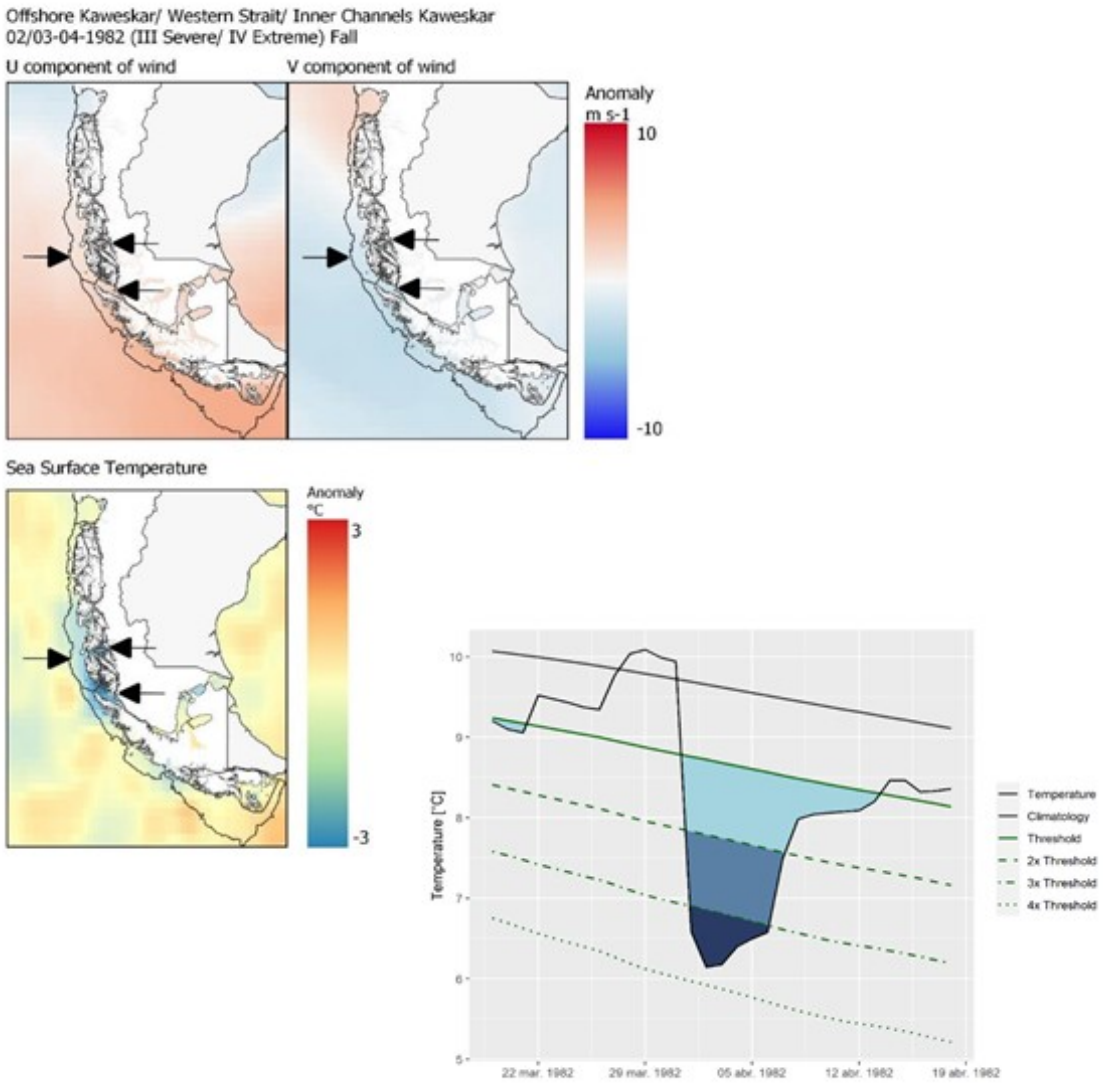


Figure A.4: 2) MCS: CE2 1982a, E4 1982b, C1 1982

3) MCS CE1 1982a

even	event_nan	start_date	peak_date	end_date	category	i_max	var (sd)	duration	days_mod	days_sto	days_severe	days_extreme	season	name
4	CE1 1982a	19-04-1982	**20-04-1982**	23-04-1982	III Severe	-2.83	0.33	5	0	3	2	0	Fall	Gulf of Penas

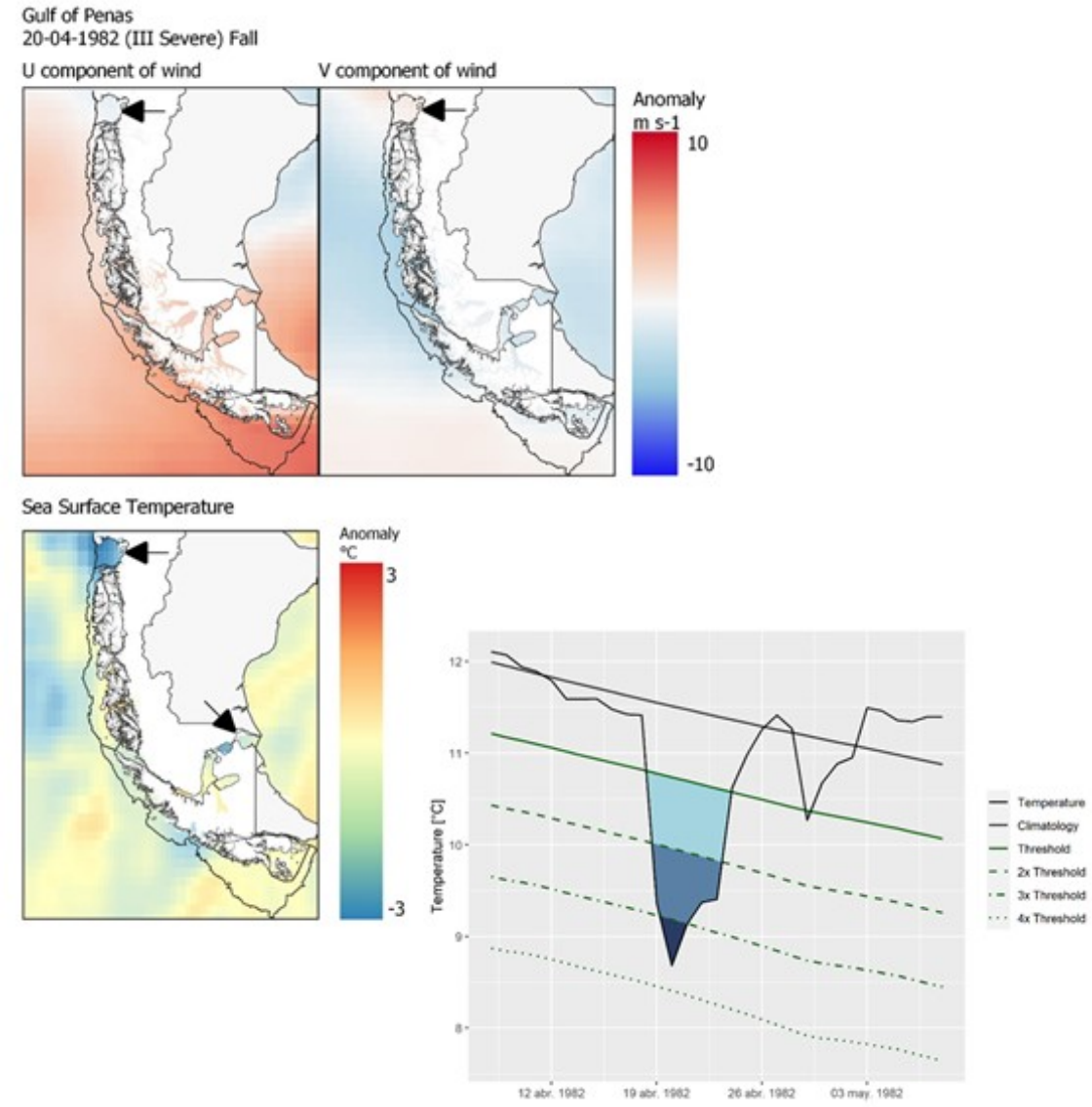


Figure A.5: 3) MCS: CE1 1982a

4) MCS E1 1982b

even	event_nan	start_date	peak_date	end_date	category	i_max	var (sd)	duration	days_mod	days_sto	days_severe	days_extreme	season	name
4	E1 1982b	05-07-1982	**26-07-1982**	19-10-1982	III Severe	-2.36	0.41	107	68	37	1	0	Winter/ S	Eastern Strait

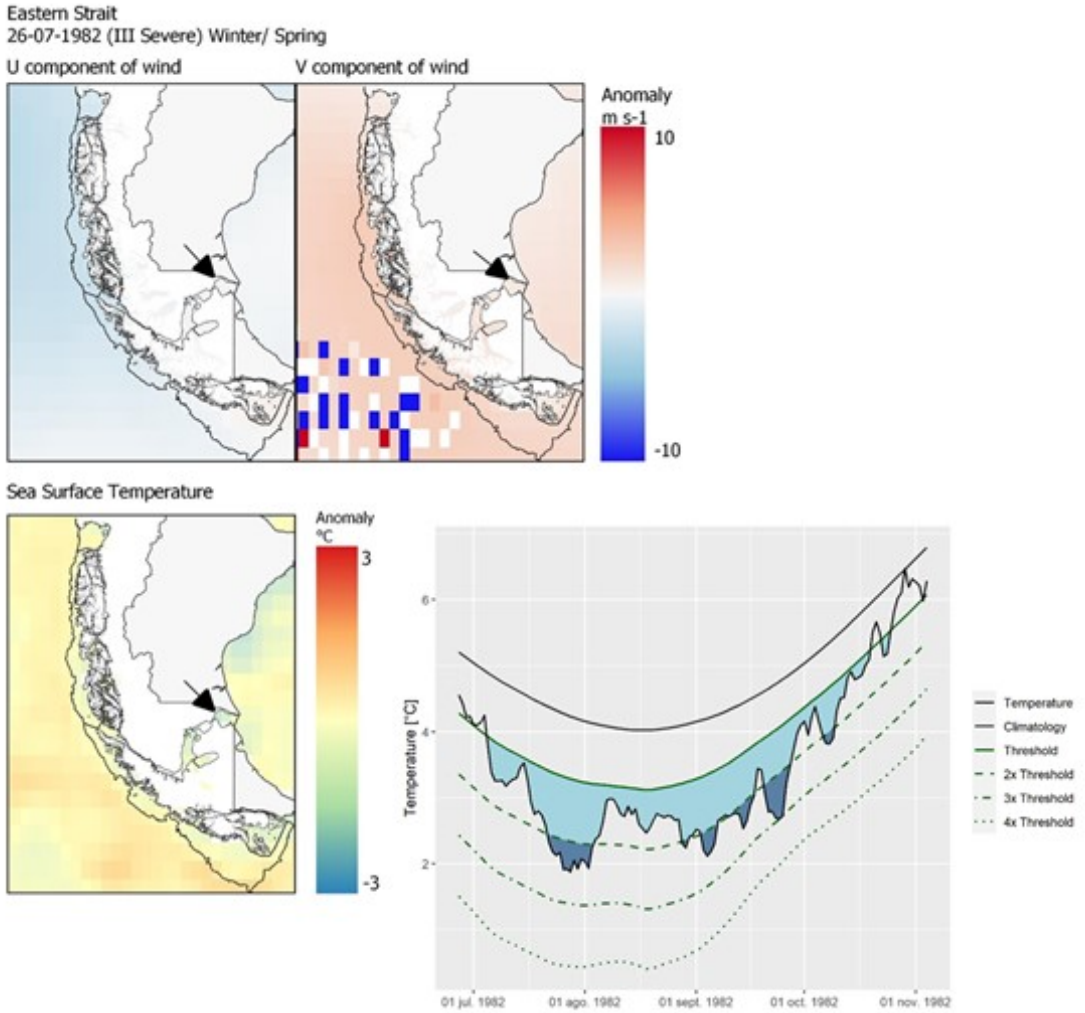


Figure A.6: 4) MCS: E1 1982b

5) MCS E3 1982

even	event_nan	start_date	peak_date	end_date	category	i_max	var (sd)	duration	days_mod	days_sto	days_severe	days_extreme	season	name
5	E3 1982	20-09-1982	**21-09-1982**	25-09-1982	IV Extreme	-1.84	0.26	6	0	1	4	1	Winter	Bahia Inutil Strait

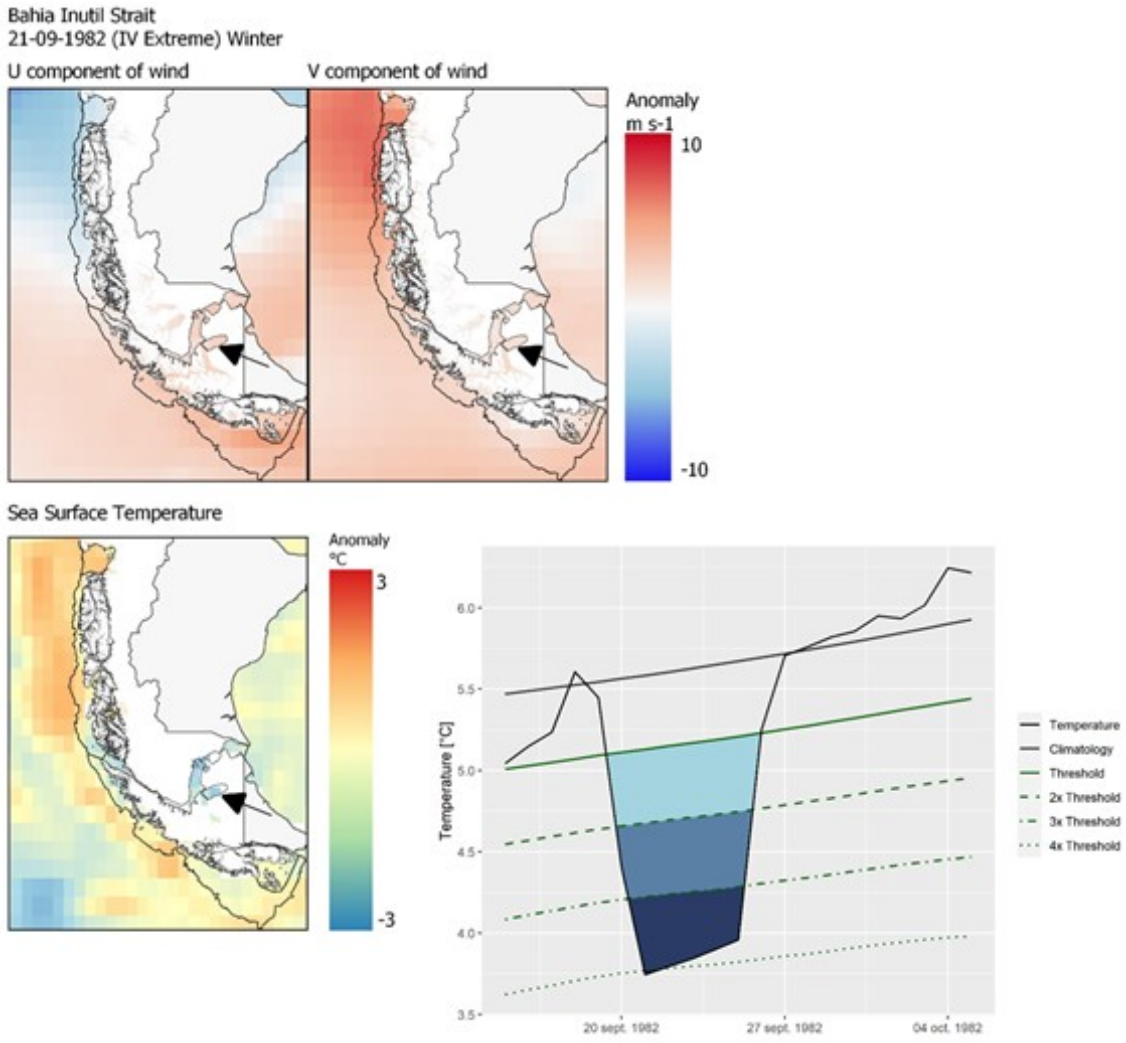


Figure A.7: 5) MCS: E3 1982

6) MCS E1 1984b

even	event_nan	start_date	peak_date	end_date	category	i_max	var (sd)	duration	days_mod	days_sto	days_severe	days_extreme	season	name
9	E1 1984b	04-05-1984	**17-08-1984**	02-11-1984	III Severe	-2.56	0.44	183	88	92	2	0	Fall/ Spri	Eastern Strait

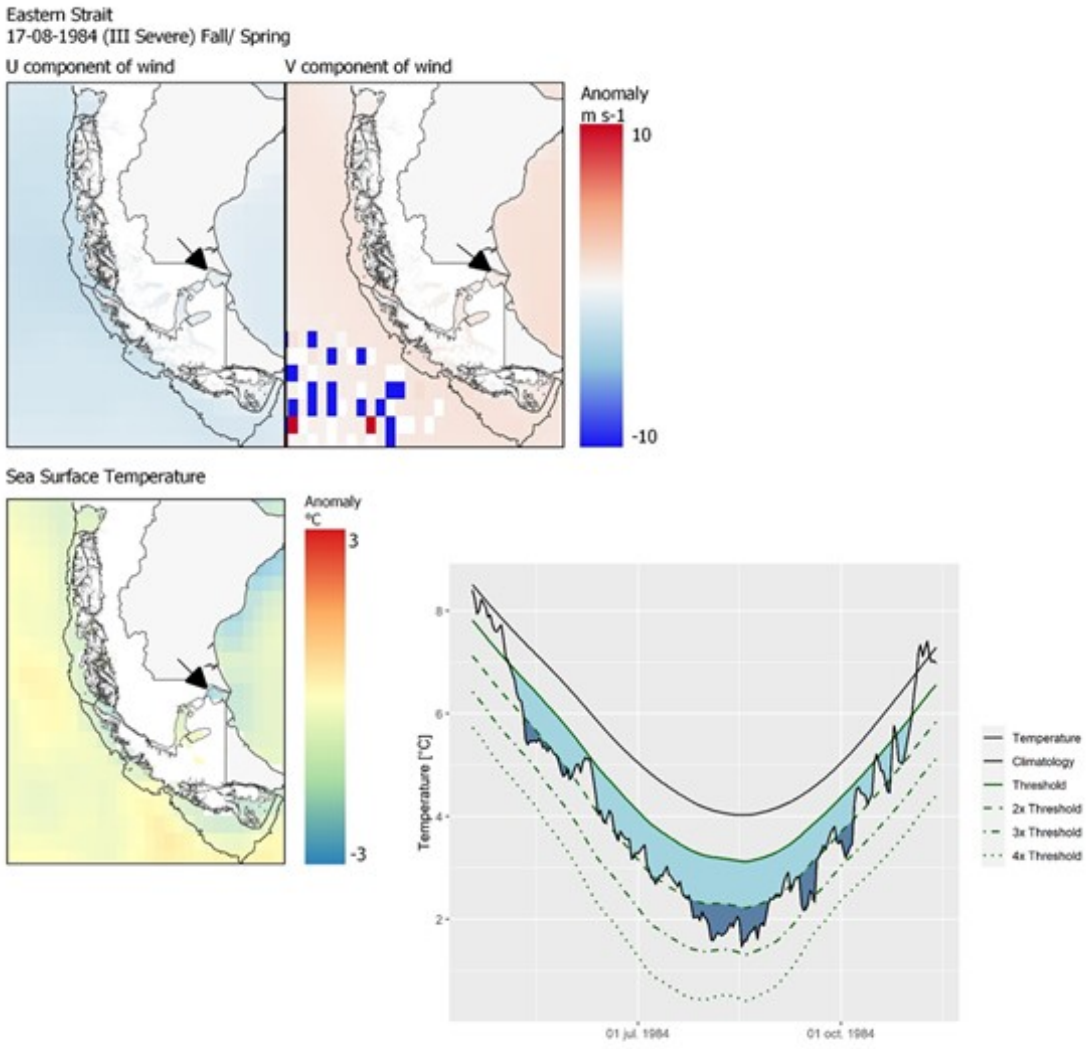


Figure A.8: 6) MCS: E1 1984b

7) MHW E2 1984b
MHW E3 1984
MHW CE2 1984

even	event_nan	start_date	peak_date	end_date	category	i_max	var (sd)	duration	days_mod	days_sto	days_severe	days_extreme	season	name
3	E2 1984b	15-12-1984	**26-12-1984**	30-12-1984	IV Extreme	2.62	0.53	16	1	8	1	6	Spring	Central Strait
4	E3 1984	18-12-1984	**26-12-1984**	30-12-1984	III Severe	2.64	0.44	13	3	7	3	0	Spring	Bahia Inutil - Strait
7	CE2 1984	15-12-1984	**27-12-1984**	30-12-1984	III Severe	2.53	0.52	16	5	8	3	0	Spring	Offshore Kaweskar

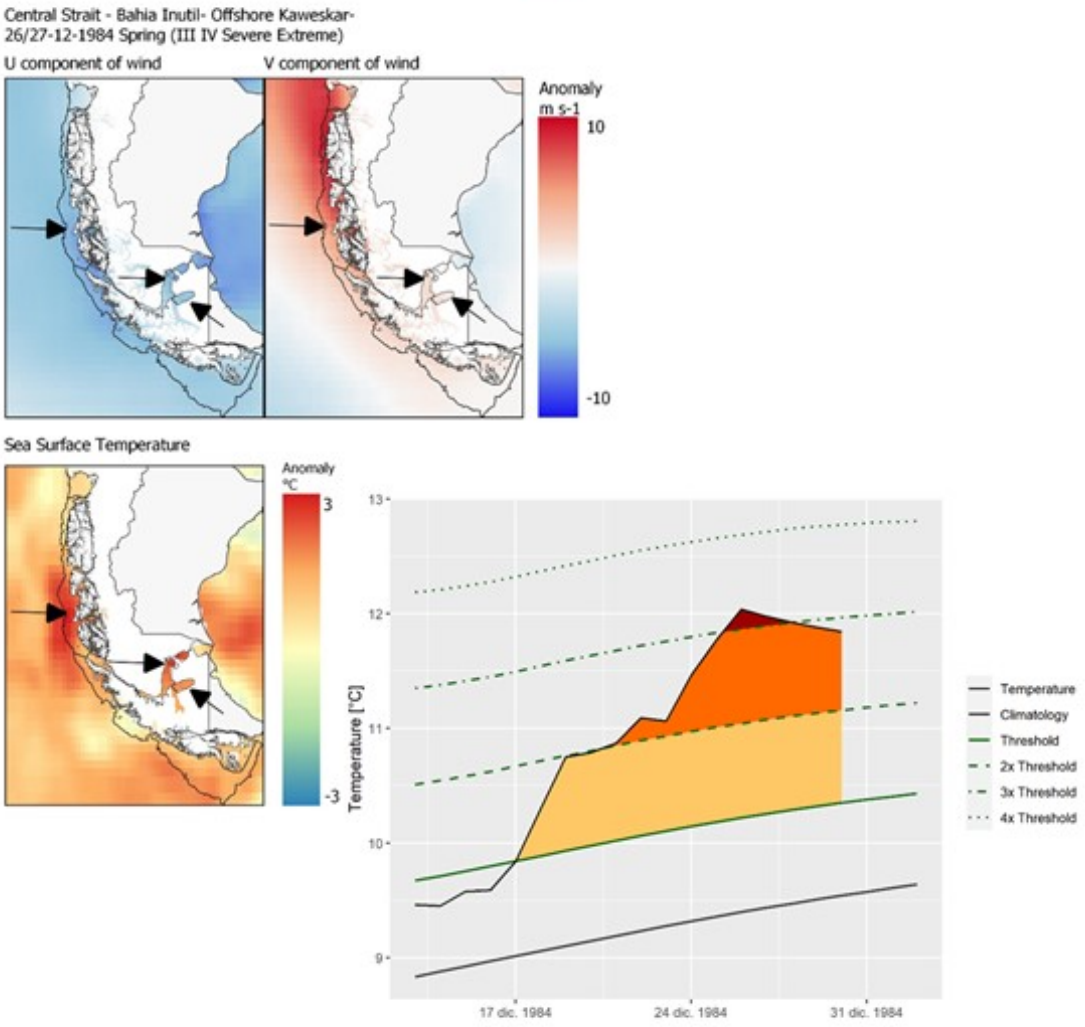


Figure A.9: 7) MHW: E2 1984b, E3 1984, CE2 1984

8) MCS CE1 1991

even	event_nan	start_date	peak_date	end_date	category	i_max	var (sd)	duration	days_mod	days_sto	days_severe	days_extreme	season	name
28	CE1 1991	29-05-1991	**31-05-1991**	16-06-1991	III Severe	-2.47	0.62	19	12	4	1	0	Fall	Gulf of Penas

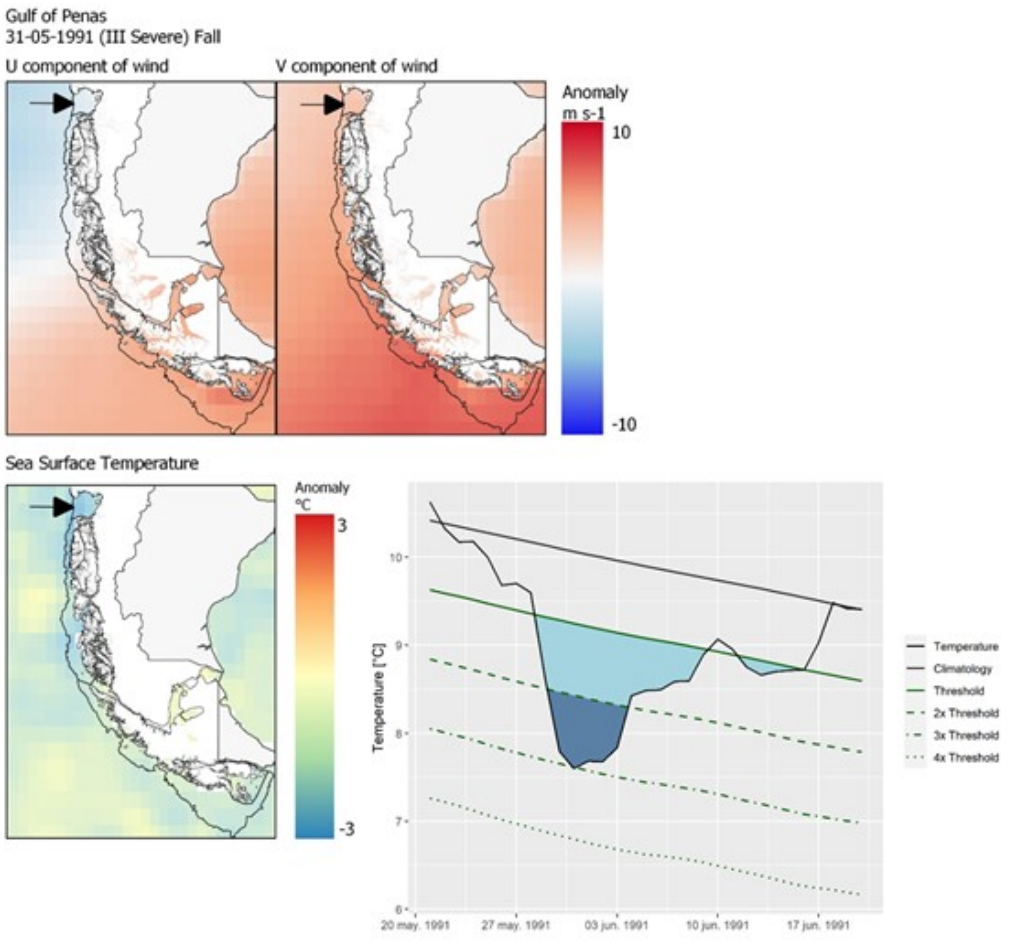


Figure A.10: 8) MCS: CE1 1991

9) MCS BH2 1995a

even	event_nan	start_date	peak_date	end_date	category	i_max	var (sd)	duration	days_mod	days_sto	days_severe	days_extreme	season	name
26	BH2 1995a	18-04-1995	**22-04-1995**	26-04-1995	III Severe	-1.94	0.57	9	6	1	2	0	Fall	Nassau Hornos

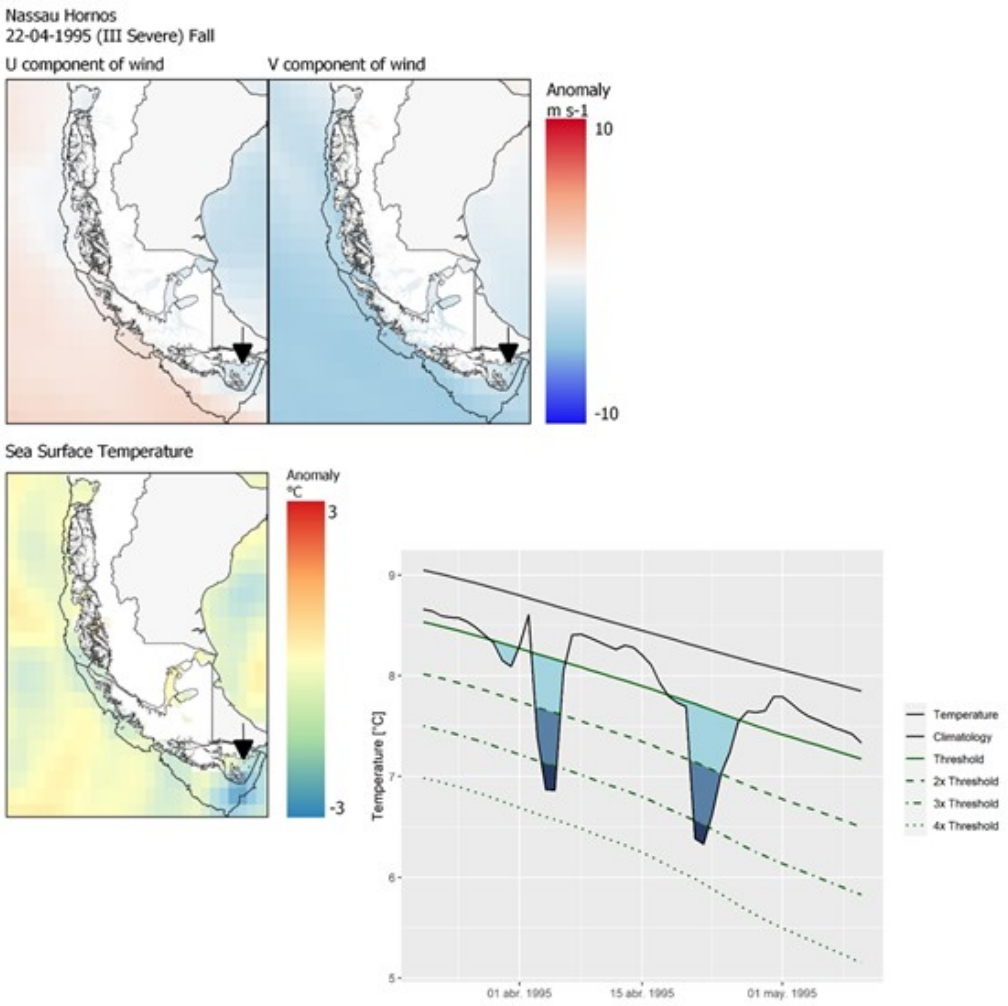


Figure A.11: 9) MCS: BH2 1995a

10) MHW CE1 1998b
CE3 1998a, BH2 1998, C1 1998b E4 1998b
BH1 1998 E2 1998b E1 1998

even	event_nan	start_date	peak_date	end_date	category	i_max	var (sd)	duration	days_mod	days_sto	days_severe	days_extreme	season	name
28	CE1 1998b	24-05-1998	**05-07-1998**	12-09-1998	III Severe	2.19	0.4	112	57	52	3	0	Fall/ Win	Gulf of Penas
35	CE3 1998a	10-04-1998	**05-07-1998**	11-08-1998	III Severe	2.32	0.38	124	74	43	4	0	Fall/ Win	Offshore Magallanes
28	BH2 1998	14-04-1998	**13-07-1998**	06-09-1998	IV Extreme	2.42	0.4	146	80	44	18	1	Fall/ Win	Nearshore Nassau Hornos
40	C1 1998b	10-06-1998	**14-07-1998**	13-09-1998	III Severe	3.01	0.57	96	52	33	11	0	Fall/ Win	Inner Channels Kaweskar
35	E4 1998b	17-06-1998	**14-07-1998**	05-08-1998	III Severe	3.84	0.72	50	19	29	2	0	Fall/ Win	Western Strait
35	BH1 1998	02-06-1998	**24-07-1998**	03-08-1998	III Severe	2.93	0.62	63	31	21	10	0	Fall/ Win	Nearshore Beagle Ballenero
30	E2 1998b	12-04-1998	**31-07-1998**	14-09-1998	III Severe	1.58	0.22	156	87	66	2	0	Fall/ Win	Central Strait
37	E1 1998	19-03-1998	**05-09-1998**	15-09-1998	III Severe	2.35	0.3	181	83	94	4	0	Winter	Eastern Strait

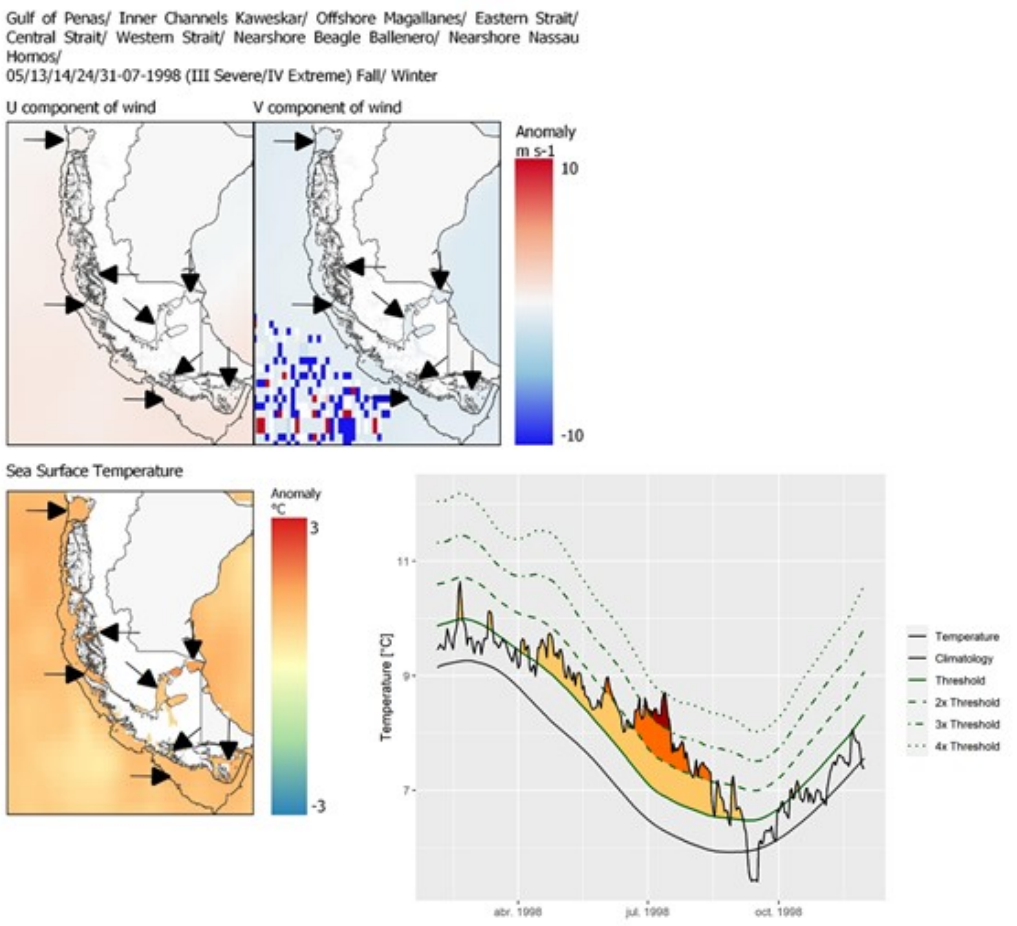


Figure A.12: 10) MHW: CE1 1998b, CE3 1998a, BH2 1998, C1 1998b, E4 1998b, BH1 1998, E2 1998b, E1 1998

11) MCS E4 2007b

even	event_nan	start_date	peak_date	end_date	category	i_max	var (sd)	duration	days_mod	days_sto	days_severe	days_extreme	season	name
67	E4 2007b	13-12-2007	**17-12-2007**	23-12-2007	III Severe	-2.83	0.62	11	6	4	1	0	Spring	Western Strait

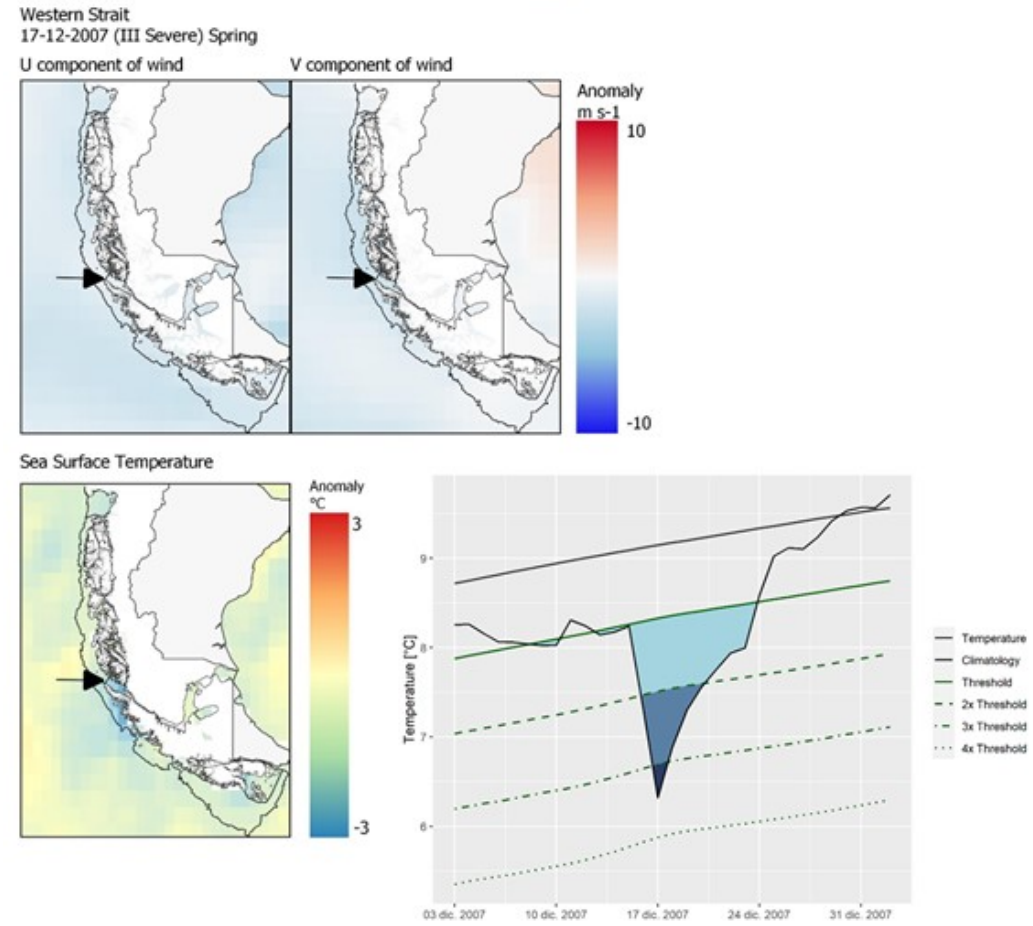


Figure A.13: 11) MCS: E4 2007b

12) MCS E3 2008

even	event_nan	start_date	peak_date	end_date	category	i_max	var (sd)	duration	days_mod	days_sto	days_severe	days_extreme	season	name
46	E3 2008	18-08-2008	**29-08-2008**	05-09-2008	III Severe	-1.85	0.39	19	15	2	2	0	Winter	Bahia Inutil Strait

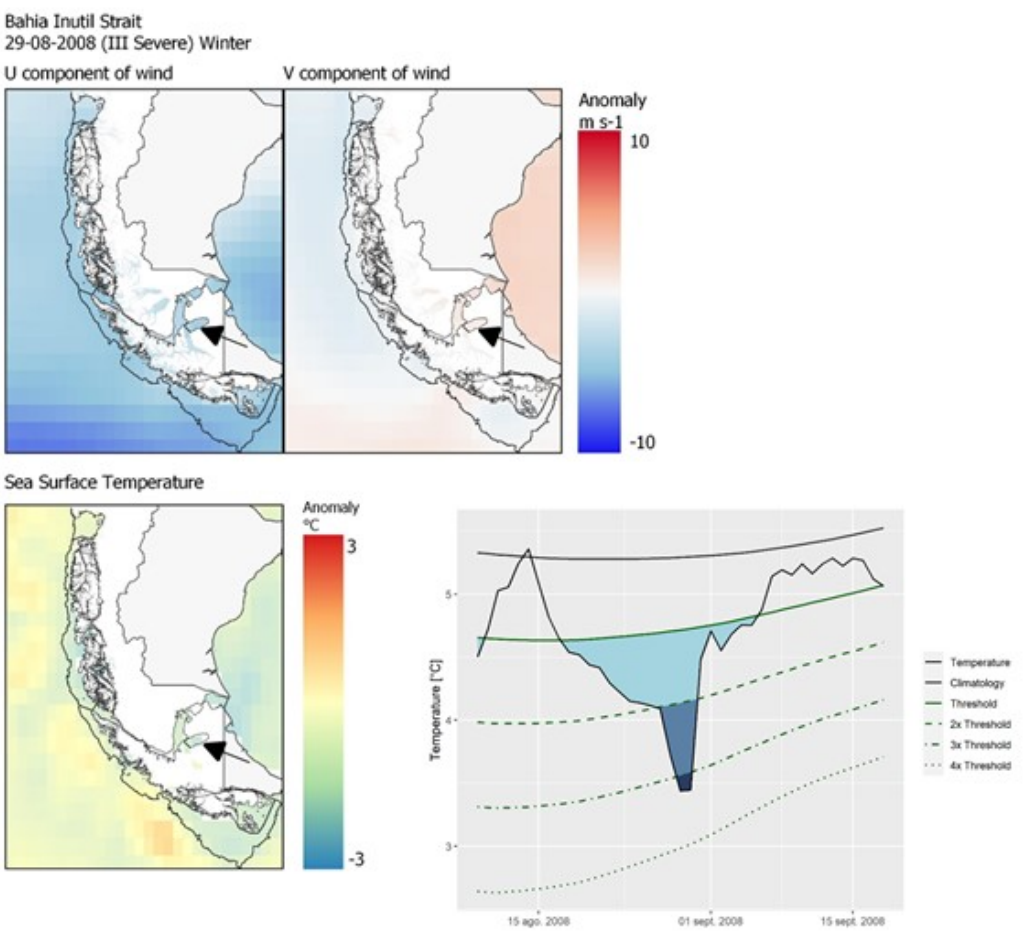


Figure A.14: 12) MCS: E3 2008

13) MCS E3 2011

even	event_nan	start_date	peak_date	end_date	category	i_max	var (sd)	duration	days_mod	days_sto	days_severe	days_extreme	season	name
63	E3 2011	03-05-2011	**09-05-2011**	11-05-2011	III Severe	-1.84	0.45	9	6	1	2	0	Fall	Bahia Inutil Strait

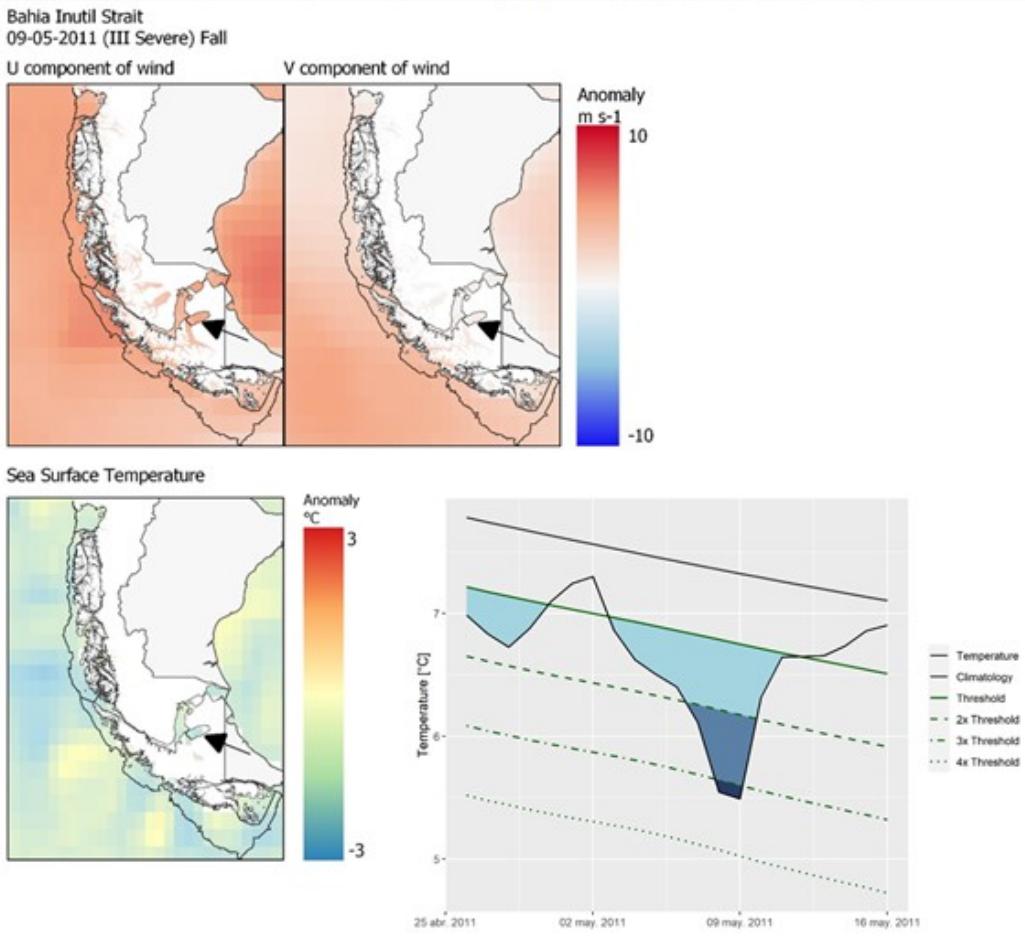


Figure A.15: 13) MCS: E3 2011

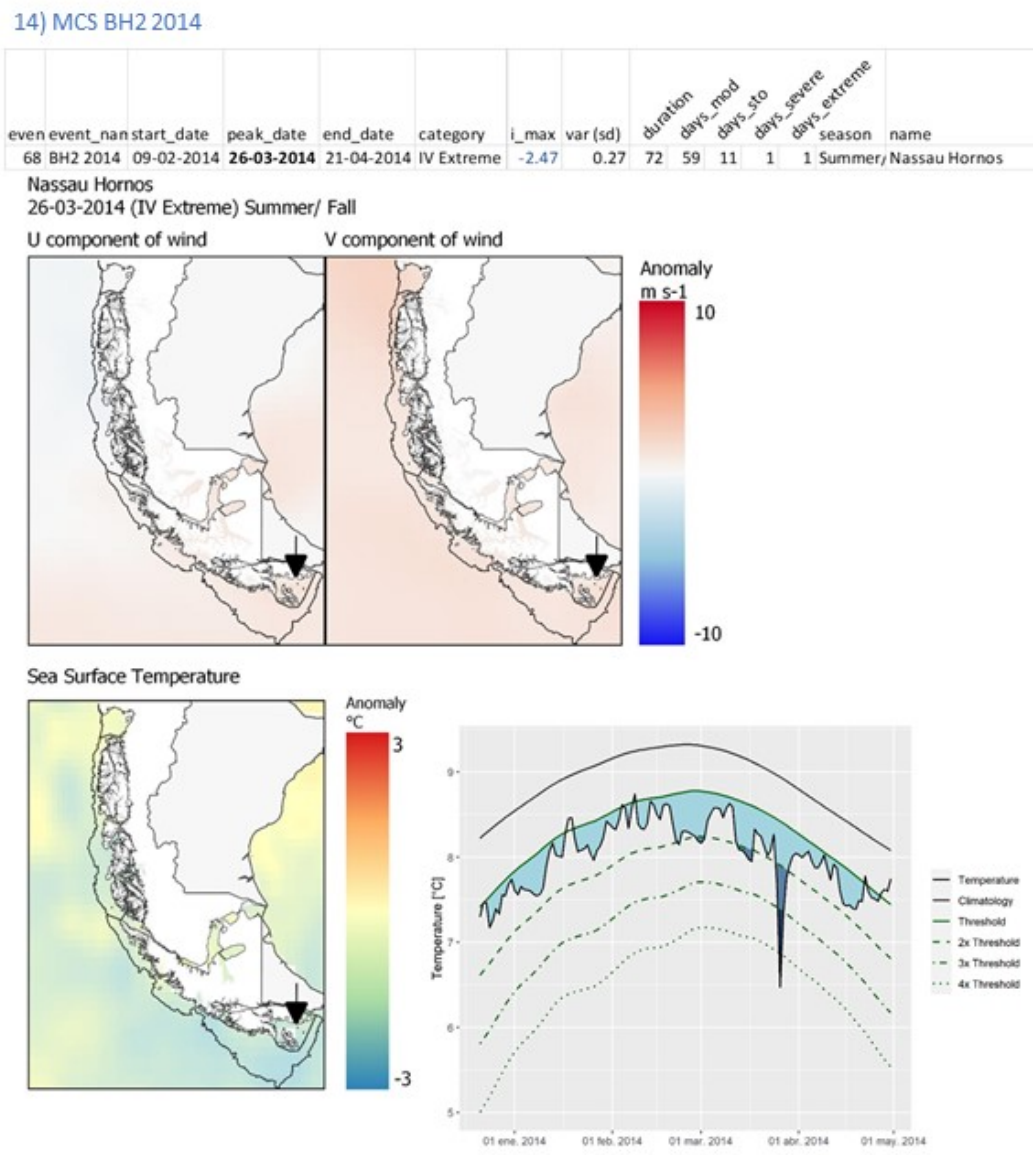


Figure A.16: 14) MCS: BH2 2014

15) MCS E4 2015

even	event_nan	start_date	peak_date	end_date	category	i_max	var (sd)	duration	days_mod	days_sto	days_severe	days_extreme	season	name
92	E4 2015	04-07-2015	**07-07-2015**	19-07-2015	IV Extreme	-5.93	1.4	16	7	4	2	3	Winter	Western Strait

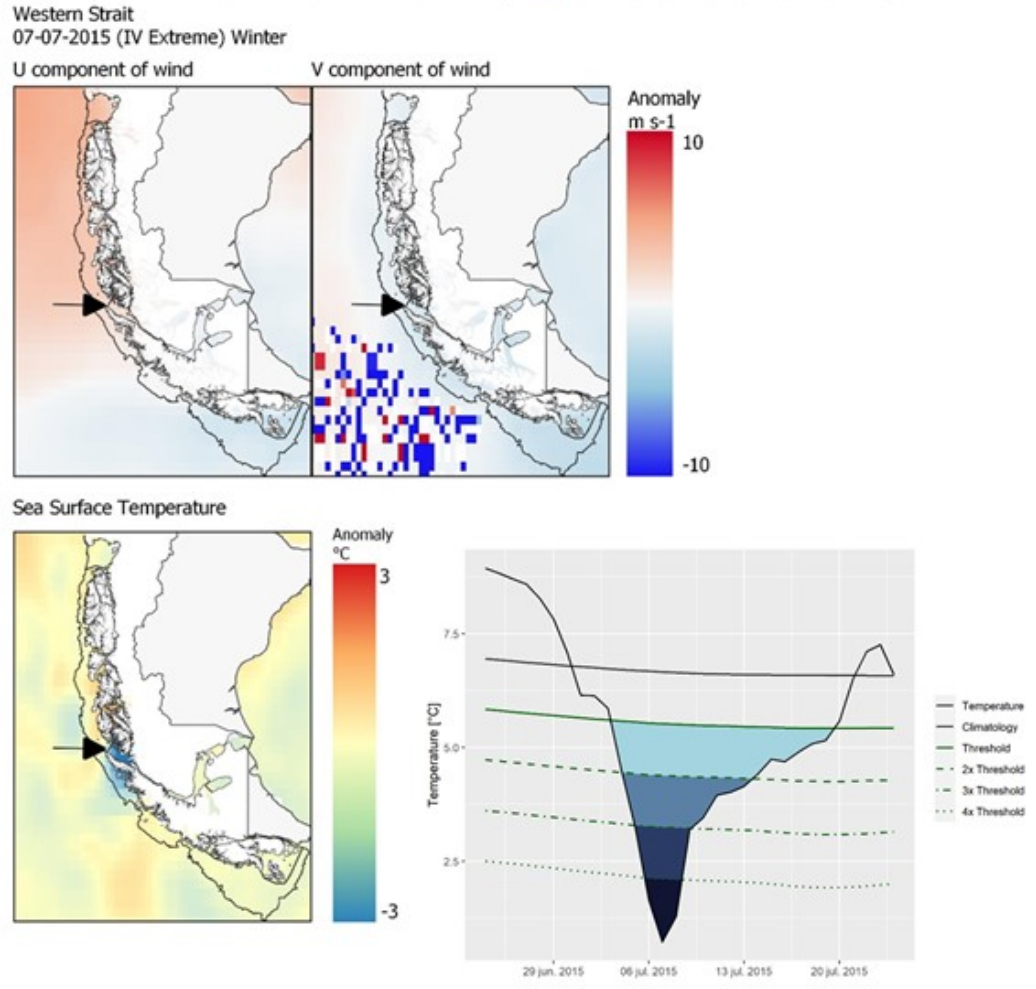


Figure A.17: 15) MCS: E4 2015

16) MCS C1 2015b

even	event_nan	start_date	peak_date	end_date	category	i_max	var (sd)	duration	days_mod	days_sto	days_severe	days_extreme	season	name
85	C1 2015b	12-08-2015	**23-08-2015**	06-09-2015	III Severe	-2.58	0.41	26	9	15	2	0	Winter	Inner Channels Kaweskar

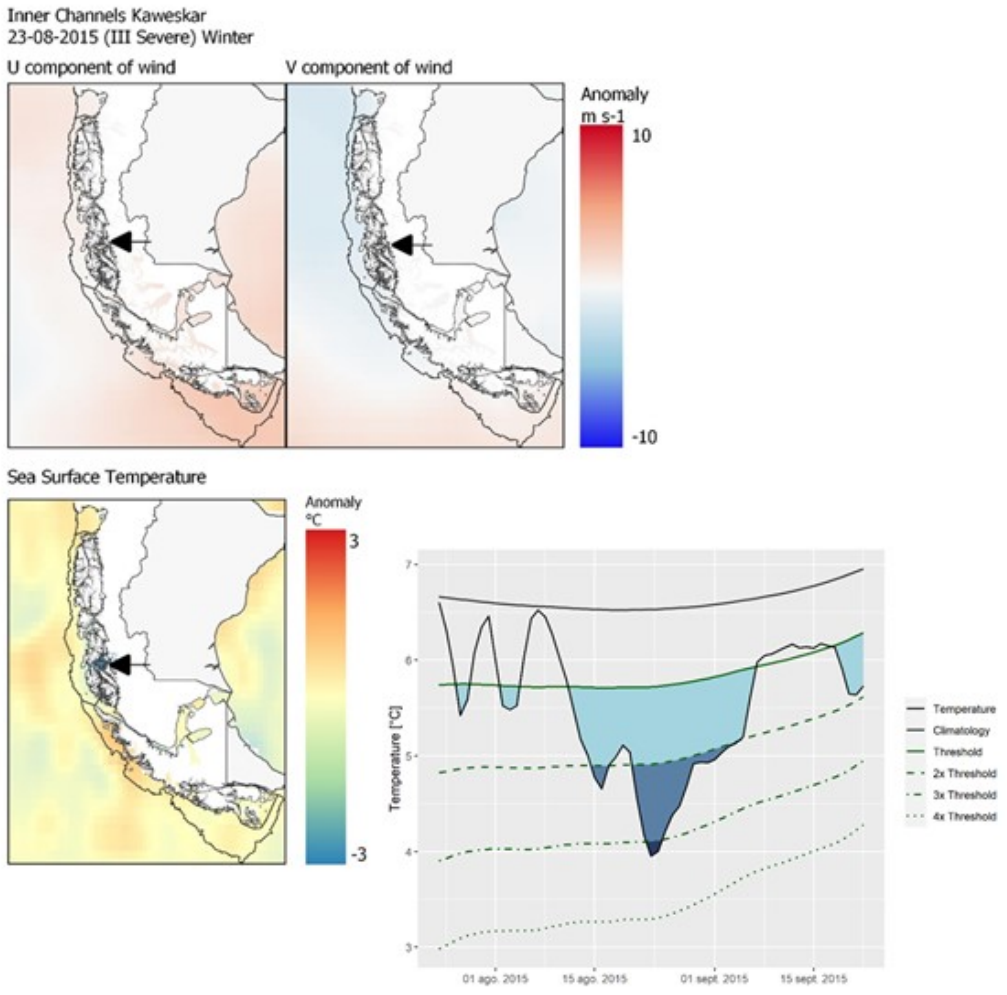


Figure A.18: 16) MCS: C1 2015b

17) MCS BH1 2015

even	event_nan	start_date	peak_date	end_date	category	i_max	var (sd)	duration	days_mod	days_sto	days_severe	days_extreme	season	name
90	BH1 2015	23-08-2015	**27-08-2015**	28-08-2015	III Severe	-2.53	0.62	6	4	1	1	0	Winter	Nearshore Beagle Ballenero

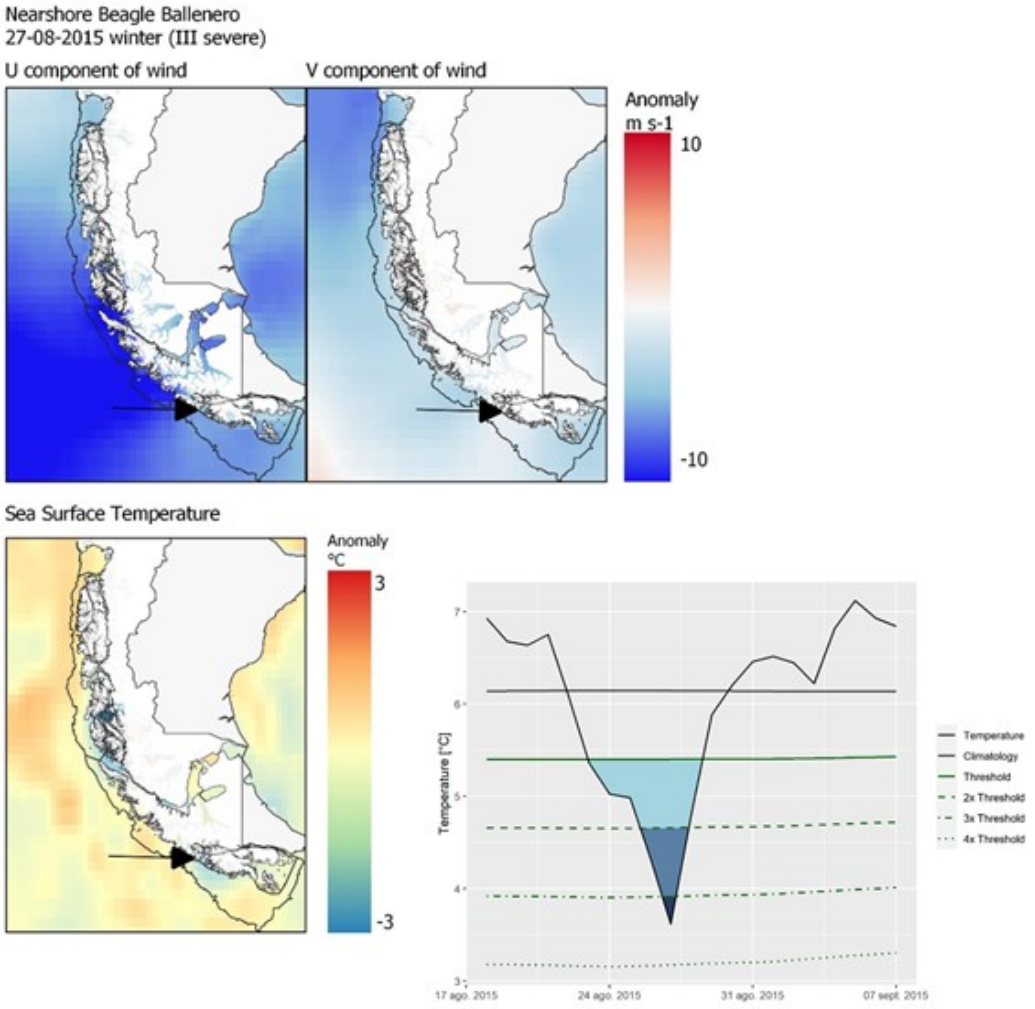


Figure A.19: 17) MCS: BH1 2015

18)
MHW CE2 2016a
MHW CE1 2016a

even	event_nan	start_date	peak_date	end_date	category	I_max	var (sd)	duration	days_mod	days_sto	days_severe	days_extreme	season	name
64	CE2 2016a	14-01-2016	**21-01-2016**	08-02-2016	III Severe	2.5	0.45	26	18	7	1	0	Summer	Offshore Kaweskar
62	CE1 2016a	12-01-2016	**22-01-2016**	15-02-2016	III Severe	3.62	0.63	35	25	7	3	0	Summer	Gulf of Penas

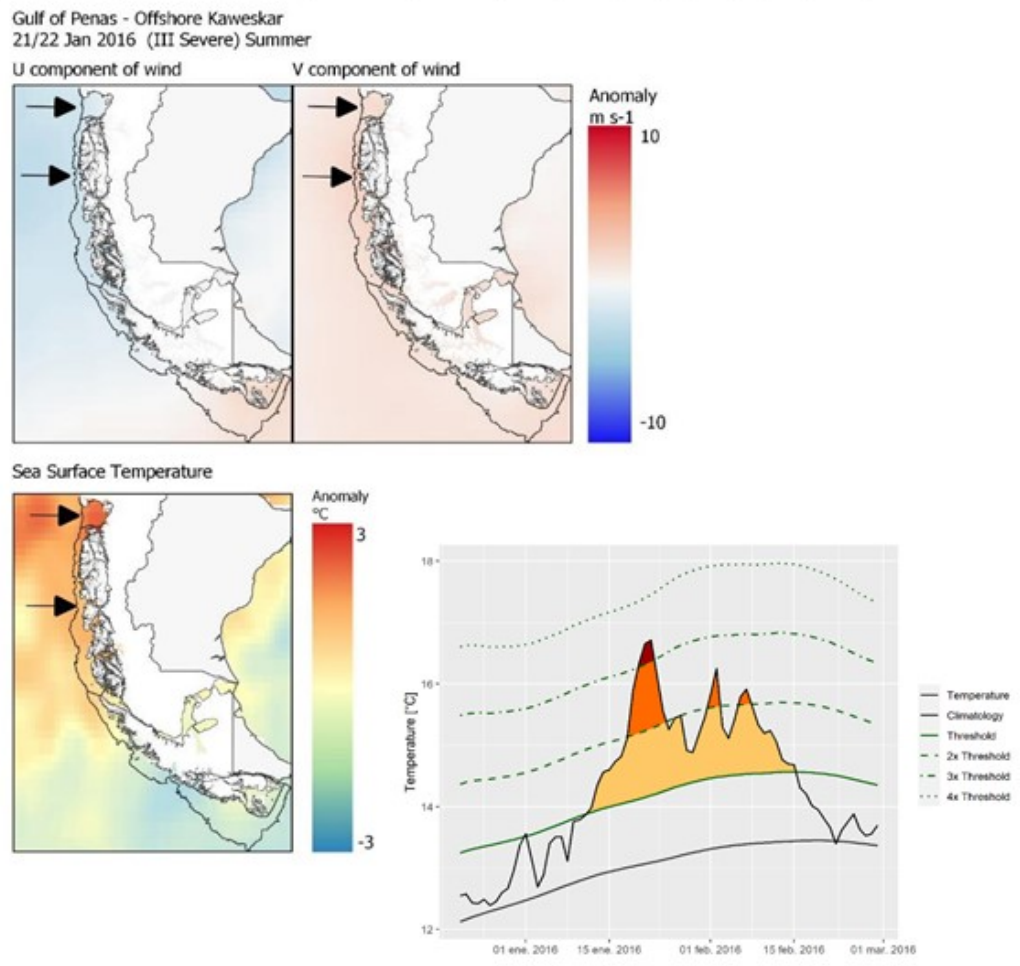


Figure A.20: 18) MHW: CE2 2016a, CE1 2016a

19) MCS BH2 2016

even	event_nan	start_date	peak_date	end_date	category	i_max	var (sd)	duration	days_mod	days_sto	days_severe	days_extreme	season	name
73	BH2 2016	14-04-2016	**18-04-2016**	09-05-2016	IV Extreme	-4.65	1.26	26	5	5	2	14	Fall	Nassau Hornos

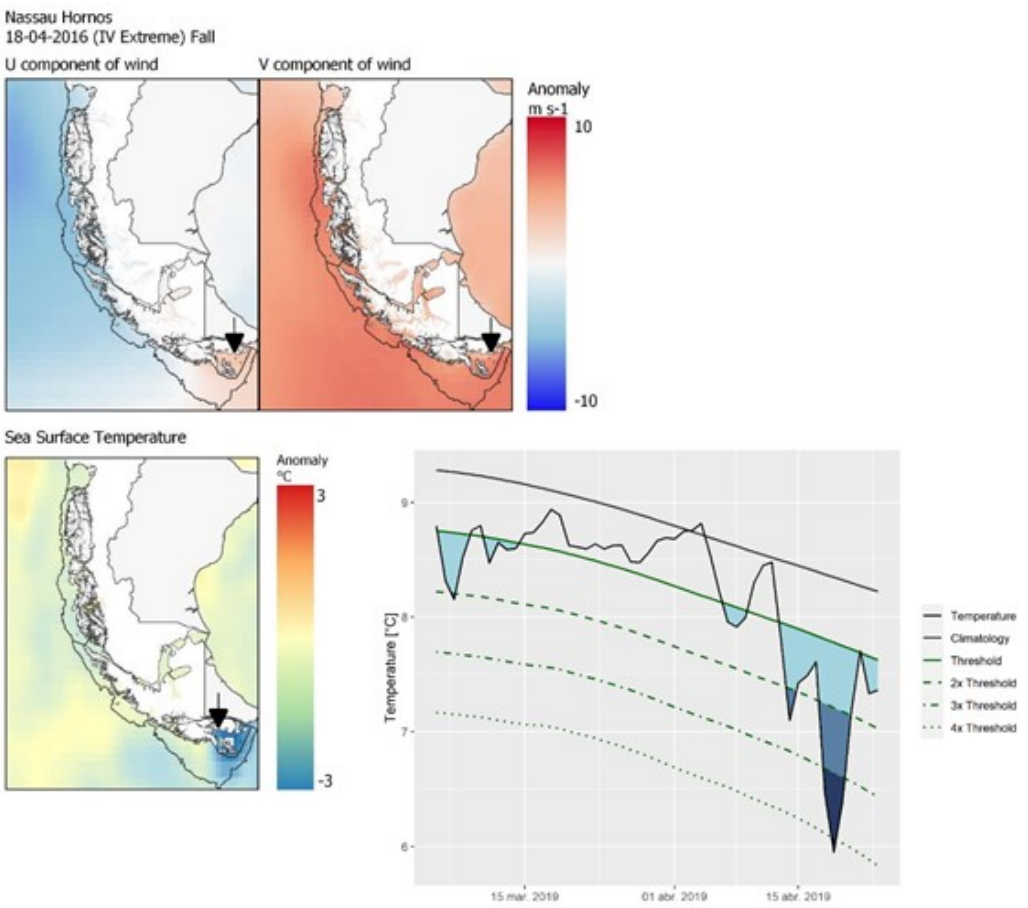


Figure A.21: 19) MCS: BH2 2016

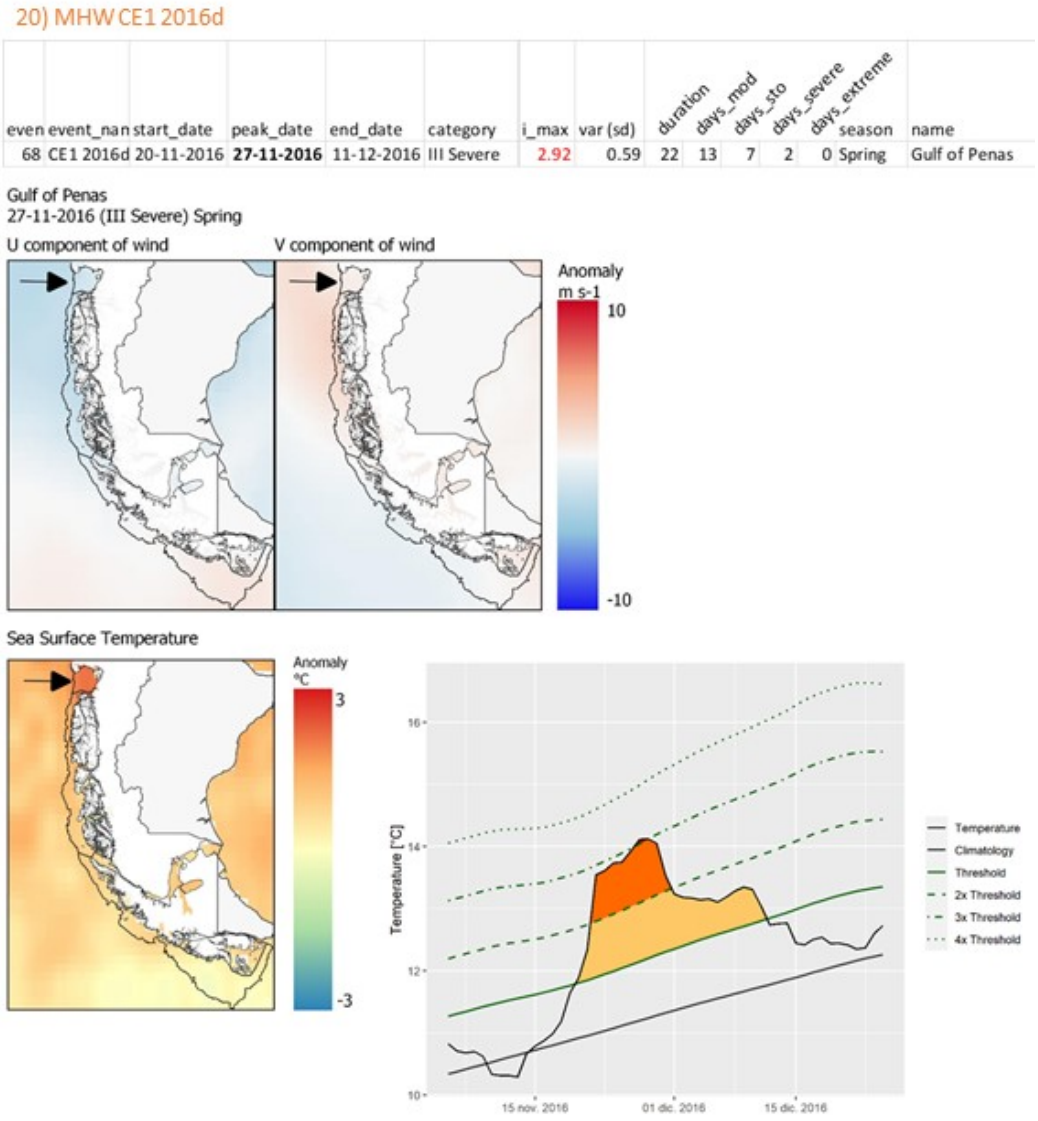


Figure A.22: 20) MHW: CE1 2016d

21) MCS BH1 2017

even	event_nan	start_date	peak_date	end_date	category	i_max	var (sd)	duration	days_mod	days_sto	days_severe	days_extreme	season	name
94	BH1 2017	05-08-2017	**07-08-2017**	18-08-2017	IV Extreme	-3.43	0.86	14	8	3	1	2	Winter	Nearshore Beagle Ballenero

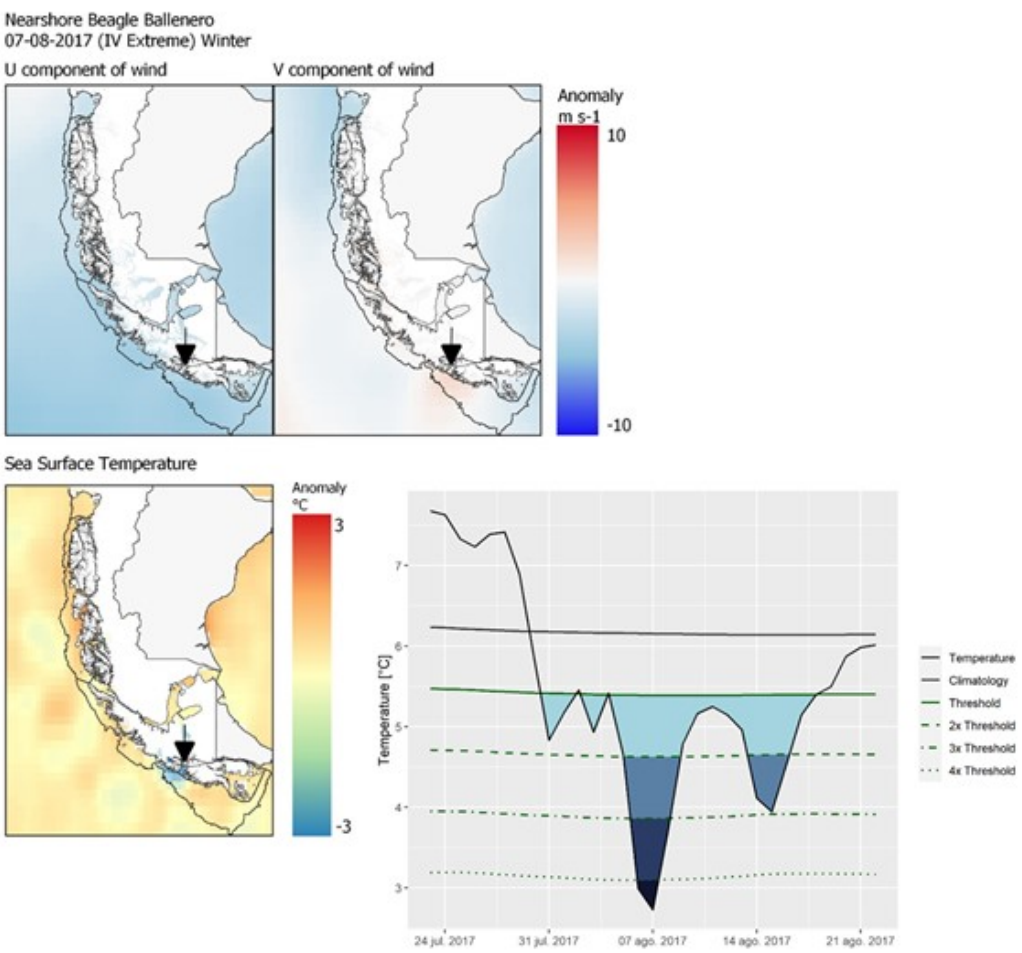


Figure A.23: 21) MCS: BH1 2017

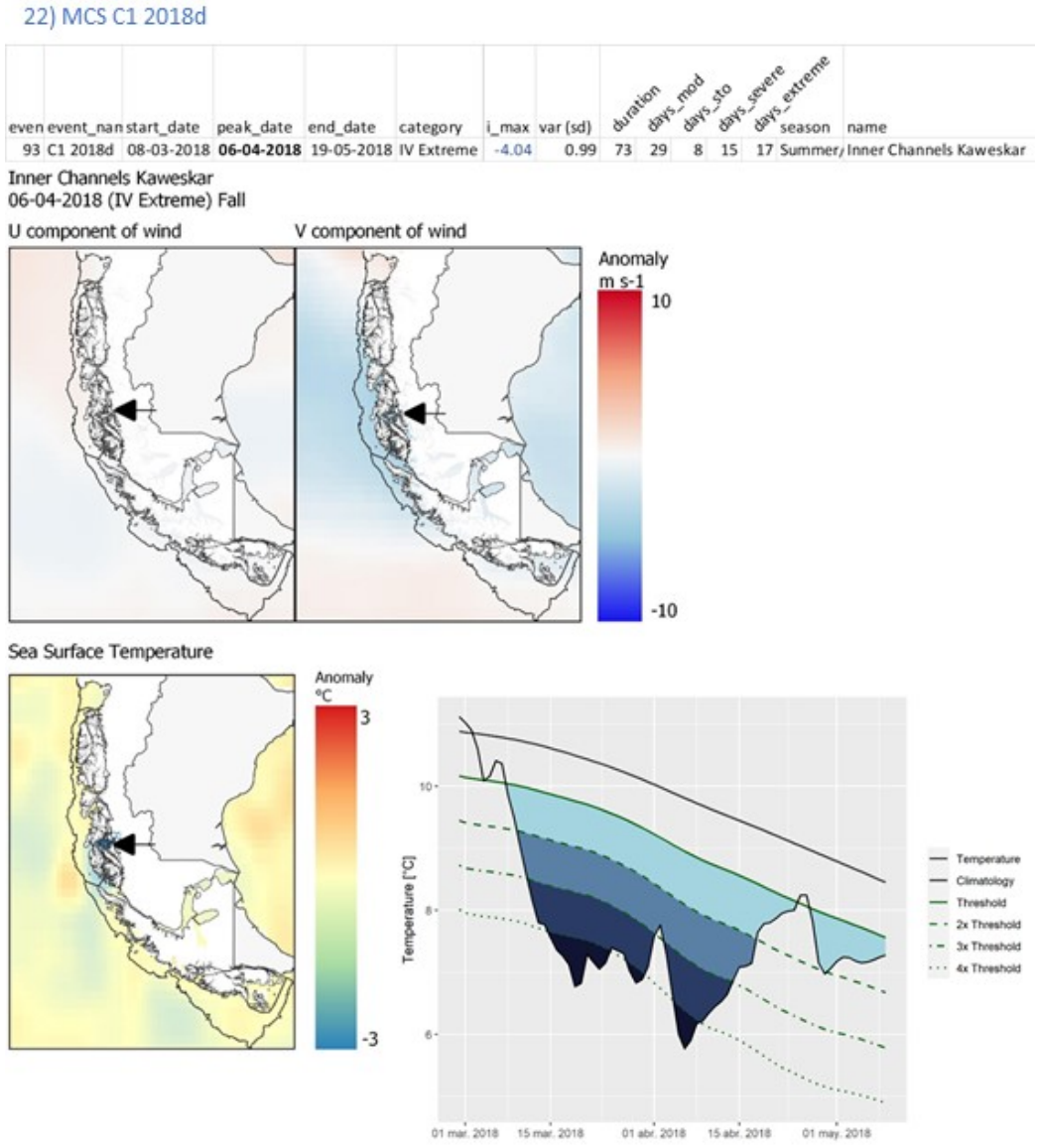


Figure A.24: 22) MCS: C1 2018d

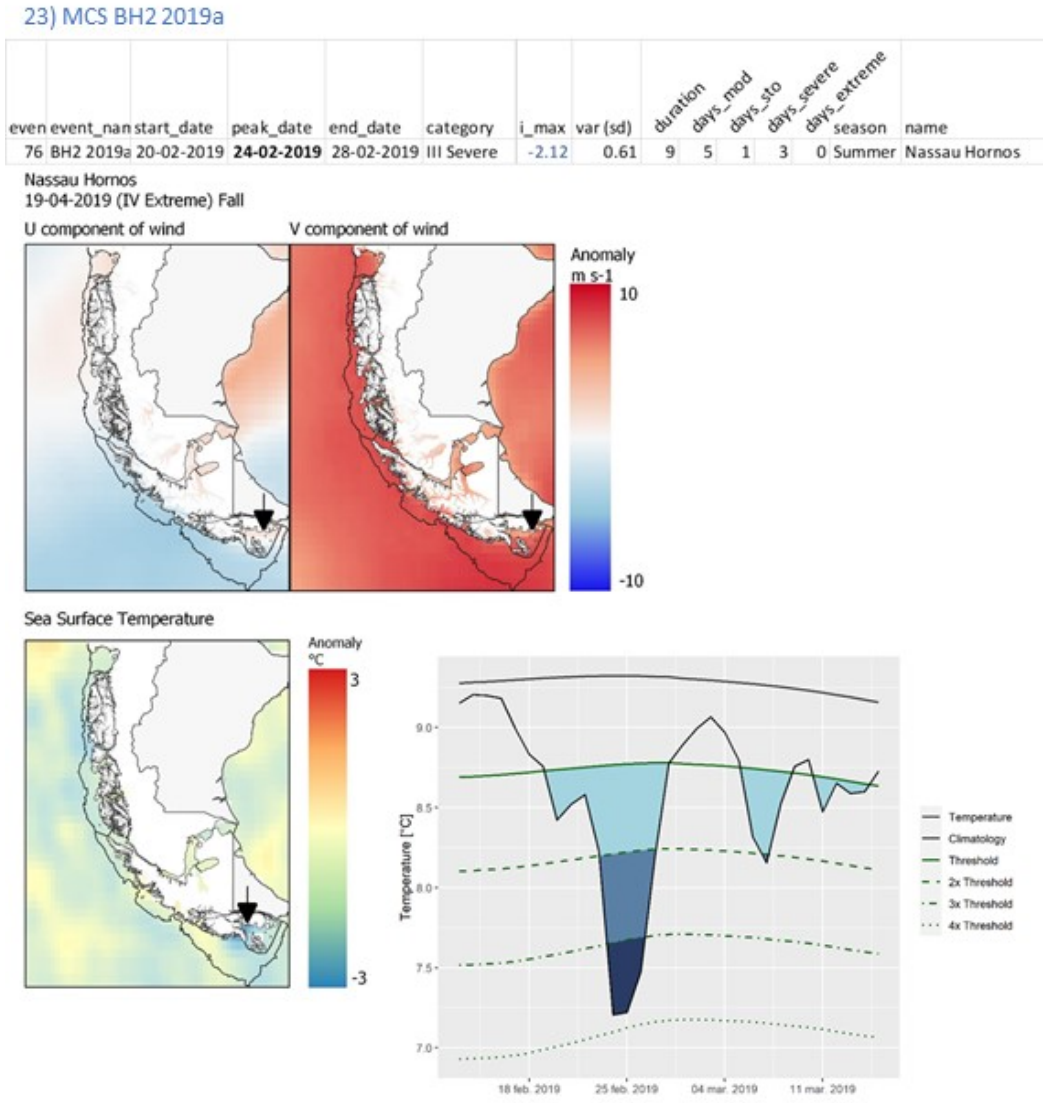


Figure A.25: 23) MCS: BH2 2019a

24) MCS BH2 2019b

even	event_nan	start_date	peak_date	end_date	category	i_max	var (sd)	duration	days_mod	days_sto	days_severe	days_extreme	season	name
77	BH2 2019b	13-04-2019	**19-04-2019**	21-04-2019	IV Extreme	-2.4	0.6	9	5	1	2	1	Fall	Nassau Hornos

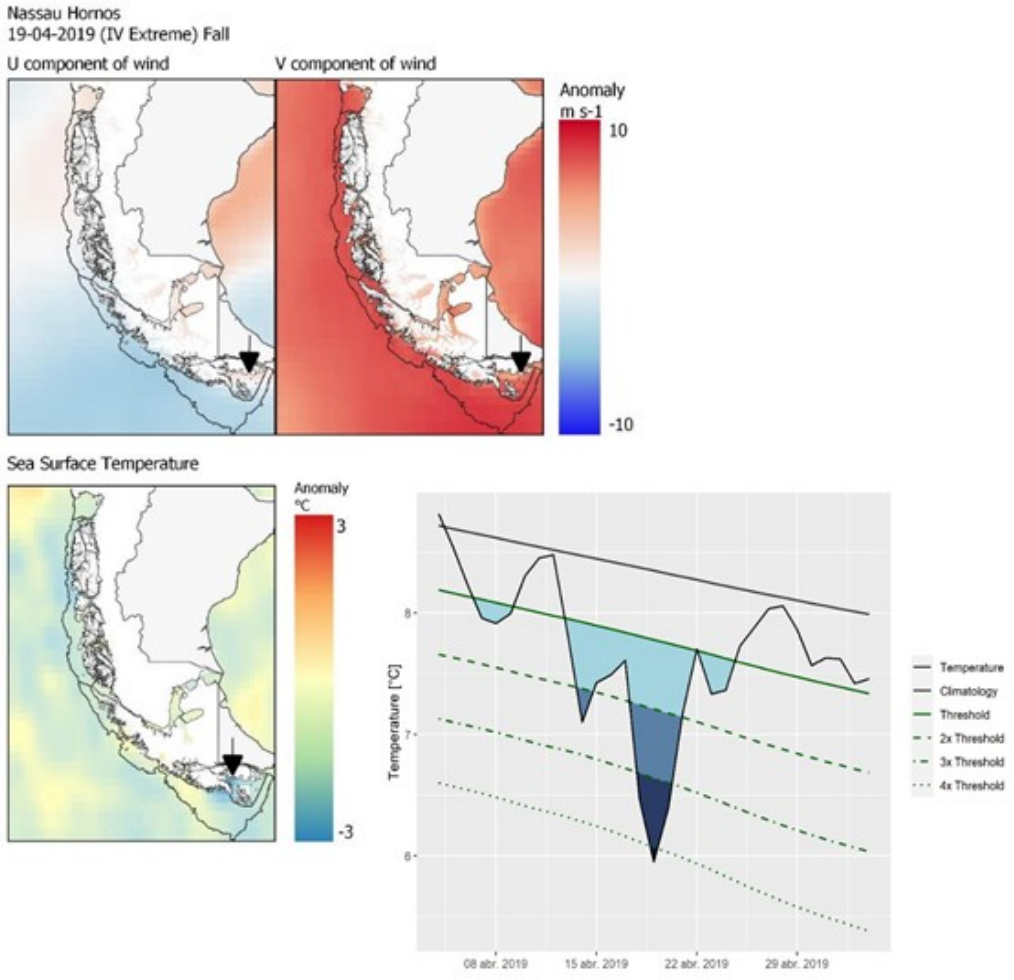


Figure A.26: 24) MCS: BH2 2019b

25) MCS E2 2019

even	event_nan	start_date	peak_date	end_date	category	i_max	var (sd)	duration	days_mod	days_sto	days_severe	days_extreme	season	name
84	E2 2019	02-06-2019	**05-06-2019**	07-06-2019	III Severe	-2.09	0.51	6	1	3	2	0	Fall	Central Strait

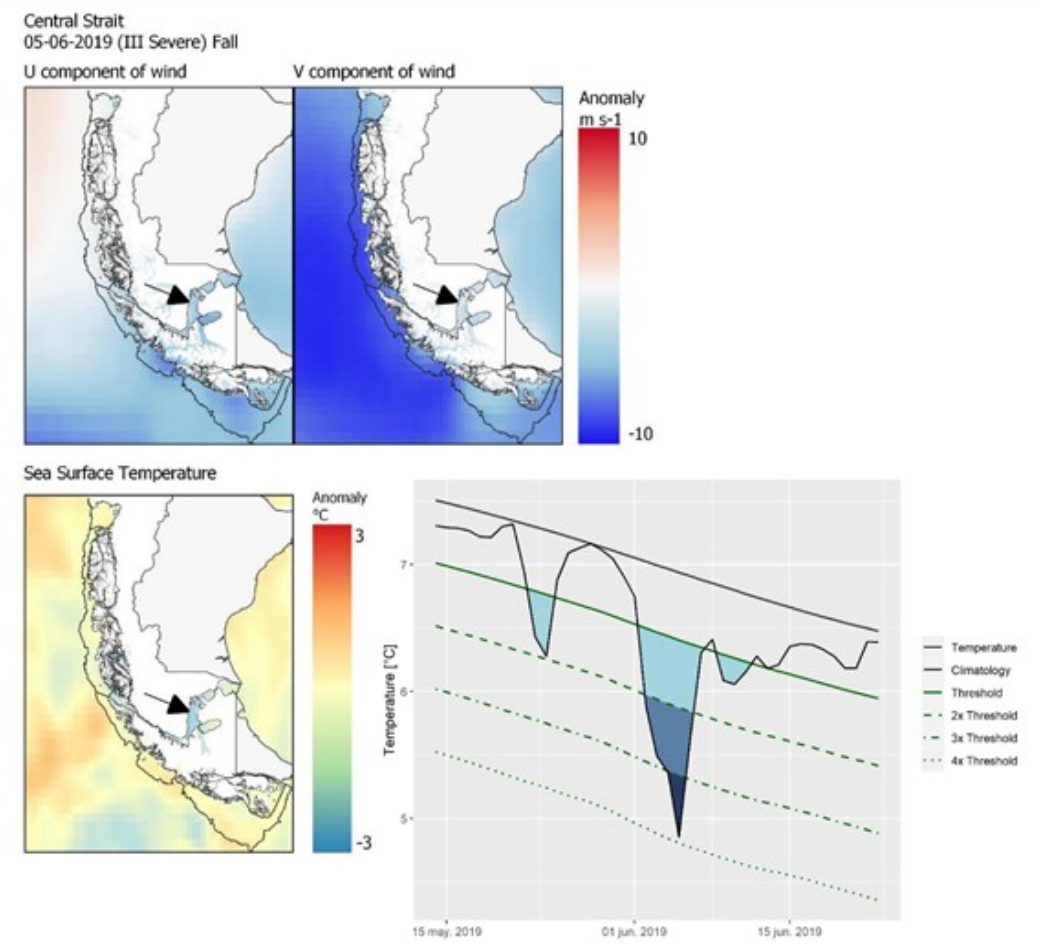


Figure A.27: 25) MCS: E2 2019

26) MCS BH1 2019

even	event_nan	start_date	peak_date	end_date	category	i_max	var (sd)	duration	days_mod	days_sto	days_severe	days_extreme	season	name
96	BH1 2019	15-08-2019	18-08-2019	21-08-2019	III Severe	-2.89	0.75	7	2	3	2	0	Winter	Nearshore Beagle Ballenero

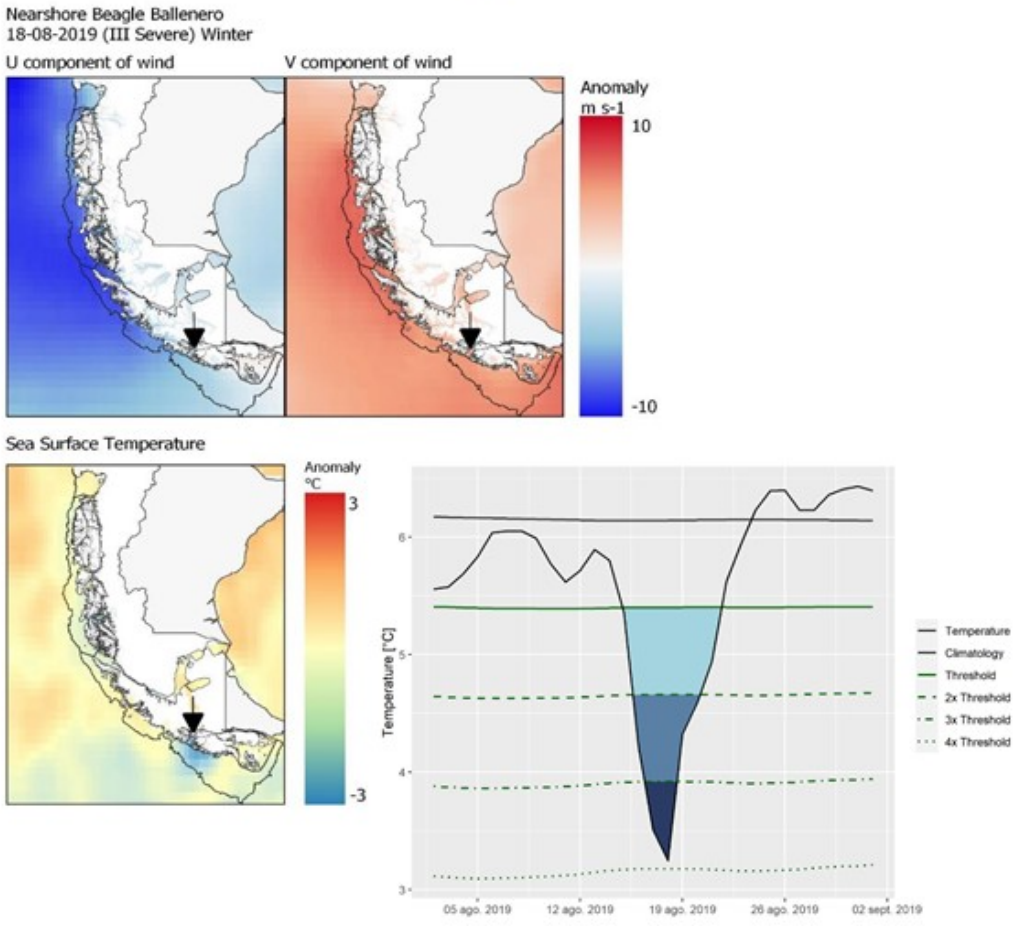


Figure A.28: 26) MCS: BH1 2019

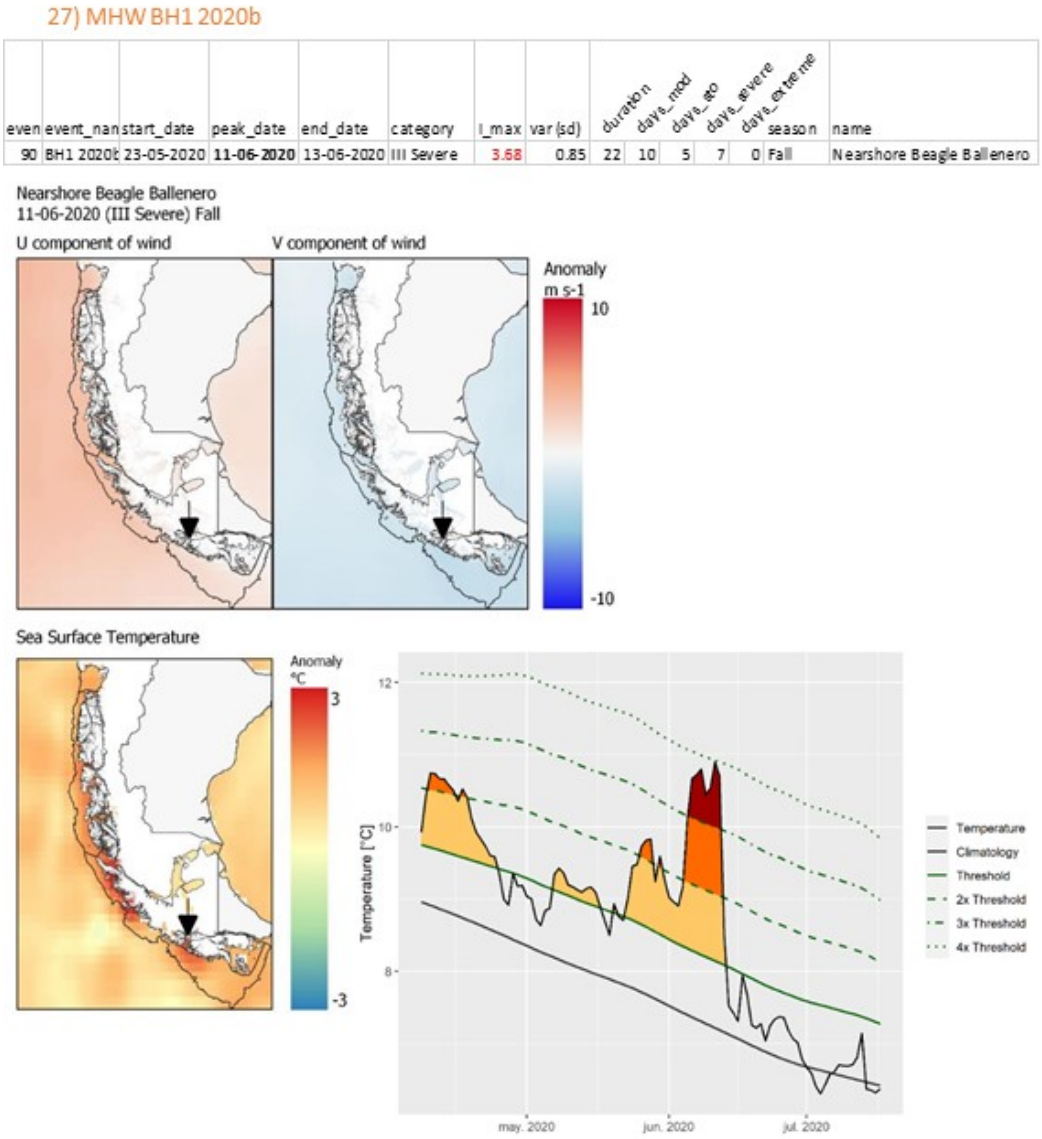


Figure A.29: 27) MHW: BH1 2020b